Contract No. 777564

INNOVATIVE RUNNING GEAR SOLUTIONS FOR NEW DEPENDABLE, SUSTAINABLE, INTELLIGENT AND COMFORTABLE RAIL VEHICLES

Deliverable 3.2 – New actuation systems for conventional vehicles and an innovative concept for a two-axle vehicle

Due date of deliverable: 30/09/2019

Actual submission: 27/09/2019

Leader/Responsible of this Deliverable: Rickard Persson, KTH

Reviewed: Yes

Document status		
Revision	Date	Description
1	29.06.2018	Skeleton
2	12.04.2019	State-of-art study included
3	16.07.2019	Draft, KTH and HUD contributions added
4	17.07.2019	Draft, POLIMI contribution added
5	23.07.2019	Draft, complete
6	22.08.2019	Language reviewed
7	30.08.2019	For TMT review
8	13.09.2019	Updated after TMT review
9	27.09.2019	Final version after TMT and quality check

This project has received funding from Shift2Rail Joint Undertaking under the European Union's Horizon 2020 research and innovation programme under grant agreement No 777564.

Dissemination Level		
PU	Public	X
CO	Confidential, restricted under conditions set out in Model Grant Agreement	
CI	Classified, information as referred to in Commission Decision 2001/844/EC	

Start date of project 01/09/2017 Duration 25 months

REPORT CONTRIBUTORS

Name	Company	Details of Contribution
Rickard Persson	KTH, Kungliga Tekniska Högskolan	Executive summary 1. Introduction 4.1 Introduction to two-axle vehicles with active suspension 5. Summary and conclusions
Bin Fu	POLITECNICO DI MILANO (POLIMI),	2. State of the art analysis (together with Rocco Libero Giossi)
Rocco Libero Giossi	KTH, Kungliga Tekniska Högskolan	2. State of the art analysis (together with Bin Fu) 4. Two-axle vehicle with active suspension (except 4.1, 4.4.2 and 4.5)
Stefano Bruni Egidio Di Gialleonardo Bin Fu Binbin Liu	POLITECNICO DI MILANO (POLIMI)	3. New actuation systems for conventional bogies (except 3.6)
Luis Baeza	University of Southampton (ISVR)	3.6. Effect of actuator dynamics on ride comfort / waterbed effect
Xiaoyuan Liu	University of Huddersfield (HUD)	4.2. MBS model (together with Rocco Libero Giossi) 4.4.2. Actuator in series with spring 4.5. Active steering of independently rotating wheels
Roger Goodall	University of Huddersfield (HUD)	Language checker

EXECUTIVE SUMMARY

The work package T3.2 generates and studies actuation concepts for conventional bogies as well as for an innovative single axle running gear intended for a two-axle vehicle. The active systems include active wheelset steering, aiming to reduce the wheel (and rail) wear and active secondary suspension with the aim to improve the vibrational ride comfort. Independently rotating wheels are studied for the single axle running gear as an alternative to the conventional solid axle. The studies include modelling and intensive simulation in a multi-body-simulation environment.

A conventional bogie vehicle with passive suspension can be designed to provide an acceptable vibrational ride comfort and wheel wear. Still, active wheelset steering will significantly reduce the wheel and rail wear in curves by controlling the angle of attack between wheel and rail. Locating the actuator in series with the longitudinal wheelset guiding stiffness gave better performance than installation in parallel to the same stiffness.

A method to evaluate the severity of different failure modes and fault-tolerant capability of different actuation schemes for wheelset steering is proposed. The quantified severity factor and Risk Priority Number can provide a good base for assessing and comparing different active steering schemes regarding their tolerance to faults. Implementing a redundant actuation scheme is an effective method to improve the fault tolerance of actuation system, whilst without any redundancy or passive back-up, the risks of safety issues will significantly increase in case of potentially dangerous failure modes.

The effects of different classic control strategies for semi-active suspension through a simple one-quarter vehicle model and full vehicle model have been investigated for the conventional bogie. In general, continuous controls produce better vibration attenuating effects than two-state controls. A trained Neural Network has been used to estimate the current required to generate the desired damping force for a given working condition of the Magneto-rheological damper. Still, the error between the actual damping force produced by the damper and the desired value can significantly degrade the performance of the semi-active suspension. Therefore, the control for the damper needs to be carefully designed.

A single axle running gear has potential for significant weight savings compared to conventional bogie designs. The savings come from reduced size of the components and reduced number of components. The single axle running gear needs unconventional wheelset guidance to maintain wheel and rail wear at levels comparable to a vehicle with conventional bogies. The reason is the longer wheelbase for the two-axle vehicle compared to the two axles in a bogie. A possible solution is a frequency dependent bush replacing the passive wheelset guidance. This is a passive solution with marginal additional cost to a conventional wheelset guidance. Active wheelset steering can provide even better performance promising significantly reduced wheel and rail wear. The frequency dependent bush will only work for solid axle wheelsets, while active wheelset steering

works for independently rotating wheels as well. Driven independently rotating wheels become an interesting solution as no actuator is needed for the wheelset steering. Active wheelset steering will reduce the flange wear to such an extent that the focus on the control will be shifted to how the wear is distributed over tread. The active wheelset steering can control the location of the rolling contact point on the wheels. Distributing the contact over the wheel may lead to much longer wheel turning intervals. The single axle running gear will need active suspension to improve the vibrational ride comfort. This is caused by the single-stage suspension, which is unable to attenuate the vibrations initiated by the track irregularities. An active suspension has the potential to achieve even better ride comfort compared to a vehicle with conventional bogies.

ABBREVIATIONS AND ACRONYMS

ADD	Acceleration-Driven-Damping
AIRW	Actuated Independently Rotating Wheels
ANFIS	Adaptive Neuro-Fuzzy Interference System
ASW	Actuated Solid-axle Wheelset
AY-FS	Actuated Yaw-Force Steered
BP	Back Propagation
DCW	Differential Coupling Wheelset
DIRW	Driven Independently Rotating Wheels
DOF	Degrees Of Freedom
DSW	Directly Steered Wheels
EHA	ElectroHydraulic Actuator
EMA	ElectroMechanic Actuator
ERI	Extended Range Integration
ERRI	European Rail Research Institute
FMEA	Failure Mode and Effect Analysis
FRS	Front Radial Steering
GPS	Global Positioning System
HALL	Hydraulisches AchsLenkerLager
HOD	Hold-Off-Device
HPI	High-Pass Integration
IRW	Independently-Rotating Wheel (or Wheelset)
KRRI	Korea Railroad Research Institute
JNR	Japanese National Railways
LMI	Linear Matrix Inequality
LQG	Linear Quadratic Gaussian
LQR	Linear Quadratic Regulator
LRC	Light Rapid Comfortable
MBS	Multi-Body Systems
MPC	Model Predictive Control
MPPT	Maximum Power Point Tracking
MR	Magneto-Rheological
NGT	Next Generation Train
NLA	Non-compensated Lateral Acceleration
NSGA	Non-Dominated Sort Genetic Algorithm
PDP	Positive Displacement Pumps
PID	Proportional Integral Derivative
PPRV	Pressure Proportional Regulator Valves
RPN	Risk Priority Number
PSD	Power Spectral Density
RMS	Root Mean Square
SYC	Secondary Yaw Control

TABLE OF CONTENTS

LIST OF FIGURES

LIST OF TABLES

1. INTRODUCTION

The target of work package WP3 is to analyse the technical solutions for active suspension and control technology on the market in railway and non-railway applications. Based on this information new concepts are generated and an authorisation process of vehicles with active suspension proposed to reach a manageable homologation process.

The work package T3.2 generates and studies actuation concepts for conventional bogies as well as for an innovative single axle running gear intended for a two-axle vehicle. The active systems include active wheelset steering, aiming to reduce the wheel (and rail) wear and active secondary suspension with the aim to improve the vibrational ride comfort. Independently rotating wheels are studied for the single axle running gear as an alternative to the conventional solid axle. The studies include modelling and intensive simulation in a multi-body-simulation environment.

A conventional bogie vehicle with passive suspension can be designed to provide an acceptable vibrational ride comfort and wheel wear. The work on the conventional bogies therefore focuses on performance enhancements and control strategy. The aim is here to find out what control strategies are needed to further improve the performance.

A single axle running gear with just one suspension stage (a conventional bogie has two) has much less scope to provide an acceptable vibrational ride comfort and level of wheel wear. Improved wheelset steering and active suspension are needed to ensure good performance. The intention is to design a simple running gear that with use of as simple as possible updates can provide performance in line with a passively suspended conventional bogie.

The performance is reported for a selected set of performance indicators: ride comfort, track forces, wheel wear and energy consumption.

2. STATE OF THE ART ANALYSIS

2.1 INTRODUCTION TO STATE-OF-THE-ART ANALYSIS

Over the last half-century, railway technologies are developed in a way that more and more electronics, sensors and controllers are applied with traditional mechanical structures to meet the new requirements for higher speed, better ride quality, and more strict safety issues. Some relevant technologies in railway engineering have been well developed and put in practical use in sub-systems including train management, communication, traction and braking controls, etc. In contrast, only limited implementations of active technologies have been introduced to improve the dynamics of the railway vehicle. Tilting trains, as one of the successful applications of active suspensions, have shown large benefits, which facilitate the further exploration of it in recent years. Since the suspension of rail vehicles is a complicated system aimed at achieving different functions, active suspension technologies proposed with different aims and configurations are developed in various forms. Major reviews were published in 1983, 1997, 2003 and 2007 [1]–[4]. A systematic state-of-art review is presented in this chapter with the inclusion of recent studies on active suspension. In sub-section 2.2, the general concepts and classifications of active suspension are explained. Based on the classifications, tilting trains, active secondary suspension and active primary suspension are introduced in sub-sections 2.3 to 2.5.

2.2 BASIC CONCEPTS OF ACTIVE SUSPENSION AND CLASSIFICATIONS

2.2.1 Basic concepts of active suspension

For a passive suspension, stiffness and damping parameters decide the frequency response of a system. However, the external excitations of the vehicle suspension system include deterministic (track layout) and stochastic (track irregularity) excitations in different frequency ranges. Therefore, design of a passive suspension with fixed parameters becomes a trade-off solution for different scenarios. In contrast, a substantial improvement can be achieved by implementing active suspension which features combined utilization of sensors, electronic controller and actuators. Figure 1 summarizes the generic workflow of active suspension.

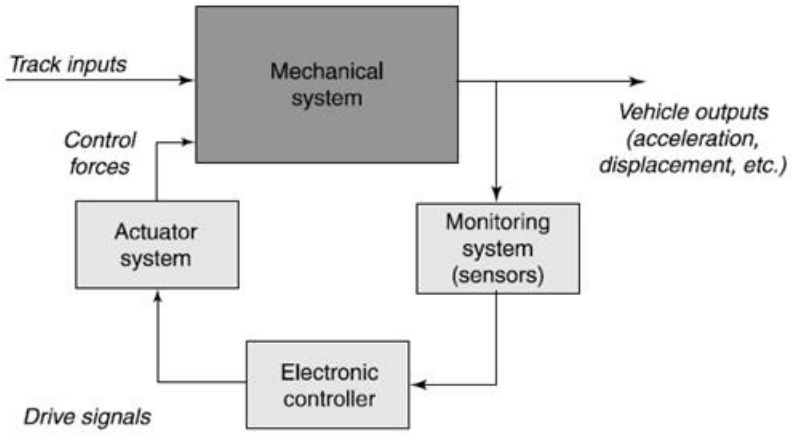

Figure 1 - Workflow of active suspension [5]

In an active suspension, the monitoring system will gather the information of vehicles including the accelerations, velocities and displacements directly and indirectly from sensors and filters. Some other information, such as vehicle position and track layout could be obtained from the Global Position System (GPS) and track layout database. This information will be analyzed in a controller designed in advance to achieve specific targets and then force demand given to control actuators to manipulate the mechanical system to the desired motion.

2.2.2 Different classifications for active suspension

(1) Classification based on suspension position

There are different sorts of approaches to classify the various active suspension technologies. A natural way is to categorize the technologies into three types:

(a) tilting trains,
(b) active primary suspension
(c) active secondary suspension

Active primary suspension is meant to improve the stability, guidance and curve negotiation behaviours for the solid-axle wheelset and independently rotating wheels. With different targets, the interesting frequency range and control strategies could be entirely different. Further classification for active primary suspension is referend in the following chapters. A active secondary suspension is aimed at improving the ride quality and often also controlling the quasi-static motion of the car-body (Hold-off Device). Tilting trains can tilt the car body to a desired rolling angle in curves so that the lateral acceleration felt by the passengers will be reduced allowing higher curve-negotiation speed. Tilting trains theoretically belong to active secondary suspension and can be combined with other active schemes like Hold-Off-Device (HOD), but as a distinctive and well-developed technology, it is reasonable to separate it from active secondary suspension. The sequence of the following chapters is organized based on this classification.

(2) Classification based on degree of control

Semi-active and fully-active are two categories introduced from the perspective of the degree of control. A clear distinction between the two technologies can be noticed in Figure 2. The fully active control requires a power supply to produce the desired force and the motion of mechanical structure can be fully controlled. In contrast with neither power supply nor actuation system, the only controllable variables in semi-active suspension are parameters of passive suspension, usually a varying damper constant. As the force generated in semi-active suspension still is dependent upon the speed of the damper, the improvement of vehicle dynamics performance is naturally constrained. For instance, semi-active control cannot create the desired force as the fully-active suspension can do in the low-frequency or quasi-static scenarios. However, the simplicity of the semi-active damping makes it easier to implement and therefore it may be a good trade-off between passive suspension and fully-active suspension.

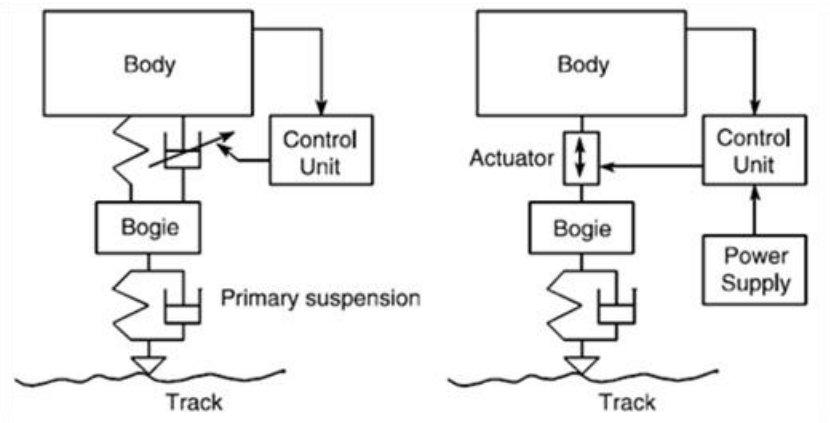

Figure 2 - Schematic diagram for the principles of semi-active (left) and fully-active (right) suspensions

Semi-passive and adaptive/adjustable passive concepts are similar to the semi-active control. The difference lies in if the characteristic of passive suspension varies according to the variables influenced by the dynamic system or not.

(3) Classification based on functions

Another kind of classification for active suspension is from the way in which control of suspension may be utilized [1]. Four types are categorized as follows:

(a) isolating the vehicle body from track irregularity (i.e. ride comfort);
(b) controlling kinematic modes of the bogie (i.e. stability);
(c) positive steering and guidance of wheelsets (i.e. active steering);
(d) special functions in addition to passive suspensions (i.e. tilting trains, HOD)

Since the purposes of active suspension decide control targets and the interesting frequency range, the active control schemes consisting of technologies of controllers, sensors and actuators will vary according to the types. Therefore, the classification based on types helps the organization of description for control strategies and other parts. In this state-of-the-art review work, the idea of

this kind of classification is applied within each sub-section. For instance, when it comes to the active primary suspension system, the control strategies are introduced from perspectives of their types.

2.3 TILTING TRAINS

Car-body tilting is a well applied technology in railway vehicles. Its aim is to reduce the lateral acceleration perceived by the passengers by rolling the car-body inwards during curve negotiation. This solution leads to an increased comfort perceived by the passengers that eventually permits a higher speed during curves reducing the overall travelling time. As reported by Persson et. al. in [6], the running time benefit can be up to 10% for a tilting train with respect to a non-tilting one with the same top speed.

A first attempt of tilting mechanism was introduced in the late 1930s ([7]) while the first operating tilting coach was developed in 1938 by Atchison, Topeka and Santa Fe Railway ([8]). In the 1980s natural tilting trains were introduced in Spain with the Talgo Pendular trains ([9]). The first mass production of actively tilting trains was introduced in Canada with the LRC in 1981 followed by Italy with the ETR450 and in Sweden with the X2000 in the 1990s, while the first high-speed train was introduced in Japan in 2007 with the Shinkansen Series N700 ([6]).

The main distinction between tilting trains is between natural and active tilting. In natural tilting the roll of the car-body is obtained thanks to the centrifugal force acting on the car-body itself. The natural tilting is possible only if the car-body centre of gravity is placed below the tilt centre. In Figure 3 a representation of this mechanism is shown.

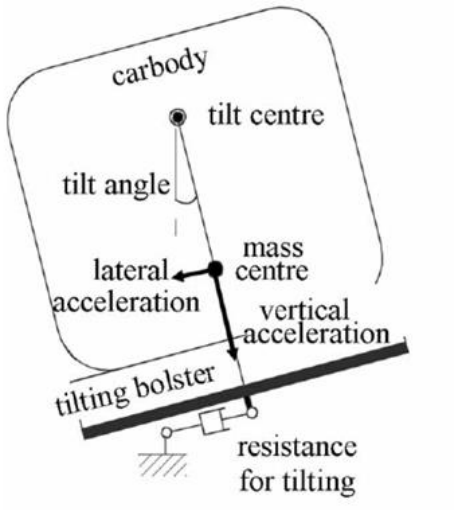

Figure 3 - Natural Tilting [6]

One commercial success of the natural tilting is Talgo trains ([10]), in which the natural tilting is achieved by placing the air springs in a high position, in this way shifting the tilting centre. In Figure 4 the Talgo configuration is shown.

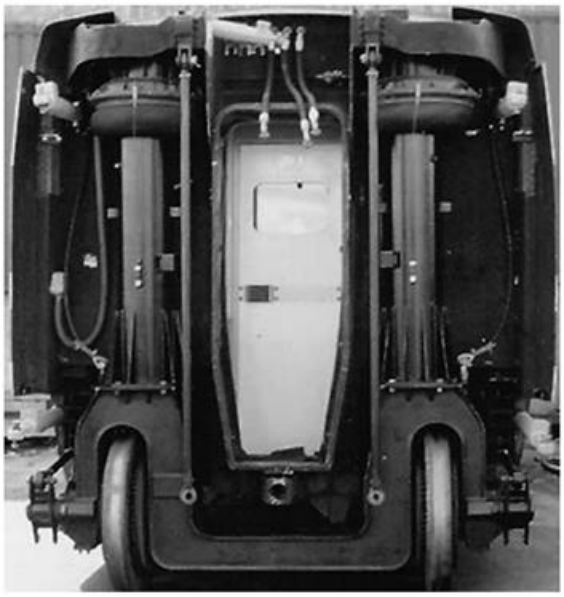

Figure 4 - Talgo Train [10]

As stated by Persson et. al. in [6], natural tilting is a purely mechanical system and it is a failsafe and low-cost system. Nevertheless, the position of the car-body centre of gravity allows lateral motion of it increasing the risk of overturning. Moreover, the car-body moment of inertial will delay the tilt motion in transition curves increasing the possibility of motion sickness in sensitive passengers. On this purpose, often a controlled natural tilting is applied. In this configuration, shown in Figure 5, an additional actuator is introduced. Its main purpose is to reduce lateral fluctuation in transition curves. Additionally, it is used to start the tilt motion before the curve negotiation to reduce the delay in the tilt motion and decrease the possibility of motion sickness.

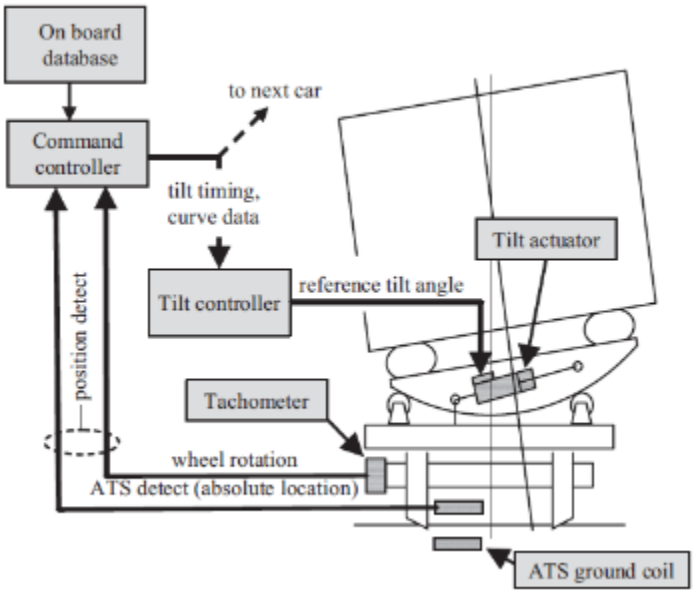

Figure 5 - Controlled Natural Tilting [6]

The second type of tilting is the active one. In this configuration, although the centre of gravity doesn't have to be lower than the tilt centre because the motion is provided by dedicated actuation, this is nearly always arranged so the vehicle comes upright in the case of control failure. Figure 6 gives an example of an active tilting mechanism.

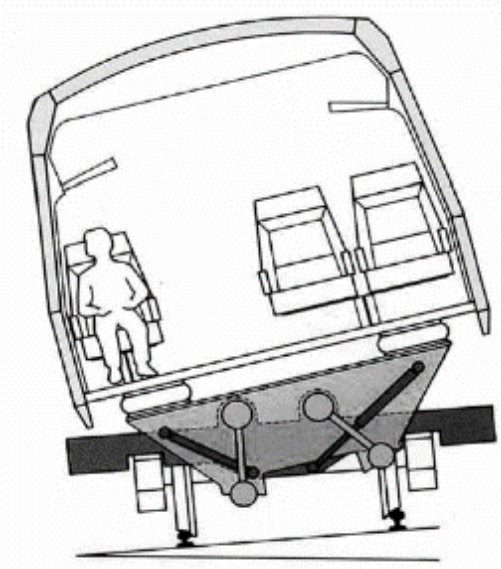

Figure 6 - Active Tilt Mechanism [6]

As well reported by Persson et. al. in [6], tilting control evolved from the so called “nulling” controller to the precedence control strategy. These control strategies are shown in Figure 7.

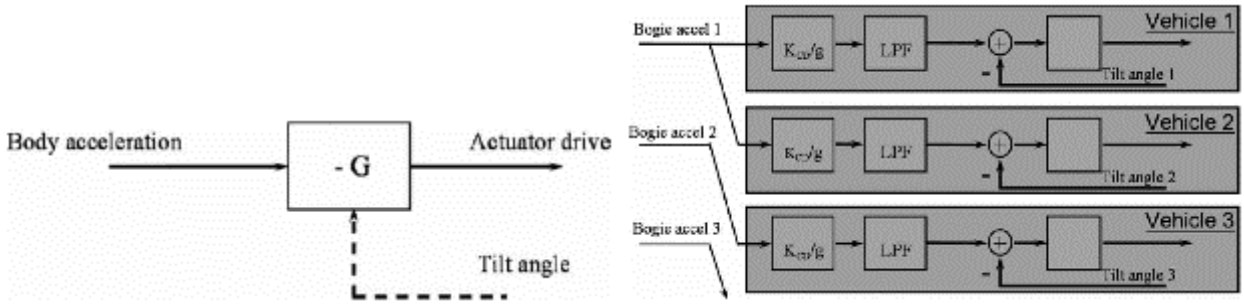

Figure 7 - Tilting Controls: nulling control (left), precedence control (right) [6]

In the “nulling” controller the lateral acceleration of the car-body is measured through the usage of an accelerometer and a negative feedback is used to tilt the car-body to bring the carbody lateral acceleration close to zero. This type of approach finds difficulties due to the strong coupling of between roll and lateral motion of the car-body modes. To solve the problem, the acceleration was then measured in a non-tilting part, thus the bogie. A low-pass filter must be added in this case to attenuate the acceleration contribution due to track irregularities causing delay in transition curves. Thus, the precedence control was introduced. In this approach the signal generated from the vehicle in front is used to command the subsequent vehicle. The filtering delay is in this case carefully designed to fit the precedence time corresponding to a vehicle length. Despite the fact that precedence control is now one of the most used strategies in European tilting trains, research is continuing to improve the performance by studying the possibility of track knowledge control or improving the control on the actuation systems or to remove it by applying local vehicle measurements alone.

In the field of local vehicle measurements, Zamzuri et. al. in [11] shows a promising utilization of a Proportional Integral Derivative (PID) nulling-type control with fuzzy correction scheme. In the study the proposed controller is compared with a fuzzy extension of a conventional PI controller showing improved performances. Subsequently, Zhou et. al. in [12] used a combination of tilt and active lateral secondary suspension control. A decentralization method is used to control separately tilting and lateral dynamics based on measurements of lateral acceleration, actuator roll and suspension deflection. Nevertheless, as previously mentioned in vehicle measurements can introduce issues in the control application. To counteract this problem Zhou et. al. in [13] introduced a robust state estimation based on H_∞ filtering to estimate the vehicle body lateral acceleration and true cant deficiency. The H_∞ filtering is then compared with a standard Kalman filter showing good results.

Facchinetti et. al. in [14] and [15], using a similar approach of Zhou in [12] of a combination of tilting and active lateral control, studied the possibility of using active air-springs and pneumatic secondary suspension. A combination of feedforward and feedback actions is introduced, and their effectiveness is tested on a full-scale test stand consisting of one bogie and a ballast mass

reproducing the inertia of half car-body. A similar approach in terms of feedforward and feedback combination is used to control interconnected hydraulic actuators by Colombo et. al. in [16]. The scopes of interconnected hydraulic actuators are to actuate the car-body tilting and provide the same car-body to bogie stiffness as a conventional anti-roll bar. Three different control approaches are performed showing that a combination of feedforward, PID and Sky-hook controls provides the best performance in terms of ride comfort for an acceptable actuation power requirement. An alternative approach is studied by Jacazio et. al. in [17]. An adaptive PID control is developed with the objective of minimize the hydraulic actuators power losses maintaining the required dynamic performances. The adaptation is based on the outside temperature and the force to be developed by the actuators. Simulation results based on real track data shows a saving of 10 to 20 % of the electric power required by train auxiliary systems. Although hydraulic actuators are described in some above references, electro-mechanical actuators are now adopted in many new European tilting trains because their high efficiency [6].
An enhancement in tilting control is the utilization of stored track data to predict the upcoming curve and reduce the delay in the actuation system. An example of this is given by Hauser in [18]. Here lateral acceleration and roll and yaw signals are combined with the track data to compute the command angle to be provided by the actuator. Another usage of stored track data is given by Persson et. al. in [19]. Here a new tilting algorithm is used for on-track tests to reduce motion sickness. The algorithm is fed with the stored track data and the position of the vehicle on the track provided by a positioning system to select the appropriate data. The approach is tested on 100 subjects giving promising results both on comfort improvements and motion sickness reduction.

2.4 ACTIVE SECONDARY SUSPENSION

2.4.1 Principles and configuration for active secondary suspension

Two general functions of the secondary suspension system in bogie vehicle are to attenuate vibration (>1 Hz) from track irregularity to improve the passenger ride comfort and meanwhile to bear static and quasi-static (<1 Hz) load from the car body to bogie with constrained deflection. however, the stiffness of conventional passive springs has opposite effects to the two targets. Solutions are provided if active secondary suspension technologies are applied. Three applicable backgrounds are explained as are shown in Figure 8.

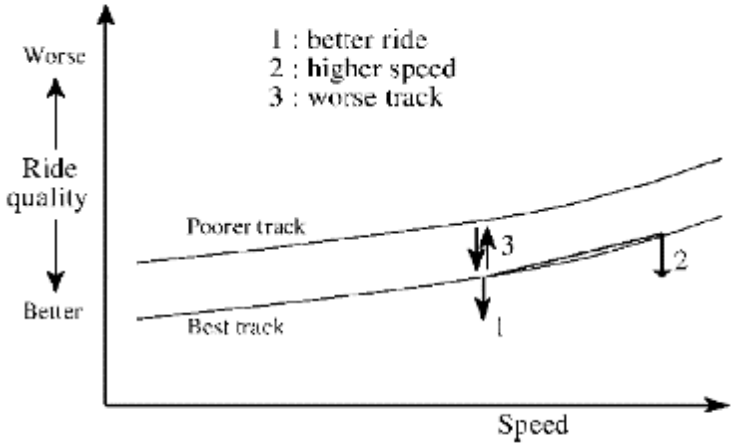

Figure 8 - The applicable backgrounds for active secondary suspension [4]

(1) Improve passenger ride comfort at current speed and track condition
(2) Enable higher speed with no sacrifice of ride quality
(3) Reduce the requirement for track maintenance with no sacrifice of ride quality

In the operational service, the ride quality of railway vehicle with passive suspension is usually satisfactory, which means that the first applicable background is not so attractive while the next two potentials still make the implementation of active secondary suspension worthwhile.
For the configuration of the active secondary suspension, actuators are generally placed between the bogie and the car-body in lateral or vertical directions. The passive air springs can also be modified to be actuators to control the vibration at a low-frequency range (<2Hz) [20]. Figure 9 gives a general representation of the active secondary suspension system.

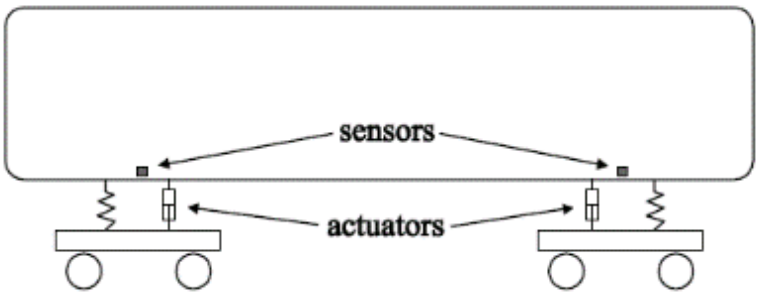

Figure 9 - Active Secondary Suspension System [21]

The further mechanical configurations of active secondary suspension can be introduced in terms of the relationship with passive springs, as are shown in Figure 10.

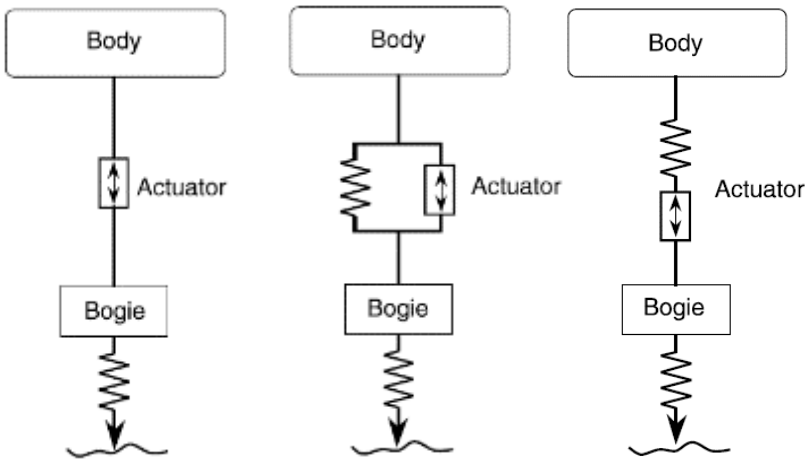

Figure 10 - Mechanical configurations of active secondary suspension

Actuators can directly replace the original passive springs from bogie to car-body and independently control the motion of the vehicle. However, considering the dynamic characteristics of different actuators, it is more practical to implement actuators in addition to passive springs in parallel and in series as the complement to the lack of capability of actuators in some cases. When paralleled with actuators, passive springs can carry the static and quasi-static load in the vertical and lateral directions which in turn reduces the requirement for actuators and thereby enables small dimensions of actuators. When connected in series with actuators, the passive springs can isolate the high-frequency excitations that actuation system cannot react because of the intrinsic limitation of itself.

A special configuration for active secondary suspension proposed by Mei [22] is implementing actuators between the adjacent car bodies in a train set, which is illustrated in Figure 11. The number of actuators can be reduced through this configuration. The working environment is friendly to sensors and actuators as severe vibration has been filtered above secondary suspension, which leads to higher reliability of the actuation system. In the research [22], two vertical actuators are arranged between the adjacent car-bodies and another two vertical actuators from bogie to car-body are configurated at the two ends of the trainset as an optional complement to further enhance the ride quality of the front and the rear car bodies. Zhou applied a similar configuration in the lateral direction [23]. The control strategies for this configuration are very different and will be discussed in the next chapter.

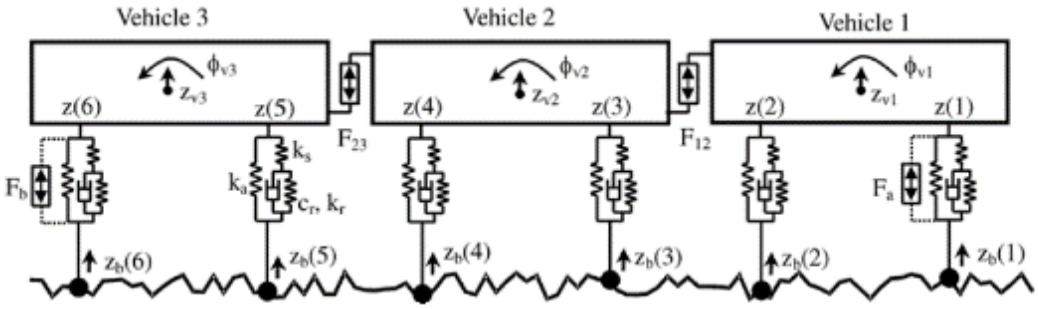

Figure 11 - Configuration for inter-vehicle actuation system [22]

When the active secondary suspension is considered from the perspective of vibration modal, except for longitudinal oscillations, the remaining five car body motions could be involved. Lateral and yaw motion alone or together are controlled by active lateral suspension, while the active vertical suspension is meant to attenuate bouncing and pitching vibrations. Rolling control can be realized by either lateral or vertical active control, which is mainly discussed in the last chapter for tilting trains. It is common to consider different motions in one control scheme which is also known as modal separation control.

2.4.2 Active Secondary suspension control strategies

2.4.2.1 Full-active control in high bandwidth

High bandwidth system deals with stochastic vibration excited from track irregularity to improve passenger ride comfort. Before the introduction to the control strategies, it is worth mentioning that there are different methods to evaluate the ride comfort. The factors in EN 12299 [24], and Ride Index W_Z [25] are usually used which take into consideration the R.M.S. value of frequency-weighted accelerations on the car-body floor. The weighting functions are used to reflect the human interpretation of ride comfort. The human body is most sensitive in the range between 0.5 to 10 Hz. The weighting functions vary depending on the method. Figure 12 gives an example of weighting functions.

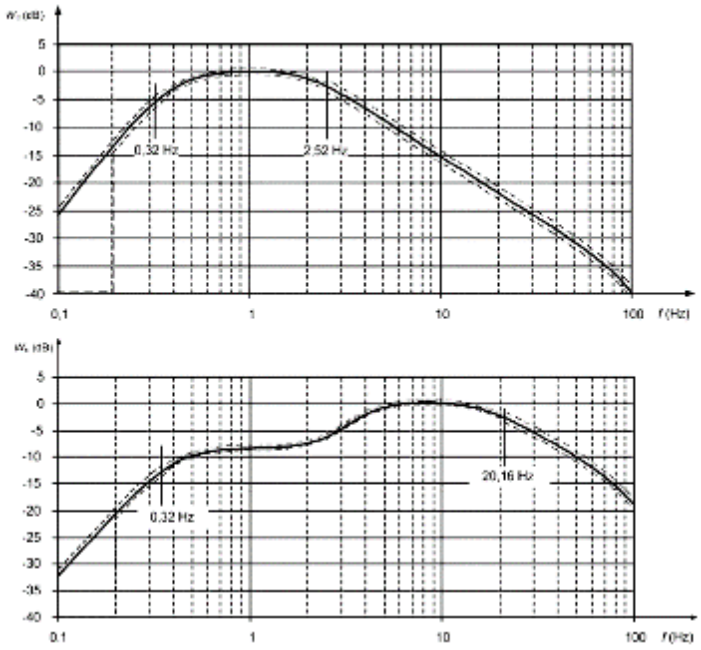

Figure 12 – Lateral (top) and vertical (bottom) weighting curves, EN 12299 [24]

Rigid car-body modes are generally in a frequency range around 1 Hz while elastic modes around 8 to 15 Hz (Orvnäs in [26]). Thus, it is important to design properly the secondary suspension system to avoid unacceptable levels of ride quality. Moreover, the general request of higher speeds in rail vehicle applications imposes lighter car-bodies resulting in lower structural stiffness, which eventually results in lower natural frequencies. This effect tends to worsen the situation of ride comfort. Once a passive system is optimized, a good way to improve passenger comfort is the usage of an active (or semi-active) suspension system to suppress undesired vibrations coming from the track.
Different control strategies and control ideas are introduced in the following parts.

(a) Sky-hook damping control

Sky-hook damping control, also known as absolute damping, is introduced by Karnopp in [27], and has been one of the simplest and most effective control techniques for vibration isolation. The basic assumption for Sky-hook control is that the subject is connected to the sky. Equation 1 gives the principles of sky-hook control for a railway vehicle.

$$\boldsymbol{F_{sky} = -C_s \dot{x}_2} \qquad \textbf{(1)}$$

where F_{sky} is the desired force acting on car-body, C_s is controllable damping and $\dot{x_2}$ is the velocity of the car body in the lateral or vertical direction. In practice, the damper must still be mounted between the car body and the bogie as illustrated in Figure 13. It is difficult to accurately produce the desired force acting on car body as the bogie is always vibrating.

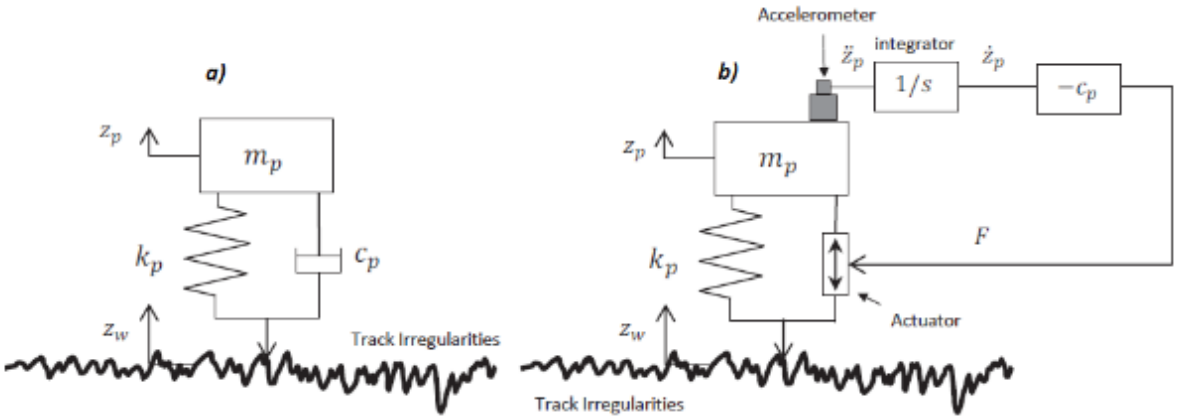

Figure 13 - Sky-hook damping for 1 DOF

The ride quality on tangent track can be significantly improved by applying sky-hook damper, but the deflection of suspension is enlarged on deterministic track features like curves and gradients. In the real case, the car body and bogie velocities are produced by integration of acceleration. Consequently, the integration of quasi-static acceleration as the lateral acceleration in curves must be avoided. The accelerations are therefore high-pass filtered before the integration. This solution will also mitigate any thermal drift in the sensors. Figure 14 gives the workflow for sky-hook damping.

Figure 14 - The workflow for sky-hook damper [28]

Thanks to the simplicity of sky-hook control, it is the one that finds application in full-size vehicle tests (Qazizadeh et. al. in [29], [30] and Sugahara et. al. in [31], [32]). In scientific studies, the Sky-hook damping is also used as reference to prove the effectiveness of other refined control techniques (Gopala Rao et. al. in [33], Sugahara et. al. in [32] and [31], Pacchioni et. al. in [34] and Orukpe et. al. [35]).

The damping factor (gain) for Sky-hook control can be set as critical damping, but this is not necessarily the best choice. Efforts are made to improve the performances of Sky-hook control. Li et. al. in [36] explored linear and non-linear approaches with different filtering techniques to improve ride comfort and minimize suspension deflection. Turnip et. al. in [37] introduces a sensitivity approach to improve Sky-hook performances at high frequencies. Hammood et. al. in [38] used a gain-scheduling approach based on the difference between car-body and bogie speeds to improve the performances while Yusof et. al. in [39] used Non-Dominated Sort Genetic Algorithm II (NSGA II) to optimize control gain and actuator stiffness. Gopala Rao et. al. in [33] develops a method to

choose the Sky-hook gain, showing that with a careful choice of the control parameters Sky-hook performances can match the performances of a Linear Quadratic Regulator (LQR).

(b) H_∞ Control

H_∞ Control is a robust model-based control technique using measurement feedback to produce a stable controller that handles unmodelled uncertainty and dynamics behaviour. A graphical representation of this control is given in Figure 15.

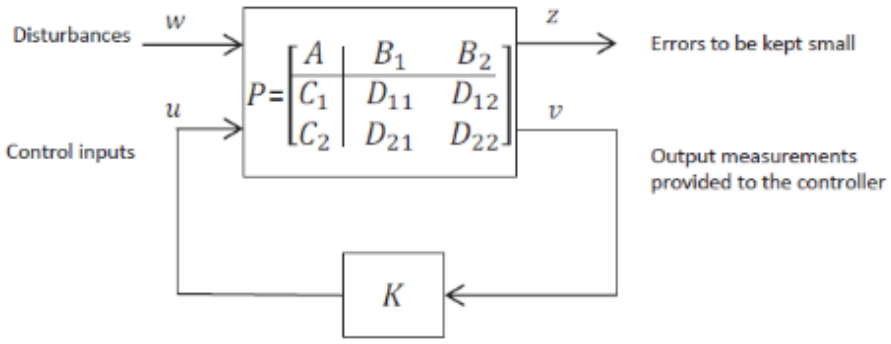

Figure 15 - H_∞ Control Scheme

H_∞ was introduced into control theory in the late 1970s. One of the first applications of H_∞ control to the control of vehicle modes is carried out by Hirata et. al. in [40] and [41] where lateral roll and yaw motions are successfully attenuated in the low frequency region. This type of control is extensively used by Kamada et. al. in [42]–[44]. Here, the effectiveness of the control strategy is shown both with simulations and experimental results on a 1:6 scale model of Shinkansen vehicle. The usage of the H_∞ control is especially useful in [42] where piezoelectric actuators are used. The robust H_∞ control overcome the problem of unmodelled behaviours and uncertainty on parameters of the piezoelectric actuators. An H_∞-Sky-hook control is developed by Leblebici et. al. in [45] showing the possibility of achieving good amplitude reduction near the resonance frequencies of the car-body. The development of a H_∞-Sky-hook control is possible due to the measurement feedback approach. A comparison in performance evaluation is carried out between Sky-hook control Model Predictive Control (MPC) based on mixed H_2/H_∞ using Linear Matrix Inequality (LMI) by Orukpe et. al. in [35]. It is shown through simulations that MPC better suppresses the bounce motion of the vehicle than the classical Sky-hook control while keeping the suspension deflection within a similar range and producing comparable forces.

(c) Linear Quadratic Gaussian (LQG) Control

Linear Quadratic Gaussian (LQG) Control is a combination of Linear Quadratic Regulator (LQR) and a Kalman filter to create a model-based control. A graphical representation of this control is given in Figure 16.

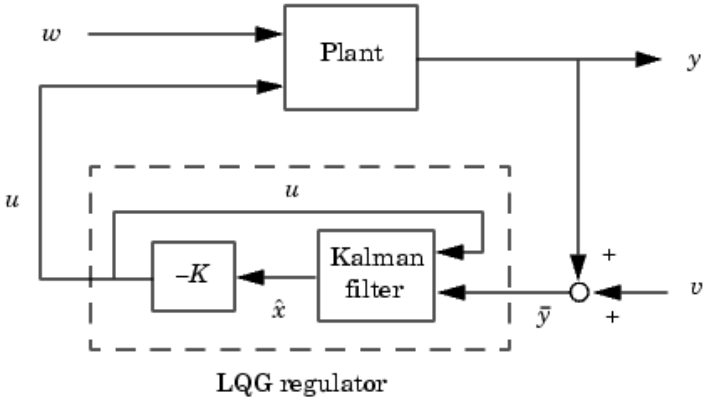

Figure 16 - LQG Control Scheme

A successful implementation of LQG is applied by Gong et. al. in [46], where it is combined with preview control. It is shown that LQG control is effective in control of both rigid and elastic modes together over a wide frequency range. An interesting application is studied by Leblebici et. al. in [47]. Here a lumped track model is introduced, and it is proven through simulations that the LQG control counteracts effectively bounce and pitch motions of the car-body. A quarter car model with non-linear suspensions is studied by Nagarkar et. al. in [48] where NSGA II is used to optimise PID and LQR control parameters with a multiple objective problem compromising ride comfort, suspension space and control force. Sugahara et. al. in [32] compares the usage of Sky-hook Damping and LQG control both by simulation and test on a full-scale model results. It is shown that LQG control works better when the natural frequency of the first bending mode of the car-body is far from the bogie one while the Sky-hook Damping improves the response when these two are close to each other. A similar approach is applied by Pacchioni et. al. in [34]. Here, it is shown that with a careful choice of the gains similar effects can be produced by Sky-hook and LQG. Nevertheless, as discussed by Sugahara et. al. in [31], LQG control can be a precise control but it can suffer of unmodelled uncertainty or even dynamics that can cause a drastic decrease in the controller performances.

(d) Fuzzy Logic Control

Fuzzy Logics comes from the definition of Fuzzy Sets which was first introduced by Zadeh in [49] in 1965. By definition, a Fuzzy Set is a set to which a variable may belong partially. This gives the possibility to the Fuzzy Logic to decide accordingly to a defined linguistic rule which output (control input) choose depending on the combination of the inputs it takes (error between reference signal and system output or measurements). A graphic representation of a Fuzzy Logic implementation is given in Figure 17.

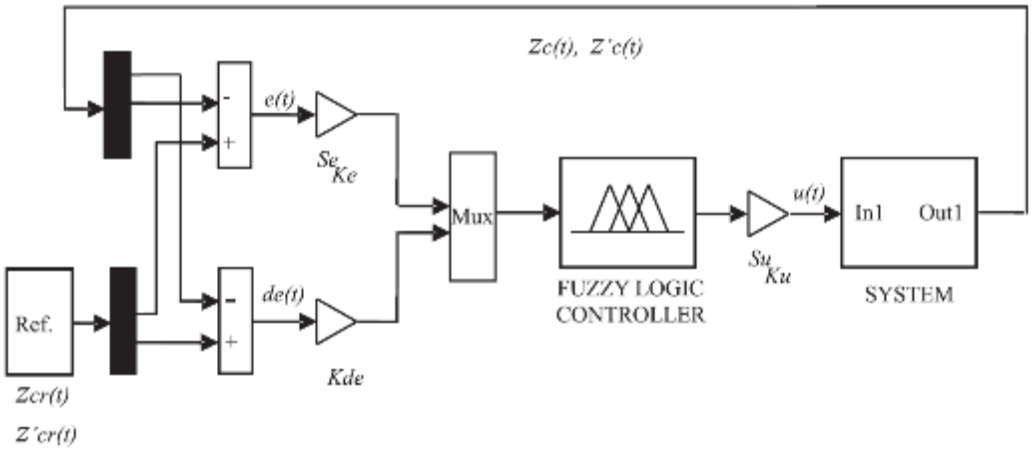

Figure 17 - Fuzzy Control Scheme [50]

Fuzzy Logic Control is successfully applied by Guclu et. al. in [50] on a tram with a three bogie configuration. Good results are presented in time and frequency domain with simulation results. In a subsequent work Guclu et. al. [51] compares the results obtained with a PID control with Fuzzy Logic Control. Both the controls are tuned with the usage of Genetic Algorithms. It is shown by simulations that the Fuzzy one improves the performances. A self-tuning Fuzzy Logic approach is implemented by Sezer et. al. in [52] achieving good results in terms of acceleration reduction and proving the robustness of the implemented approach against car-body mass variation. The simulation results are shown in terms of time and frequency domain analysis showing that low frequency amplitude is properly attenuated.

(e) Modal control approach

The target of modal control is to attenuate different motions efficiently using one common control strategy. The modal decomposition is achieved by processing the acceleration mounted on different positions of the car body. Then for suppressing each single modal, the desired actuation forces will be calculated separately, and these forces will be superimposed so that finally the different vibration modals can be damped at the same time. Orvnäs applied this idea to design control schemes for lateral, yaw and roll motions control in [53] as well as for bounce, pitch and roll motions control in [21]. The control scheme proposed and applied in [53] is shown in Figure 18. In this scheme, sensors mounted on front and rear position of car-body will measure lateral accelerations. Then the sum and difference of the two signals are processed to reflect the lateral oscillation and yaw motion separately. Then forces aimed at controlling motions will be generated according to sky-hook or H_∞ control. Moreover, the lateral acceleration of bogie is processed by the low pass filter and half bogie mass is used as a gain to form the force reference for HOD function. The idea of modal control is also applied in the studies by Hammood et. al. in [38], Sugahara et. al. in [54], Yusof et. al. in [39], and Qazizadeh et. al. in [29], [30].

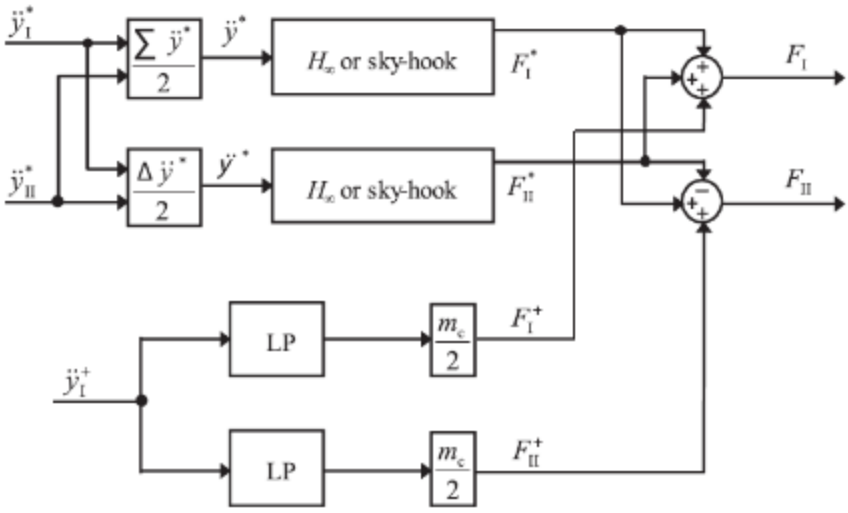

Figure 18 - Modal control considering lateral and yaw motion with conjunction of HOD [53]

(f) Model-based control

The inter-vehicle actuation system, as a special arrangement, has unique control strategy. When actuators connect the adjacent car bodies, the motions of them are coupled so that the whole trainset should be considered as a complete system. Furthermore, as each car body is equally important, the ride quality of each body should be optimised, which means in the control strategy, the control objectives are multiplied with an increasing number of car bodies. The complexity of the system makes it extremely difficult to apply the mentioned control strategies where dynamic system model and space-state functions are required, while multi-objective Genetic Algorithms are introduced and proved to get satisfied effects.

In paper [22], a three-car-body train set is studied, where the R.M.S values of acceleration are measured from the front, middle (dependent on front and rear variables) and rear positions and the sum of nine components form the objective function as is shown in the Equation 2:

$$J = \frac{\sqrt{\sum_{i=1}^{6} r.m.s.(\ddot{z}(i)) + r.m.s.(\ddot{z}_{v1}) + r.m.s.(\ddot{z}_{v2}) + r.m.s.(\ddot{z}_{v3})}}{9} \quad (2)$$

Each desired actuator force is decided by six variables that enable objective function at a minimum value. Equations 3 and 4 present the method for calculation.

$$F_{12} = \sum_{i=1}^{6} G_{12}(i)\dot{z}(i) \quad (3)$$

$$F_{23} = \sum_{i=1}^{6} G_{23}(i)\dot{z}(i) \quad (4)$$

Constraint function could be introduced to limit the deflection of suspension in low bandwidth, see Equation 5.

$$d(i) = \max\left[abs\left(z(i) - z_b(i)\right)\right] \quad where\ i = 1, 2, \dots 6 \quad (5)$$

In this way, the knowledge of vehicle dynamic model is not required. The control is purely based on an optimal mathematic model. This control scheme also named as Model-based approach in [5] can be applied for other multi-objective control targets. Weighting factors need to be configured to reflect the importance of different control targets. An example is given in Equation 6:

$$\int (q_1 a_b^2 + q_2 x_{db}^2 + r F_b^2) dt \quad (6)$$

where, a_b, x_d and F_a are body acceleration, suspension deflection and actuator force respectively and the coefficients in front of the index are their weighting factors.

2.4.2.2 Full active control in low bandwidth (Hold-off-Device)

Hold-off-Device(HOD) is first proposed by Allen in [55]. It is a typical application of active control in low bandwidth. The target of this application is generating a force in the lateral direction to counteract the movement of the car body in curves so that the car body will be maintained in centring position and the contact of stiff bump stop will be avoided. As a result, the ride comfort will be improved, and bump stop clearance can be reduced to enhance the width of the car body. In another way around, with the current suspension deflection unchanged, HOD allows softer secondary spring which could mean a better ride comfort. Besides, the stability and overturning in the crosswind can also be improved as the centre of car body mass which is determined by car body motion will be restricted.
For the control strategy, the low-pass filters are used to process the lateral acceleration of bogie so that the track layout information will be extracted. The desired force to be generated by actuators can be calculated by the following Equation 7, where, $(z - z_t)$ is the suspension deflection.

$$F_a = -K_L \int (z - z_t) d_t \quad (7)$$

In paper [56] electro-hydraulic actuators are applied in the lateral direction. The product of lateral acceleration of bogie and half mass of car body is used to generate the reference force.

2.4.2.3 Semi-active control

Semi-active control should be compared with the above full-active control strategies. The idea of the sky-hook damper, H_∞ control, LQG control etc. can also be applied in a semi-active actuation system. The most frequently used strategies based on sky-hook damper are introduced as follows. The basic definition for the classic sky-hook control Equation 1 presents the ideal force with the assumption that one end of damping is connected to the sky rather than to the bogie as in reality. Two classic strategies are proposed: Two-state sky-hook control (also known as On-off sky-hook control) and Continuous (also known as linear control) sky-hook control.

(1) Two-state/On-off Sky-hook control

Two-state Sky-hook control is the most primary control strategy. The damper is only required to have two states: high damping state C_{max} and low damping state C_{min}. Low requirement for semi-active damper makes it easy to implement in real practice.

$$C_s = \begin{cases} C_{max} & \dot{x}_2\,(\,\dot{x}_2 - \dot{x}_1\,) \geq 0 \\ C_{min} & \dot{x}_2\,(\,\dot{x}_2 - \dot{x}_1\,) < 0 \end{cases} \quad (8)$$

Equation 8 presents the control method where C_s is the only controllable variable in semi-active control, determined by the sign of directions of car-body velocities ($\dot{x}_2$) and relative velocity of dampers ($\dot{x}_2 - \dot{x}_1$). Because dampers are connected between the bogie and car-body. The real sky-hook control force can be calculated through Equation 9.

$$F_{sky} = \begin{cases} -C_{max} \cdot (\,\dot{x}_2 - \dot{x}_1\,) & \dot{x}_2\,(\,\dot{x}_2 - \dot{x}_1\,) \geq 0 \\ -C_{min} \cdot (\,\dot{x}_2 - \dot{x}_1\,) & \dot{x}_2\,(\,\dot{x}_2 - \dot{x}_1\,) < 0 \end{cases} \quad (9)$$

(2) Continuous/ Linear Sky-hook Control

From the above equation, it is known that the damping force exerted is not the ideal force according to the definition of sky-hook control. Thus, the continuous Sky-hook control is consequently proposed, shown in Equation 10.

$$C_s{}' = \begin{cases} \min\left[C_{max} \cdot \frac{\dot{x}_2}{(\dot{x}_2 - \dot{x}_1)}, C_{max}\right] & \dot{x}_2\,(\,\dot{x}_2 - \dot{x}_1\,) \geq 0 \\ \max\left[C_{min} \cdot \frac{\dot{x}_2}{(\dot{x}_2 - \dot{x}_1)}, C_{min}\right] & \dot{x}_2\,(\,\dot{x}_2 - \dot{x}_1\,) < 0 \end{cases} \quad (10)$$

Compared with Equation 8 the damping changes continuously with measured velocities from car-body and bogie. This control law means a higher requirement for adjustable damping technologies and also another controller for the damper to generate the desired force timely and accurately.

The poor effect of Sky-hook control in high frequency excites the refining work for the classic sky-hook damper. Acceleration-Driven-Damper (ADD) is introduced by Savaresi in [57] to improve the damping effect in high-frequency range and later a mixed sky-hook and ADD control strategy is proposed to take advantages of the two controls and provide good effects over a wider frequency range in [58]. A bogie -based Sky-hook control is compared with classic car-body based Sky-hook by Hudha in [59]. The simulation results of a 17 DOF dynamic model show that the bogie-based control can better attenuate the vibration in terms of lateral, roll and yaw motion. LQG control law is applied by Wang in [60] and [61] where MR damper is used to reduce the vibration in lateral, yaw and roll directions. Three working modes of semi-active control (passive-off, passive on and semi-active) are investigated and the semi-active suspension is proved to be fail-safe. Zhong investigated H_∞ as system controller and Adaptive Neuro-Fuzzy Interference System (ANFIS) inverse control as MR damper controller. The lateral, yaw and roll acceleration can be reduced by 30% according to the simulation results in [62].

2.4.3 Implementation of active secondary suspension

2.4.3.1 Implementation of Active secondary suspension in lateral direction

In the early 1980s, British Rail Research carried out theoretical and a series of experimental studies for active suspension [63]. The assessment methods for ride comfort and limitation of passive suspension were thoroughly analysed. The experiment tests for both vertical and lateral active suspension with different actuator technologies were undertaken. In the vertical direction, electromagnetic actuators were mounted on Mark III coach with BT10 bogie in parallel with vertical air-spring. An alternative was an air pump actuator which can vary the pressure and volume of air spring by an electric motor. According to the measured acceleration, around 50% vibration reduction can be achieved at 1-2Hz. For the lateral active control, servo-hydraulic actuators were placed in parallel with air-spring using modal control of lateral and yaw, and vibration from 0.5-2Hz is significantly eliminated. Electromechanical actuators were also involved in the field test for lateral active suspension and had been proved fail-safe when a failure of control system happens.

In the 1990s, Fiat Pendolino implemented HOD function through pneumatic actuators in addition to tilting technology in operation. But in later stage, the centring function is realized by tilting devices and actuators are removed [28].

In mid 1990s, Siemens in Austria carried out field tests on prototype vehicle where tilting, lateral centring, lateral and vertical semi-active technologies were put together [64]–[66].The integrated active control strategy improved overall dynamic performance including reduced lateral acceleration of bogie and constrained lateral displacement of the car body on curves.

KTH and Bombardier Transportation in Sweden explored and developed active suspension in the program Green Train since 2005 [67]. Active lateral suspension and active vertical suspension were implemented on Regina 250 and tested in field railway from 2007 to 2013 [30], [53], [56]. HOD is included in suspension to centre the car-body in curves. Sky-hook control and the more advanced H_∞ control were explored. It proves that both control strategies have similar performance in terms of car body lateral acceleration, but H_∞ can yield lower car body displacement compared with Sky-hook control.

In recent years, Korea Railroad Research Institute (KRRI) carried out roller rig tests and field tests for active lateral suspension [68]. Electromagnetic actuators were investigated, and Sky-hook control law was applied in these experiments. Both urban vehicle and intercity vehicle were tested on roller rig tests. The lateral accelerations can be reduced by 12dB for both types of vehicle at the peak frequency. In the field tests, only the inter-city vehicle was involved, where the active lateral suspension was implemented in the mid passenger car of a five-car train set. The field tests are in good agreement with the rig tests. Besides, a fail-safe control scheme was proposed and implemented in the field test. The control commands for active suspension will be weakened (60%) or deactivated when the vehicle speed and temperature signals beyond the “yellow” and “red” limits. Redundant sensors were also implemented to achieve the fail-safe target as is presented in Figure 19.

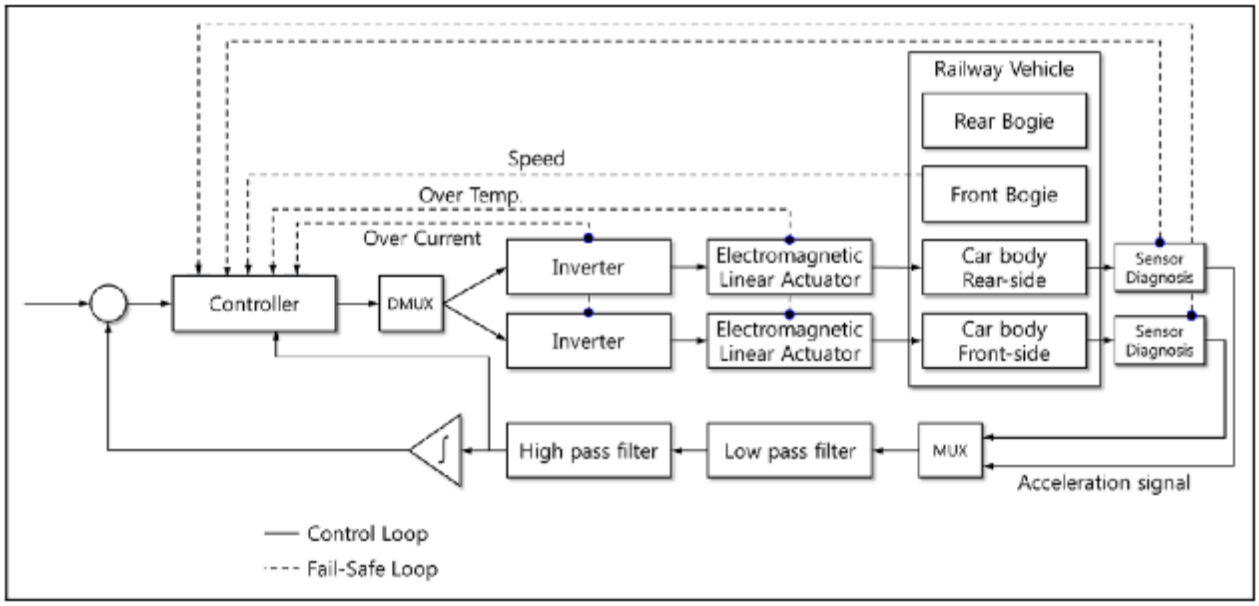

Figure 19 - Fail-safe control scheme for active lateral suspension system [68]

Japan started the research for active suspension in the 1980s and has launched the first commercial train with fully active suspension in 2001. In the first phase at the beginning of the 1980s, the old Japanese National Railways (JNR) tested lateral active suspension with pneumatic actuators which reduced 50% of vibration at 120km/h [69]. After the privatization of JNR, the JR-East in 1991 made field tests on Series 400 EC train where pneumatic actuators and H_∞ control was adopted for full active suspension in lateral direction and maximum testing speed up to 240km/h. In 1993, a new field test on Star 21 with maximum speed 425km/h was carried out. Both tests validated the similar effects that 50% or more lateral vibration can be reduced by active suspension. At the same time, JR West installed lateral pneumatic actuators in the test train WIN 350 and prototype of Series 500 EC [70] (see Figure 20). Hitachi tested an active suspension with hydraulic actuators on WIN 350. Kawasaki Heavy Industries made field tests on test Train 300X also with hydraulic active suspension based on $\boldsymbol{H}_\infty$ control law. Above contents are the major field tests before the real implementation of active suspension. Some other research about rig test and investigation for $\boldsymbol{H}_\infty$ control in the same period can be referred to in Paper [41], [71].

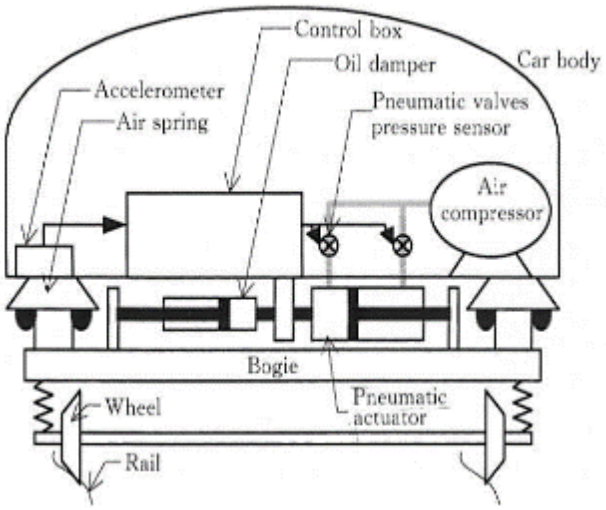

Figure 20 - Prototype of Series 500 EC [70]

In 2001, the operation of Series E2 and E3 Shinkansen trains started the commercial use of fully active suspension. In these vehicles, pneumatic actuators are implemented on the end cars and the green car (first class car), and semi-active suspensions are installed in all cars [28]. $\boldsymbol{H}_\infty$ control law is adopted to eliminate the yaw and roll car-body vibration. After that, the fully active suspension is further explored and developed in the project Fastech 360, aimed at developing higher speed train. The test train 360S and 360Z installed higher bandwidth electro-magnetic actuators [72]. More advanced technologies for fully active in Series E5 and E6 has applied electro-mechanical actuators in all cars in 2011 and 2013 [73].

2.4.3.2 Implementation of Active secondary suspension in vertical direction

As previously shown the application of active control can improve the dynamic response of a railway vehicle in terms of passengers' comfort. Different types of control strategies and actuator technologies can be applied. Nevertheless, in terms of real-world implementations, few solutions are tested concerning active control.

Extensive tests on a 1:6 scaled Shinkansen vehicle are done by Kamada et. al. in [42]–[44]. In his studies, the control strategy applied is a robust H_∞ modal control. The 1:6 scaled experimental set-up is shown in Figure 21.

Figure 21 - Experimental Set-up in [42] – [44]

In [42], 5 modes are considered: two rigid modes and three elastic modes. A weighting function for disturbance suppression (W_s) is chosen separately for each considered mode. A combination of linear and stack piezoelectric actuators are used. 20 piezoelectric actuators are used. The tasks are split between the two different actuators types. Linear actuators are used to control the first two rigid modes while the piezoelectric ones are used to suppress the three elastic ones. Satisfactory experimental results are obtained when the combination of linear and piezoelectric actuators is used. Subsequently in [43] the usage of pneumatic actuators in parallel with the air spring is considered. due to the reduction of the number of actuators used the controllable modes considered are the first two rigid and the first elastic bending ones. Despite rigid body modes are effectively suppressed, the control performance become worse near the elastic vibration modes due to the non-linearity of the electric-pneumatic valve. Lastly in [44], air suspensions are directly used to control the first and second rigid modes and the first bending mode. The air spring is controlled by pressure control and accelerometers are placed at the edges and the centre of the 1:6 scaled vehicle. Here, the weighting function for disturbance suppression (W_s) of each considered mode are summed with the other to give the final weighting function. In this way a modal separation is kept without applying a proper on-line modal decomposition. Satisfactory results are obtained for the scaled vehicle and for a simulated full-size vehicle but here a careful model of the pressure valve should be considered.

Experimental results are shown on a full-size vehicle Shinkansen laboratory vehicle by Sugahara et. al. in [31]. Here, a combination of variable axle dampers and air-springs with a build-in orifice control valve is applied. A view of the experimental test components is given in Figure 22.

Figure 22 - Test Plant (left), Air spring (centre) and axle damper (right) [31]

The axle dampers are used to control the first bending mode while air springs to control bounce and pitch. A comparison between Sky-hook and LQG control logics is made showing that LQG gives rise to a more precise result while Sky-hook acts on a wider frequency range. This is partially caused by the sensitivity of LQG control logic to unmodeled dynamics. An improvement of 3.6 dB in ride quality is reported during experiments compared to the expected 4.7 dB.
On-track tests are carried out by Qazizadeh et. al. in [29] and [30]. Here, secondary lateral and vertical dampers are replaced by electro-hydraulic actuators on the high-speed train Regina 250. A view of the actuator replacement is given in Figure 23.

Figure 23 - Actuator replacement in Regina 250 [29], [30]

A modal sky-hook approach is used on a two car-body train in which one car mounts conventional suspension and the other mounts the active devises. Accelerations are taken on the car-bodies above the secondary suspensions. The measurements are performed at speeds up to 200 km/h, showing 44% reduction of weighted acceleration compared to the passive reference car.

2.4.3.3 Implementation of Semi-active secondary suspension

In the early 1990s, UK started an initial exploration of semi-active suspension on a rig test at the GEC-Alsthom Engineering Research Centre [74], aimed at studying the potential of semi-active damper in secondary lateral position. In the experimental work, a simplified scale rig test was applied where an electrohydraulic actuator produced excitation to simulate the bogie vibration. The damper and stiffness were achieved by external pipework and solenoid valve enabling high and low damping rates. A unique two-state control strategy was proposed based on a solo velocity of the car-body and a limit value was optimised as judgment for high or low damping rate. The switch damper scheme can produce more than 25% improvement of ride index (according to EN12299 [24]).

In the middle of 1990s, on-track tests were made in Sweden of secondary lateral semi-active suspension on X2000 train set [75]. A control strategy based on sky-hook was applied to attenuate the lateral and yaw motion of the car-body. A mixed hydraulic and electromagnetic actuator was created to enable continuously variable damping rates. In the field test, semi-active devices were mounted on the driving trailer car at the end of the train set. The R.M.S values of lateral acceleration decreased by 30% from 0.8 - 2 Hz but increased below 0.8 Hz.

At around the same time, Siemens carried out field tests for semi-active suspension in Austria [64]–[66]. Two lateral and two vertical hydraulic dampers with continuously adjustable damping valves were mounted in addition to the electromechanical tilting and pneumatic lateral positioning devices on the prototype bogie SF 600. The ideal damping force was calculated based on Sky-hook control and method of “lookup table” was used to produce demanded current signals. Field Measurements show that the ride quality can be improved by 15% in terms of RMS acceleration.

Korea carried out the studies for semi-active suspensions through rig tests and field tests in the last decade [76]–[80]. Yu-Jeong Shin used 1:5 scaled (see Figure 24) [76]–[78] and full-scale [78] roller rig test to study the effects of semi-active lateral suspension with magnetorheological damper at different speed ranges. The classic Sky-hook control and H_∞ control in a later stage were applied to suppress the vibration. After that, an experiment for ride quality was undertaken on field tests [80]. The semi-active MR damper with Sky-hook control scheme provides 29% improvement compared with the passive system.

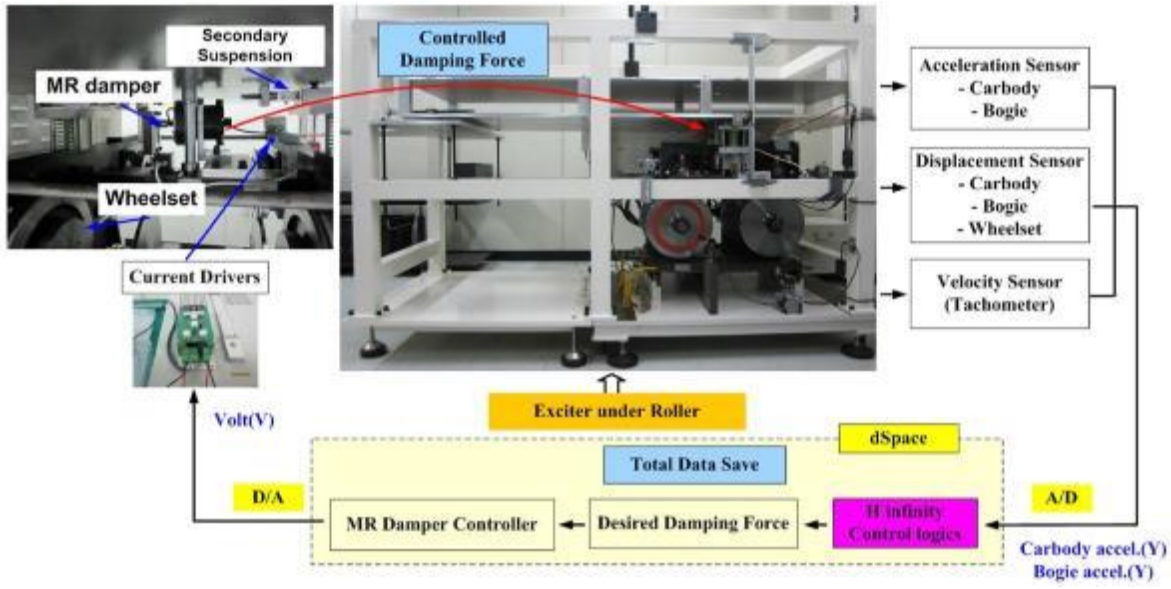

Figure 24 - Measurements and control loop for 1:5 scale roller rig test [77]

Japan started the exploration on semi-active suspension technologies in the early 1990s and has applied the technologies into commercial use since the end of 1990s. All the semi-active dampers are focused on the lateral direction [70].

In 1994, JR-West used test train WIN350 to explore the performance of semi-active suspension where 6-stage variable dampers were implemented, and control was based on sky-hook control law. Field tests illustrate that 30% vibration at a speed of 300km/h can be reduced by implementing semi-active suspension. Figure 25 gives a set-up of semi-active lateral suspension for test train WIN350. After that, the Series 500 Shinkansen EC trains got this technology which enables ride quality in 300 km/h being equal to the one at 270km/h without semi-active suspension.

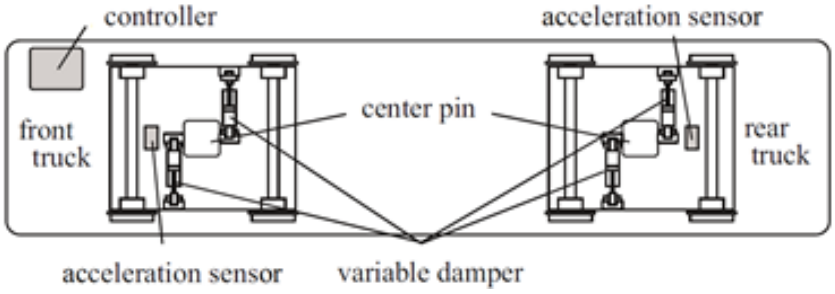

Figure 25 - Set-up of the semi-active system used for test train WIN350 [69]

JR-Central installed semi-active suspension on Series 300 EC in 1994 for field tests. The control and variable dampers were similar to the ones of JR-West. The semi-active suspension can reduce the lateral vibration by 4dB of riding quality level L_T measured in the position of rear-end car. The

control scheme was improved by introducing delay compensator and a bandpass filter to achieve a larger controllable frequency range. Series 700 Shinkansen EC trains installed this system and started the operation since 1999.

2.5 ACTIVE PRIMARY SUSPENSION

2.5.1 Principles and configuration for active primary suspension

For conventional vehicles with passive suspension system, the compromise between stability and curve negotiation behaviour has to be made even if steering mechanisms have been proposed [81]. In contrast controlling wheelset kinematics by applying active suspension can provide flexible solutions to ensure the stability and curving behaviours simultaneously [1],[2]. The implementation of active primary suspension is expected to produce greater monetary benefits than active secondary suspension due to its relation to the wheel-rail contact, which is the major contributor to maintenance costs, especially for the track.

The wheelsets can be generally classified into two types according to the mechanical structures of wheelsets: Solid-axle wheelsets and Independently Rotating Wheels (IRW). For each solid-axle wheelset, two wheels mounted rigidly on one axle have the same rotating speed. Consequently, longitudinal creepage is produced and it enables the ability of guidance and self-centring, but meanwhile it causes instability and unwanted wear of rail and wheel. By contrast, for independently-rotating wheels, two unconstrained wheels will lose guidance and self-centring ability and increase risk of flange contact and derailment. In general, ‘stability’ and ‘curving’ should be considered in the study of active primary suspension for solid-axle wheelset, and ‘guidance’ is added for independently-rotating wheels.

Because of the natural difference between solid-axle wheelset and independently-rotating wheels described above, it is intuitive to split the active primary suspension into two parts, one for solid-axle wheelset, the other for independently-rotating wheels. The mechanical structures and control strategies could be correspondingly different between these two parts. All five configurations [4] [82] of active primary suspension schemes are gathered in Figure 26, where configurations (a) and (b) are for solid-axle wheelset, configurations (c), (d) and (e) are for independently-rotating wheels), which will be explained further in following parts.

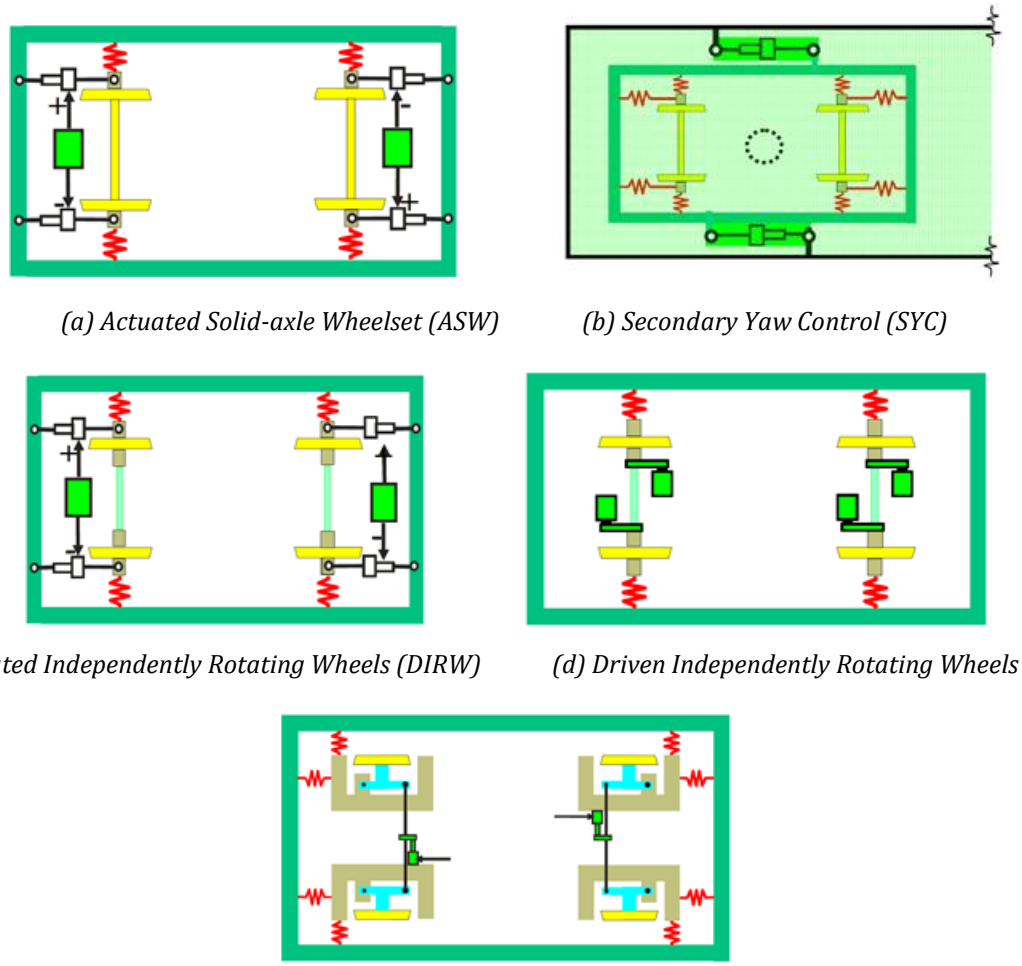

(a) Actuated Solid-axle Wheelset (ASW) *(b) Secondary Yaw Control (SYC)*

(c) Actuated Independently Rotating Wheels (DIRW) *(d) Driven Independently Rotating Wheels (AIRW)*

(e) Directly Steered Wheels (DSW)

Figure 26 - Five configurations for active primary suspension

2.5.2 Solid-axle wheelsets

2.5.2.1 Actuated Solid-axle wheelset (ASW)

(1) General concepts and mechanical configurations

Applying yaw actuations and lateral actuations are two general solutions of kinematic control of wheelset to improve the steering and stability [3]. While from the perspective of mechanical configurations, three schemes are introduced. Yaw torque on wheelset could be applied directly by one yaw actuator mounted between bogie and wheelset as shown in Figure 27(a) or in a more practical way of utilizing two actuators in the longitudinal direction at ends of the wheelset, as indicated in Figure 27(b). Lateral actuation, as its name suggests, is achieved by two lateral actuators (see Figure 27(c)), which can enhance both the stability and curving performance. Comparison between yaw actuation and lateral actuation was carried out based on a simplified

two-axle vehicle model [83]. It is shown that the lateral actuation requires a larger force to achieve the same stability of the vehicle than with the yaw actuator. Moreover, the lateral schemes risk deterioration of ride quality.

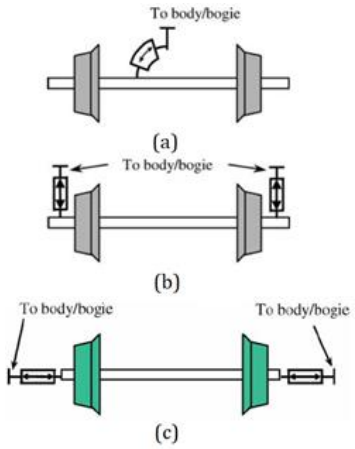

Figure 27 - Mechanical schemes for solid-axle wheelsets

(2) Combination of actuation and passive spring

The combined passive primary spring can significantly affect the effectiveness of steering and stability performance, as well as the control strategies and specification (such as required maximum force, power) for the actuation technologies. If primary spring is remained in parallel with yaw actuators in the longitudinal direction to ensure the stability of the vehicle, a higher force is required for the actuator to cancel out the action of the passive spring on curves. However, keeping passive suspension is still an efficient approach to guarantee fault tolerance of the actuation system which is a crucial issue for the implementation of active primary suspension. One classical active primary architecture named 'yaw relaxation' was proposed by Shen et. al. in [84], in which spring is arranged in series with the actuator, working as traction rod, shown in Figure 28. On the tangent track, the stability is ensured by the passive spring and actuation system working in low bandwidth frequency range (usually below 1Hz). On curves, the 'traction rod' works in active mode to steer the wheelset with low forces. Detailed descriptions about the control strategies are presented in the later section 2.5.2.3.

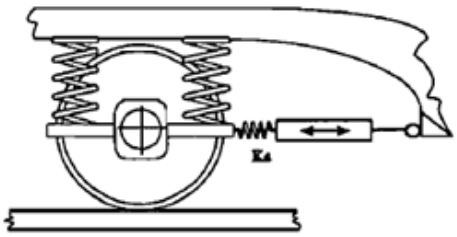

Figure 28 - Yaw relaxation scheme [84]

2.5.2.2 Secondary Yaw Control (SYC)

Secondary yaw control was proposed by Diana firstly in order to improve stability in tangent track and curving performance of a tilting train in [85] and [86]. Yaw torque from car-body to bogie is produced by two longitudinal electro-mechanical actuators in the position where the original passive yaw damper is mounted. The schematic scheme is shown in Figure 29. The SYC can enhance the vehicle critical speed and reduce track shift force. Although it is reasonable as well to classify the SYC into active secondary suspension, it is introduced here as the function of SYC is providing stability and steering instead of improving ride quality, similar to the typical active primary suspension.

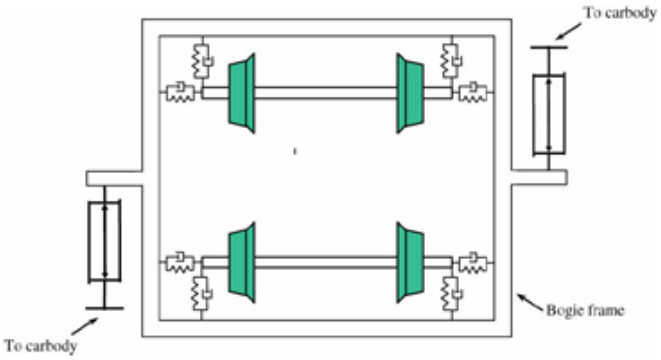

Figure 29 - Secondary Yaw Control (SYC)

Based on the concept of SYC, a new active suspension Actuated Yaw-Force Steered (AY-FS) is proposed by Simson in [87]–[89] in the background of heavy hauling locomotives. In this concept, force steering linkage is added on the SYC. This concept can be considered as the combination of SYC and passive steering linkages which can force the wheelset into ideal position according to the geometrical relationship among the bogie, the car body and the linkages, as is presented in Figure 30. It can significantly improve the curving behaviours with traction force.

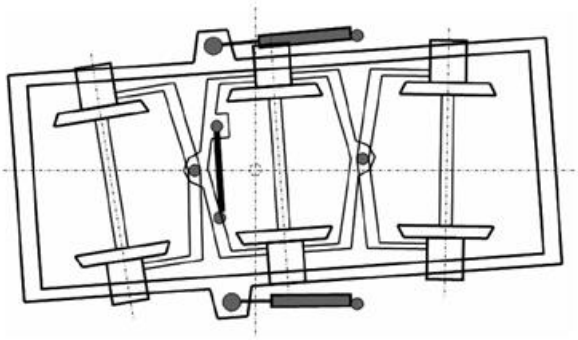

Figure 30 - Actuated yaw force steered bogie (AY-FS)

2.5.2.3 Control strategies for Steering and Stability

(1) Steering Control

The fundamental objective of implementing active primary suspension is improving curving behaviour. Wear number/wear index and equality of track shift force among different wheelsets are often used as two indicators to evaluate curving behaviour. The general principles of steering on curves can be divided into three categories which are present as follows.

(1.a) Radial Control (imperfect control)

The idea of radial control is to make each wheelset to take a radial alignment position. In other words, the attack angle of wheelset should be controlled to be zero on curves. Based on this concept, the schemes of steering bogie by means of utilizing passive linkages or coupling of wheelsets in the same bogie have been proposed in [81] and [90]. But this control concept produces perfect curving behaviour at the only condition that cant deficiency is zero which seldom take places in the real operation service. A non-zero angle of attack is needed to provide lateral creepage force to balance the un-compensated lateral force in normal cases.

(1.b) Perfect Steering control based on creepage force

The definition of perfect steering from Goodall and Mei [5] is described that the longitudinal creepage forces on wheels on the same axle should be equal or be zero if no traction or braking force is applied. At the same time, the equal lateral creepage force on each wheelset should be achieved. However, in operational service, there is no economic and accurate approach to measure the creepage force. Therefore, some equivalent indicators that can be formulated from ideal steering conditions are proposed in the real case, which is explained from (1.b.1) to (1.b.4).

(1.b.1) Control strategy based on lateral position of wheelset as control target [91], [92]

Zero longitudinal force (without traction and braking force) and equal lateral force mean pure rolling of each wheel. Yaw actuation system can apply a yaw torque to control the lateral position of the wheelset to achieve the pure rolling. The schematic strategy is presented in Figure 31.

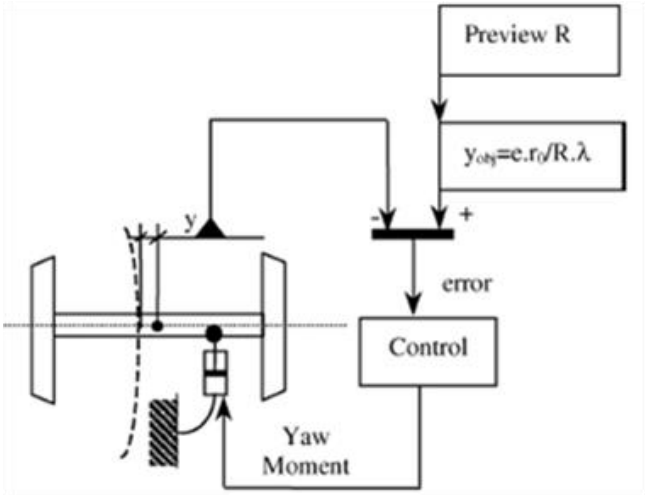

Figure 31 - Control strategy based on lateral position of wheelset as control target

The ideal lateral displacement of the wheelset can be calculated as follows:

$$\mathbf{y} = \frac{\mathbf{er_0}}{\boldsymbol{\lambda}\mathbf{R}} \quad \textbf{(11)}$$

where e is the half track clearance; r_0 is the rolling radius, λ is the wheel conicity, and R is the curve radius. Therefore, the measured signals required for this concept include wheel conicity, curve radius and difficult measured lateral displacements of the wheelset.

(1.b.2) Control strategy based on yaw moment applied from primary suspension

This control strategy known as Yaw Relaxation is first proposed by Shen and Goodall in [84] and some followed studies were carried out by J. Perez and S. Shen in [91] and [92] respectively.
The force applied to the wheelset can be divided into two parts: the force from wheel-rail contact, and the force transmitted from the bogie. The two opposite creepage forces applied on two wheels exert yaw torque and in the ideal steering condition this torque should be zero. If the inertia force of wheelset is neglected, the yaw torque on wheelset from bogie should be reduced to zero, which become the control target in this strategy. Measurement for this yaw torque could be realized by the longitudinal force applied on the axle box, i.e. the sum of longitudinal force at traction rod/longitudinal actuator and the force on primary suspension (like passive springs above the axle-box). In the real case, the former force could be measured from the actuation system and the latter one could be obtained by measuring the deflection of springs and the knowledge of stiffness characteristics. While the measurement error could be introduced in this part as stiffness could vary at different load cases. Shen also pointed out that this control strategy could be refined if a pair of wheelsets are taken into account instead of a wheelset alone [84]. The frequency range of the actuation system should be below the natural frequency of hunting motion to avoid the possible instability caused by dynamics of the actuation system.

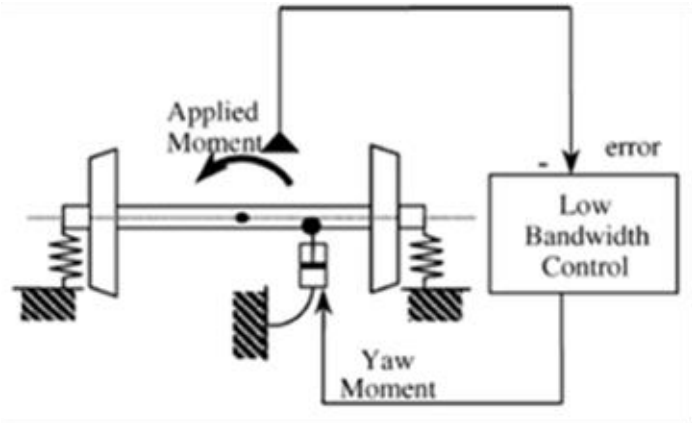

Figure 32 - Control strategy based on yaw moment applied from primary suspension

The knowledge required for this concept includes actuator forces and the longitudinal forces from passive springs (stiffness and deflection of spring).

(1.b.3) Control strategy based on ideal angle of attack

Equal ideal angle of attack for each wheelset is another indicator to achieve the equal lateral contact force of wheelsets [92]. The ideal angle for each wheelset is determined by track data (curvature and super-elevation), cant deficiency (vehicle speed) and creep coefficient. Feedforward control could be implemented to simplify the control design and avoid instability of the system. This control strategy can involve many inaccurate factors such as creep coefficient. The effectiveness of the longitudinal actuator could also be influenced by the stiffness of primary suspension. Therefore, the application of feedback control will improve the effectiveness of steering significantly.

(1.b.4) Control strategy based on same position/movement of wheelsets

In this control strategy, the specific ideal angle of attack or ideal lateral displacement is not needed. Instead, the zero difference of the angle of attack, lateral displacement of wheelsets will be used as a control target. The force or deflection of primary suspension in lateral and longitudinal directions will be measured as indicators to eliminate the difference of wheelsets motions.

In summary, aiming at perfect steering control, the four strategies are based on the same principle about creepage forces. In the ideal condition that all the parameters can be accurately measured, the four control strategies can all provide perfect steering effect. While if the real sensor and uncertainty of measurement are considered, the steering effect of these control strategies could be deteriorated and present different characteristics. Table 1 compares the difference among the above control schemes.

Table 1 - Comparison of different schemes for Perfect Steering Control

ID.	Control target	Measurement
1.b.1	Ideal lateral displacement	wheel conicity, curve radius, lateral displacement of wheelset
1.b.2	Zero yaw moment applied from primary suspension	actuator force in longitudinal direction, longitudinal force of passive spring (stiffness and deflection of spring)
1.b.3	Ideal angle of attack	curve radius, cant deficiency, creep coefficient, angle of attack
1.b.4	Equal lateral displacement and angle of attack	Lateral and longitudinal force or deflection of primary suspension

(1.c) Ideal steering control in hauling locomotives coupler force

Despite that perfect steering principle described in (1.b) is generally accepted, Simson and Cole modified this principle as 'Modified perfect locomotive steering' and proposed a new principle named 'Ideal locomotive steering' to make steering strategies more suitable in the background of hauling locomotives [87]. The general idea is briefly introduced as follows.

Firstly, the perfect steering principle cannot be achieved in hauling locomotives. It is difficult to keep the heavy haul train at a constant speed on curves because of the running resistance of the heavy train [87]. The high longitudinal train forces will cause lateral forces on couplers and consequently introducing yaw moment on locomotives which cannot be balanced if equal longitudinal and lateral contact force on each wheelset are achieved in the definition of perfect steering in (1.b).

Therefore, the modified definition of perfect steering is proposed that the lateral creepage force of wheels on the same bogie should be equal but the lateral creep forces on leading bogie and rear bogies are different to cancel out the yaw moments of coupler forces. The longitudinal creep forces should be equal on each wheelset. Besides, the definition of ideal locomotive steering under traction condition is presented where longitudinal creep forces of wheels could be different but the direction should be the same as traction force. The lateral wheel contact forces, lateral creepage forces and angle of attack of wheelset on the same bogie should be equal.

(1.d) Other Controls

For SYC, reducing/equalizing track shift forces of the two axles on the same bogie is the major control target. When the vehicle passes a specific curve radius with a particular non-compensated acceleration, the referenced forces actuators will be obtained from a lookup table conducted by a vast number of simulations considering different running sceneries.

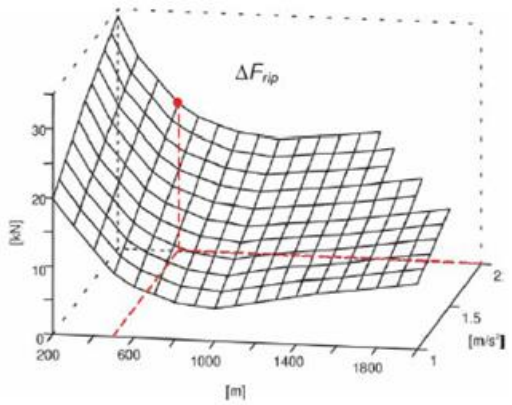

Figure 33 - Lookup table for calculating actuation force

For AY-FS, the yaw angle of bogie in the first control strategy based on knowledge of the track curvature and the calculation method is presented in the study. With a known target yaw angle, the difference between measured yaw angle and target angle will be input signal and produced by the

PID controller to introduce desired yaw torque on the bogie. The second control strategy is based on ideal control which has been described in the control principle in (1.c)

(2) Stability Control

The self-excited oscillation of solid-axle wheelset introduces instability of the vehicle system. Achieving stabilization is the primary interest of active primary suspension apart from steering. Yaw angle of the wheelset, lateral velocity of wheelset and yaw angular velocity of wheelset are three indicators to reflect the instability of wheelset and based on these indicators, three control strategies are proposed to stabilize the kinematic modes of the wheelset.

Active lateral damping and active yaw damping are two similar control strategies. The former one applies lateral forces that are proportional to the yaw velocity of the wheelset, while the latter one introduces yaw torques that are proportional to the lateral velocity of the wheelset. The stabilization effects of these two control strategies are theoretically verified in [3] based on a model of two-axle vehicle. The active yaw damping is preferable to active lateral damper as it requires lower actuation force and can produce better ride quality [83]. The active yaw damping effect is validated by experimental test by Pearson et. al. in [93].

The third stability control strategy is named as 'Sky-hook spring' (also known as 'Absolute yaw stiffness') is inspired by the ineffectiveness of passive yaw stiffness in [36] and [94]. In passive primary suspension, springs will produce yaw force that is proportional to the relative motion between bogie and wheelset. But ideal yaw force should be proportional to the absolute yaw motion of wheelset. Increasing stiffness of spring can enhance the effect of yaw force and thereby the stability will be improved. But the effect will still be deteriorated by the motion of bogie. In order to solve this ineffectiveness, 'Sky-hook spring' is proposed where the yaw motion of wheelset is measured with respect to an ideal sky-hook. The yaw force acting on wheelset is proportional to the measured absolute yaw angle of wheelset with a high-pass filter to remove the low frequency signal related to curving [94]. Table 2 presents the above three control strategies.

Table 2 - Comparison of three control strategies for stability

Control strategy name	Input/measurement	Output	Note
Active lateral damping	Yaw angular velocity of the wheelset	Lateral force proportional to input signal	
Active yaw damping	Lateral velocity of the wheelset	Yaw torque proportional to input signal	
Sky-hook spring/ Absolute stiffness	Absolute yaw angle of wheelset	Yaw force proportional to input signal	The yaw angle could be measured and processed from yaw accelerometer

For SYC, the stabilization of the vehicle is achieved by two longitudinal actuators worked as the more efficient secondary yaw damper. The referenced forces of actuators can be calculated as follows, which are in the opposite sign of the relative speed (v_{rel}) between bogie and car-body in longitudinal direction. c_v is a gain like viscous damping. The delays from sensors and action of the actuator is considered by introducing term $m_v a_x$.

$$\boldsymbol{F_{ref} = -(c_v v_{rel} + m_v a_x)} \quad \textbf{(12)}$$

For AY-FS, the yaw angle of bogie can be measured by the yaw actuators and ideal yaw angle of bogie is calculated based on the knowledge of track curvature. The misalignment yaw angle of the bogie from measured value to ideal value is input signal and control force is produced by PID control.

2.5.3 Independently Rotating Wheels

In order to overcome the well-known trade off problem between running safety and curving performance in conventional solid-axle axle wheelsets, Independently Rotating Wheels (IRW) were introduced. This configuration provides a drastic change in the wheelset configuration allowing the wheels on the same axle to independently rotate with respect to each other. In this way the dependency between the yaw and lateral movement of the wheelset is removed, allowing the possibility of virtually eliminating the longitudinal creep force at the wheel-rail interface. Thus, pure rolling is no more dependent on the lateral position of the wheelset. This significantly reduces the wear and removes the hunting motion (Goodall et. al. [95] and Pérez et. al. [96]). Additionally, if the usage of two-axle railway vehicles is considered together with IRWs, as described by Kurzeck et. al. in [97] for the “Next Generation Train” (NGT) project, a double-deck trainset configuration with continuous floors on both levels is possible. One of the first applications of IRW was presented in 1941 by Talgo in which passive steering capability is achieved by special linkages between wheels (Carballeira et. al. in [98]). The first Talgo solution is shown in Figure 34. IRWs are also applied to low speed applications such as tramways (Meyer in [99]).

Figure 34 - Talgo solution of 1941 [98]

Nevertheless, some drawbacks are generated when the constraint between the wheels is removed. In fact, the absence of coupling between the wheels leads to the loss of the self-guidance ability (Perez et. al. [96] and Goodall et. al. [95]) that will eventually lead to flange contact. It is farther demonstrated by Goodall et. al. in [95] through the usage of a linearized model of a two-axle vehicle that dynamic instability is still present for the IRWs configuration. Moreover, the longitudinal creep force on the wheel-rail interface can't be considered completely negligible and they can still affect the stability of the wheelset (Cho et. al. [100] and Sugiyama et. al. [101]). Active solutions on Independently Rotating Wheels (shortly named IRW) are first introduced by Mei et.al. in [3] and [102]. The absence of self-guidance capability and the risk for dynamic instability will lead to poor ride, noise and wear, and must be taken care of, either by passive solutions as applied by Talgo or by active control. This aspect is clearly pointed out in the literature by Mei et. al. in [102], Goodall et. al. in [95] and Gretzschel et. al. in [103].

In order to achieve guidance and stability, different types of mechatronic configurations of the IRW can be used. As defined by Bruni et. al. in [4] and [82] and subsequently adopted as definitions, it is possible to divide the active secondary suspension related to the IRWs in three main categories. Actuated Independently Rotating Wheels (AIRW), introduced by Mei et. al. in [102], Driven Independently Rotating Wheels (DIRW), introduced by Gretzschel et. al. in [103] and Directly Steered Wheels (DSW), introduced by Aknin et. al. in [104]. These concepts will be discussed in the subsections 2.5.3.1, 2.5.3.2 and 2.5.3.3 respectively.

Despite that active control seems to provide superior solutions to fundamental issues for high speed applications of the IRWs some passive configurations are proposed. The most noticeable is the Spanish Talgo train in which a steering mechanism based on Watt's linkage allows correct passive steering on steady curves (Figure 35). In this case the train must be articulated, reducing the flexibility for vehicle configuration changes. It is shown by Baeza et. al. in [105] and [98] that the dependency of the dynamic behaviour of the system on the vehicle velocity is reduced with respect to conventional wheelset vehicles.

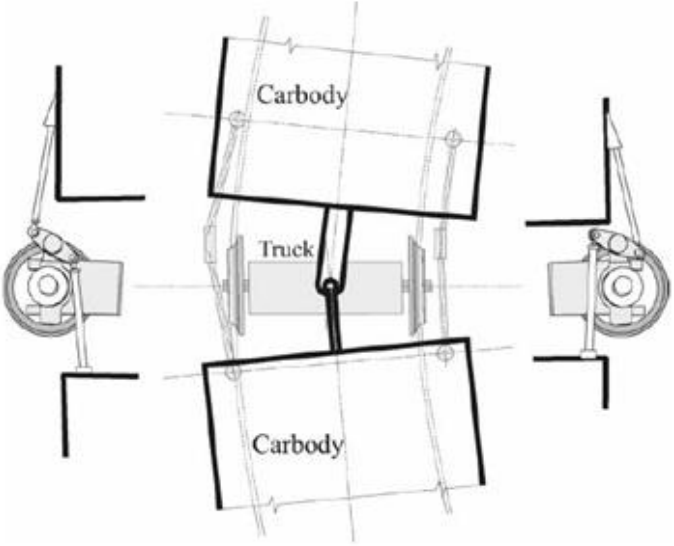

Figure 35 - Talgo's Steering Mechanism [105]

A Differential Coupling Wheelset (DCW) based on a clutch type slip differential (Figure 36) is proposed by Wu et. al. in [106]. This configuration can potentially solve the problem of both conventional solid-axle wheelsets and IRWs. In fact, its aim is to have a solid-axle wheelset like behaviour for tangent track and large radius curves when the clutch is closed and an IRWs like behaviour in very tight curves (curve radius less than 60 m) when the clutch is opened. A similar concept was previously introduced by Geuenich et. al. in [127], in which although the clutch was actively controlled.

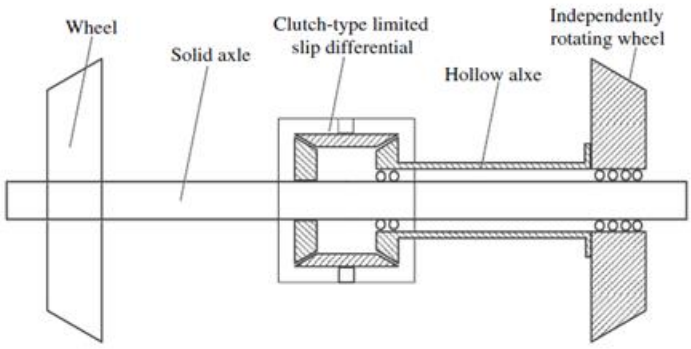

Figure 36 - Differential coupling wheelset [106]

An independently-rotating wheelset using inverse tread conicity (Figure 37) is proposed instead by Suda et. al. in [107]. The self-steering capability is achieved through a negative tread conicity that leads to a self-restoring yaw moment.

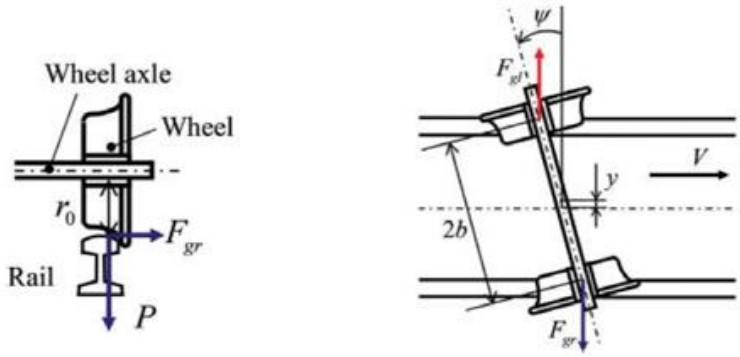

Figure 37 - IRW with Inverse tread [107]

The above-mentioned passive configurations can be solutions to the IRWs guidance and steering problems, but the superior performance that can be achieved by an active system favours the latter.

2.5.3.1 Actuated Independently Rotating Wheel (AIRW)

The concept of AIRWs (Figure 26(c)) is based on the possibility of controlling the yaw and lateral displacement of the common axle on which the independently-rotating wheels are mounted with an external actuator. This can be done even by the direct application of a torque to the axle (Goodall et. al. in [95], [108], [109] and Mei et. al. in [110]) or by generating it through the usage of a linear actuator (Pérez et. al. in [96], [111]). The example of Figure 15 shows this last possibility. Using a two-axle linear model, it is proved by Mei et. al. in [83] that the torque required to steer the AIRW is lower than the one required by a common solid-axle vehicle due to the absence of longitudinal passive suspension that restricts the yaw displacement. A combination of AIRW and DIRW is though presented by Perez et. al. in [111]. The control logics proposed during the years to solve the stability and guidance problems will be discussed in subsection 2.5.3.4.

2.5.3.2 Driven Independently Rotating wheel (DIRW)

The concept of DIRWs (Figure 26(d)) is based on the possibility of controlling the speed of the two wheels of one axle autonomously. This was done firstly by applying a differential torque provided by electric servomotors through a gearbox connecting the two wheels (Gretzschel et. al. in [103], [112]). More often, thanks to the advances in asynchronous induction motor control methods, an AC motor is assigned to each wheel. These are then used to provide traction, wheel guidance and stability control. The motors can be externally mounted and connected to the wheelset through a gearbox (Pérez et. al. in [111], Liang et. al. in [113], [114], Ahn et. al. in [115] and Lu et. al. in [116]) as shown in Figure 26(c) or embedded inside the wheels (Mei et. al. in [117], Ji et. al. in [118] and in the “Next Generation Train” project in [97], [119]–[121]). The absence of additional actuators leads to reduced space requirement, reduced cost and improved reliability makes the DIRW solution attractive and thus it is more studied in recent years. Due to the absence of additional

actuators, that leads to a reduction of the space required by the wheelset frame, and to the possibility to provide both traction and control within the same system, the DIRW solution is the most attractive and thus it is more studied in recent years.

2.5.3.3 Directly Steered Wheels (DSW)

The concept of DSW (Figure 26(e)) is based on the removal of the axle between the wheels and that the wheels are mounted on a separate frame connected by a steering rod. In this way the two wheels can be directly steered. An active action can be made applying a displacement to the steering rod (Aknin et. al. in [104] and Wickens in [122], [123]) as shown in Figure 6 or by controlling differential torque through hub-mounted traction motors (Powell in [124]). A configuration of DSW having self-steering capability is presented by Michitsuji et. al. in [125]. Despite being one of the most primitive ideas of IRWs it is also one of the most advanced and visionary. It is also shown by Wickens in [123] that the stability issue achieved through active control is less affected by friction and traction then with other types of active control. Nevertheless, this idea is one of the less studied.

2.5.3.4 Control strategies for guidance and steering

(a) Stability Control

For what concerns AIRW, a first approach to solve the stability problem was introduced by Goodall et. al. in [95] in which yaw damping is introduced actively in the system through a feedback of the difference between the wheelset and car-body yaw velocity. This choice was done partially by observing the necessity of the usage of realistic sensors to implement control logics. Moreover, in his studies Goodall introduces a proposal of the adaptation of the control effort based on the train speed (Goodall et. al. [95], [109]). Subsequently, Mei and Goodall in [108] developed an H_∞ control using μ-synthesis based on the same concept expressed above. This was done to overcome the problem of parameter variation, non-modelled actuator dynamics and the necessity of a simple model to describe the very complex model of a real train. In the work of Perez et. al. ([96], [111]) instead, the problem of stability is less evident because he considered a conventional bogie vehicle with longitudinal suspension.

On DIRW the first approach was introduced by Gretzschel et. al. in [103], [112]. Here the stability is obtained by feeding back the yaw velocity of the leading axle into a PID controller that sets the direction and the amount of torque to be produced by the steering motor through a gearbox that connects the two wheels on the same axle. Gretzschel combined simulation and experimental results based on a 1:5 scaled test rig that was scaled following the strategy proposed in [126]. Mei et. al. [117] use embedded permanent magnet synchronous motors in the wheels, to actively apply yaw stiffness through the differential torque generated by the two motors. This solution is high-pass filtered to influence only kinematic frequencies and not interfere with the guidance and curving action. Based on the same principle the stability action for this control is tested in a test rig and compared with simulation results by Liang and Iwnicki in [113], [114].

On the DSW configuration, stabilization is achieved by simply applying guidance control with a large stability margin with respect to the speed as shown by Wickens in [122], [123]. In [123],

Wickens compares stability limits of conventional passive vehicle, yaw relaxation control, ASW and DSW showing that only for the DSW configuration no stability limits are found for speed and equivalent conicity variation.

(b) Guidance and Steering Control

Two main approaches are introduced for the guidance problem concerning the AIRW configuration. The first approach is proposed by Goodall et. al. in [95], [109] and it is based on the fundamental concept that for a conventional wheelset the two wheels rotate at the same speed. Thus, the external actuator will steer the IRW wheelset such that the speed difference of the two wheels is set to zero. In this way a solid-like wheelset behaviour will be achieved. The problem of adaptation is introduced too. As mentioned for the stability part, an H_∞ control using μ-synthesis is subsequently developed in [108]. The second approach is proposed by Pérez et. al. in [96], [111]. To avoid flange contact he proposes a feedback approach on the lateral clearance that sets this to zero. Because of the impracticality of measuring the lateral displacement of the wheelset with respect to the centre line, in his work Pérez derives a reference signal for the wheel speed difference based on the curvature of the track and the velocity of the train. The reference value is obtained from the dynamic equations that describe the system. The wheels speed difference is found to be related to the rest of the variables by a first order transfer function with low time constant that allows to neglect this contribution in the frequency range of the guidance control. The relation in then further simplified by considering the quasi-static condition during curving.

As mentioned in subsection 2.5.2.2, for DIRW more research has been carried out especially concerning guidance. By using an experimental regression model that correlates the difference in the rotational speed of the wheels and their lateral deviation, a PID control based on the minimization of the creepage forces through the measurements of lateral displacement and yaw angle of the wheelset is proposed by Gretzschel et. al. in [103], [112]. The control is successfully tested on a 1:5 scaled test rig. By a combination of AIRW and DIRW concepts, Perez et. al. in [111] provide steering with the AIRW concept and guidance with the DIRW concept. For the guidance part a traction control is applied to maintain the differential traction torque equal to zero. In his work Pérez firstly introduces the dynamic model of the synchronous motor through the separation method of field and armature windings equations. This method is generally used to control synchronous machines and it allows to represent the rotating voltage and current vector into two separate equations representing the imaginary and real parts of them through simpler windings equations. The control is then designed considering the field current constant. Within the “Next Generation Train” project, a PD control is used by Kurzeck et. al. in [119] to set the lateral displacement of the IRW wheelset to zero through the differential torque control of the two motorized wheels. In his study, Kurzeck focused on the peak torque and power required due to track irregularities. Here, a torque limiter is introduced, and a pattern search optimization is used to tune the controller with the objective of reduce the wear on curved track with irregularities. Using the same control approach to restore the guidance used by Kurzeck ([119]) but focusing on the synchronous motor control as done by Pérez ([111]), Ahn et. al. in [115] successfully show the effectiveness of the control on a 1:5 scaled test rig. A feedforward action is introduced by Grether

in [120] to compensate the gyroscopic moment introduced into the system in transition curves. This concept is then used by Heckmann et. al. in [121] in combination with a feedback control on lateral displacement, yaw angle and yaw velocity of the wheelset. In his work Heckmann also introduced a gain scheduling approach based on the vehicle velocity to avoid possible instability conditions caused by the control action. Controlling the two wheels of the IRW to have the same speed and thus acting as a solid-axle wheelset, Ji et. al. in [27] studied the dependency between the synchronous control accuracy and the rail-wheel clearance, proposing an optimized tread profile to reduce this dependency. Using the lateral displacement and the yaw angle of the IRW wheelset as feedback, Lu et. al. in [116] developed a robust torque control using μ-synthesis. To reduce the complexity of the model, the control was based only on the model of the IRW wheelset using the bogie force and torque as external inputs. The simulation results are then experimentally validated on a 1:5 scaled test rig.
On DSW a first approach for guidance is proposed by Wickens in [122] where the wheels are steered by an angle proportional to the tracking error. The tracking error is here defined as the error of the vehicle position with respect to the track centreline. Subsequently, a passive bogie with self-steering capability is introduced by Michitsuji and Suda in [125]. Here a feedforward action is introduced to improve the vehicle behaviour during the transition curve by compensating the disturbances that derives from the time variation of the track curvature. The effectiveness of the solution is shown by simulation results and experimental ones carried out on a 1:10 scaled test rig.

2.6 SUMMARY

Active suspension for railway vehicles can be considered by definition as a technology with the inclusion of electronics like sensors, controllers and actuators. Over the past 40 years, it has developed into a comprehensive combination of various technologies which can substantially improve the dynamic behaviours of the vehicle in different aspects.
This section presented a state-of-the-art analysis of active suspension including its latest development. The concepts and classifications of active suspension are fully explained which lays down the foundation for the subsequent studies and helps the organization of the multi-target research work for this complex system. Then, tilting trains, active secondary suspension and active primary suspension are introduced in terms of principle configuration, control strategy and implementation status. Based on this previous research, the new exploration and challenging work are carried out in this project and presented in the next sections.

3. ACTIVE SUSPENSION SYSTEMS FOR CONVENTIONAL BOGIES

3.1 INTRODUCTION

In this section, the conventional bogie with targeted operational speed 160km/h is used as the research subject and active suspension technologies including active steering system and semi-active secondary vertical suspension are studied. The control strategies for these active systems are investigated and quantitative beneficial effects are assessed based on Multi-Body Systems (MBS) simulation. Furthermore, the fault-tolerance of different active steering schemes is investigated in this part.

In Section 3.2, the MBS simulation model for conventional bogie vehicle and actuators are introduced. These models then will be adopted in all the following research topics from Section 3.3 to Section 3.5. In Section 3.3, active steering is investigated in terms of mechanical schemes, control strategies and their effects. Two control strategies for active steering are introduced and simulations in different scenarios are performed to quantify the beneficial effects of active steering in service. After the validation of substantial interest of active steering, safety issues are considered for the implementation of this technology, as they directly affects the kinematics of the wheelset. Therefore, in Section 3.4 a fault-tolerant design of the active steering system is studied. An approach to quantifying the fault tolerance of active steering system is proposed based on the concept of Risk Priority Number (RPN) value and MBS simulations are performed to study the impacts of failure modes. Nine different active steering schemes are compared, and case studies are presented for further explanation. Finally, Section 3.5 introduces the semi-active secondary vertical suspension for improving vertical ride comfort. Several “classic” control strategies such as Skyhook and Acceleration-Driven-Damping(ADD) are compared and we also proposed a new control strategy, named Maximum Power Point Tracking(MPPT), which has a good impact on ride comfort and would be simpler to implement and less expensive compared to other studied control strategies.

3.2 MBS MODEL

3.2.1 Multibody dynamics model of rail vehicle

Despite three different research topics being investigated in Section 3, the vehicle multibody simulations are all performed to analyse the dynamics of the railway vehicle. A “Baseline passive vehicle model” was built in SIMPACK, considering the reference vehicle with bogies defined by the Simulation Group common to WP1, WP2 and WP3 of Run2Rail. For the study of active steering and of semi-active secondary suspensions, the model is slightly modified. In both cases, the model of the control and actuation system is built using a co-simulation with Simulink. In the second case, the effect of car body flexibility is introduced, as this effect is highly relevant to ride comfort.

The passive baseline model is proposed based on an inter-city trailer vehicle and is targeted to a maximum service speed of 160km/h. This model has one car-body, two bogies and four wheelsets.

For the passive primary suspension, one coil spring at the top of each axle-box carries the vertical load and provides a small part of yaw stiffness, and in longitudinal direction, the traction rod mounted between the axle-box and bogie transmits the longitudinal force and provides most of the yaw stiffness. In secondary passive suspension, air springs are implemented to produce soft stiffness, and each bogie has one lateral damper, two vertical dampers and two yaw dampers. The mass properties and passive suspension parameters are examined and modified by a group of experts in rail vehicle dynamics to ensure that the model is representative. The major parameters of the passive baseline model are presented in Table 3.

Table 3 - Parameters of the baseline model for conventional bogie vehicle

Parameters of vehicle dynamics model	Unit	Value
Axle load (tare condition)	t	11
Wheelbase	mm	2500
Base of bogie	m	16.000
Diameter of wheel (new)	mm	860
Wheel and rail profile	- / -	S1002/UIC60
Rail cant	-	1:40
Mass of car body	t	30
Mass of frame	t	3
Mass of wheel-set	t	1.8
Stiffness of primary coil spring in x/y direction	MN/m	1.8
Stiffness of primary coil spring in z direction	MN/m	1.2
Stiffness of traction rod bushing in x/z direction	MN/m	10
Stiffness of traction rod bushing in y direction	MN/m	3
Stiffness of airspring in x/y directions	MN/m	0.15
Stiffness of airspring in z direction	MN/m	0.25
Secondary vertical damper	kN/m/s	30
Secondary lateral damper	kN/m/s	60
Secondary anti-hunting damper	kN/m/s	200
Equivalent stiffness of anti-roll bar	MN/rad	1.5

Based on this table, the passive vehicle model is built in SIMPACK as is presented in Figure 38. Apart from the described baseline SIMPACK model, in Section 3.5 a simple one-quarter vehicle model is built in Simulink to study the principle of the different control strategies and the SIMPACK baseline model is also modified by importing a finite element car body model to explore the vibration of flexible car body in a higher frequency range. These models are further described in Section 3.5.1.

To simulate the dynamics of the vehicle with active suspension, the passive vehicle model in SIMPACK and active actuation system built in Simulink are combined and co-simulation between the two software is performed.
For active steering system, the actuator force generated from actuation model in Simulink will be sent back into the SIMPACK vehicle model to manipulate the kinematics of wheelsets whilst for the semi-active secondary suspension system, the damping force will be produced to attenuate the vibration of car body. The detailed introductions for actuation models can be found in the corresponding sections.

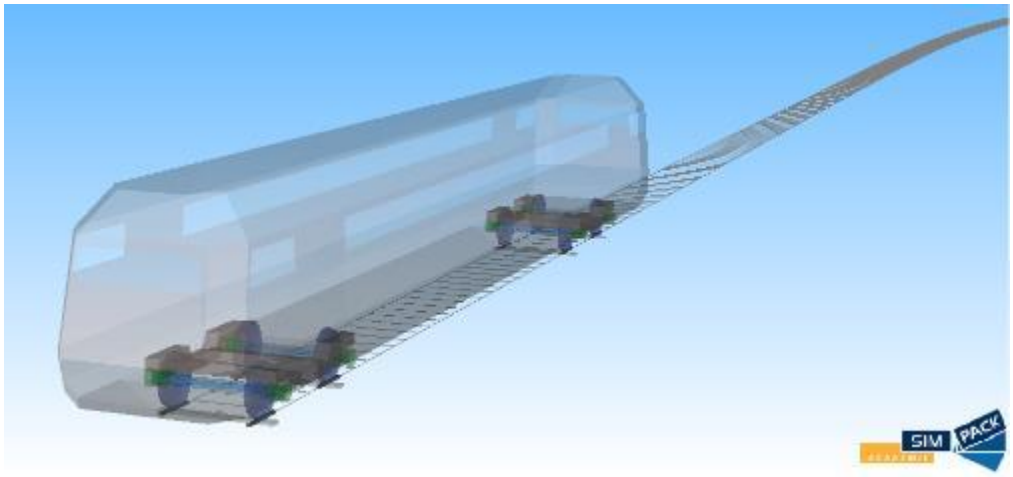

Figure 38 - The baseline model built in Software SIMPACK

In the simulations, two types of track irregularities are considered: ERRI high-level track irregularity [131] and a measured track irregularity which will be referred to as “110 track”.

3.2.2 Electro-hydraulic actuator model

In Section 3.3 and Section 3.4, electro-hydraulic actuation models are built in Simulink Sim-scape to study their dynamic effects. Section 3.3 considers an interconnected electro-hydraulic actuation model, which is schematically shown in 3.4. For each wheelset, the right and left actuators are combined in one system and they will always move in opposite directions. The high and low pressures produced from pumps work together with 5/3 (port/position) and 3/3 directional valves to control the flow of hydraulic oil and to control the motion of cylinders. The opening area of orifices in the valves can be proportionally controlled by the command signal. In the active steering system, the control target is the displacement of cylinder and a PID controller is introduced to achieve the desired displacement. In tangent track, the actuator works in passive mode, which means the orifice of valves is closed and the compressibility of hydraulic oil will generate stiffness and damping effects. The high and low pressures are set to 60 bar and 20 bar respectively and the maximum actuator force is configured as 20 kN.

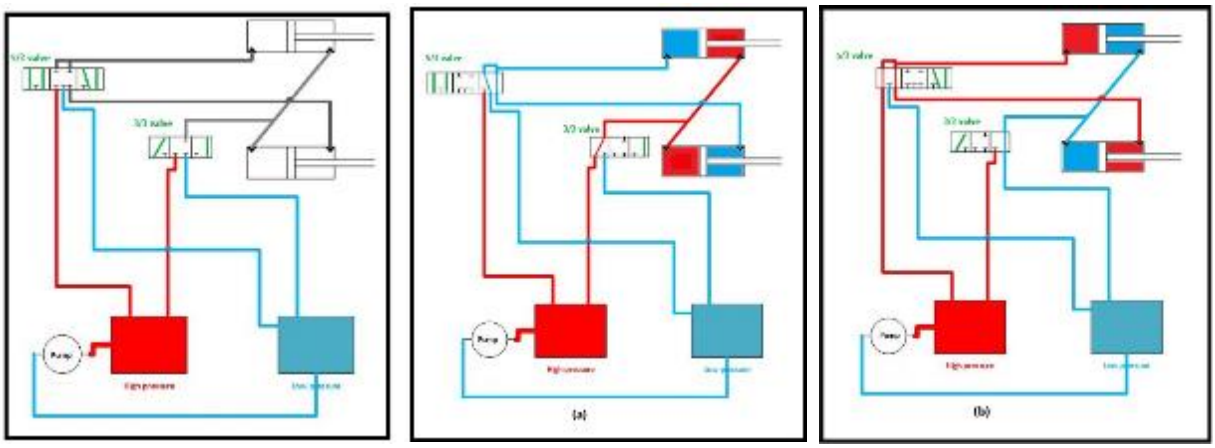

(a) Passive mode (b) move to positive direction (c) move to negative direction

Figure 39 - Inter-connected hydraulic actuator model and its working modes

In Section 3.4, a simple electro-hydraulic actuator model is adopted as well to investigate the effects of different configurations for the actuating system in terms of fault tolerance. This system controls a single actuator located on one side of the bogie, so the synchronisation of the steering command shall be ensured by the control system. For each wheelset, two actuation systems are implemented and they are assumed to work independently. A relatively simple 4/3 directional valve is used to control the flow direction and the area of orifices can be controlled for the flow rate, i.e. the velocity of the cylinder. The principle of this simple actuator is shown in Figure 40.

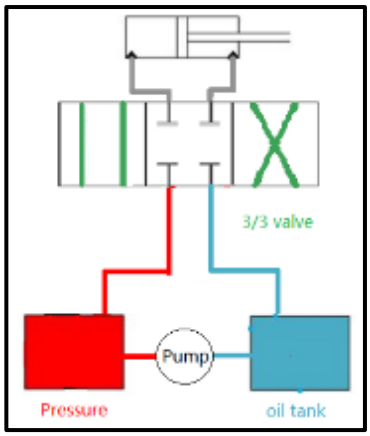

Figure 40 - The principle of simple hydraulic actuator

Apart from the actuator models, it is worth mentioning that in Section 3.5, a dynamic model of Magneto-rheological (MR) Damper is introduced to study its effects on semi-active vertical suspension, which is explained in detail in Section 3.5.3.

3.3 ACTIVE STEERING OF SOLID-AXLE WHEELSETS

3.3.1 Control strategies for active steering system

The active steering system can be achieved by different mechanical arrangements of actuators in primary suspension as is introduced in Section 2.5.2, but the most commonly used scheme is applying actuators in longitudinal direction between the bogie side frames and two ends of the wheelsets, as is shown in Figure 41(a), so that the actuator can move the axle box longitudinally, thus producing the steering of the wheelset. The configuration for longitudinal passive spring is important to the effectiveness of active steering system. When a passive spring is kept in parallel with the actuator, as shown in Figure 41(b), additional actuator force is required to cancel out the stiffness effect of the spring. However, the passive spring can serve as a back-up for active steering to ensure safety when active system fails in service. Both arrangements are considered in the following analyses.

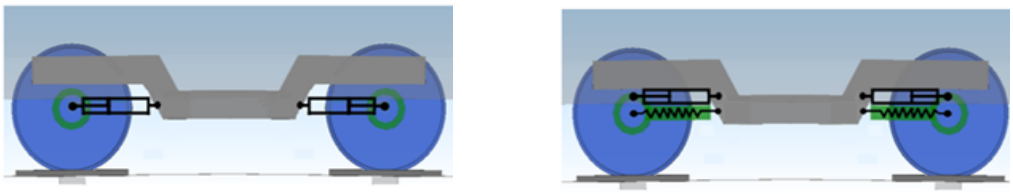

(a) Active steering without passive spring (b) Active steering with passive spring in parallel

Figure 41 - Arrangement of two active steering schemes

The control of active steering system proposed here is based on displacement control of actuators. When a vehicle passes curves, the radial position of front and rear wheelsets is schematically shown in Figure 42 (a).

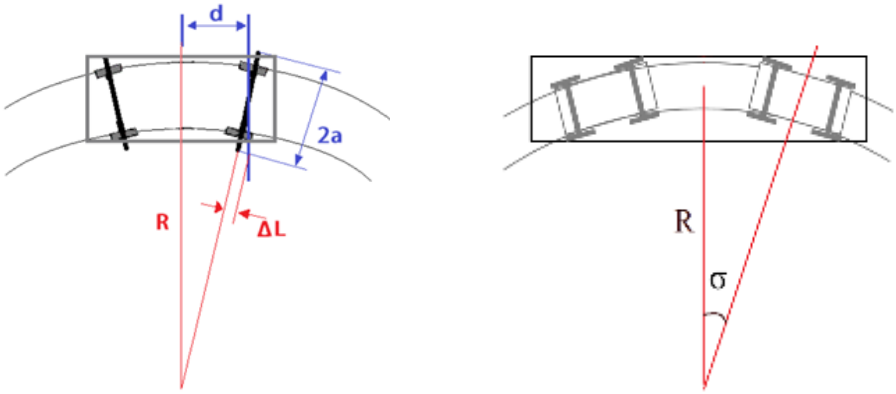

(a) Radial position of wheelset (b) Yaw angular of bogie

Figure 42 – Radial position of wheelset and yaw angle of bogie

The displacement of actuator ΔL is calculated according to Equation (13) to create a radial position of the wheelset

$$\Delta \mathbf{L} = \frac{\boldsymbol{d}}{\boldsymbol{R}} \cdot \boldsymbol{a} \quad \textbf{(13)}$$

where d represents the half wheelbase, and a is half distance between the right and left actuators; 1/R is the track curvature. There are two methods to obtain the track curvature and according to these methods, we develop two control strategies: (1) control strategy based on gyroscope sensors and (2) control strategy based on a database of track curvature and geo-referentiation of the vehicle.

(1) Control strategy based on gyroscope sensors

The first method to estimate the track curvature is presented in Equation (14).

$$\mathbf{R} = \frac{\boldsymbol{V}}{\dot{\sigma}} \quad \textbf{(14)}$$

where V is the longitudinal speed of the vehicle and $\dot{\sigma}$ is the absolute yaw angular velocity (yaw rate) of bogie, the absolute yaw angle of bogie is shown in Figure 42(b). The yaw rate $\dot{\sigma}$ can be measured by a gyroscope sensor mounted on the bogie and a first-order filter is implemented to filter out the unwanted noise signals coming from track irregularities.
To test this method, simulations are performed on a curve with radius R400 with transition length 60 m at speed 58.2 km/h (non-compensated lateral acceleration equal to 0). Figure 43 presents the accurate curvature and estimated curvature when ERRI high-level track irregularity [131] is applied and is not applied. Without track irregularity, the estimated curvature is completely the same as the accurate one on the full curve, while with track irregularity, the estimated curvature is fluctuating around the accurate value, within an acceptable tolerance.

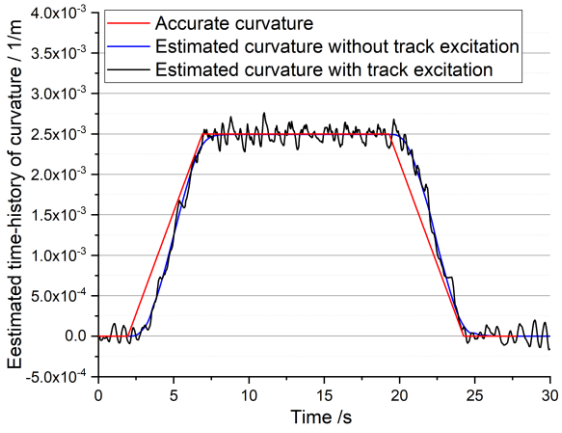

Figure 43 - Compassion between the accurate curvature and estimated curvature

In Figure 43, a delay between the accurate curvature and estimated curvature can be clearly observed which mainly comes from the first-order low-pass filter. The delayed curvature estimation will create a delayed referenced displacement of actuator. Furthermore, the response time of the electro-hydraulic actuation system can enlarge the delay effect between the ideal action and actual action of actuators.
One solution to alleviate this problem is applying Precedent control strategy where the control signal for the actuators mounted on the first leading wheelset is used as precedent command and it will be actively delayed to control the actuators behind. This delay time is carefully calculated considering the vehicle speed and distances between the first wheelset and the following wheelsets. More importantly, this active delay can compensate for the effects of delay between the accurate track curvature and estimated track curvature, and also the response time of electro-hydraulic actuators. Moreover, implementing this control principle can reduce the number of sensors for the following wheelsets and bogies, saving cost and simplifying the implementation of active steering system. However, the delay on the first leading wheelset still cannot be compensated.
The control workflow is schematically shown in Figure 44.

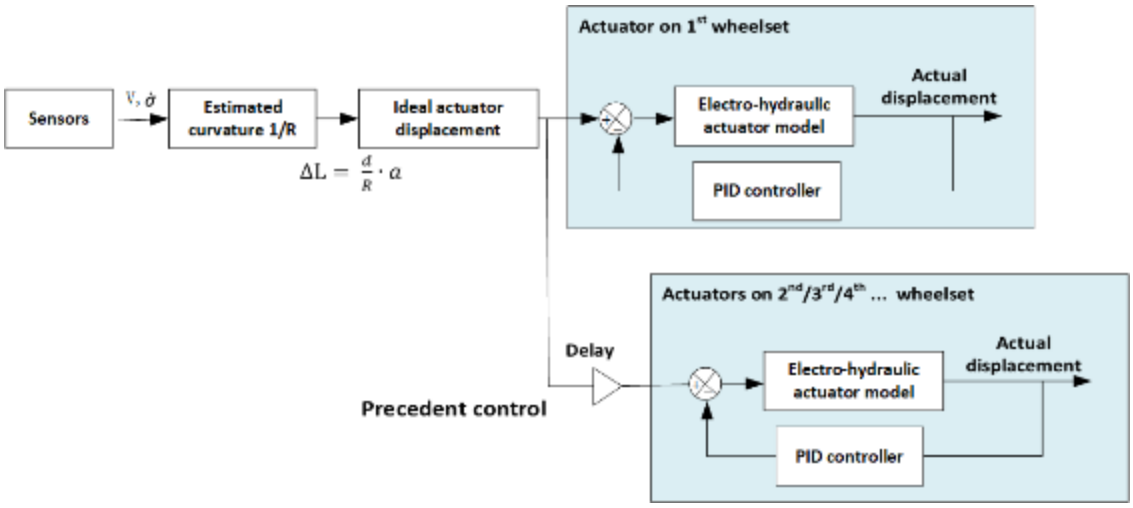

Figure 44 - Workflow of first active steering control

According to the above description, MBS simulations are performed on curve R400 at 82.2 km/h (non-compensated lateral acceleration: 0.65m/s^2) to explore the active steering effects. In these simulations, the longitudinal passive springs are disabled. Figure 45 to Figure 47 compare the wheelset angle of attack, guiding force and wear number between the passive suspension and active steering suspension when track irregularity is not applied.

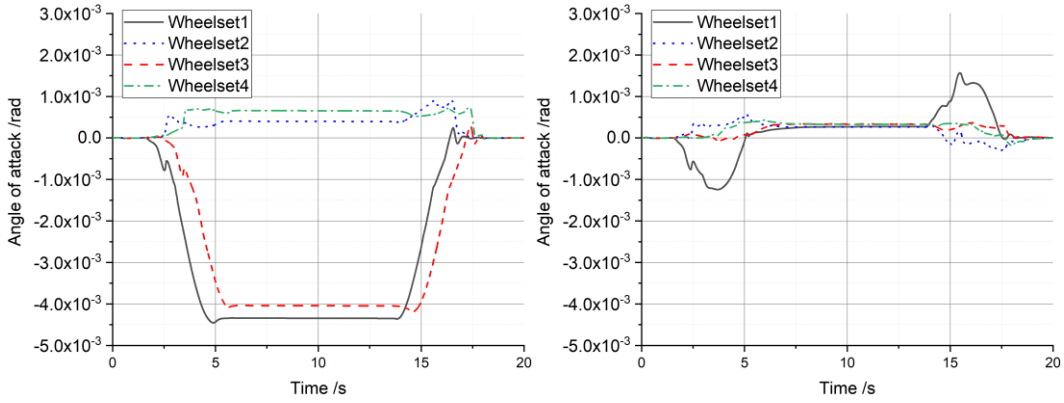

(a) Passive scheme (b) Active steering scheme

Figure 45 - Wheelset angle of attack with no track irregularity

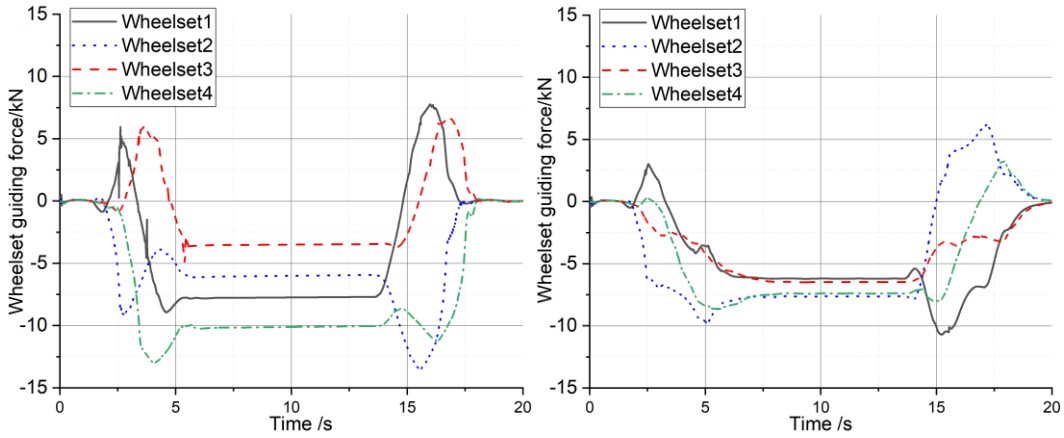

(a) Passive scheme (b) Active steering scheme

Figure 46 - Wheelset guiding force with no track irregularity

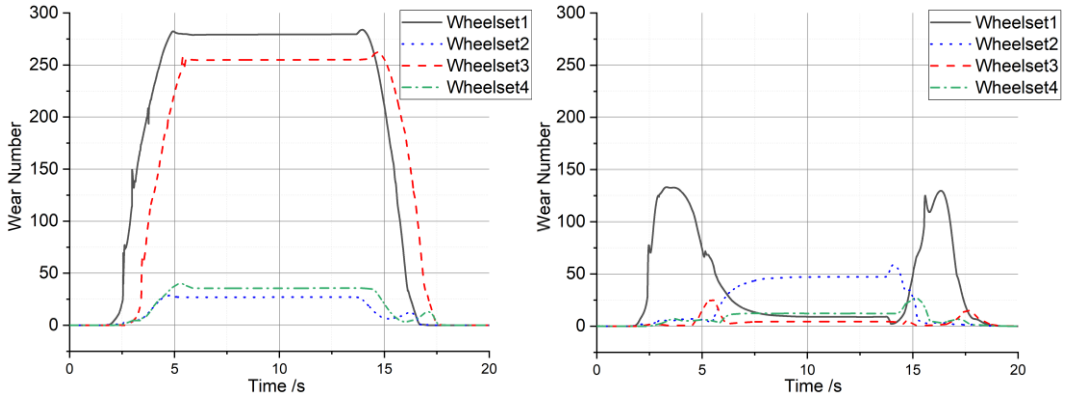

(a) Passive scheme (b) Active steering scheme

Figure 47 - Wheelset wear number with no track irregularity

With active steering system, the angle of attack is drastically reduced especially for the leading wheelsets on both bogies, and the four wheelsets have similar attack angle, which means that the wheelsets have similar posture when passing the curve. As a result, the guiding forces of the four wheelsets become more even and the maximum guiding force decreases from 10kN to 7.5kN, which may allow higher speed on curves. Furthermore, active steering significantly reduced the wear number. However, for the leading wheelset, two curve transition zones see peak values due to the delay of hydraulic actuators' movement. As the precedent control is applied, this phenomenon doesn't take place on the following wheelsets.

The above simulations are performed again with track irregularity and the results are presented in Figure 48 to Figure 50.

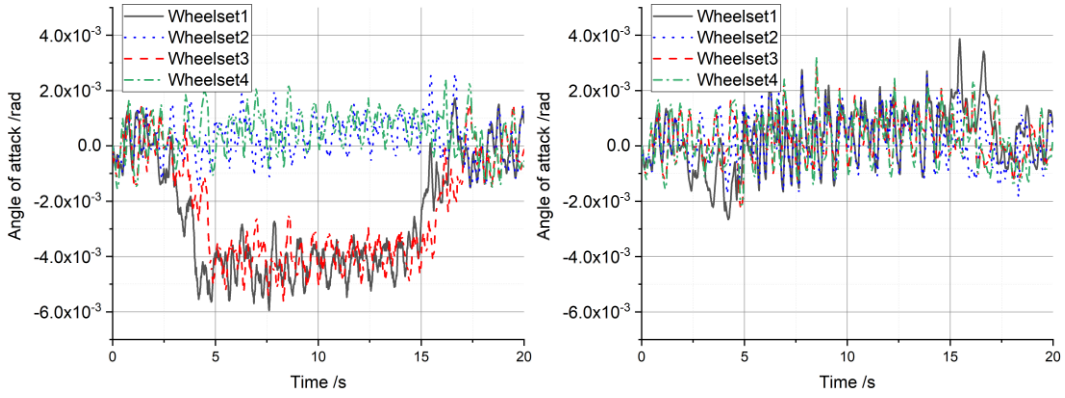

(a) Passive scheme (b) Active steering scheme

Figure 48 - Wheelset angle of attack with track irregularity

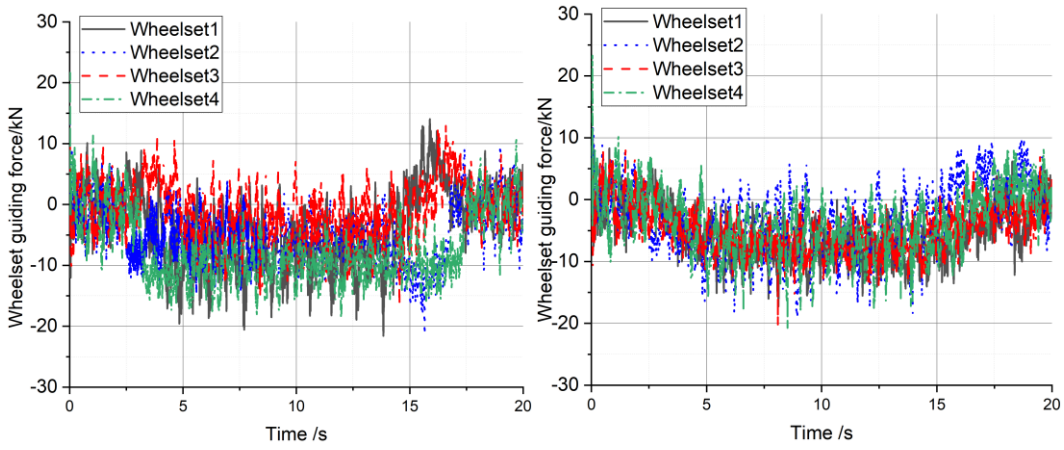

(a) Passive scheme (b) Active steering scheme

Figure 49 - Wheelset guiding force with track irregularity

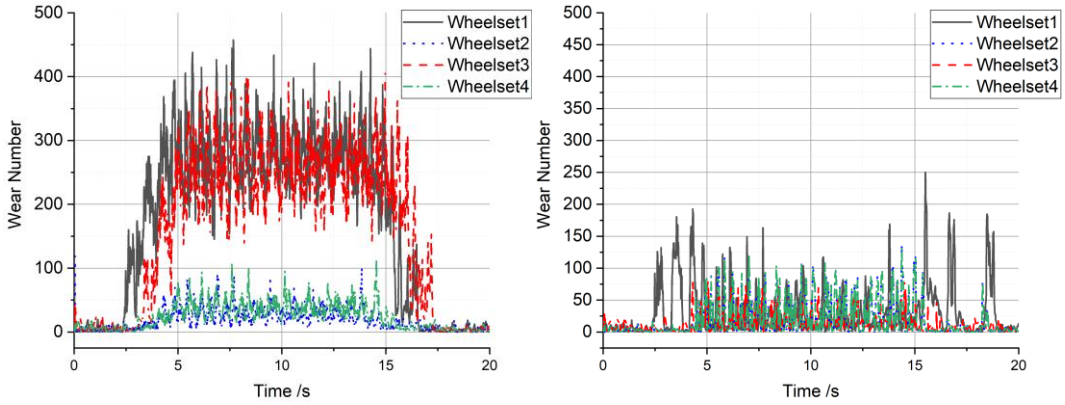

(a) Passive scheme (b) Active steering scheme

Figure 50 - Wheelset wear number with track irregularity

With presence of track irregularity, despite of the oscillations being observed, the active steering dramatically improves the performance at curve negotiation, similar to the results with no track irregularity.

(2) Control strategy based on track curvature database and Geo-localisation technology

In this section, we explore a new control strategy based on utilization of track curvature database and geo-localisation technology. From the above description, the estimation for track curvature can introduce the time delay and track irregularity leads to the fluctuation. If the information of track curvature is stored in a database and geo-localisation technology is applied to locate the vehicle on track, the curvature can be obtained by means of lookup-table. The error of this method mainly comes from the tolerance of the geo-localisation system, but some technologies like Kalman filter can be used to combine different information on vehicle localisation e.g. from balises, GPS signal and odometry to generate more accurate measurement to locate vehicle position.
To simulate this control strategy in Simulink, the track position and corresponding curvature are stored in a table and the leading wheelset position on track is measured and exported to the actuation system. To compensate for the response time of electro-hydraulic actuator, we add a short distance calculated as the multiplication of delay time and vehicle speed on the wheelset position. This strategy is shown in Figure 51.

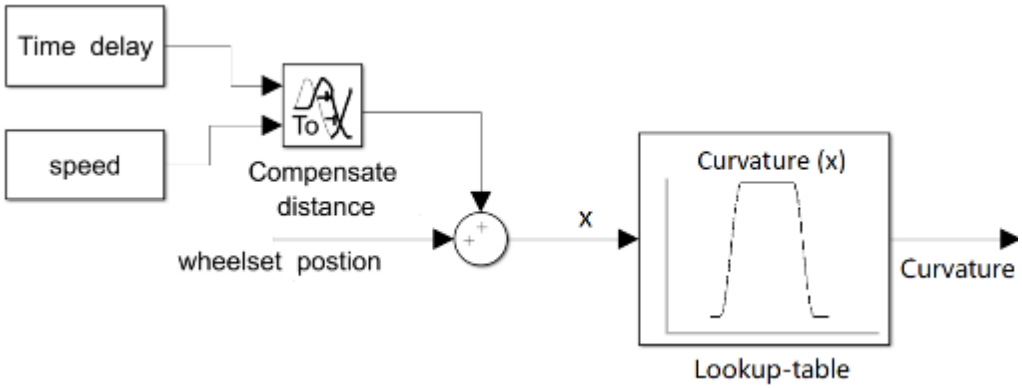

Figure 51 - Control strategy to obtain the ideal track curvature

This control strategy is simulated without track irregularity and compared with the first control strategy based on gyroscope sensors. The simulation results are displayed in Figure 52.

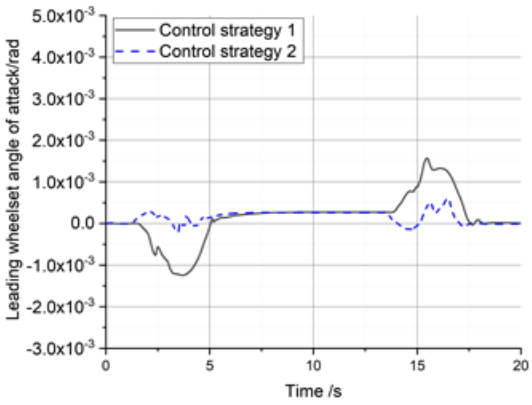

(a) Angle of attack

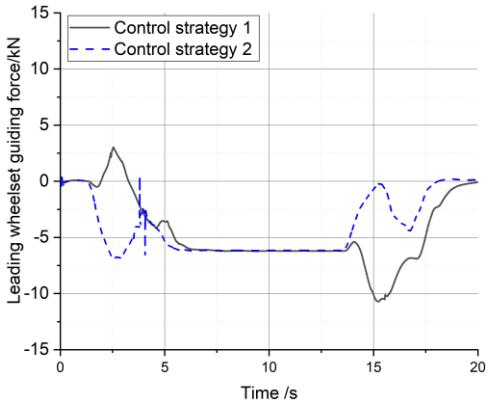

(b) Wheelset guiding force

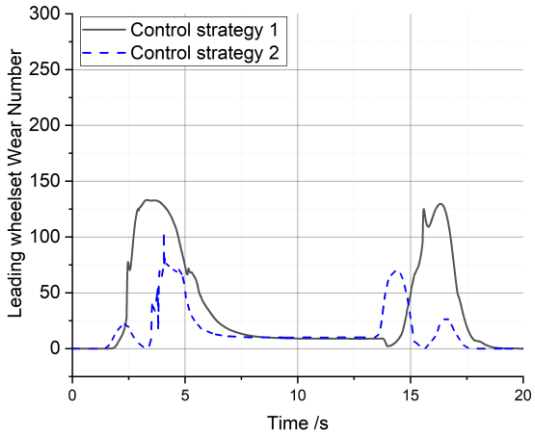

(c) wear number

Figure 52 - Performance of leading wheelset with two control strategies (no track irregularity)

It can be seen that the control strategy based on the track curvature database can produce a better effect in curve transition part, whilst on full curve, the two control strategies have the same performance, because in this part the obtained track curvature and the referenced displacement of actuators are the same. The comparison with track irregularity is also performed and presented in Figure 53 and the features of the two control strategies are similar to the simulations performed with no track excitation.

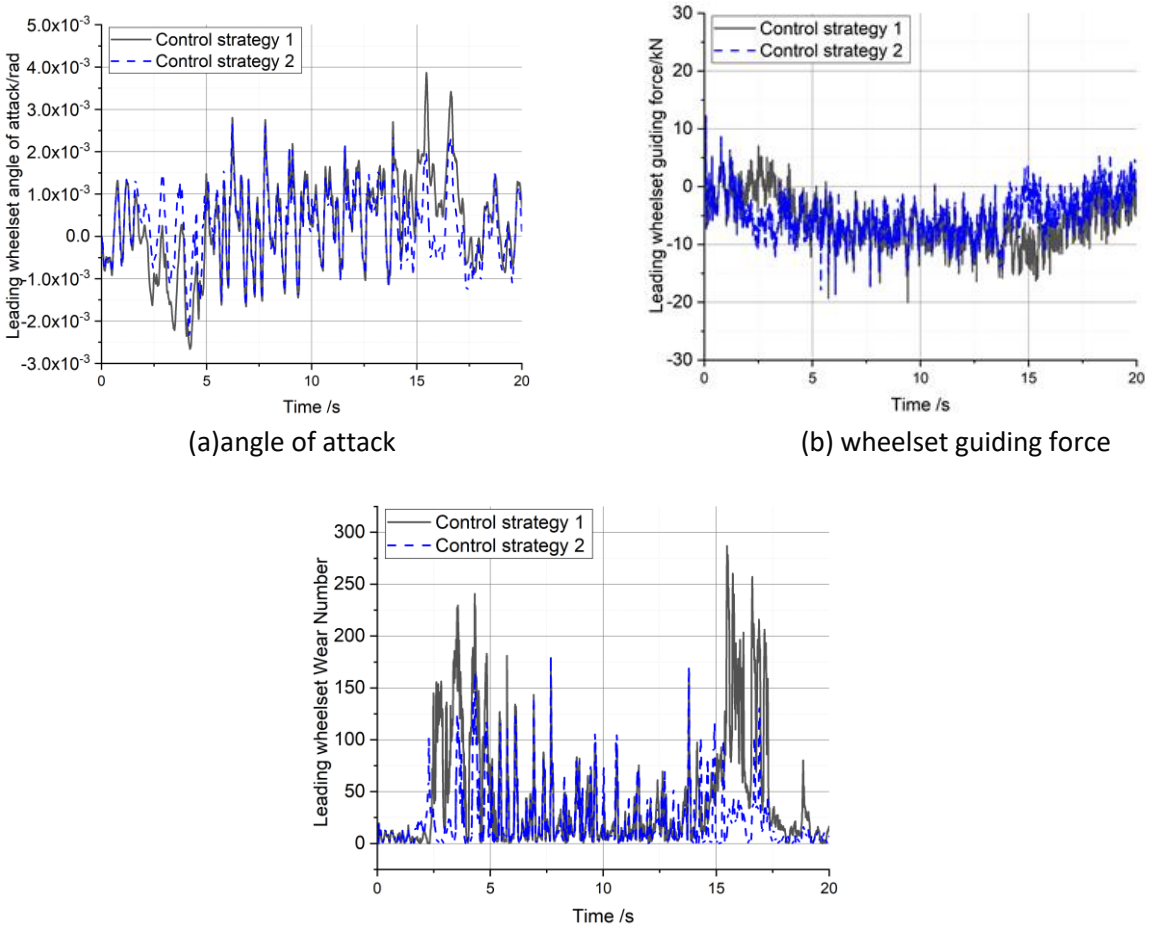

(a)angle of attack

(b) wheelset guiding force

(c) wear number

Figure 53 - Performance of leading wheelset with two control strategies (with track irregularity)

As the two control strategies have negligible difference on full curve and in the following simulation work, active steering performance on full curves is considered. We only applied the second control strategy for the following simulations.

3.3.2 Simulation results in different scenarios

To make comprehensive evaluation on the active steering effects, simulations are performed at different combinations of speed and track layout. Table 4 summarizes the simulation scenarios where curves R250, R400, R600, R1500 are selected to represent the tight curve, small curve, middle curve and large curve. The curve passing speeds are also configured considering three typical situations.

Table 4 - Simulation scenarios

Curve radii	Curve transition	Super-elevation	Case 1 NLA 0.65 [m/s^2]	Case 2 NLA 0 [m/s^2]	Case 3 Speed 10 [km/h]
R [m]	L [m]	h [mm]	V1 [km/h]	V2 [km/h]	NLA [m/s^2]
250	100	150	72,7	56,4	-1,0
400	80	100	82,2	58,2	-0,6
600	80	80	95,5	63,8	-0,5
1500	60	60	142,4	87,3	-0,4

The ERRI high level track irregularity [131] is applied and characterized Wear number is obtained as mean value over the period on the full curves.

Table 5 summarizes the wear number of the leading wheelset when paralleled springs are disabled. Around 90% of wear number can be reduced with exception of large curve R1500, whilst Table 6 presents the simulation results with presence of passive springs paralleled with actuators. In this configuration, the steering effects are drastically degraded on the narrow curves with R250 and R400, while on relatively large curves, the steering effects tend to be more even.

Table 5 - Wear number in different scenarios with no passive spring in parallel with actuator

Curve radii	Case 1 NLA 0,65 [m/s^2]			Case 2 NLA 0 [m/s^2]			Case 3 10 [km/h]		
R [m]	Passive	Active	Improvement [%]	Passive	Active	Improvement [%]	Passive	Active	Improvement [%]
250	487.20	38.73	92.05	526.55	43.35	91.77	519.75	57.17	89.00
400	281.63	21.90	92.22	309.31	22.90	92.60	346.97	30.89	91.10
600	187.70	23.23	87.62	204.73	20.35	90.06	221.15	17.67	92.01
1500	51.69	21.66	58.09	61.86	15.09	75.60	67.15	19.26	71.32

Table 6 - Wear number in different scenarios with passive spring in parallel with actuator

Curve radii	Case 1 NLA 0.65 [m/s2]			Case 2 NLA 0 [m/s2]			Case 3 10 [km/h]		
R [m]	Passive	Active	Improvement [%]	Passive	Active	Improvement [%]	Passive	Active	Improvement [%]
250	487.20	313.81	35.59	526.55	351.05	33.33	519.75	352.23	32.23
400	281.63	135.09	52.03	309.31	147.67	52.26	346.97	170.36	50.90
600	187.70	48.90	73.95	204.73	52.52	74.35	221.15	56.26	74.56
1500	51.69	26.12	49.46	61.86	19.76	68.06	67.15	22.29	66.81

3.4 FAULT-TOLERANT ANALYSIS FOR ACTIVE STEERING SYSTEM

The active steering has been studied in Section 3.3 and the beneficial effects have been revealed from the simulations, but when it comes to the implementation, cost-benefit and safety-critical issues must be considered seriously.

The cost-benefit of active primary suspension is particularly attractive as this technology has the potential to provide substantial benefits in terms of lower maintenance costs and reduced impacts on wheels and the track. However, as active steering directly affects the kinematics of the wheelset, safety issues are concerned in case the actuation system fails in service. As a result, a fault-tolerant design of the active steering system is crucial for the implementation of the technology.

In this work, we propose an approach to analyse the fault tolerance of active steering system where the concept of Risk Priority Number (RPN) from Failure Mode and Effect Analysis (FMEA) is adopted and multibody simulations are performed to study the impacts of failure modes. Based on this method, nine different active steering schemes are compared, and case studies are presented for further explanation.

3.4.1 Methodology for fault-tolerant analysis

3.4.1.1 Failure Mode and Effect Analysis and Risk Priority Number

Failure Mode and Effect Analysis (FMEA) is a systematic approach to evaluate the potential failure modes of the system and their effects [129]. It was firstly proposed for the design of aircrafts and now has been successfully applied in many other industries to reduce the impacts of failure and to improve the reliability of the system. In FMEA, a core concept is calculating Risk Priority Number (RPN) which involves three factors: the Severity of the failure in terms of economic losses and injury to people, the Occurrence defined as the likelihood that the failure rate will actually take place, and also the Detectability of the fault, i.e. the ability to detect the failure mode through inspection and/or monitoring. As is shown in Equation (15), the RPN is calculated as the multiplication of the levels of Severity, Occurrence and Detection, which are characterized from 1 to 10.

$$\mathbf{RPN=Severity \times Occurrence\ (\times Detectability)} \qquad \mathbf{(15)}$$

In the background of active suspension system, if a frequent failure mode of actuation system has a severe impact on safety and is difficult to detect, the system needs to be improved in the design process to avoid this failure mode, for instance through redundancy of critical subsystems / components. A seminal work presented in [132] adopted the RPN value to study the failures of active suspension for the first time. Following this work, we propose a quantitative method to assess the PRN value where the severity is focused upon as is introduced in Section 3.4.2.

3.4.1.2 Vehicle dynamics simulation and severity level estimation

The failure modes of actuation system have various impacts on vehicle and track systems which are hard to predict even with knowledge of vehicle dynamics. The simulation for vehicle and actuation system thus is necessary to investigate the failure effects.

In Europe, the vehicle acceptance norm EN 14363 [128] presents the safety evaluation criterion by measuring two assessment quantities in the normal method: the sum of guiding forces of left and right wheels $\sum Y_{max}$ and the derailment coefficient $(Y/Q)_{max}$. According to EN 14363, the measured time-histories of quantities are processed firstly by a 20 Hz lower-pass filter and then by the sliding mean method with window length 2 m and step length 0.5 m. After that, the 99.85 percentile value from the time-history data is obtained as the characteristic value to be compared with the limit value for the safety evaluation.

When a failure of the active suspension occurs, the increase of the assessment quantities and remaining margin from the limit value reflect the severity levels, and based on this, we establish the severity factor s to quantify the impacts according to Equation (16),

$$\boldsymbol{s(x) = \frac{x^n - F_n^n}{F_l^n - F_n^n} \ (n = 2)} \qquad \textbf{(16)}$$

where x is the assessment quantity considered (either $\sum Y_{max}$ or $(Y/Q)_{max}$), F_n is the value of the assessment quantity in the healthy condition of the suspension; F_l is the limit value for the assessment quantity according to EN14363 [128]. The severity factor s is computed for all relevant assessment quantities and the maximum value is chosen.

An example of simulated derailment coefficient x and corresponding severity factor s is shown in Figure 54 where F_n and F_l are 0.3 and 0.8 respectively. When exponent n is set to 2, the gradient of severity s over x is increasing. In other words, the variation of severity factor will be more sensitive to x when the assessment quantity in faulty condition becomes close to the threshold value. This weighted effect meets the common expectation for severity assessment. The factor s can be used as an independent indicator for severity evaluation. When it is greater than 1, the $\sum Y_{max}$ or $(Y/Q)_{max}$ exceeds the limit value, resulting in the chance of unsafety.

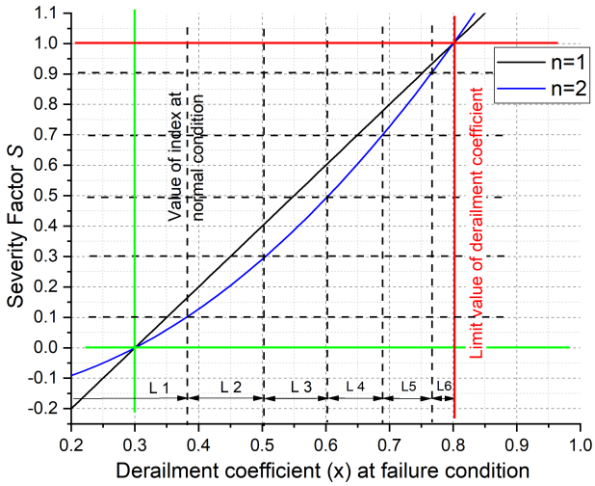

Figure 54 - **Example of severity factor *s* for derailment coefficient**

In order to build the connection between the severity factor s and Severity ranks for RPN calculation, 10 levels of severity are defined based on EN 60812 [129], and the corresponding severity factor s is graded as shown in Table 7 As the limit values of factors defined in EN 14363 [128] are conservative for safety guarantee, the situation of "s=1" is not graded in the top level of severity but in Rank 7 that starts to have a risk of injured passengers and a small chance of derailment.

Table 7 - **Description of severity levels for railway vehicle**

Severity factor	Severity rank	Impact	Description
s<0.1	1	no impact	No recognizable effect
0.1≤s<0.3	2	very little	Noticed by few passengers
0.3≤s<0.5	3	little	Impacts on vehicle and infrastructure in long term
0.5≤s<0.7	4	very low	Noticed by many passengers
0.7≤s<0.9	5	low	Impacts on vehicle and infrastructure in mid term
0.9≤s<**1.0**	6	moderate	Impacts on vehicle and track in short term
1.0≤s<1.1	7	high	Risk of injured people and small chance of derailment
1.1≤s<1.3	8	very high	Severe impacts on vehicle and infrastructure in short term
1.3≤s<1.5	9	very unsafe	Risk of many injured people and few dead people
s≥1.5	10	catastrophic	Risk of many dead people and the line closed for weeks

Then the Severity level can be obtained for calculating RPN. A method to quantify the Occurrence level is introduced in Section 3.4.3, whilst Detection is not considered in this work because a realistic estimation of this factor would require the knowledge of the detailed implementation of the active steering system in a specific application, including the implementation of any supervision system.

3.4.2 Simulation model

The principle of active steering is applying actuators between wheelsets and bogie in the longitudinal direction as is introduced in Section 3.3. Nine practical schemes labelled as “A1, A2, …, C3” are presented in the three-by-three matrix as shown in Figure 55.

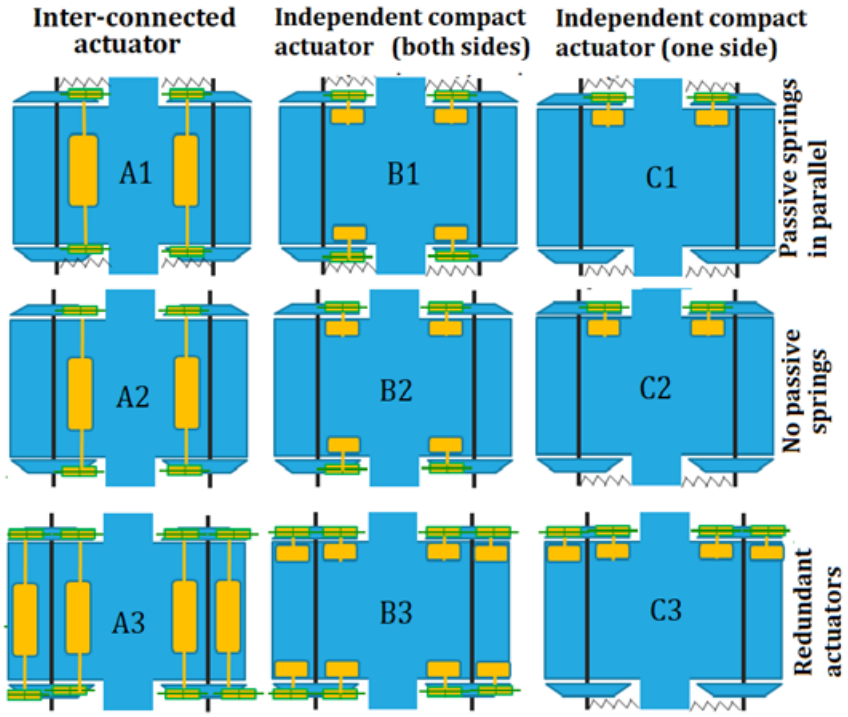

Figure 55 - **The “three by three” active steering schemes**

The schemes labelled with “A” adopt inter-connected electro-hydraulic actuation system where the left and right actuators for each wheelset are combined in one system. By contrast, the schemes marked with “B” and “C” implement simple compact actuators for each wheel which is less likely to fail. The schematics of the inter-connected and compact hydraulic actuators are shown in Figure 56: in both cases, the maximum force that can be generated by the actuator is 20 kN. For schemes “C”, actuators are applied only on one side of the bogie whilst at the other side a passive suspension is used as a trade-off scheme between the benefits and the costs. These schemes therefore include

a total number of actuators which is one half compared to the corresponding schemes “B”. The schemes in the first row with “1” include passive springs in parallel with actuators to enhance fault tolerance, but in these cases, higher actuator force is required to cancel out the action of passive springs. The schemes in the third row with “3” have redundant actuations as the back-up in case one fails in service so that the safety is expected to be ensured. The schemes “2” have neither passive springs nor redundant actuators.

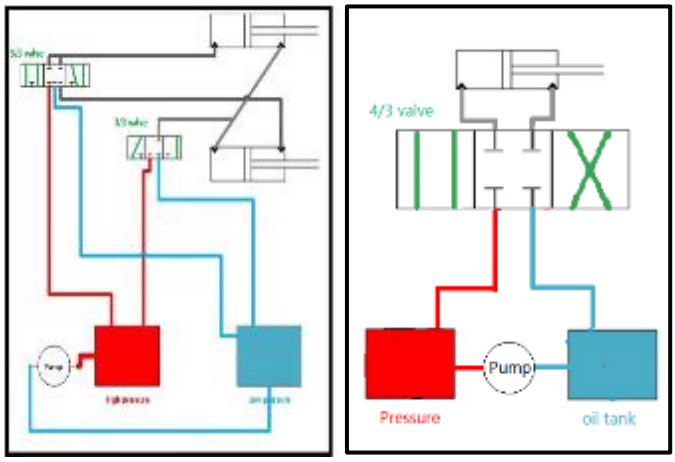

Figure 56 - **Interconnected and simple actuator models**

On curves, the control strategy for active steering is based on the ideal radial position of the wheelset in which the elongation of the actuator is controlled to force the wheelset in desired positions. On tangent track, the actuation system operates in passive mode where the compressibility and flow of hydraulic oil will generate stiffness and damping effects to mimic the behaviour of a passive primary suspension. The detailed description of the control strategy in curve is described in Section 3.3.

The active steering systems are implemented in a MBS model of the baseline vehicle with bogies defined by the “Simulation group”. The main parameters of this vehicle model are presented in Table 3. Two extreme simulation scenarios are considered to investigate the impacts of failure modes of actuation system. In Scenario 1, the vehicle runs on tangent track at the maximum test speed of 176 km/h (110% of max. operational speed), while in Scenario. 2, the vehicle negotiates a short radius curve R250m with superelevation of 150 mm at speed 73 km/h (non-compensated lateral acceleration: 0.65m/s^2). A measured track irregularity “track irregularity 110” is applied in both scenarios.

3.4.3 Case studies for fault-tolerant analysis

3.4.3.1 Introduction of typical failure modes and estimation for Occurrence

The active steering actuation system can be a complicated electro-hydraulic or electro-mechanical system. For electro-hydraulic actuator, each sub-structure such as the motor, valve, controller could suffer failure mechanisms leading to the malfunction of the actuation system. However, in spite of the variety of possible failure causes, the failure modes of the system can be summarized in a limited number of relevant cases, as summarized below.

(1) Inversion control: The actuator is producing force in the opposite direction possibly due to an error occurring in the controller or to an incorrect installation of sensors or actuators.

(2) Max force: The incorrect signals of sensors and controllers may lead to a situation in which the actuator generates the maximum force to push or pull the wheelset. In the following simulations, the maximum force is set to 20 kN.

(3) Random force: The actuator could produce a random force because of a failure occurring in the valves, controllers or sensors. To simulate the random force, a white noise signal is created and then a 5 Hz low-pass filter is applied to reflect the limited bandpass of the actuators. Finally, the time history of random force is normalized in the range of [-20 kN, 20 kN] as is shown in Figure 57.

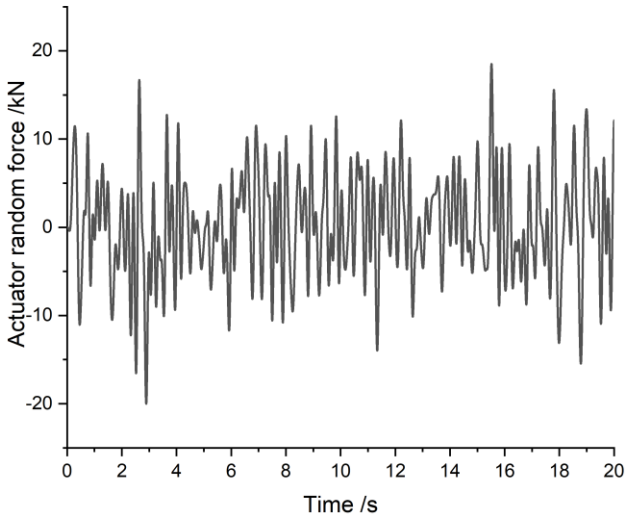

Figure 57 - Actuator random force fed into the dynamics model

(4) Free (Zero force): It means that there is no force between the two ends of the actuator which could be caused by a mechanical failure of the actuator or by severe leakage of hydraulic oil, for instance, the fracture of the cylinder or even a missing actuator. The failure mode “Free” could

degrade the stability of the vehicle. In the Multibody simulation, “0” actuator force will be used to simulate the case “Free”.

(5) Zero/No input signal: In this failure mode, there is no control signal or the signal for actuator is zero and thereby the valves will work in passive mode. This case is the normal working status on tangent track but on curves it will introduce additional stiffness and the wheelsets have to overcome this effect for curve negotiation.

Based on the above description, the configurations for failure modes on the front bogie are summarized in Table 8.

Table 8 - The simulation configurations for the failure modes

(A: schemes A1, A2, A3; B/C: schemes B1, B2, B3, C1, C2, C3)

	Tangent track	Curve R250	Configuration for actuator
Inversion control	×	✓	A/B/C: All actuators on first bogie
Max force	✓	✓	A: Front interconnect actuator (FL+FR) B/C: Front Left
Random force	✓	✓	A: Front interconnect actuator (FL+FR) B/C: Front Left
Free (Zero force)	✓	✓	A: Front interconnect actuator (FL+FR) B/C: Front Left
Zero/No input signal (Passive)	×	✓	A: Front interconnect actuator (FL+FR) B/C: Front Left

The main subsystems of the two types of hydraulic actuators and their estimated failure rates are shown in **Table 9** according to some empirical data. As the structure of the inter-connected hydraulic actuator is more complex than the singe compact actuator and the number of some components are doubled, for instance, the valves and motors, the failure rates of these components on inter-connected actuators are 2-4 times larger than those of compact actuator, whilst as control electronics, sensors and cables are the same or similar, these subsystems are assumed to have the same failure rates for both configurations of the actuating system.

Table 10 presents the causes of several failure modes from the perspective of sub-system and consequently, the failure rates for one actuation system can be computed according to Equation (17). where $p_{subsystem,i}$ is the failure rate of the ith subsystem associated with the failure mode.

$$\boldsymbol{P_{actuator}} = \mathbf{1} - \prod(\mathbf{1} - \boldsymbol{p_{subsystem,i}}) \quad \textbf{(17)}$$

Table 9 - Failure rates of sub-systems of two hydraulic actuators (Failure rate: number of failures per operating hour, unit: h^{-1})

Failure Rate $p_{subsystem}$	Sub-system						
	Motor	Pump	Cylinder	Valves	Control electronics	Cabling	Sensors
Compact hydraulic actuator	10×10^{-6}	30×10^{-6}	1×10^{-6}	10×10^{-6}	10×10^{-6}	4×10^{-6}	20×10^{-6}
Inter-connected hydraulic actuator	20×10^{-6}	60×10^{-6}	2×10^{-6}	40×10^{-6}	10×10^{-6}	4×10^{-6}	20×10^{-6}

Table 10 - Causes and failure rates of typical failure modes

Fault mode	Sub-system							Failure rate for one actuation system $p_{actuator}$	
	Motor	Pump	Cylinder	Valves	Control electronics	Cabling	Sensors	Compact actuator	Inter-connected actuator
Free (Zero force)	✗	✗	✓	✗	✗	✗	✗	1×10^{-6}	2×10^{-6}
Zero signal (Passive)	✗	✗	✗	✓	✓	✓	✓	44×10^{-6}	74×10^{-6}
Max force	✗	✗	✗	✗	✓	✗	✓	30×10^{-6}	30×10^{-6}
Inversion	✗	✗	✗	✗	✓	✓	✓	34×10^{-6}	34×10^{-6}
Random force	✗	✗	✗	✓	✓	✓	✓	44×10^{-6}	74×10^{-6}

Assuming that each actuation system will work independently and has no interface with others, then the failure rate of the actuation systems on one bogie can be estimated according to Equation (18), where n is the number of the actuation systems implemented on one bogie.

$$\boldsymbol{p_{bogie} = 1 - (1 - p_{actuator})^n} \quad \textbf{(18)}$$

Considering the three by three actuation schemes, the failure rate matrix for the schemes are presented in Equation (19) where $p_{actuator,1}$ is the failure rate of the failure mode on the inter-connected actuation system and $p_{actuator,2}$ is the failure rate for the compact actuation system.

$$\boldsymbol{P_{bogie} = \begin{bmatrix} 1-(1-p_{actuator,1})^2 & 1-(1-p_{actuator,2})^4 & 1-(1-p_{actuator,2})^2 \\ 1-(1-p_{actuator,1})^2 & 1-(1-p_{actuator,2})^4 & 1-(1-p_{actuator,2})^2 \\ 1-(1-p_{actuator,1})^4 & 1-(1-p_{actuator,2})^8 & 1-(1-p_{actuator,2})^4 \end{bmatrix}} \quad \textbf{(19)}$$

The failure rates of the actuation system in one bogie are computed based on Equation (19), using the actuator failure rates from Table 10. Then the levels of Occurrence are graded based on Table 11, which is proposed based on EN 60812 [129].

Table 11 - Ten levels of occurrence and failure rate

Occurrence Rank	Impact	Failure rate [1/hour]
1	Low	$P<1\times10^{-7}$
2		$1\times10^{-7}\leq P<1\times10^{-6}$
3		$1\times10^{-6}\leq P<5\times10^{-6}$
4	Moderate	$5\times10^{-6}\leq P<2\times10^{-5}$
5		$2\times10^{-5}\leq P< 1\times10^{-4}$
6		$1\times10^{-4}\leq P< 4\times10^{-4}$
7	High	$4\times10^{-4}\leq P<1\times10^{-3}$
8		$1\times10^{-3}\leq P< 2\times10^{-3}$
9	Very high	$2\times10^{-3}\leq P< 5\times10^{-3}$
10		$P\geq 5\times10^{-3}$

The resulting Occurrence matrixes for different failure modes are:

$$\boldsymbol{O}_{\text{inversion}}=\begin{bmatrix}5&6&5\\5&6&5\\6&6&6\end{bmatrix}\quad \boldsymbol{O}_{\text{max}}=\begin{bmatrix}5&6&5\\5&6&5\\6&6&6\end{bmatrix}\quad \boldsymbol{O}_{\text{rand}}=\begin{bmatrix}6&6&5\\6&6&5\\6&6&6\end{bmatrix}$$

$$\boldsymbol{O}_{\text{free}}=\begin{bmatrix}3&3&3\\3&3&3\\4&4&3\end{bmatrix}\quad \boldsymbol{O}_{\text{passive}}=\begin{bmatrix}6&6&5\\6&6&5\\6&6&6\end{bmatrix} \tag{20}$$

3.4.3.2 Case studies

(1) Failure mode: Inversion Control

Inversion Control could be one of the most severe failure modes when a vehicle negotiates curves as the actuator will exert inverse force on wheelset so that the kinematics of wheelset could be in the worse situation for curve negotiation. In the following part, Inversion control will be used as an example to show how fault-tolerant analysis is performed.

As the actuation system on tangent track works in passive mode, so this failure is simulated only on tight curve R250. In normal condition and in failure mode “Inversion control”, the time histories

of derailment coefficient for actuation schemes B1, B2 and B3 are compared in Figure 58 to Figure 60.

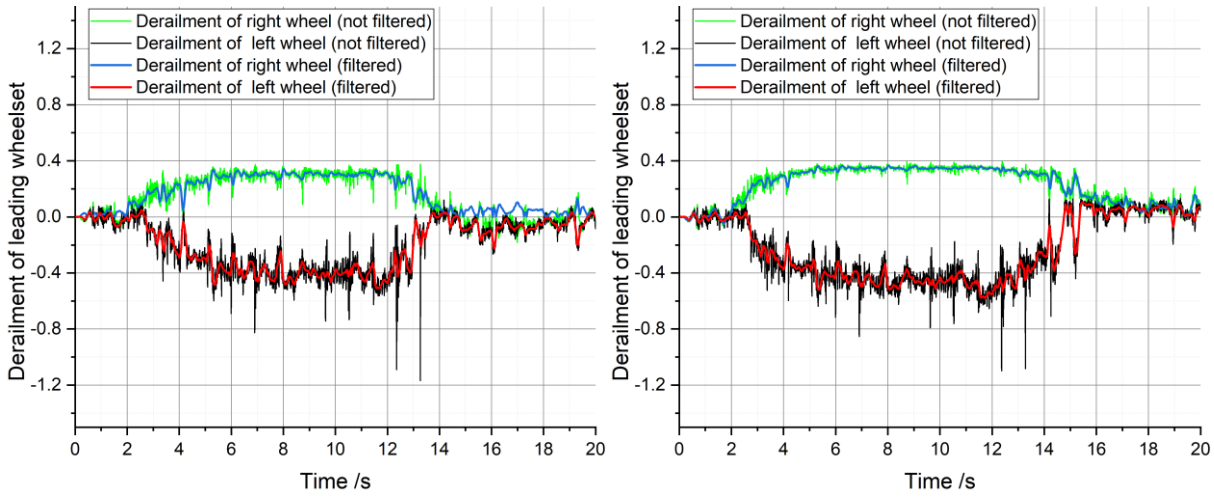

(a) Normal control (b) Inversion control

Figure 58 - Time history of derailment coefficient (Y/Q) for scheme B1 in (a) normal control and (b) Inversion control

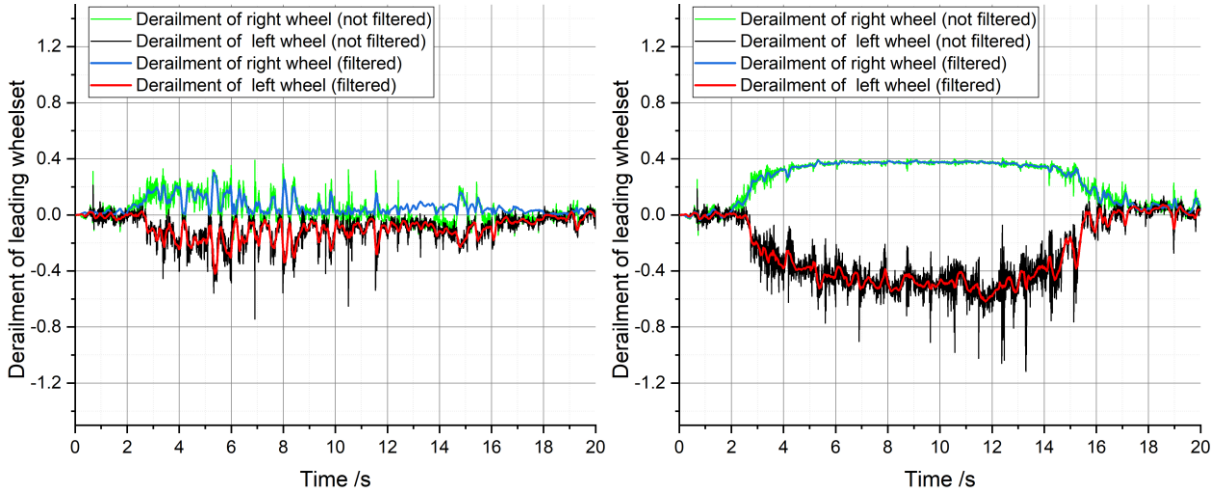

(a) Normal control (b) Inversion control

Figure 59 - Time history of derailment coefficient (Y/Q) for scheme B2 in (a) normal control and (b) Inversion control

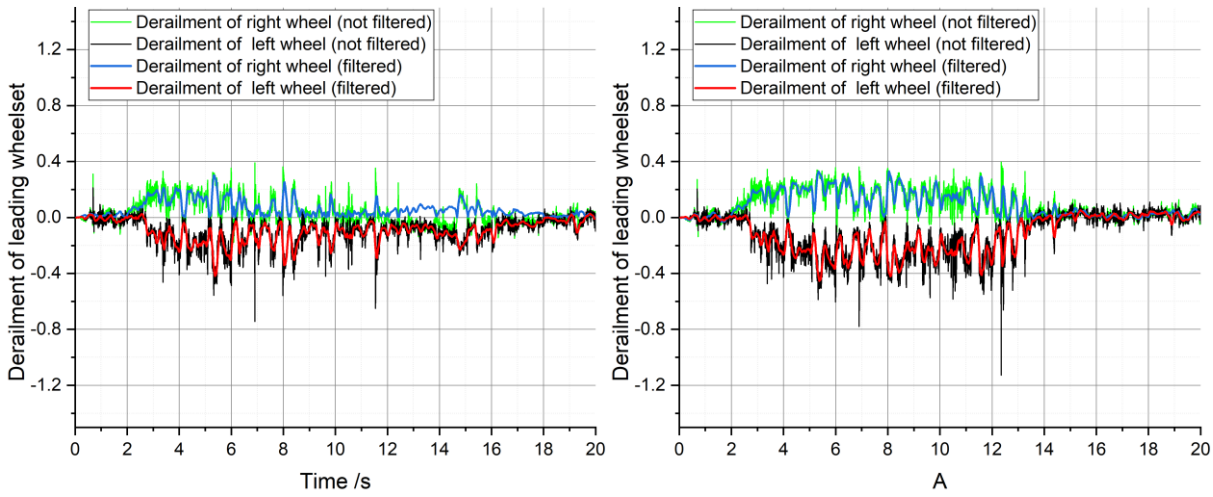

(a) Normal control (b) Inversion control

Figure 60 - Time history of derailment coefficient (Y/Q) for scheme B3 in (a)normal control and (b)Inversion control

For schemes B1 and B3, as passive springs or redundant actuators are applied, the Inversion control doesn't make significant rise of derailment coefficient, whilst for scheme B2, the amplitude of derailment coefficient increases but with 20Hz lowpass filter and the sliding mean defined in EN 14363 [128], the derailment coefficient is still under the limit value 0.8.

The corresponding track shift forces are presented in Figure 61 to Figure 63. For schemes B1 and B3, the track shift force doesn't change drastically, whilst the failure mode on scheme B2 introduces much larger track shift force. However, when the filters are applied, the track shift forces in all schemes can still meet the safety requirement.

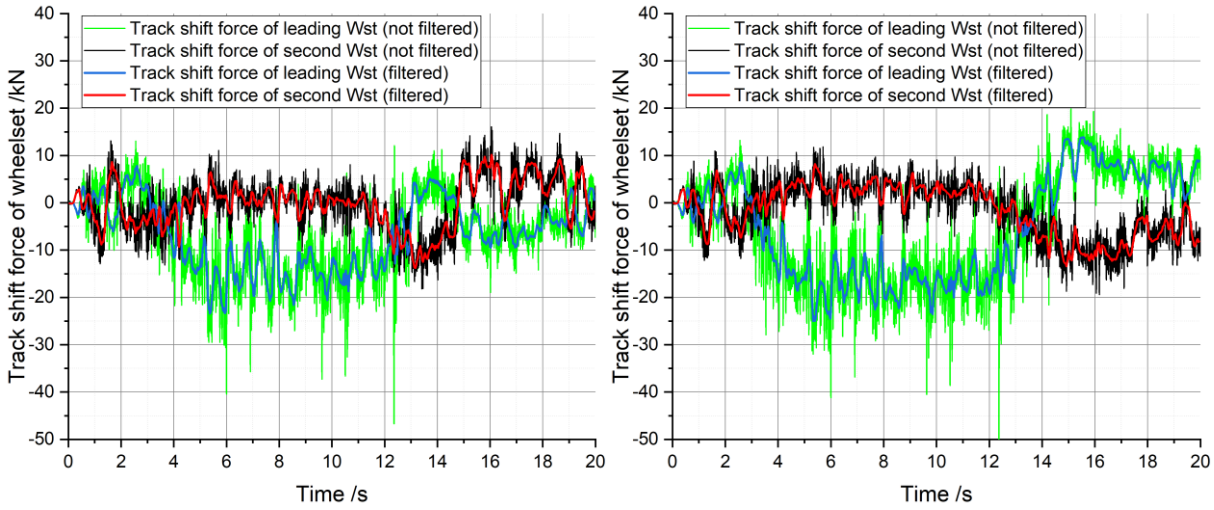

(a) Normal control (b) Inversion control

Figure 61 - Time history of track shift force for scheme B1 in (a) normal control and (b) Inversion control

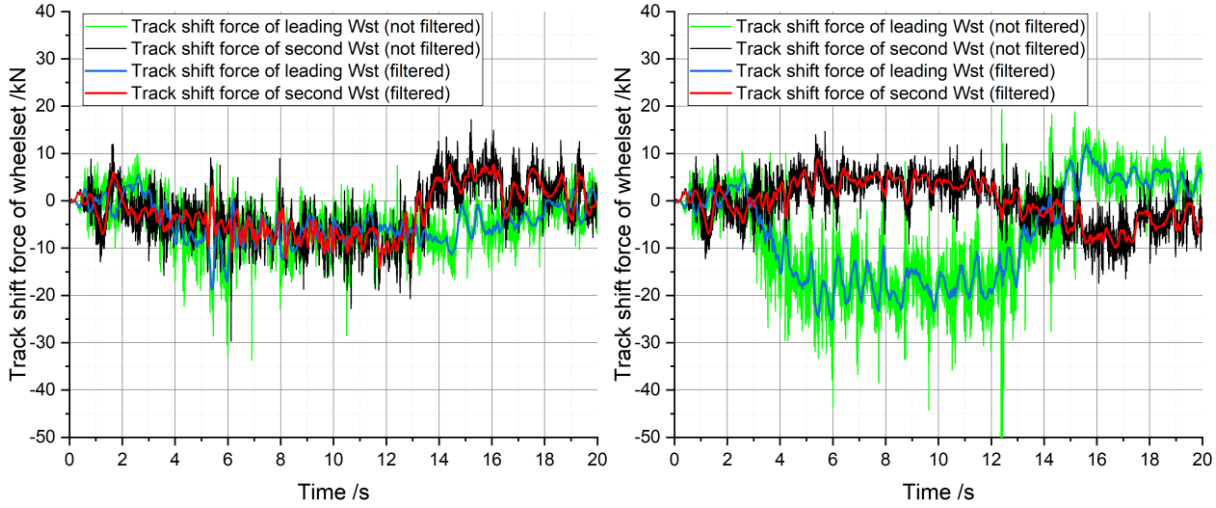

(a) Normal control (b) Inversion control

Figure 62 - Time history of track shift force for scheme B2 in (a) normal control and (b) Inversion control

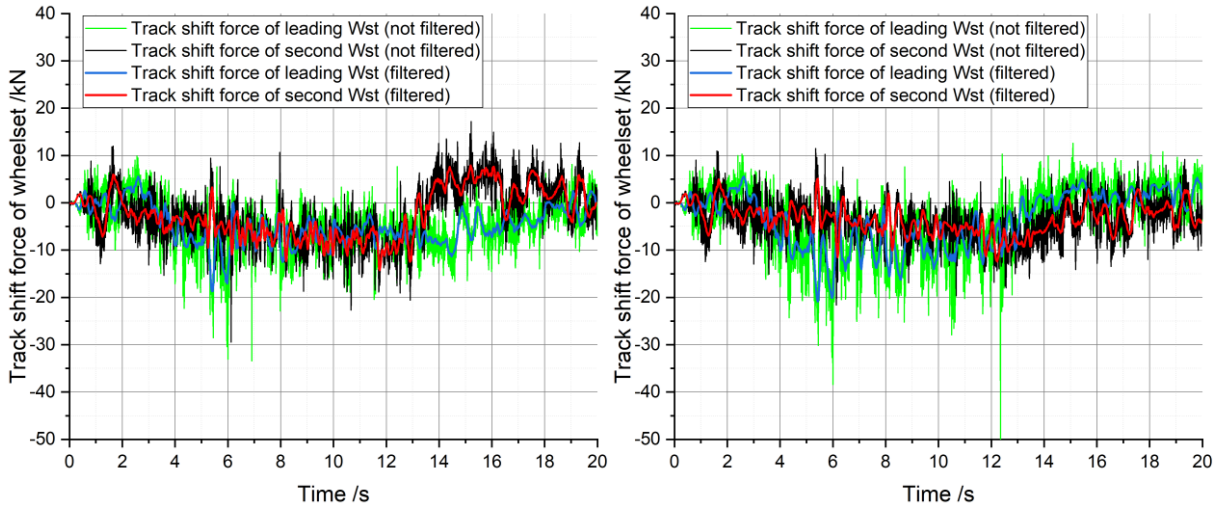

(a) Normal control (b)Inversion control

Figure 63 - Time history of track shift force for scheme B3 in (a) normal control and (b) Inversion control

Based on the above simulations, the characterised values for derailment coefficient and track shift force (the maximum value between the leading wheelset and second wheelset) in all three-by-three schemes are obtained and presented in Figure 64(a) and (b).

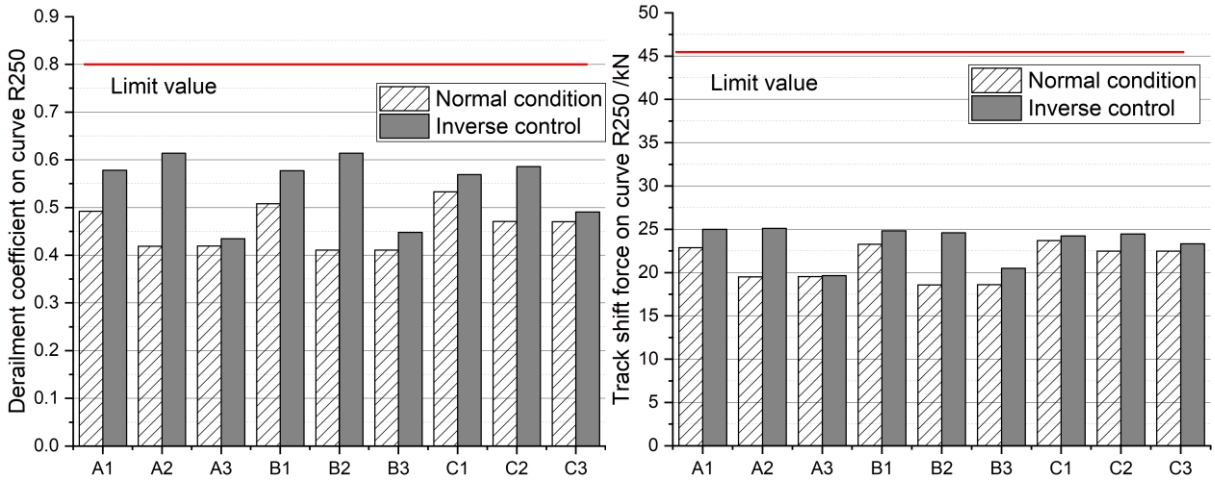

(a) (b)

Figure 64 - (a) Derailment coefficient and (b) track shift force on Curve R250 in normal condition and Inverse control

The increase of the factors from the normal condition to the failure condition is clear, especially for schemes A2, B2 and C2 in which neither passive springs nor redundant actuators are implemented

as the back-up. The values of factors then are processed to severity levels s according to the method described in Section3.4.2.

$$S = \begin{bmatrix} s_{A1} & s_{B1} & s_{C1} \\ s_{A2} & s_{B2} & s_{C2} \\ s_{A3} & s_{B3} & s_{C3} \end{bmatrix} \quad (21)$$

$$S_{Y/Q,\text{inverse}} = \begin{bmatrix} 2 & 2 & 2 \\ 3 & 3 & 2 \\ 1 & 1 & 1 \end{bmatrix} \quad S_{\sum Y,\text{inverse}} = \begin{bmatrix} 1 & 1 & 1 \\ 2 & 2 & 1 \\ 1 & 1 & 1 \end{bmatrix} \quad S_{\text{inverse}} = \begin{bmatrix} 2 & 2 & 2 \\ 3 & 3 & 2 \\ 1 & 1 & 1 \end{bmatrix} \quad (22)$$

The matrix S, as shown in Equation (21), is used as the form to display the severity levels for the three-by-three actuation schemes. The first and second matrix in Equation (22) present the severity levels based on derailment coefficient and track shift force respectively and the higher severity level between the two is selected as the comprehensive assessment, as shown in the third matrix.

(2) Failure mode: Max force

With the same method as is illustrated for Inversion control, the failure mode Max force is simulated. For the sake of brevity, we only present the bar charts for derailment coefficient and track shift force on tangent track and tight curve R250 as are shown in Figure 65 and Figure 66. The severity values are presented in Equation (23) and Equation (24).

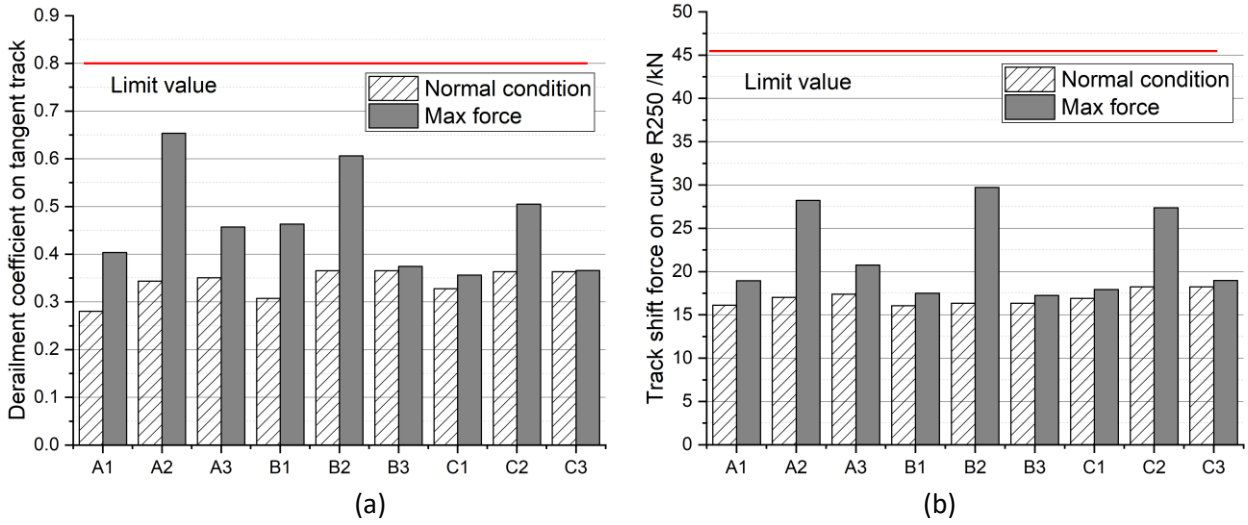

Figure 65 - (a) Derailment coefficient and (b) track shift force on tangent track in normal condition and Maximum force

$$S_{\frac{Y}{Q},\text{maxforce},1} = \begin{bmatrix} 2 & 2 & 1 \\ 4 & 3 & 2 \\ 2 & 1 & 1 \end{bmatrix} \quad S_{\sum Y,\text{maxforce},1} = \begin{bmatrix} 1 & 1 & 1 \\ 2 & 3 & 2 \\ 1 & 1 & 1 \end{bmatrix} \quad S_{\text{maxforce},1} = \begin{bmatrix} 2 & 2 & 1 \\ 4 & 3 & 2 \\ 2 & 1 & 1 \end{bmatrix} \quad (23)$$

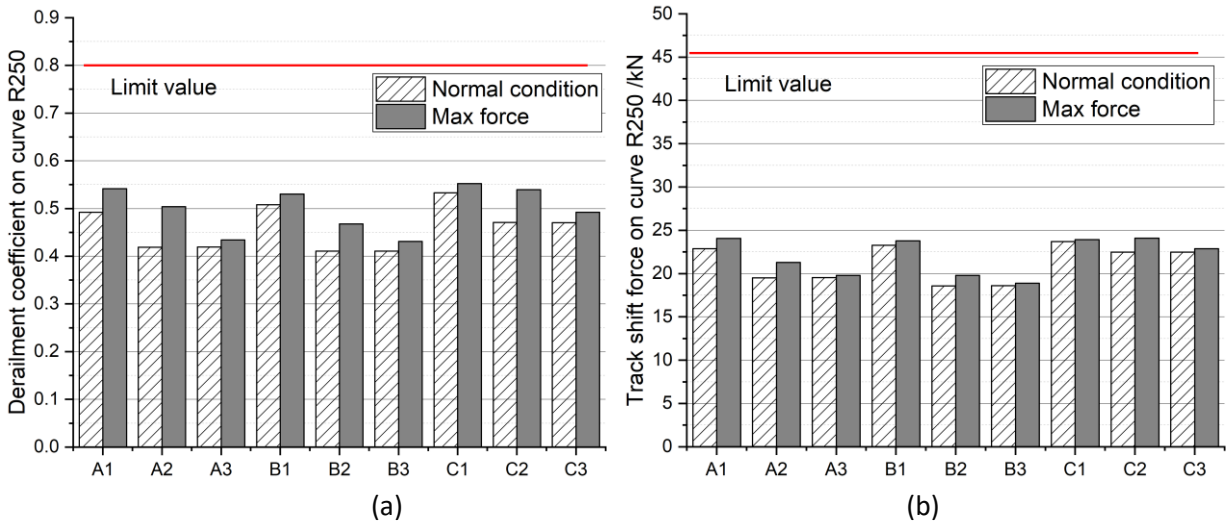

Figure 66 - (a) Derailment coefficient and (b) track shift force on R250 in normal condition and Maximum force

$$\boldsymbol{S}_{\frac{Y}{Q},\mathbf{maxforce,2}} = \begin{bmatrix} \mathbf{2} & \mathbf{1} & \mathbf{1} \\ \mathbf{2} & \mathbf{2} & \mathbf{2} \\ \mathbf{1} & \mathbf{1} & \mathbf{1} \end{bmatrix} \quad \boldsymbol{S}_{\sum Y,\mathbf{maxforce,2}} = \begin{bmatrix} \mathbf{1} & \mathbf{1} & \mathbf{1} \\ \mathbf{1} & \mathbf{1} & \mathbf{1} \\ \mathbf{1} & \mathbf{1} & \mathbf{1} \end{bmatrix} \quad \boldsymbol{S}_{\mathbf{maxforce,2}} = \begin{bmatrix} \mathbf{2} & \mathbf{1} & \mathbf{1} \\ \mathbf{2} & \mathbf{2} & \mathbf{2} \\ \mathbf{1} & \mathbf{1} & \mathbf{1} \end{bmatrix} \quad \textbf{(24)}$$

Based on the figures and severity values, the failure mode Max force on tangent track is more severe than the situation on tight curve R250. In this failure mode, the vehicle is still safe in extreme conditions.

(3) Failure mode: Random force

Based on the same method, the simulation results for failure mode Random force are presented in Figure 67 and Figure 68, and corresponding severity values are presented in Equation (25) and Equation (26).

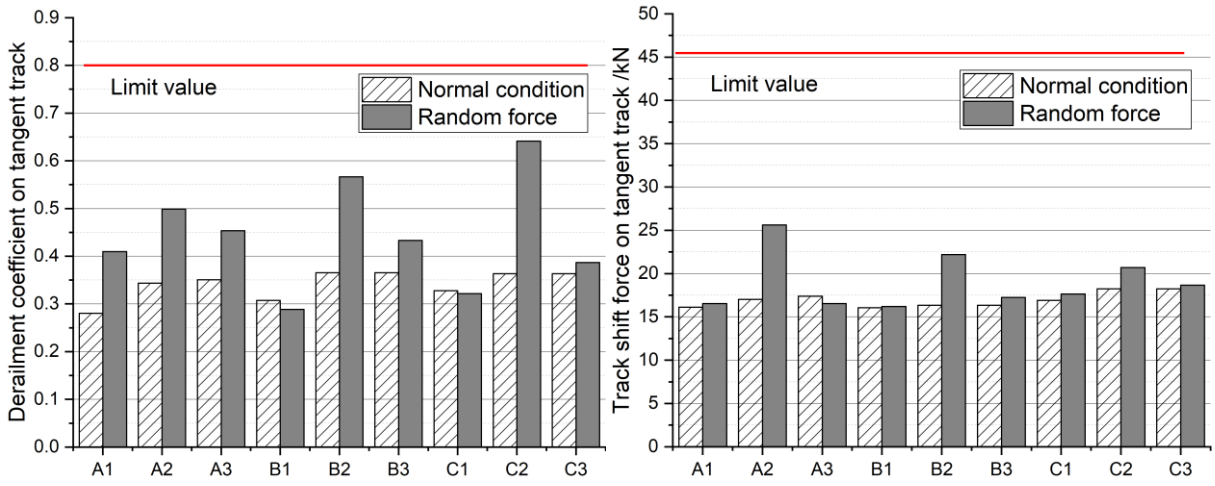

Figure 67 - (a) Derailment coefficient and (b) track shift force on tangent track in normal condition and Random force

$$\boldsymbol{S}_{\frac{Y}{Q},\mathbf{randforce},1} = \begin{bmatrix} \mathbf{2} & \mathbf{1} & \mathbf{1} \\ \mathbf{2} & \mathbf{3} & \mathbf{4} \\ \mathbf{1} & \mathbf{2} & \mathbf{1} \end{bmatrix} \quad \boldsymbol{S}_{\sum Y,\mathbf{randforce},1} = \begin{bmatrix} \mathbf{1} & \mathbf{1} & \mathbf{1} \\ \mathbf{2} & \mathbf{2} & \mathbf{1} \\ \mathbf{1} & \mathbf{1} & \mathbf{1} \end{bmatrix} \quad \boldsymbol{S}_{\mathbf{randforce},1} = \begin{bmatrix} \mathbf{2} & \mathbf{1} & \mathbf{1} \\ \mathbf{2} & \mathbf{3} & \mathbf{4} \\ \mathbf{2} & \mathbf{2} & \mathbf{1} \end{bmatrix} \quad (25)$$

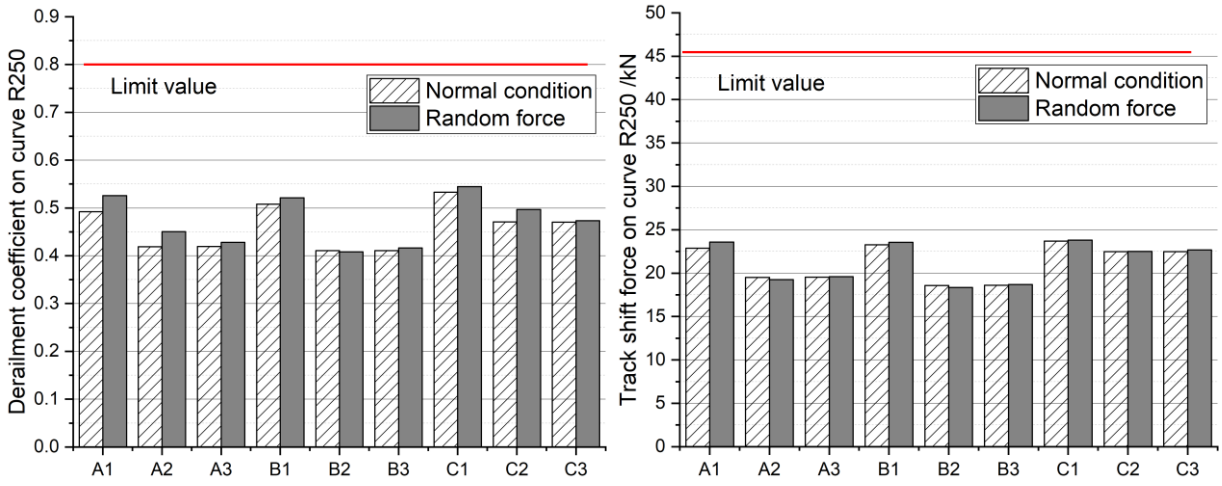

Figure 68 - (a) Derailment coefficient and (b) track shift force on curve R250 in normal condition and Random force

$$\boldsymbol{S}_{\frac{Y}{Q},\mathbf{maxforce},2} = \begin{bmatrix} \mathbf{1} & \mathbf{1} & \mathbf{1} \\ \mathbf{1} & \mathbf{1} & \mathbf{1} \\ \mathbf{1} & \mathbf{1} & \mathbf{1} \end{bmatrix} \quad \boldsymbol{S}_{\sum Y,\mathbf{maxforce},2} = \begin{bmatrix} \mathbf{1} & \mathbf{1} & \mathbf{1} \\ \mathbf{1} & \mathbf{1} & \mathbf{1} \\ \mathbf{1} & \mathbf{1} & \mathbf{1} \end{bmatrix} \quad \boldsymbol{S}_{\mathbf{maxforce},2} = \begin{bmatrix} \mathbf{1} & \mathbf{1} & \mathbf{1} \\ \mathbf{1} & \mathbf{1} & \mathbf{1} \\ \mathbf{1} & \mathbf{1} & \mathbf{1} \end{bmatrix} \quad (26)$$

From these results, the Random force can increase the severity on tangent track, similar to the effects of the failure mode Max force.

(4) Failure mode: Free (Zero Force)

For failure mode Free (Zero force), Figure 69 and Figure 70 present the bar charts for derailment coefficient and track shift force on tangent track and tight curve R250 and corresponding severity values are presented in Equation (27) and Equation (28).

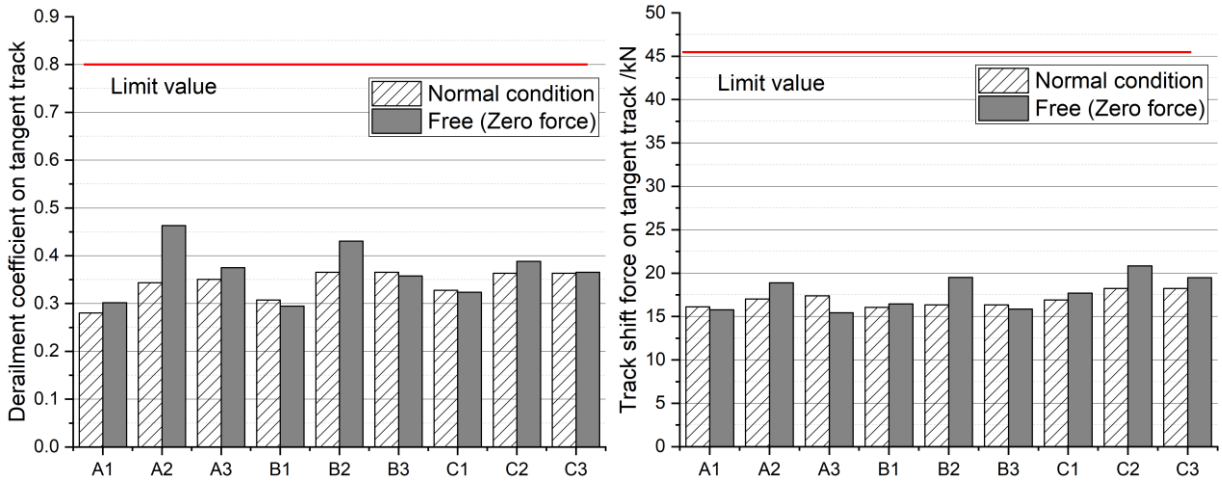

Figure 69 - (a) Derailment coefficient and (b) track shift force on tangent track in normal condition and Free

$$\boldsymbol{S}_{\frac{Y}{Q},\mathbf{free},1} = \begin{bmatrix} 1 & 1 & 1 \\ 2 & 2 & 1 \\ 1 & 1 & 1 \end{bmatrix} \quad \boldsymbol{S}_{\sum Y,\mathbf{free},1} = \begin{bmatrix} 1 & 1 & 1 \\ 1 & 1 & 1 \\ 1 & 1 & 1 \end{bmatrix} \quad \boldsymbol{S}_{\mathbf{fress},1} = \begin{bmatrix} 1 & 1 & 1 \\ 2 & 2 & 1 \\ 1 & 1 & 1 \end{bmatrix} \tag{27}$$

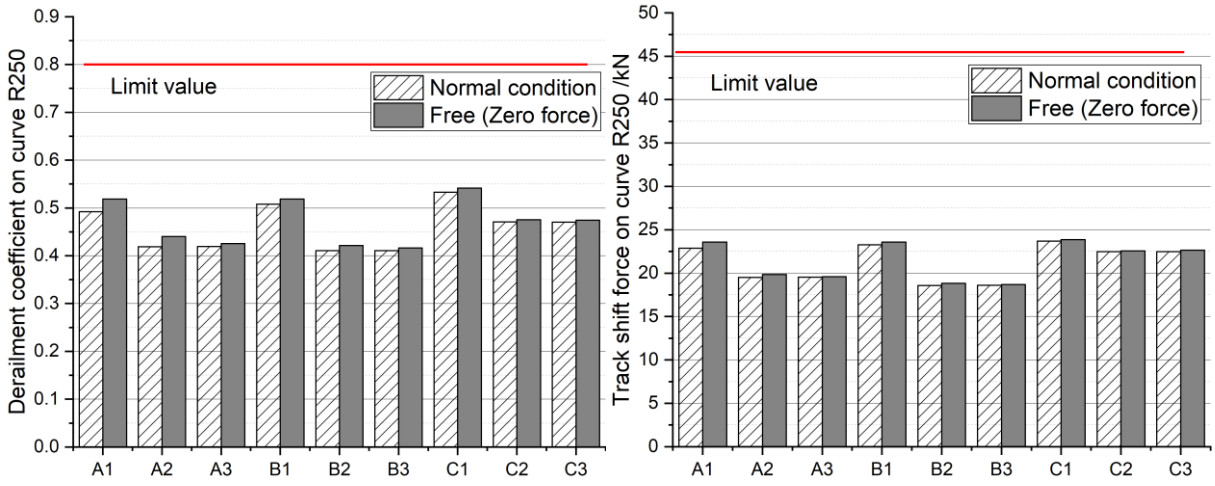

Figure 70 - (a) Derailment coefficient and (b) track shift force on curve R250 in normal condition and Free

$$\boldsymbol{S}_{\frac{Y}{Q},\mathbf{free},2} = \begin{bmatrix} 1 & 1 & 1 \\ 1 & 1 & 1 \\ 1 & 1 & 1 \end{bmatrix} \quad \boldsymbol{S}_{\sum Y,\mathbf{free},2} = \begin{bmatrix} 1 & 1 & 1 \\ 1 & 1 & 1 \\ 1 & 1 & 1 \end{bmatrix} \quad \boldsymbol{S}_{\mathbf{free},2} = \begin{bmatrix} 1 & 1 & 1 \\ 1 & 1 & 1 \\ 1 & 1 & 1 \end{bmatrix} \tag{28}$$

The failure mode Zero force in the above simulations shows limited degradation of dynamic behaviours, and there is no sign of vehicle instability arising from the lack of longitudinal stiffness. This is because, in the original passive bogie, the anti-hunting damper and the coil spring above the axle-box still ensure a good stability even when a large part of the primary longitudinal stiffness is lost at one side of wheelset. If the anti-hunting damper is removed, the failure Zero force will have a much more severe impact at high speed.

(5) Failure mode: Zero/No Signal (Passive mode)

As the passive mode is the normal status when the vehicle runs on tangent track, therefore the failure mode Zero/No signal (passive mode) is only simulated on curve R250. Figure 71 presents the derailment coefficient and track shift force and corresponding severity values are displayed in Equation (29). Based on the simulation, the Passive mode has negligible impacts on safety.

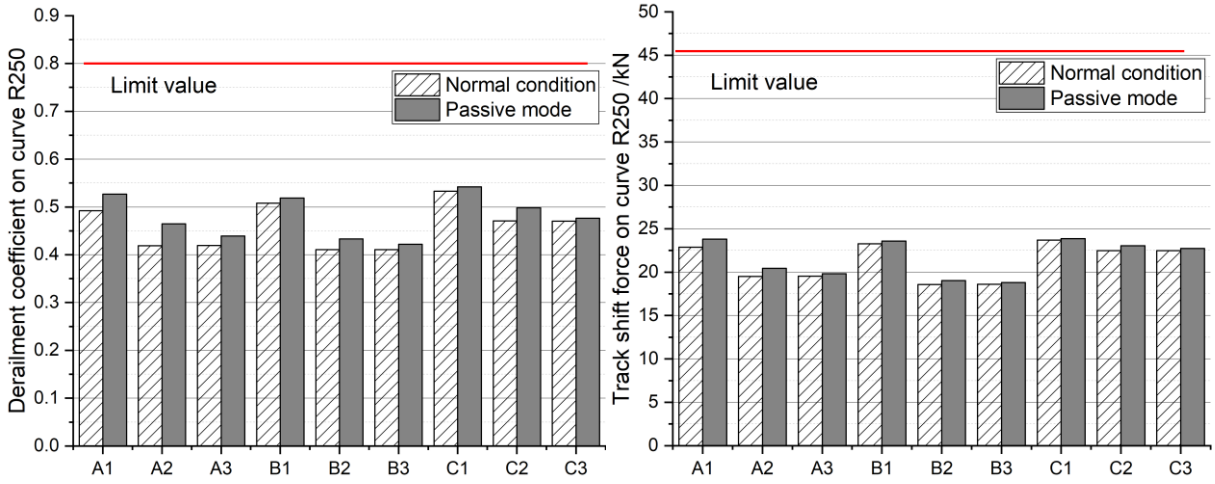

Figure 71 - (a) Derailment and (b) track shift force on curve R250 in normal condition and Passive mode

$$\boldsymbol{S}_{Y/Q,\text{passive}} = \begin{bmatrix} 1 & 1 & 1 \\ 1 & 1 & 1 \\ 1 & 1 & 1 \end{bmatrix} \quad \boldsymbol{S}_{\sum Y,\text{passive}} = \begin{bmatrix} 1 & 1 & 1 \\ 1 & 1 & 1 \\ 1 & 1 & 1 \end{bmatrix} \quad \boldsymbol{S}_{\text{passive}} = \begin{bmatrix} 1 & 1 & 1 \\ 1 & 1 & 1 \\ 1 & 1 & 1 \end{bmatrix} \qquad (29)$$

Finally, all the Severity values are summarized in Table 12, showing that the Max force, Random force and Inversion control are first three dangerous failure modes, followed by Free and Zero signal. Implementing redundant structure is effective to ensure the safety, while without back-up for actuation system the severity levels will increase, but in all conditions analysed here, the vehicle still meets the safety requirement.

Table 12 - Severity levels of different actuation schemes in typical failure modes

	Inversion	Max force		Random force		Free (Zero force)		Zero signal (passive)
Schemes	R250	Tangent	R250	Tangent	R250	Tangent	R250	R250
A1	2	2	2	2	1	1	1	1
B1	2	2	1	1	1	1	1	1
C1	2	1	1	1	1	1	1	1
A2	3	4	2	2	1	2	1	1
B2	3	3	2	3	1	2	1	1
C2	2	2	2	4	1	1	1	1
A3	1	2	1	2	1	1	1	1
B3	1	1	1	2	1	1	1	1
C3	1	1	1	1	1	1	1	1

As for the RPN values, because the Detection level is not involved in this work, the Severity value and Occurrence value are multiplied for RPN calculation, as is shown in Table 13. This table clearly reveals the risks of failure modes and also the capability of fault tolerance of different actuation schemes. In general, the actuation schemes with neither passive springs nor redundant structures have high risks of safety issues, and the failure modes Random force, Max force and Inversion control need more attention. Apart from making comparisons between different schemes, the RPN value can also be used to evaluate the improvement between the previous and modified schemes in the design process.

Table 13 - RPN values of different actuation schemes in typical failure modes

	Inversion	Max force		Random force		Free (Zero force)		Zero/No signal (passive)
Schemes	R250	Tangent	R250	Tangent	R250	Tangent	R250	R250
A1	10	10	10	12	6	3	3	6
B1	12	12	6	6	6	3	3	6
C1	10	5	5	5	5	3	3	5
A2	15	20	10	12	6	6	3	6
B2	18	18	12	18	6	6	3	6
C2	10	10	10	20	5	3	3	5
A3	6	12	6	12	6	4	4	6
B3	6	6	6	12	6	4	4	6
C3	6	6	6	6	6	3	3	6

It should be noted that the above conclusions for different failure modes cannot be directly extended to other railway vehicles, because the severity of failure modes is not only determined by the active actuation system, and is also affected by the parameters of the passive suspension, which will differ for different vehicle designs.

3.5 SEMI-ACTIVE SECONDARY VERTICAL SUSPENSION

The target of this section is to explore the different control strategies for semi-active secondary vertical suspension and their effects on ride comfort of railway vehicles. A simplified one-quarter vehicle dynamics model and a full MBS model of the vehicle with flexible car body are implemented to test the semi-active suspension and a model of MR damper and its control are considered to study the effect of its dynamic behaviour. Several classic control strategies are compared and new ones are proposed, named Maximum Power Point Tracking (MPPT) and Modified MPPT, which can provide satisfying performance and are easier to implement.

3.5.1 Simulation models and their configurations

To understand the control strategies for semi-active secondary vertical suspension and validate their effects in the rail vehicle, two dynamics models are considered: 1 simple one-quarter vehicle model built in Simulink and 2 the full vehicle model built in SIMPACK.

(1) One-quarter vehicle model in Simulink

Based on the classic one-quarter vehicle model, a modified vehicle model was proposed, as is shown in Figure 72 where an additional virtual mass is connected to the car body with spring and damper to generate vibration at around 8Hz, to simulate the high-frequency vibration from flexibility of the car body. By doing so, the model can be used to test the attenuating effects of semi-active suspension in a relatively high frequency range. The parameters of this simple model are scaled according to the baseline SIMPACK model, and are presented in Table 14. In the semi-active control, the damping force between the bogie and car body is generated from the damper according to the control strategy considered.

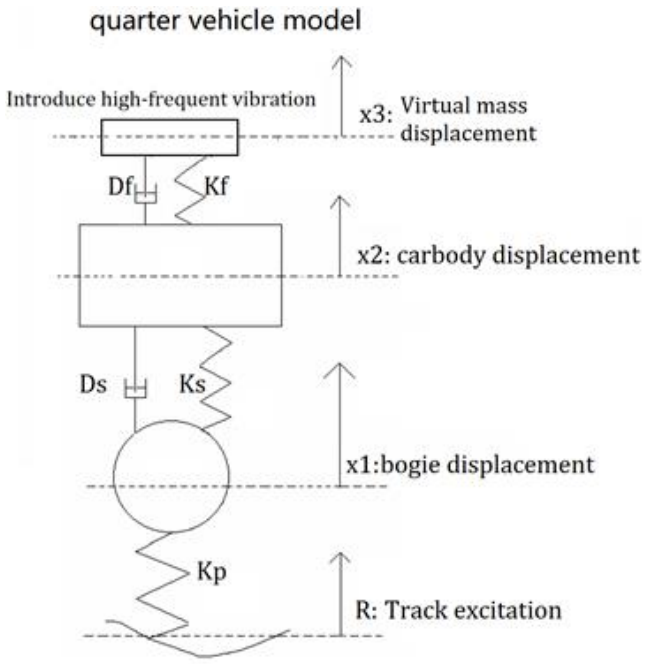

Figure 72 – Modified one-quarter vehicle model

Table 14 - Parameters of modified one-quarter vehicle model

Parameters	Value
Mass of car body	7.5 t
Mass of bogie	1.25 t
Virtual mass	1 t
Primary stiffness K_p	1 MN/m
Secondary stiffness K_s	0.15 MN/m
Secondary damping D_s	30 kNs/m
Stiffness of virtual mass	2.2MN/m
Damping of virtual mass	500Ns/m

(2) Full vehicle model in SIMPACK

Further to the simple one-quarter vehicle model, a complete MBS vehicle model was defined in SIMPACK. The original baseline model described in Section 3.2 was modified to make it consistent with a finite element model of a flexible car body available from a project partner. In this way, it is possible to consider the ability of the semi-active suspension and related control strategy to mitigate high-frequency vibration (in a range up to 30 Hz) excited by car body flexible modes. The first

bending mode of this flexible car body is at around 8 Hz and the other flexible modes below 30 Hz are all included in this model. The full vehicle model with flexible car body is shown in Figure 73.

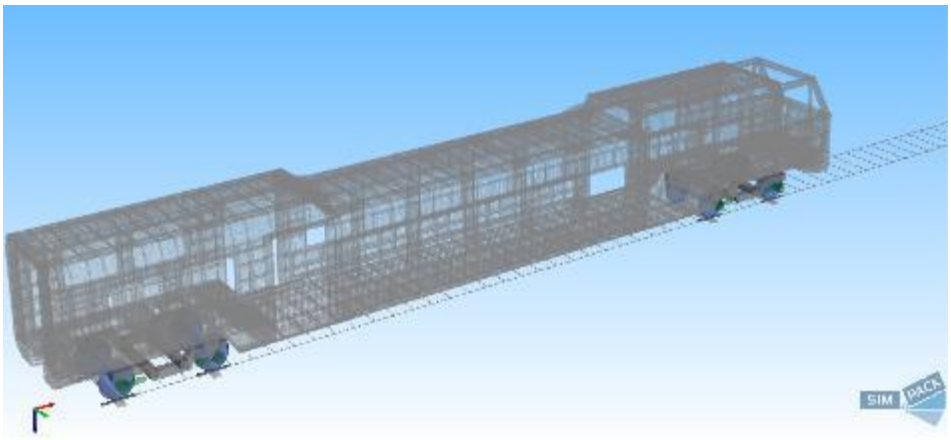

Figure 73 - Full vehicle model considering car body flexibility

3.5.2 Control strategies for semi-active secondary vertical suspension

There are various types of control strategies for semi-active suspension. According to the functionality of the damper technologies, the control strategies can be divided into two basic categories: two-state (on-off) control and continuous control. In two-state control, the semi-active damper is switched between two states providing the minimum and maximum damping effect. By contrast, the continuous control strategies can only be applied with the dampers which can generate damping varying continuously. The control strategies analysed in this work are listed in Table 15.

Table 15 - The category of control strategies

Two-state control strategies	Continuous control strategies
(1) Two-state Skyhook control	(1) Continuous Skyhook control
(2) Two-state ADD control	(2) Continuous ADD control
(3) Two-state Mixed ADD & Skyhook control	(3) Continuous Mixed ADD & Skyhook control
	(4) MPPT
	(5) Modified MPPT

3.5.2.1 Two-state Skyhook and Continuous Skyhook

(1) Two-state Skyhook control

The basic definition for the classic Skyhook control in railway suspension is presented in Equation (30):

$$\boldsymbol{F_{sky} = -C_s \dot{x}_2} \tag{30}$$

where C_s is the controllable damping; $\dot{x}_2$ is the velocity of the car body in lateral or vertical direction; F_{sky} represents the desired damping force. For the two-state Skyhook control, the controllable damping C_s is set to the maximum value when the directions of car-body velocities ($\dot{x}_2$) and velocity of the damper ($\dot{x}_2 - \dot{x}_1$) have the same sign, i.e. when the force generated by the damper is producing a dissipation, and is set to the minimum value otherwise, as shown in Equation (31).

$$\boldsymbol{C_s = \begin{cases} C_{max} & if: \dot{x}_2 (\dot{x}_2 - \dot{x}_1) \geq 0 \\ C_{min} & if: \dot{x}_2 (\dot{x}_2 - \dot{x}_1) < 0 \end{cases}} \tag{31}$$

In the dynamics model, the generated damping force is calculated according to the Equation (32)

$$\boldsymbol{F_{sky} = \begin{cases} -C_{max} \cdot (\dot{x}_2 - \dot{x}_1) & if: \dot{x}_2 (\dot{x}_2 - \dot{x}_1) \geq 0 \\ -C_{min} \cdot (\dot{x}_2 - \dot{x}_1) & if: \dot{x}_2 (\dot{x}_2 - \dot{x}_1) < 0 \end{cases}} \tag{32}$$

(2) Continuous skyhook control

By comparing Equation (30) and (32), it can be seen that in the Two-state Skyhook control, actual generated damping force is different from the ideal one because of the bogie's motion, i.e. $\dot{x}_1$ not being equal to 0. Considering this, the Continuous Skyhook control is proposed to compensate for the effect of relative velocity between the bogie and car body, as presented in Equation (33).

$$\boldsymbol{C_s = \begin{cases} \min \left[C_{max} \cdot \frac{\dot{x}_2}{(\dot{x}_2 - \dot{x}_1)}, C_{max} \right] & if: \dot{x}_2 (\dot{x}_2 - \dot{x}_1) \geq 0 \\ \max \left[C_{min} \cdot \frac{\dot{x}_2}{(\dot{x}_2 - \dot{x}_1)}, C_{min} \right] & if: \dot{x}_2 (\dot{x}_2 - \dot{x}_1) < 0 \end{cases}} \tag{33}$$

3.5.2.2 Two-state ADD and continuous ADD

The control strategy Two-state Acceleration Driven Damper (ADD) has the same form as the Two-state Skyhook but the sign of car body acceleration $\ddot{x}_2$ is applied instead of car body velocity $\dot{x}_2$, as is shown in Equation (34). The ADD has been proved to be effective to attenuate high-frequency vibrations[57].

$$\boldsymbol{C_s = \begin{cases} C_{max} & if\ \ddot{x}_2 (\dot{x}_2 - \dot{x}_1) \geq 0 \\ C_{min} & if\ \ddot{x}_2 (\dot{x}_2 - \dot{x}_1) < 0 \end{cases}} \tag{34}$$

To our knowledge, a continuous form of the ADD control was not proposed so far in the literature, but based on the form of Continuous Skyhook control, it is proposed in this work as is shown in Equation (35).

$$C_s = \begin{cases} \min\left[C_{max} \cdot \frac{\dot{x}_2}{(\dot{x}_2 - \dot{x}_1)}, C_{max}\right] & if\ \ddot{x}_2\,(\dot{x}_2 - \dot{x}_1) \geq 0 \\ \max\left[C_{min} \cdot \frac{\dot{x}_2}{(\dot{x}_2 - \dot{x}_1)}, C_{min}\right] & if\ \ddot{x}_2\,(\dot{x}_2 - \dot{x}_1) < 0 \end{cases} \quad (35)$$

3.5.2.3 Two-state Mixed ADD & Skyhook and Continuous Mixed ADD & Skyhook

As is studied in [58], the control strategy of Two-state ADD has good attenuating effect for high-frequency vibrations but has poor performance in low-frequency range, whilst the Two-state Skyhook control has the opposite feature in the low and high-frequency ranges. A new control strategy is proposed aimed at taking advantage of the two control strategies and to produce good effects in all frequency ranges. Equation (36) presents this Two-state Mixed ADD & Skyhook control algorithm.

$$C_s = \begin{cases} C_{max} & if: \left(\ddot{x}_2^{\,2} - \alpha^2 \dot{x}_2^{\,2}\right) < 0\ and\ \ddot{x}_2\,(\dot{x}_2 - \dot{x}_1) \geq 0 \quad case\ 1 \\ C_{max} & if: \left(\ddot{x}_2^{\,2} - \alpha^2 \dot{x}_2^{\,2}\right) > 0\ and\ \ddot{x}_2\,(\dot{x}_2 - \dot{x}_1) \geq 0 \quad case\ 2 \\ C_{min} & if: \left(\ddot{x}_2^{\,2} - \alpha^2 \dot{x}_2^{\,2}\right) < 0\ and\ \ddot{x}_2\,(\dot{x}_2 - \dot{x}_1) < 0 \quad case\ 3 \\ C_{min} & if: \left(\ddot{x}_2^{\,2} - \alpha^2 \dot{x}_2^{\,2}\right) > 0\ and\ \ddot{x}_2\,(\dot{x}_2 - \dot{x}_1) < 0 \quad case\ 4 \end{cases} \quad (36)$$

In this equation, a new parameter α is introduced as a cross-over point between the ADD and Skyhook controls. When α tends to be zero, this control will become the ADD and if α tends to be a positive infinite value, this control is equal to Skyhook control. In order to find the suitable α, we sweep the different values normally from 1 to 10 and select the one producing the best ride comfort.

There is no definition for continuous Mixed ADD & Skyhook, so we propose this control method, shown in Equation (37), based on the form of continuous Skyhook control, as we did to define Continuous ADD.

$$C_s = \begin{cases} min\left[C_{max} \cdot \frac{\dot{x}_2}{(\dot{x}_2 - \dot{x}_1)}, C_{max}\right] & if: \left(\ddot{x}_2^{\,2} - \alpha^2 \dot{x}_2^{\,2}\right) < 0\ and\ \ddot{x}_2\,(\dot{x}_2 - \dot{x}_1) \geq 0 \quad case\ 1 \\ min\left[C_{max} \cdot \frac{\dot{x}_2}{(\dot{x}_2 - \dot{x}_1)}, C_{max}\right] & if: \left(\ddot{x}_2^{\,2} - \alpha^2 \dot{x}_2^{\,2}\right) > 0\ and\ \ddot{x}_2\,(\dot{x}_2 - \dot{x}_1) \geq 0 \quad case\ 2 \\ max\left[C_{min} \cdot \frac{\dot{x}_2}{(\dot{x}_2 - \dot{x}_1)}, C_{min}\right] & if: \left(\ddot{x}_2^{\,2} - \alpha^2 \dot{x}_2^{\,2}\right) < 0\ and\ \ddot{x}_2\,(\dot{x}_2 - \dot{x}_1) < 0 \quad case\ 3 \\ max\left[C_{min} \cdot \frac{\dot{x}_2}{(\dot{x}_2 - \dot{x}_1)}, C_{min}\right] & if: \left(\ddot{x}_2^{\,2} - \alpha^2 \dot{x}_2^{\,2}\right) > 0\ and\ \ddot{x}_2\,(\dot{x}_2 - \dot{x}_1) < 0 \quad case\ 4 \end{cases} \quad (37)$$

3.5.2.4 Maximum Power Point Tracking (MPPT)

The Maximum Power Point Tracking (MPPT) is a technique used in the photovoltaic solar system to generate maximum power in a variable condition. One classic algorithm for this problem is *Perturb and observe* where the controller adjusts the voltage by a small amount and then the output power is observed. If the power increases, further adjustments in that direction are tried until power

starts to decrease. Otherwise, if the power decreases, an adjustment is taken in the opposite direction and the procedure is repeated.
This algorithm can be implemented to attenuate the vibration of the mechanical system. In the background of semi-active suspension, the controllable variable is the damping C_{mppt} and control target can be represented as cost function $J(t)$ which is defined as the root mean square of car body acceleration in a "time window" as is shown in Equation (38)

$$\boldsymbol{J(t) = \sqrt{\frac{1}{n_w}\sum_{i=t-n_w}^{t} \ddot{x}_2(i)^2}} \quad \textbf{(38)}$$

where n_w is the number of acceleration data measured in a time window T. Assuming that acceleration values are available at discrete intervals with a constant sampling time Δt, n_w in Equation (38) is the ratio of the time window length over the sampling time $n_w = {}^{T}/_{\Delta t}$.
The control strategy is presented in Equation (39), where the current damping $C_{mppt}(t)$ equals to the damping at last step $C_{mppt}(t-1)$ plus the contribution of cost function's variation "$-coef \cdot [J(t) - J(t-1)]$". The constant parameter $coef$ decides the rate of damping variation in time. In this control strategy, the parameters coef and n_w (or window time) need to be optimized to enable the MPPT to have a good attenuating effect.

$$\boldsymbol{C_{mppt}(t) = C_{mppt}(t-1) - coef \cdot [J(t) - J(t-1)]} \quad \textbf{(39)}$$

The above mentioned algorithm can also be slightly modified as shown in Equation (40) where the cost function at current time $J(t)$ is added to affect the variation speed of damping. When the cost function becomes a relatively large value, which means the current vibration is severe, the damping will be adjusted quickly, whilst if the cost function $J(t)$ remains in a low level, the changing of damping will become slow. The control strategies based on Equation (39) and (40) are referred as MPPT and Modified MPPT.

$$\boldsymbol{C_{mppt}(t) = C_{mppt}(t-1) - coef \cdot J(t) \cdot [J(t) - J(t-1)]} \quad \textbf{(40)}$$

For these two controls, the only required measured signal is the acceleration of the car body, and therefore the MPPT will be simpler and less expensive to implement then the other mentioned control strategies.

3.5.3 Dynamics of Magneto-rheological (MR) Damper and its control

3.5.3.1 MR dynamics model

Magneto-rheological (MR) Damper is a promising technology to be implemented in the field of semi-active suspension. A dynamics model of the MR damper considered in this work is shown in Figure 74 [62].

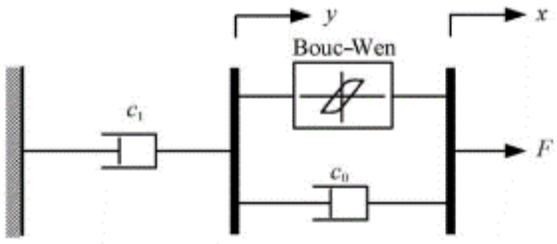

Figure 74 - Schematic of the modified Bouc-Wen model for MR damper [62]

This modified Bouc-Wen model was proposed in [62] and has been validated by experimental tests. Its mathematical model is presented in Equation (41) to Equation (43).

$$\boldsymbol{F = c_1 \dot{y}} \quad \textbf{(41)}$$

$$\boldsymbol{\dot{y} = \frac{1}{c_0 + c_1}(\alpha z + c_0 \dot{x})} \quad \textbf{(42)}$$

$$\boldsymbol{\dot{z} = -\gamma|\dot{x} - \dot{y}||z|^{n-1} - \beta(\dot{x} - \dot{y})|z|^n + A(\dot{x} - \dot{y})} \quad \textbf{(43)}$$

where F is the generated damping force; $\dot{y}$ is an internal velocity; c_1 and c_0 represent the damping coefficients at low velocities and high velocities; $\dot{x}$ is the velocity of piston and z is an evolutional variable; α, γ, β, A and n are parameters associated with the shape of the hysteresis loop. Among these parameters, α and c_0 are the functions of input current signal I, which defines the dynamic behaviour of the MR damper. Equations (44) and (45) express the relationship between the input current and parameters α and c_0

$$\boldsymbol{\alpha = \alpha_a + \alpha_b I + \alpha_c I^2} \quad \textbf{(44)}$$

$$\boldsymbol{c_0 = c_{0a} + C_{0b} I} \quad \textbf{(45)}$$

where, the new parameters α_a, α_b, α_c, c_{0a} and C_{0b}, together with the mentioned c_1 γ, β, A and n should be estimated according to experimental data of a real MR damper. A group of validated parameters as shown in Table 16 are adopted in the MR damper dynamics model [62].

Table 16 - Parameters for Modified Bouc-Wen model

Parameter	Values	Parameter	Values
c_1	91.6Ns mm^{-1}	α_a	40 N mm^{-1}
γ	0.15mm^{-1}	α_b,	2036.8 N mm^{-1}
β	0.15 mm^{-1}	α_c	-535.95 N mm^{-1}
A	4.5	c_{0a}	8.4 Ns mm^{-1}
n	2	C_{0b}	11.23 Ns mm^{-1}

A first-order filter is also implemented to reflect a 5ms response time of MR damper. According to the above description, the MR damper model is built in Simulink. To test the dynamic behaviours of MR damper, the force generated by the damper for different input current signals 0 A to 1.2A in

steps of 0.2A is computed assuming a harmonic displacement of the piston with 15mm amplitude and 1 Hz frequency. Figure 75 presents the force-velocity and force-displacement features of MR damper in these tests.

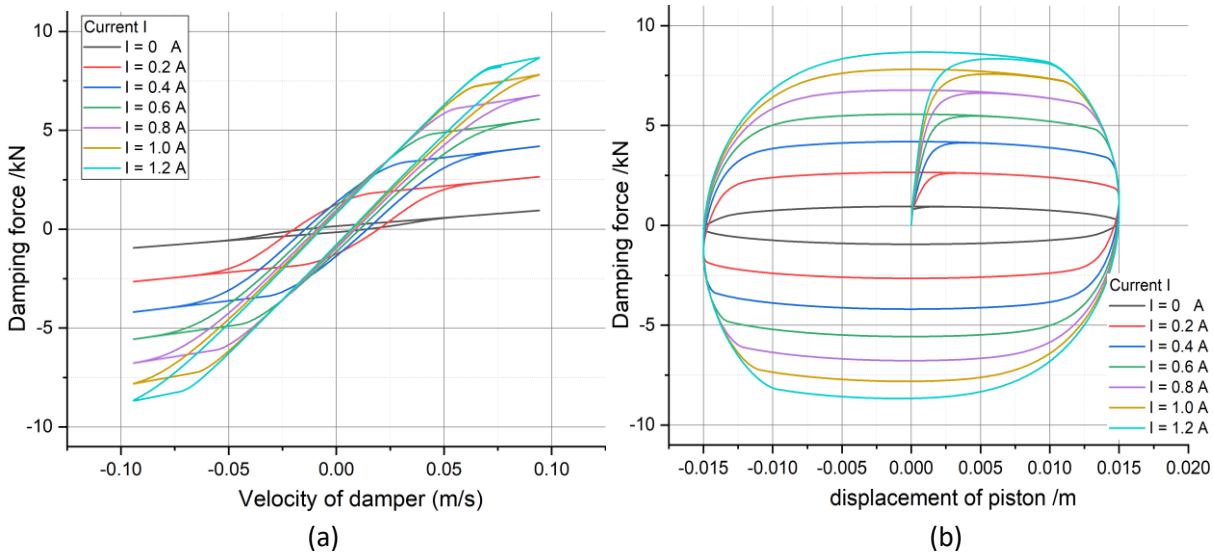

Figure 75 - The (a) force-velocity feature and (b) force-displacement feature of the MR damper

3.5.3.2 MR damper control

The positive correlation between the input current signal and damping is clearly revealed in Figure 75(a) and (b). Assuming a linear relationship between the damping force and the input current, the control strategies introduced in Section 3.5.2 for calculating ideal damping can be directly scaled for calculating the desired current signal. However, a nonlinear relationship between current and damping exists between the two quantities and therefore the ideal damping force is different from the force generated according to the above mentioned method. In order to solve this problem, a control system for MR damper is required.

For the damper model, velocity and current signals are sent into the dynamics model and the damping force is generated, whilst for the control system of MR damper, the ideal damping force and velocity are sent into the system and the required current signal needs to be computed. The workflow of the simulation for semi-active vertical suspension is schematically presented in Figure 76.

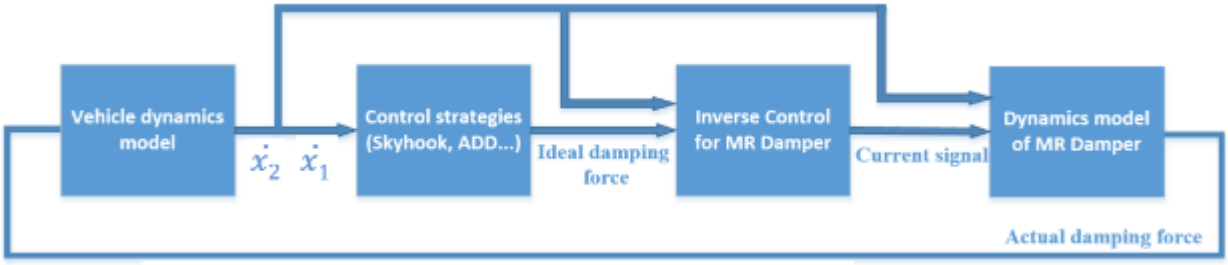

Figure 76 - The schematic workflow of the simulation considering the damper model

According to the nonlinear dynamics model of MR damper, it is impossible to get the analytic solution for calculating current signal. Therefore, the use of a Back propagation (BP) Neural Network is proposed to reproduce the relationship between the current signal, force and velocity. The structure of the Neural Network has one input layer, one output layer and two hidden layers as is shown in Figure 77.

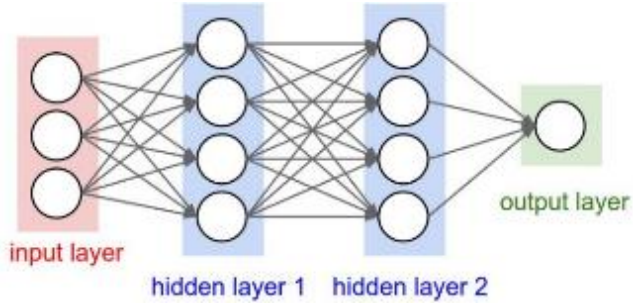

Figure 77 - The layers of the Neural Network

Considering the physical model of MR damper, we select six input signals for this Neural Network: the time history of velocity v and force F at the current step, last step, and the step before the last step and the output is the current signal. The input and output of the system are displayed in Equation (46) and (47).

$$\boldsymbol{N_{in}} = [\boldsymbol{v_k}, \boldsymbol{v_{k-1}}, \boldsymbol{v_{k-2}}, \boldsymbol{F_k}, \boldsymbol{F_{k-1}}, \boldsymbol{F_{k-2}}] \quad \textbf{(46)}$$

$$\boldsymbol{N_{out}} = [\boldsymbol{I_k}] \quad \textbf{(47)}$$

The training data comes from a forward simulation where the current signal is directly controlled by the scaling factor for generating ideal damping (with the assumption that the current is proportional to the damping). The maximum current for damper is set to 1 A. The data simulated in the first 10 seconds is used for training and data from 10 second to 20 second is used for testing.
The targeted current and estimated current from the trained Neural Network are presented in Figure 78. Furthermore, Figure 79 compares the targeted damping force and the actual damping force. From the two figures we can see the estimation effect of the trained Neural network is satisfying.

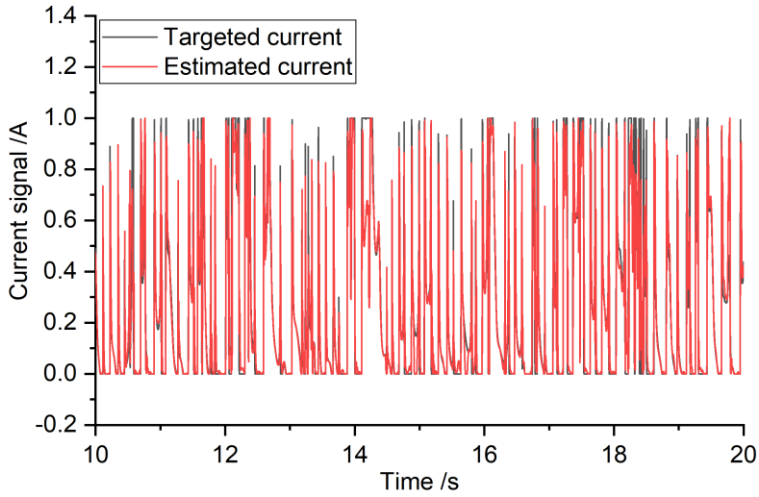

Figure 78 - Comparison between targeted current and estimated current from the trained Neural Network

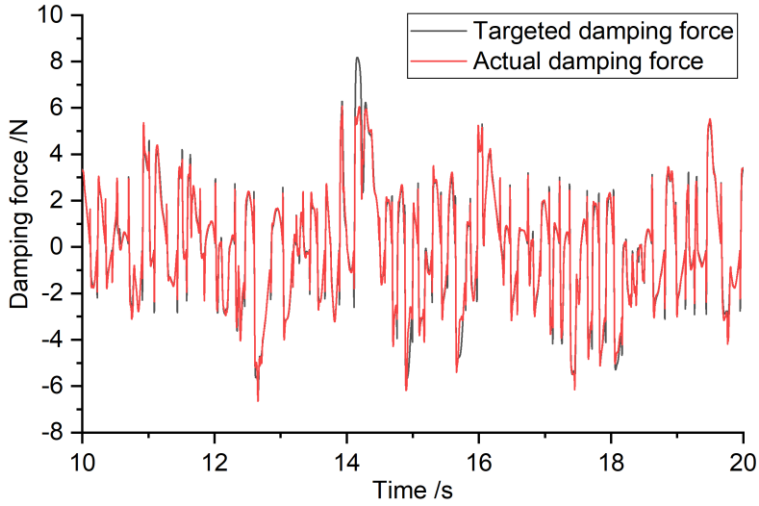

Figure 79 - Comparison between the targeted damping force and actual damping force

For the comparison shown above, the trained data and test data are selected as different time records coming from the same simulation. In order to test the effect of trained Neural Network in the workflow as is shown in Figure 76, we compared the ideal damping force and actual damping force when Two-state Skyhook control and Continuous Skyhook are implemented respectively on the one-quarter vehicle model. The results are displayed in Figure 80 and Figure 81. Despite a small difference between the ideal and actual damping forces can be observed, the control of the damper is acceptable and this trained Neural Network will be implemented in the following simulations.

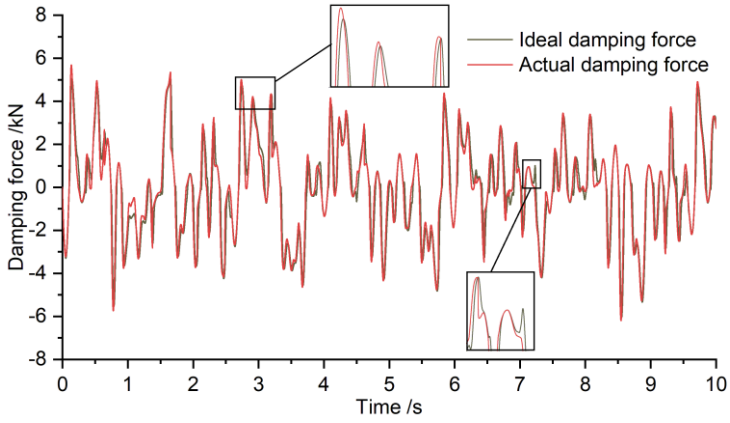

Figure 80 - Ideal damping force and actual damping force with Two-state Skyhook in one-quarter vehicle model

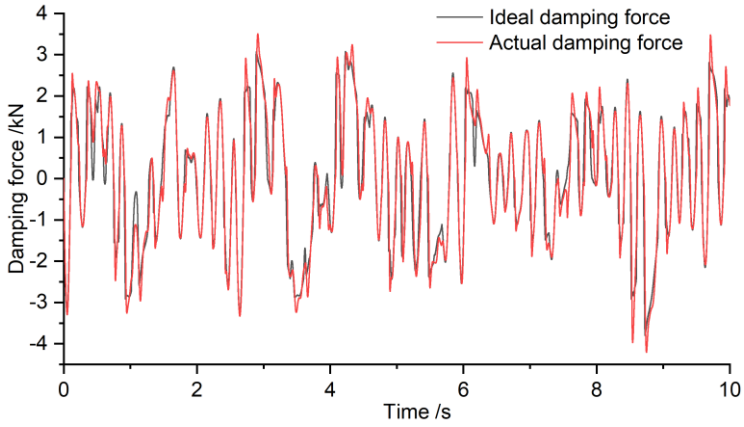

Figure 81 - Ideal damping force and actual damping force for Continuous Skyhook in one-quarter vehicle model

3.5.4 Effects of Semi-active secondary vertical suspension

3.5.4.1 Simulation results based on one-quarter vehicle

In this section, two indicators are used to evaluate the effects of semi-active vertical suspension in terms of ride comfort: 1 Root mean square of acceleration filtered by the weighting function in EN12299 [24] to consider the weighted contribution of vibrations at different frequencies; 2 Sperling ride index W_z [25]. Additionally, the Power-spectral-density (PSD) analysis is carried out to assess the vibration attenuating effects at different frequencies.

The simulations are performed at speed 150 km/h on tangent track. To simulate a poor track condition, a scale factor 2 is applied to ERRI high level track irregularity [131] in vertical direction. In the following simulations, the maximum and minimum damping are 30 kNs/m and 10 kNs/m (the

lower damping cannot be surely achieved by the MR damper) and the boundary for the current signal is [0, 1A].
For control strategies Mixed-ADD and MPPT, the parameters in these controls had been optimized before the comparison among the different controls.

(1) Simulation considering ideal MR damper behaviour

The simulation on one-quarter vehicle model was firstly performed. With ignorance of MR damper model, the ideal damping force based on the control strategies is sent into the vehicle model, and this can reveal the pure effectiveness of control strategies.
The time-history of car body acceleration can directly display the attenuating effects of different control strategies as can be seen in the example shown in the Figure 82, where the improvements can be observed when Two-state skyhook and the Continuous Skyhook are implemented.

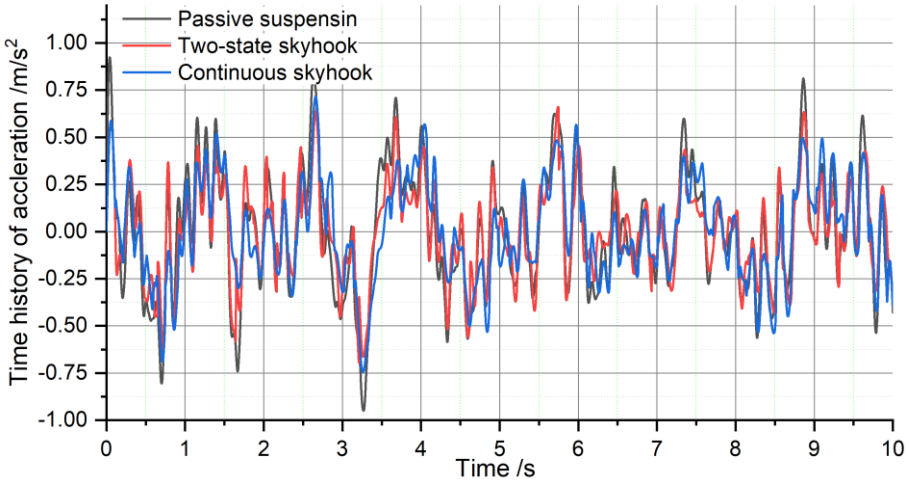

Figure 82 - The time history of acceleration with different suspension systems

The PSD analysis on car body acceleration was carried out to show the control strategies' effects in different frequencies. Figure 83 presents the PSD analysis on the effects of two-state control strategies. With respect to the passive suspension, the semi-active controls produce significant improvement in 1-5Hz. ADD can generate better effect than Skyhook control above 1Hz but in low-frequency range below 0.7Hz its effect is even worse than the passive suspension. Two-state mixed ADD & Skyhook combines the advantages of Skyhook and ADD controls: in low-frequency range under 1Hz the mixed control is better than ADD, and in frequency range 1-5Hz, it shows better effect than Skyhook.

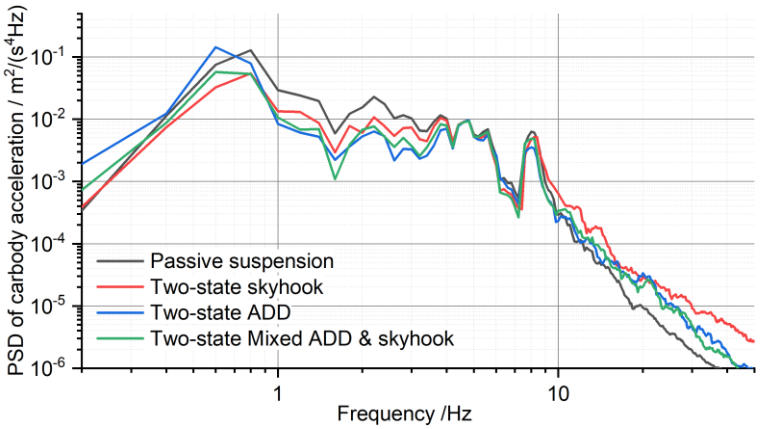

Figure 83 - PSD analysis on the effects of two-state control strategies

The PSD analysis on continuous controls is presented in Figure 84. The Continuous ADD can generate good performance in high-frequency range but still has poor behaviour in the low frequency range below 0.7 Hz. Continuous Skyhook and continuous Mixed ADD & Skyhook have a similar performance and can provide almost the best attenuating effect in 1-5Hz frequency range. The Modified MPPT is not as effective as the above three controls in the range 1-5 Hz, but can produce the best effect at around 8Hz. The modified MPPT also shows a clear improvement with respect to the original MPPT strategy. Considering that this control is simpler and easier to implement, the Modified MPPT could be a promising control strategy for the implementation of semi-active suspension.

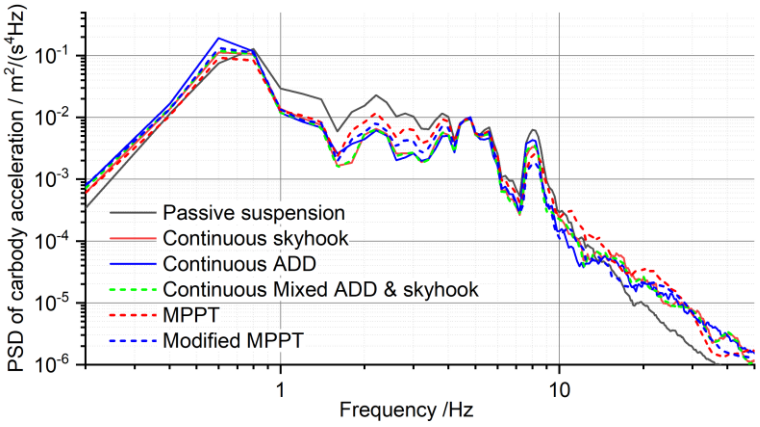

Figure 84 - PSD analysis on the effects of continuous control strategies

To evaluate the general performance of different control strategies, the RMS of filtered car body acceleration and Sperling ride index are compared in Figure 85(a) and (b). The best two control strategies are Continuous Skyhook and Continuous Mixed ADD & Skyhook which can reduce the RMS acceleration by 20%. For two-state controls, ADD shows improvement with respect to Two-

state Skyhook and Two-state Mixed ADD & Skyhook can produce further minor improvement. The continuous controls show better effects than the two-state ones except for Continuous ADD. MPPT produces the effect between two-state skyhook and two-state ADD, whilst the Modified MPPT can generate a better performance close to the overall best level.

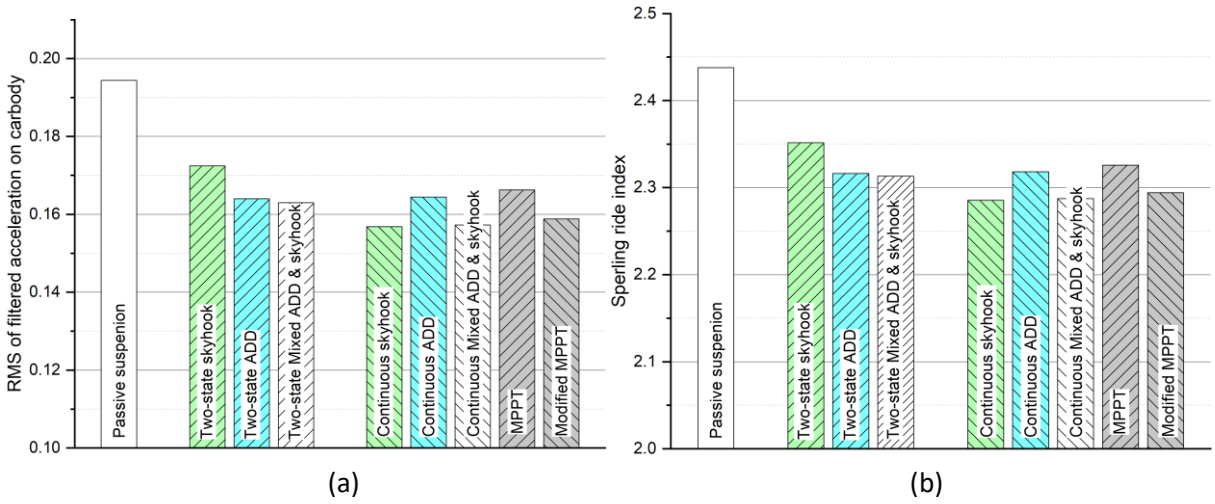

Figure 85 - Simulation results of (a)RMS value and (b)Sperling ride index with different control strategies

(2) Simulation with MR damper model

In this section, the MR damper model and its controller are considered to show the influence of dynamics of the damper. The PSD analyses are presented in Figure 86 and Figure 87 and the RMS of acceleration and Sperling ride index are compared in Figure 88.

When the dynamics of the MR damper are considered, the features of different control strategies don't have significant influence. However, as the actual force generated by the damper deviates from the ideal force, the attenuating effects of all the control strategies are reduced and the RMS of acceleration rises by 0.01-0.02 m/s^2.

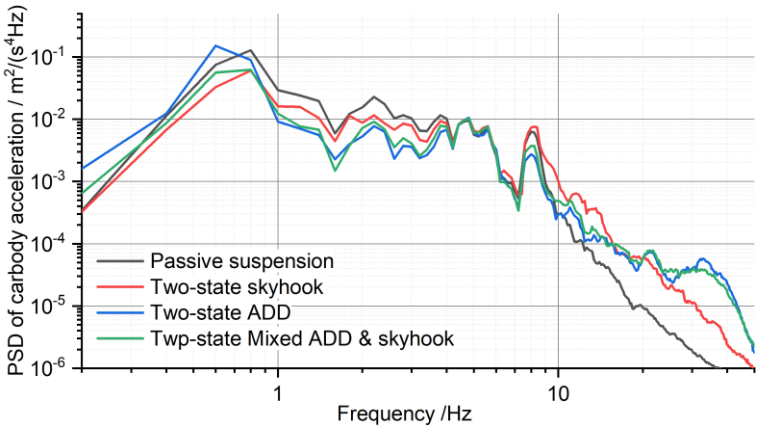

Figure 86 - PSD analysis on the effects of two-state control strategies

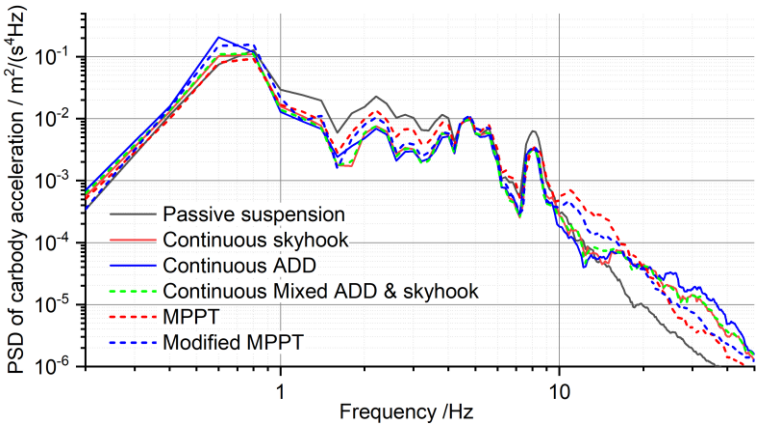

Figure 87 - PSD analysis on the effects of continuous control strategies

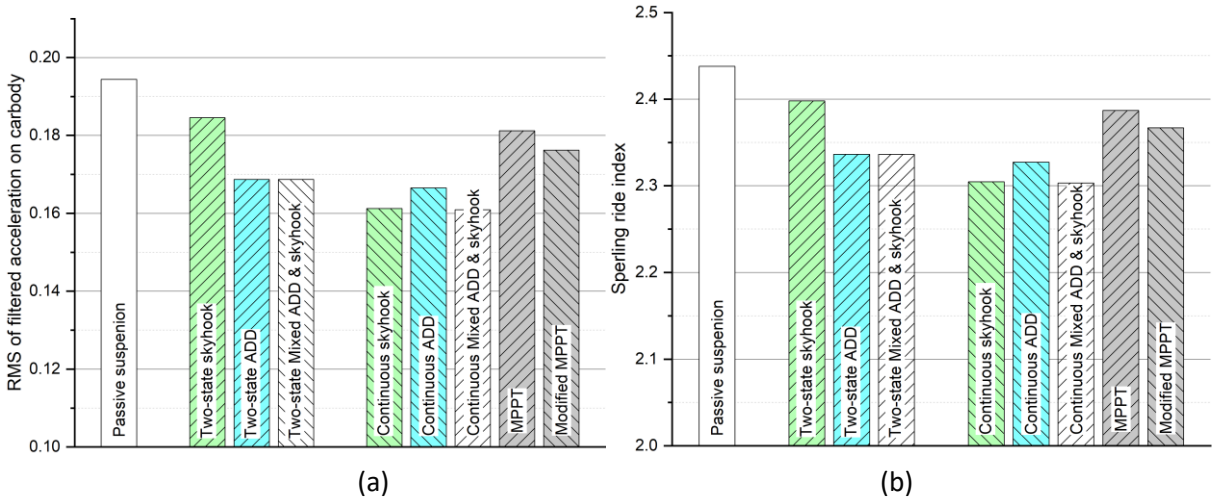

Figure 88 - Simulation results of (a)RMS value and (b)Sperling ride index with different control strategies

3.5.4.2 Simulation results based on full vehicle model

In this section, the corresponding simulations are performed based on the full vehicle model in SIMPACK. For the full vehicle model, the vibration will become more complex and as the flexible car-body is considered, higher-frequency vibrations are introduced in the system.

(1) Simulation considering ideal MR damper behaviour

When the MR damper model is not considered, the PSD analyses are performed for two-state control strategies and continuous control strategies as are shown in Figure 89 and Figure 90 respectively. Compared to the simple one-quarter vehicle mode, the full vehicle model considers additional vehicle dynamics, particularly in the 10-30 Hz frequency range. In general, all the semi-active controls can effectively attenuate the vibration from 1-7 Hz. The comparison conclusions of different control strategies are similar to the ones for one-quarter vehicle model.

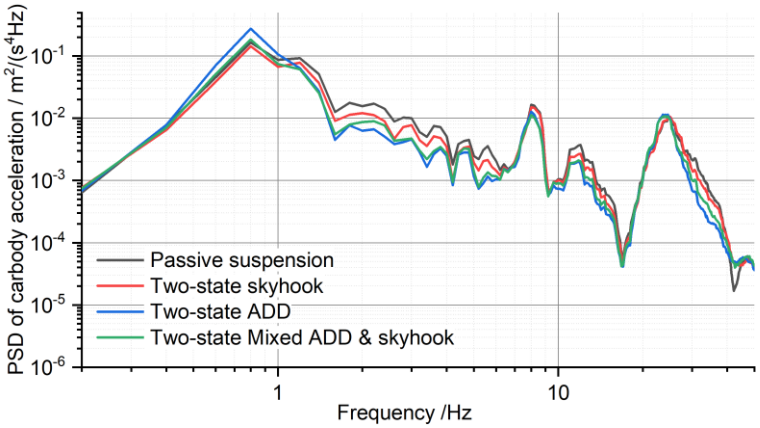

Figure 89 - PSD analysis on the effects of two-state control strategies

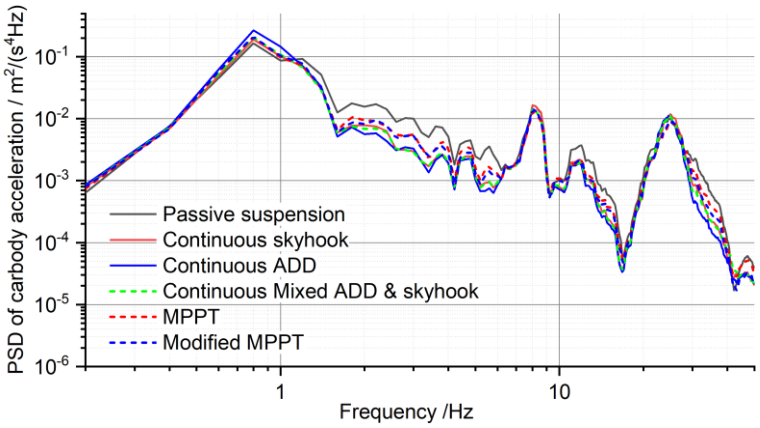

Figure 90 - PSD analysis on the effects of continuous control strategies

The RMS of filtered car body acceleration and Sperling ride index are compared in Figure 91(a) and (b). The best two control strategies are Two-state Mixed ADD & Skyhook and Continuous Mixed ADD & Skyhook. The continuous control version shows significant improvement compared to the two-state one only for Skyhook control. MPPT and improved MPPT can generate good performance, close to the overall best level.

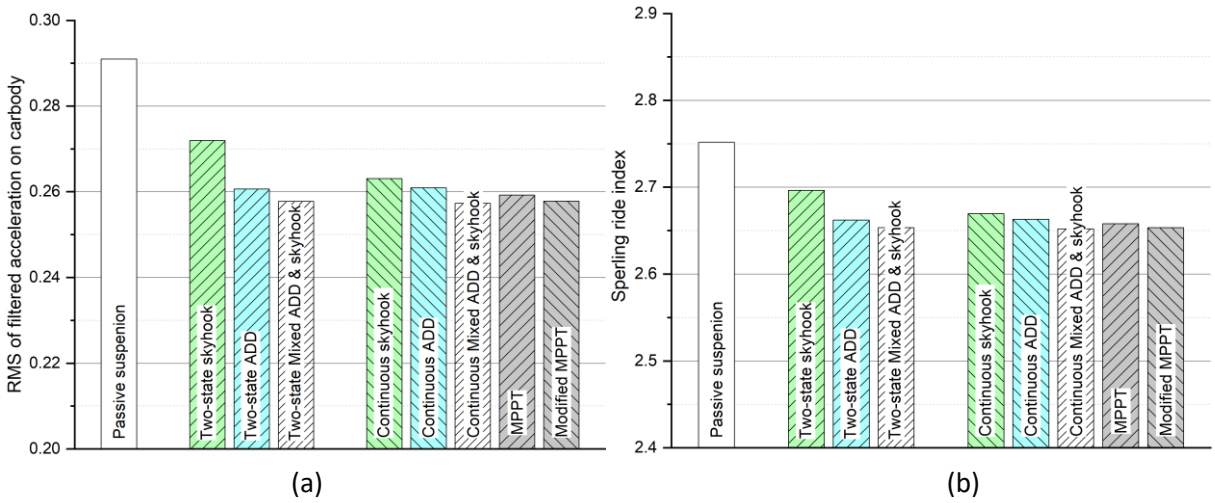

Figure 91 - Simulation results of (a)RMS value and (b)Sperling ride index with different control strategies

(2) Simulation with MR damper model

When MR damper model and its controller are considered, the RMS of filtered car body acceleration and Sperling ride index are compared in Figure 92(a) and (b).

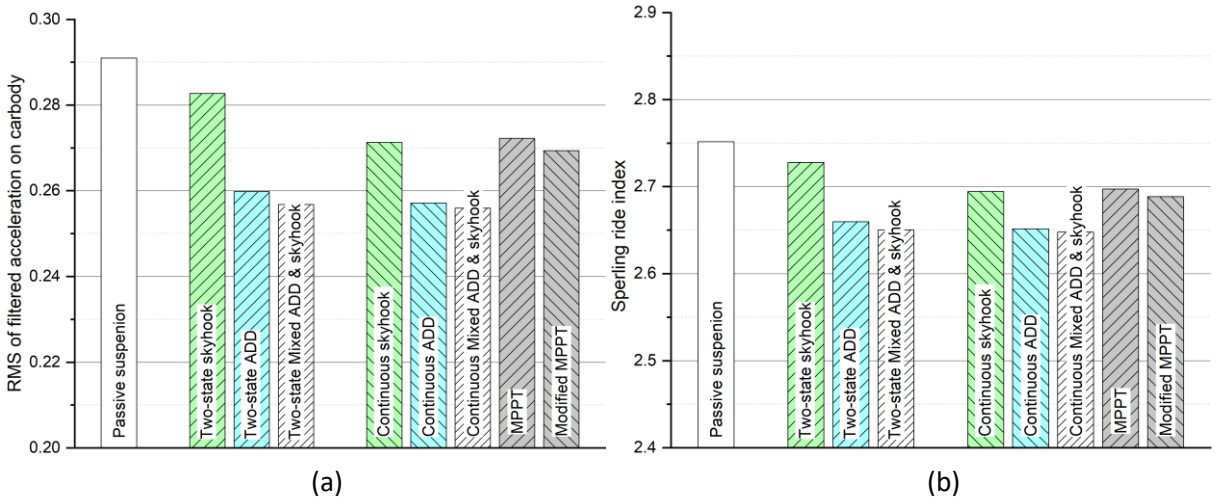

Figure 92 - Simulation results of (a)RMS value and (b)Sperling ride index with different control strategies

The improvement of ride comfort with different control strategies are revealed and some features are the same as shown in Figure 91, but the general effects of control strategies are reduced due to the difference between the ideal damping force and actual damping force, especially for Two-state and continuous Skyhook, MPPT and Modified MPPT. Despite the use of the trained Neural Network, a significant degradation of performance is observed when the dynamics of the MR damper is considered. This is probably because the working conditions for the full vehicle model are more complex than for the one-quarter vehicle mode, so that there is an inaccuracy introduced in the estimation of the current needed to generate the damping force. There are however margins to improve the estimation of the current required to drive the MR damper and this is envisaged as future line of research, extending the results obtained in this project.

3.6 EFFECT OF ACTUATOR DYNAMICS ON RIDE COMFORT / WATERBED EFFECT

The implementation of the active control for the improvement of the vibratory comfort, usually implies an increase of the dynamic response in the carbody above certain frequency. In addition to the theoretical issues associated with the feedback control of systems with linear parameters, the main limitation in the railway case is the actuator. The objective of the present section is to analyse such limitations through a study carried out by means of a model of the most performed hydraulic actuator technology.

Figure 93 sketches the hydraulic actuator of the patent EP 2039582. The figure shows (1) the cylinder, (2) two 2-ways Pressure Proportional Regulator Valves (PPRV), (3) two Positive

Displacement Pumps (PDP), (4) two check valves, and (5) the reservoir. The technology based on PPRV allows setting the maximal pressure in the actuators chambers, and consequently it enables control of the force. PPRVs do not have a very fast response, but they allow to keep the pressure below the fixed limit, even if the fluid conditions change rapidly.

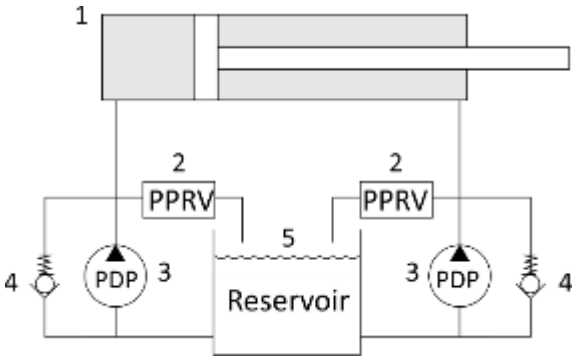

Figure 93 – Actuator hydraulic scheme

3.6.1 Actuator model

In order to model the behaviour of the actuator, the variables associated with the pressures p_{jc} and flows q_{jc} (in m^3/s) are defined in Figure 94. The reservoir pressure is supposed to be p_0 and any pressure cannot be negative.

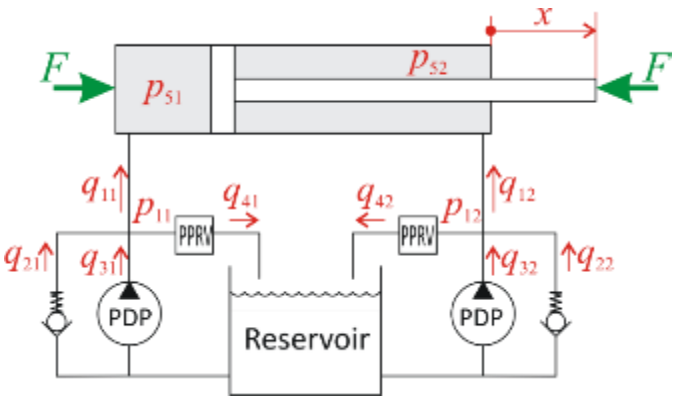

Figure 94 - Parameters of the actuator model

The equation of the fluid into the hydraulic cylinder is

$$\frac{dp_{5c}}{dt} = \frac{\beta}{V_c}\left[q_{1c} - \frac{dV_c}{dt}\right] \quad (48)$$

where the sub-index c is the chamber number (c =1, 2), β is the bulk modulus of the hydraulic fluid and V_c is the volume of the chamber. The volume of the chamber depends on the rod position as follows

$$\boldsymbol{V_c = V_{c0} \pm x A_c} \quad \textbf{(49)}$$

A_c being the effective area of the actuator chamber ($A_1 > A_2$ because the piston rod), x the piston rod position (as shown in the figure) and V_{c0} the volume of the c -th chamber when x is zero. The upper sign in $\pm$ (or $\mp$) is the actual one when c =1, and the lower is the correct if c =2. The derivative of the chamber volume with respect to the time is obtained from the last formula, and it results

$$\boldsymbol{\frac{dV_c}{dt} = \pm A_c \dot{x}} \quad \textbf{(50)}$$

A quadratic model of the flow to the cylinder and the difference of pressure between the pipe and the chamber is the following

$$\boldsymbol{q_{1c} = \pi D_1^2 \sqrt{\frac{1}{8\kappa_5 \rho}}\, sign\,(p_{1c} - p_{5c}) \sqrt{|p_{1c} - p_{5c}|}} \quad \textbf{(51)}$$

where D_1 is the pipe diameter, ρ is the density of the hydraulic fluid, and κ_5 relates the pressure fall and the flow between pipe 1 and the actuator chamber (κ_5 ≈0.5). The slope of the last equation is infinite when $p_{1c} - p_{5c} = 0$ and it may produce numerical problems. In order to prevent this issue, the last formula has been regularised by means of the following expression

$$\boldsymbol{q_{1c} = \kappa_{51}\, atan \frac{p_{1c} - p_{5c}}{\kappa_{52}}} \quad \textbf{(52)}$$

The characteristic equation of the check valve is

$$q_{1c} = 0 \; if \; p_{1c} > p_0$$

$$\boldsymbol{q_{2c} = ?\; if\; p_{1c} = p_0} \quad \textbf{(53)}$$

The proportional pressure relief valve can be modelled as follows

$$p_{1c} = p_c(\xi_c) + k_4 q_{41} \; if \; q_{41} > 0$$

$$\boldsymbol{p_{1c} = ? \qquad if\; q_{41} = 0} \quad \textbf{(54)}$$

ξ_c being the command value (ξ_c is between 0 and 1) that can be used for fixing the actuator force.

There is an electrical delay between the selected command value $\tilde{\xi}_c$ and the effective command value ξ_c, and this can be modelled by means of the following equation

$$\boldsymbol{\xi_c + z_e \dot{\xi}_c = \tilde{\xi}_c} \quad \textbf{(55)}$$

where z_e is a parameter that determines the time delay (around 0.1 s), which is mainly due to the energisation of the valve coil.

The flow at the pumps is almost constant, but there is a small reduction when the pressure increases at the pipe. The following model of the pump is adopted in the present work

$$\boldsymbol{q_{3c} = Q_c - k_c p_{1c}} \quad \textbf{56}$$

Q_c being the nominal flow at the pump, and k_c the slope that relates the flow reduction when the pressure in the pipe increases.
The balance of the different flows is

$$\boldsymbol{q_{1c} - q_{2c} - q_{3c} + q_{4c} = 0} \quad \textbf{(57)}$$

The force of the actuator is computed as follows

$$\boldsymbol{F = p_{51} A_1 - p_{52} A_2} \quad \textbf{(58)}$$

The formulae that have been presented in this section form a differential-algebraic system of equations (DAEs) that is solved by means of ode15s in MATLAB®.

Parameters of the model

The parameters that have been adopted in this work are the following

- Bulk modulus of hydraulic fluid (mineral oil): b = 1.8 10^9 Pa
- Cylinder areas: A_1=8 cm^2; A_2=6 cm^2
- Volumes of the chamber: V_{10} =56 cm^3; V_{20} =42 cm^3
- Valve electrical impedance: z_e=0.044 s, (if $\xi_c \in [0,1]$)
- Nominal pump flow: Q_1=1.6 ℓ/min, Q_2=1.2 ℓ/min
- Slope that relates the pump flow reduction: k_c= 4.0 10-14 m^3/sN
- Local pressure loss coefficient at the cylinder: κ_{51} = 107.41 ℓ/min; κ_{52} = 1.0 bar
- Pipe diameter: D_1= 0.8 cm
- Local pressure loss coefficient at the valve: κ_4 =3.5 bar min/ℓ
- Reservoir pressure: 2 bar.

3.6.2 Static response of the actuator

The static force of the actuator when $\dot{x} = 0$, $\tilde{\xi}_1 = 1$ and $\tilde{\xi}_2 = 0$ is $F = 4.23$ kN, whereas the static force of the actuator when $\tilde{\xi}_1 = 0$ and $\tilde{\xi}_2 = 1$ is $F = -2.76$ kN. The graphs in Figure 95 show the static force when varying the command value of one of the valves while the command value of the other valve is zero. From this result the asymmetric behaviour of the actuator can be seen, which is due to the different effective areas A_1 and A_2, and the pressure loss in the valves.

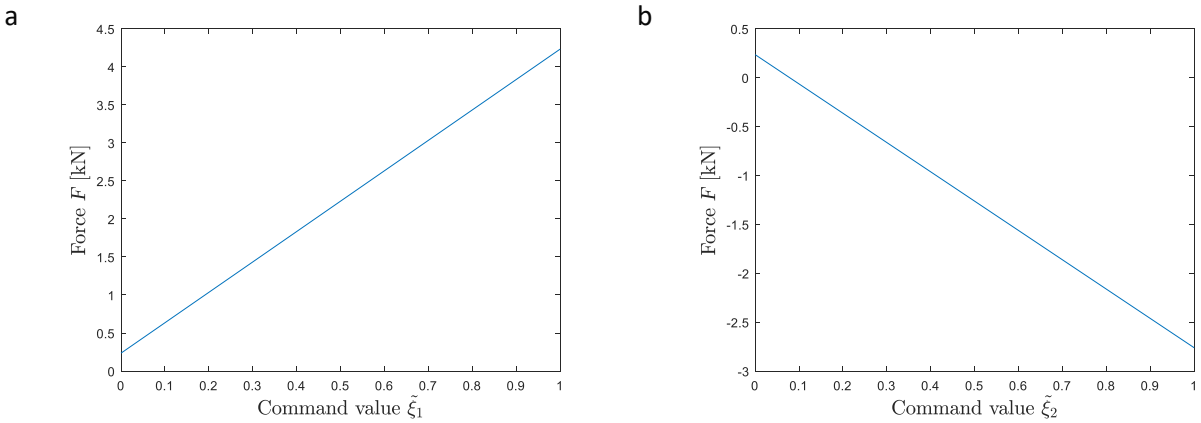

Figure 95 - Static force as a function of the command value

Due to this asymmetric behaviour, it is not obvious how to set the force in the actuator by controlling the valves independently. In order to reduce this issue, the total force in the actuator is set by applying pressure in both sides of the cylinder. The actuator is commanded in the following calculations through a global command variable ξ that takes values between -1 (maximal compressive force) and 1 (maximal extension force). The command value in each valve are then obtained by means of the following linear relationships

$$\xi_1 = \frac{1+\xi}{2} \quad (59)$$

$$\xi_2 = \frac{1-\xi}{2} \quad (60)$$

3.6.3 Dynamic response

The following results are associated with the harmonic variation of the global command variable ξ when $x = \dot{x} = 0$. Figure 96 presents the amplitude of the first harmonic of the force vs the frequency of the command variable. From this result, there is a fall of 3 dB at 3.8 Hz. It could be deduced that the actuator can be potentially suitable for increasing the vibration comfort below the cut-off frequency of the railway-vehicle secondary suspension.

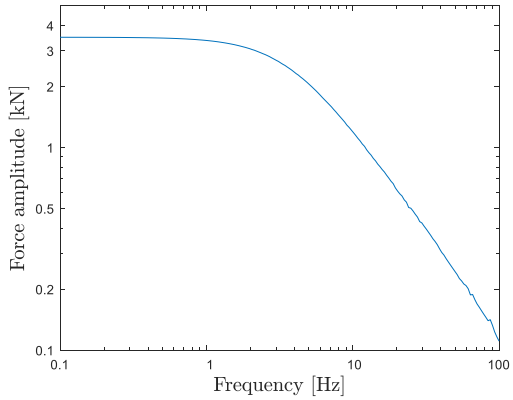

Figure 96 - Amplitude of the fundamental harmonic of the force vs the frequency of the command variable ξ

Figure 97 compares the weight of the superharmonics with respect to the fundamental frequency when the command variable ξ is harmonic and $x = \dot{x} = 0$. This calculation is done by summing the amplitudes of the force superharmonics and dividing by the amplitude of force fundamental harmonic. This result shows that the influence of the superharmonics is negligible (smaller than 1%) below 20 Hz.

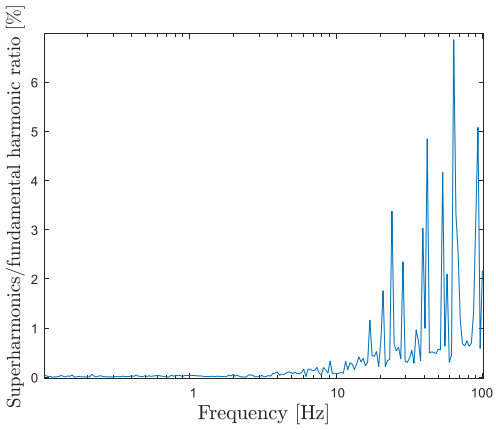

Figure 97 - Ratio between the sum of the superharmonic amplitudes and the amplitude of the fundamental harmonic of the force vs the frequency of the command variable ξ

Figure 98 presents the delay of the force with respect the command parameter. For frequencies higher than 3 Hz the delay is not a linear function of the frequency, and consequently, the force wave can be distornsioned with respect the command variable wave. Furthermore, for frequencies higher than 30 Hz the delay exceeds 90° and the control becomes instable.

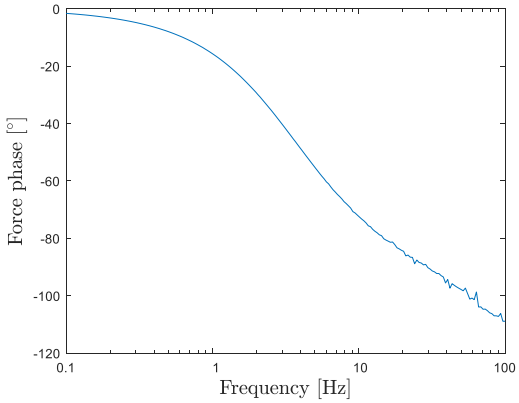

Figure 98 - Phase of the force fundamental harmonic with respect the command variable ξ , vs the frequency of the command variable

The plots in Figure 99 represents the force response when the command variable remains zero and there is a harmonic displacement at the actuator rod, which is $x = \bar{x}\, cos\, 2\,\pi f t$. In this calculation, the optimal response of the actuator should be a constant force. Nevertheless this optimal behaviour is hardly fulfilled when the velocity of the rod is not negligible.

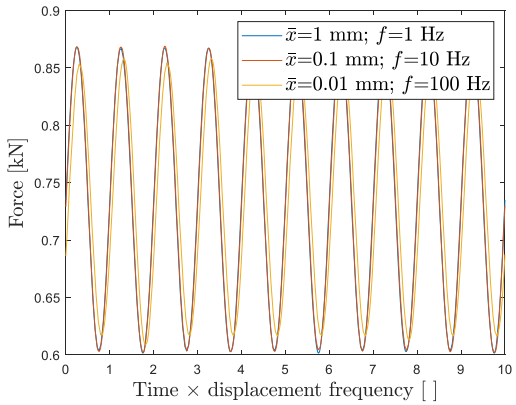

a) The velocity peak of the rod is 6.3 mm/s

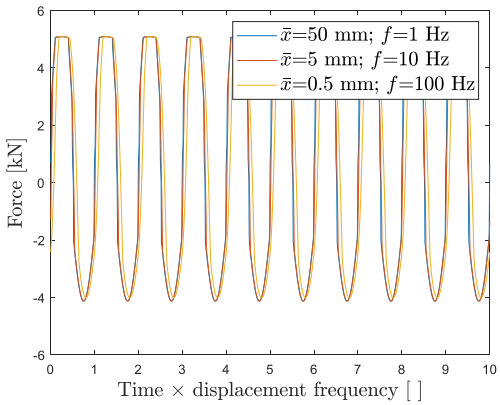

b) The velocity peak of the rod is 314.2 mm/s.

Figure 99 - Force of the actuator when the command variable ξ is zero, and the actuator rod displaces harmonically. Each plot is carried out for three different amplitude/frequency combinations that produces the same acceleration.

In the previous cases, the actuator acts like a damper but its behaviour is not linear when the rod velocity is not small, producing forces at higher frequencies than those of the rod displacement. This conclusion can be seen in Figure 100, where ten harmonics of the actuator force are represented. The excitation is a harmonic displacement of the rod. The study has been carried out for different combination of frequency and amplitude of the rod displacement. This result shows that the force introduced by the 2nd and 3rd harmonics are remarkable and they can excite until 30 Hz.

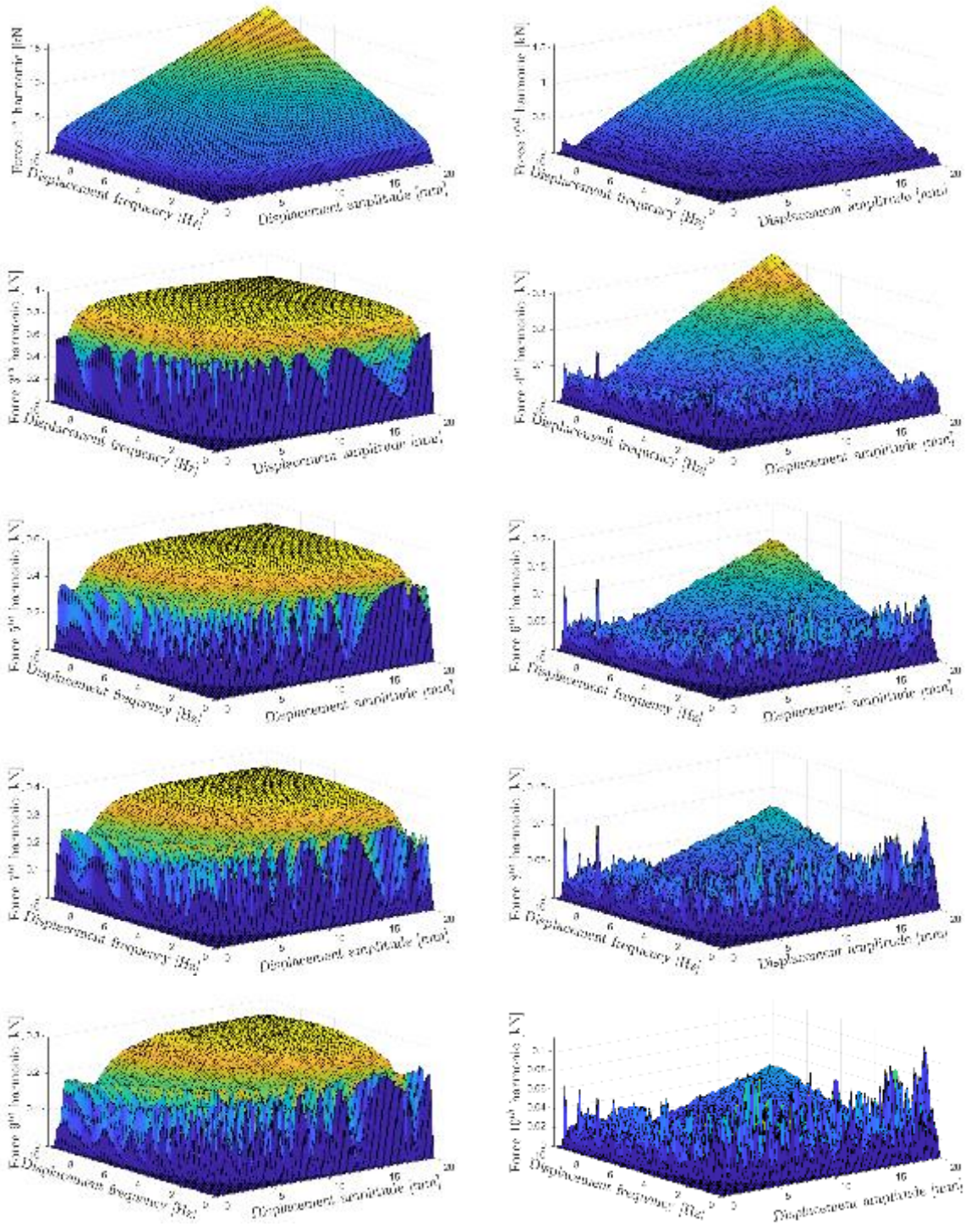

Figure 100 - Amplitude of the harmonics 1 to 10th associated with the actuator force when a harmonic displacement in the rod is applied

3.7 CONCLUSIONS ON ACTIVE SUSPENSION FOR CONVENTIONAL VEHICLES

In Section 3, active suspension technologies for conventional bogie vehicles were explored in three aspects and the conclusions are summarized in three parts as follows.

(1) Wheelset steering of solid-axle wheelset

Active wheelset steering will significantly improve the wheel and rail wear condition from tight curves to large curves by controlling the angle of attack between wheel and rail. Two different approaches to derive track curvature were investigated. The first approach uses gyroscope sensors to estimate the track curvature but the low-pass filter and response time of actuators will introduce a time delay between the ideal movement and actual movement of actuators and steering effects on curve transitions will be degraded. To solve this problem, precedent control is applied. The control signal for the actuators on the leading wheelset is used for the actuators behind, by which the time delay will be compensated and steering performance on curve transition will be improved, apart from the leading wheelset. The second approach is utilizing track curvature database and Geo-localisation technology, by which the track curvature can be accurately obtained and steering effect of all wheelsets can be improved on the curve transition. Simulations have been performed in different scenarios. Without the passive spring in parallel with actuators, the wear number can be reduced by 90% on tight curve R250, small curve R400 and middle curve R600, whilst with the passive springs, the wear improvement rate will be degraded significantly.

(2) Fault-tolerant analysis for active steering system

In this section, a method to evaluate the severity of different failure modes and fault-tolerant capability of various actuation schemes for wheelset steering is proposed. The quantified severity factor and Risk Priority Number can provide a good base for assessing and comparing different active steering schemes in regard to their tolerance to faults. Implementing a redundant actuation scheme is an effective method to improve the fault tolerance of actuation system, whilst without any redundancy or passive back-up, the risks of safety issues will significantly increase in case of particularly dangerous failure modes taking place.

(3) semi-active vertical suspension

The effects of different classic control strategies for semi-active suspension through a simple one-quarter vehicle model and full vehicle model have been investigated. In general, continuous control produces better attenuating effects than two-state control. Mixed Acceleration Driven Damping & Skyhook show the best performance among the different controllers considered.

Maximum Power Point Tracking and Modified Maximum Power Point Tracking are proposed as new control strategies and they have shown a satisfactory behaviour for the semi-active suspension. Considering that they are less expensive and easier to implement, Maximum Power Point Tracking and Modified Maximum Power Point Tracking are promising control strategies for a semi-active suspension.

To consider the dynamics of the Magneto-rheological damper, a trained Neural Network can be used to estimate the current required to generate the desired damping force for a given working condition of the damper. Even so the error between the actual damping force produced by the damper and the desired value can significantly degrade the performance of the semi-active suspension. Therefore, the control for the damper needs to be carefully designed.

4. TWO-AXLE VEHICLES WITH ACTIVE SUSPENSION

4.1 INTRODUCTION

4.1.1 Background

A single axle running gear has potential for significant weight savings compared to conventional bogie designs. The savings come from reduced size of the components and reduced number of components. One way to reduce the number of components is to combine two functions in one hardware, and in the proposed single axle running gear the frame is also utilized as anti-roll bar. Modern designs could further reduce the weight, which could also be applied on bogie vehicles. One modern design is to locate the bearing inside the wheel making the wheel axle both shorter and lighter - bogies with in-board bearings are on the market today. Another modern design is use of composite materials for the frame.

A conventional bogie vehicle with passive suspension can be designed to provide an acceptable vibration ride comfort and wheel wear. A single axle running gear with just one suspension stage (a conventional bogie has two) has less scope to provide an acceptable vibration ride comfort and level of wheel wear. Active or semi-active wheelset steering, and active suspension is needed to ensure good performance. The intention is to design a simple running gear that with as simple as possible active systems can provide performance in line with a passively suspended conventional bogie.

The new innovative vehicle will be compared to a reference vehicle on a track where the reference vehicle runs today.

4.1.2 Reference vehicle

The reference vehicle comes from Metro Madrid and is named class 8000. It consists of three cars; two driven end cars and the intermediate trailer car, see Figure 101. Key data for the reference train is given in
Table 17.

Figure 101 - Metro Madrid Class 8000

Table 17 - Key data of Metro Madrid class 8000

Property	End cars	Intermediate car
Length	18.104 m	17.000 m
Maximum service speed	120 km/h	120 km/h
Driven axles / Trailer axles	4 / 0	0 / 4
Axle load tare	9,85 tonnes	6,36 tonnes
Axle load at pay load	14.35 tonnes	11.10 tonnes
Tare load per length	2,17 tonnes / m	1,50 tonnes /m
Pay load per length	0.99 tonnes / m	1,12 tonnes / m

4.1.3 The reference track

The class 8000 is used on several lines of the Metro Madrid network. Line 10 is selected as reference as this line has sections with tight curves and other sections with relatively high speed making it suitable as a reference track.

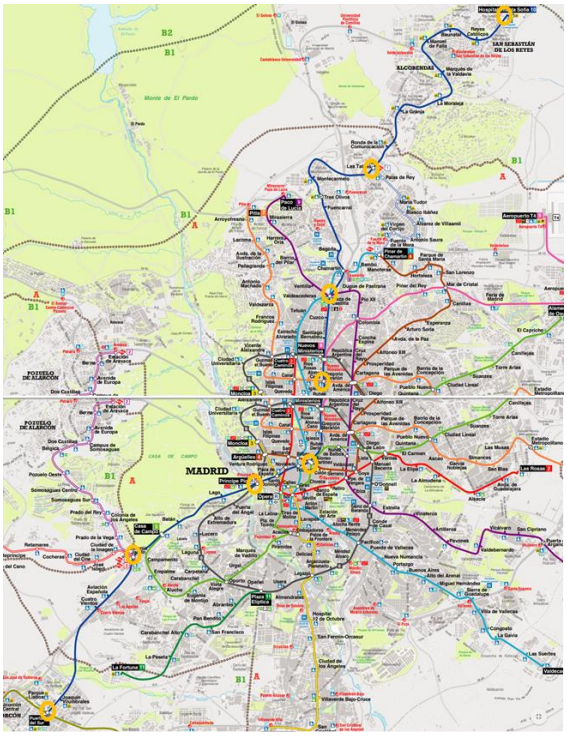

Figure 102 - Metro Madrid Line 10, map

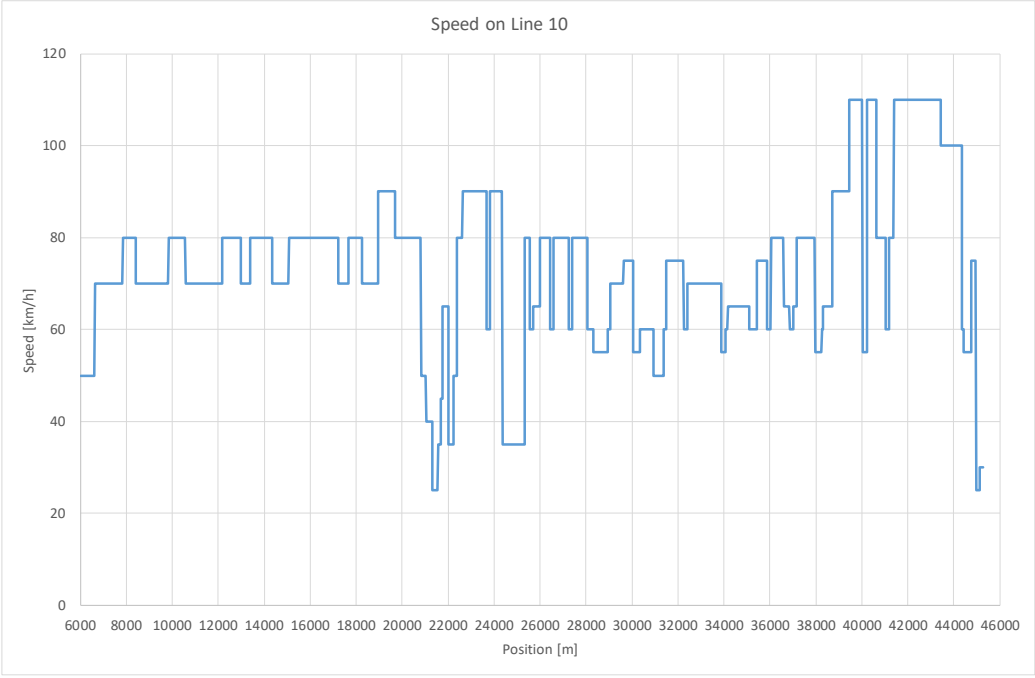

Figure 103 - Metro Madrid Line 10, speed profile

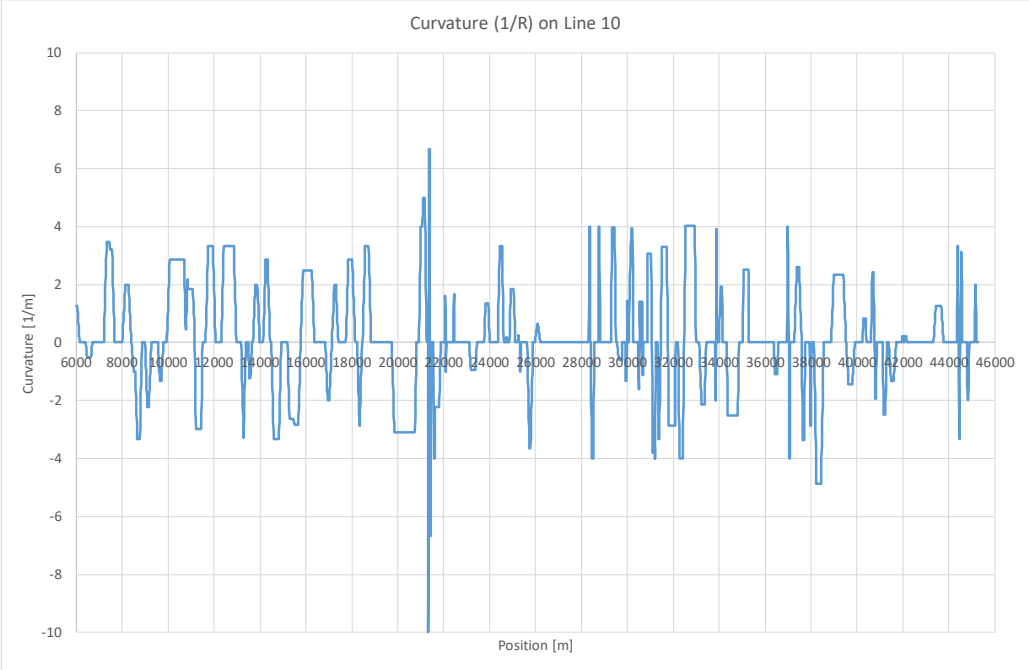

Figure 104 - Metro Madrid Line 10, curvature (1/R)

4.1.4 The innovative vehicle

The innovative vehicle should be able to run on the same track as the reference vehicle, carrying the same number of passengers per metre at the same time bringing benefits in terms of weight and cost, see Figure 105 and Table 18.

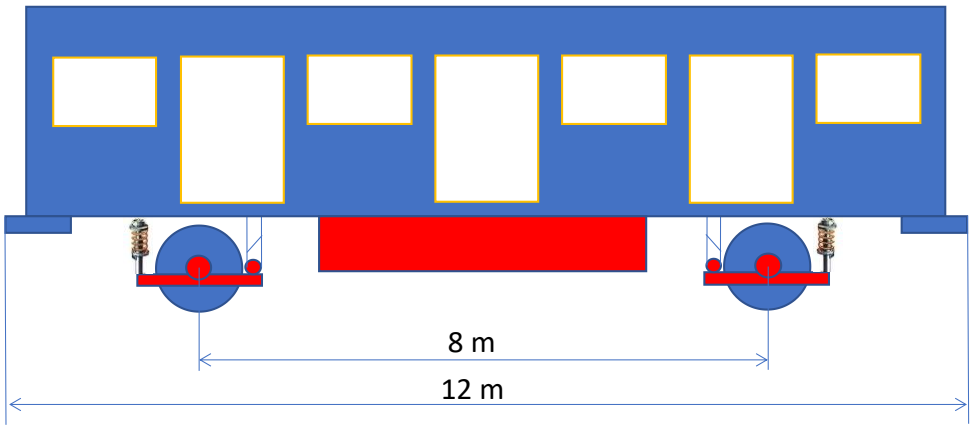

Figure 105 - The innovative vehicle

Table 18 - Parameters for the innovative vehicle

Property	Unit	Driven car	Trailer car
Length	m	12.000	12.000
Maximum service speed	km/h	120	120
Driven axles / Trailer axles	- / -	2 / 0	0 / 2
Axle load tare	t	9.06	8.28
Axle load at pay load	t	15.0	15.0
Tare load per length	t/m	1.51	1.38
Pay load per length	t/m	0.99	1.12
Axle distance	m	8.0	8.0
Wheel diameter	m	0.860	0.860
Wheel profile	-	S1002	S1002
Mass of frame and drive	kg	1500	800
Mass of wheelset	kg	1500	1200
Stiffness coil spring vertical	kN/m	150	150
Stiffness coil spring horizontal	kN/m	150	150
Stiffness rubber bushing lateral	kN/m	150	150
Stiffness rubber bushing radial	kN/m	10,000	10,000
Vertical damper	kN/(m/s)	10	10
Lateral damper	kN/(m/s)	30	30
Anti-roll stiffness	kN/rad	250	250

4.2 MBS MODEL

The vehicle model is implemented in the multi body simulation (MBS) system SIMPACK®. The vehicle representation is given in Figure 106 left. The frame model is designed to resemble the specified characteristics. Requested mass and inertia are given while the centre of mass is automatically calculated by SIMPACK®. In Figure 106 right is a representation of the implemented running gear frame. The centre of mass is displaced with respect to the geometrical centre.

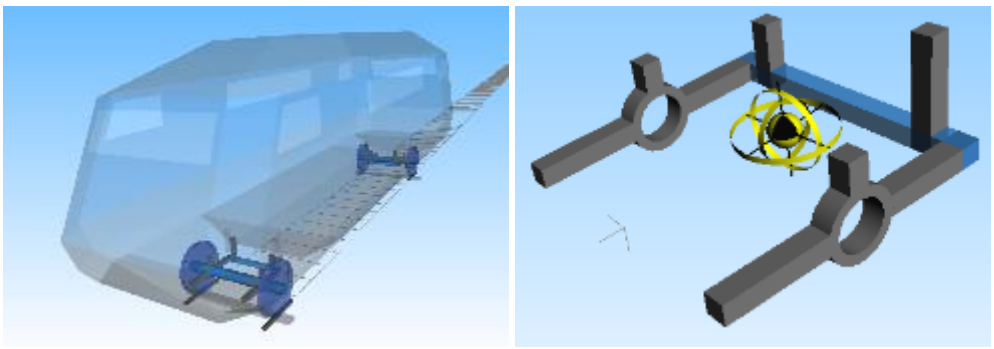

Figure 106 - MBS vehicle model (left) and frame model (right)

The suspension elements are introduced into the system. Coil spring element for the vertical suspensions, rubber spring for the lateral and longitudinal suspensions and a spring damper in series for the damping elements. The locations of the elements together with their descriptions are shown in Figure 107. The wheelset steering actuators locations are also shown.

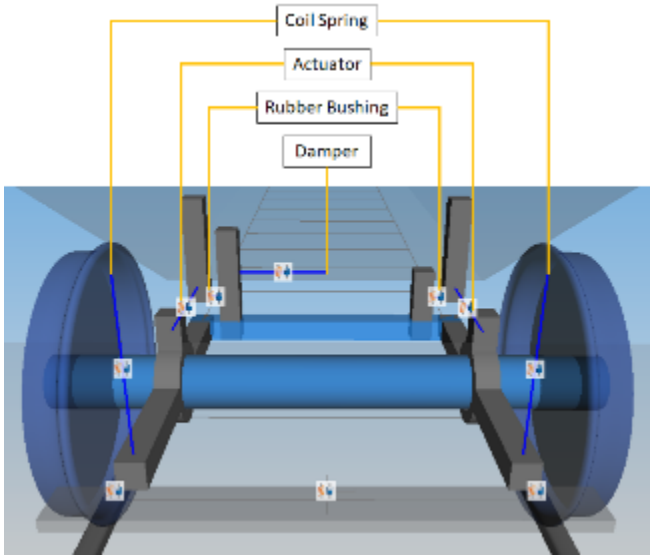

Figure 107 - Suspension locations

The vehicle's frame will be built in composite material. This generates a certain flexibility that will allow the frame itself to act as anti-roll bar. A simple representation of this behaviour is introduced. The rigid frame of Figure 106 right is split into two rigid halves connected by a torsional stiffness of 0.25 MN/rad. To grant the relative motion between the wheelset and the frame, bearings models are also introduced. In Figure 108 the split frame is shown together with the achieved main movement.

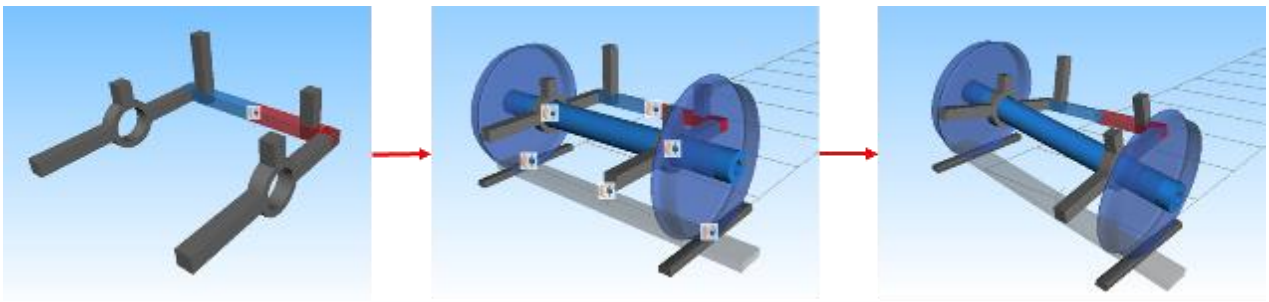

Figure 108 - Split frame representation

4.3 PERFORMANCE OF THE PASSIVE VEHICLE

As we here are aiming for a vehicle that only uses the active suspension to improve the performance, the performance of the passive vehicle is important and must be checked. The checks are generally made according to EN14363 [128], which divide the assessment in two stages, the checks reported here are:

1. Check of the sway coefficient (1st stage)
2. Safety against derailment on twisted track (1st stage)
3. Track shift forces (2nd stage
4. Safety against derailment (2nd stage)
5. Stability (2nd stage)

4.3.1 First stage assessment

The introduction of the split frame representing the flexibility of a real frame was necessary to get enough flexibility to handle the safety against derailment on a twisted track. In Figure 109 it is possible to see the difference between rigid and split frame implementation in terms of total wear number for the front (left) and rear (right) wheelsets. The vehicle is running through a 250 m curve with a cant of 150 mm at equilibrium speed. For both front and rear wheelsets, the frame flexibility improves the wear number, which is an indication of improved performance generally.

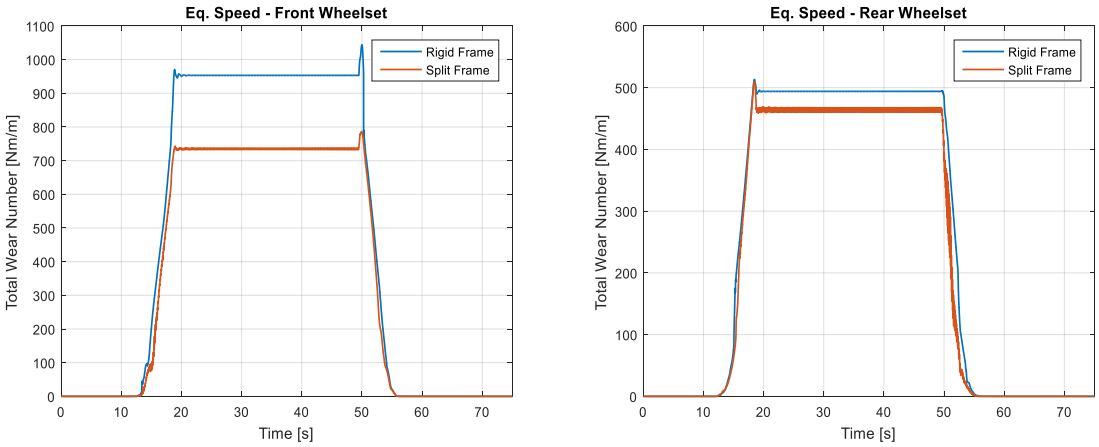

Figure 109 - Comparison of wear numbers at curve negotiation, rigid against split frame: front wheelset (left) and rear wheelset (right)

The flexibility of the frame will enhance the vehicle sway. With reference to Figure 110 the flexibility coefficient can be calculated as follows:

$$S = \frac{a_c - a_t}{a_t} = \frac{sin(\vartheta_c) - sin(\vartheta_t)}{sin(\vartheta_t)} \quad (61)$$

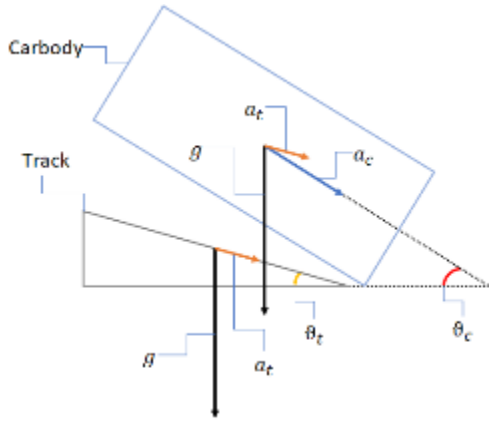

Figure 110 - Sway model calculation

The flexibility coefficent achieved with the split frame implemented is 5.5 % compared to 2.3 % with the rigid frame. The values are calculated for the vehicle at tare load and will rise with increased load to about double the value.

The first stage assessment, safety against derailment on twisted track, is carried out through simulations, in line with the methods stated by EN14363 [128]. The methods used for the assessment are the first and second indicated by the standard. These are respectively related to the wheel lift Δz the derailment ratio. The track cases are built accordingly to the standard. In Figure

111 and Figure 112 are shown the results obtained for the first and second method respectively. The red line displays the limit value for each test condition. As shown, the vehicle is safe against the derailment on twisted track in both cases.

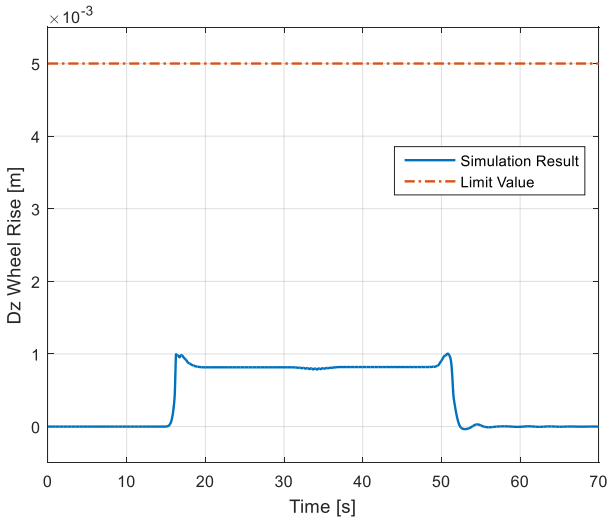

Figure 111 - Twisted track assessment EN14363 [128] - method 1

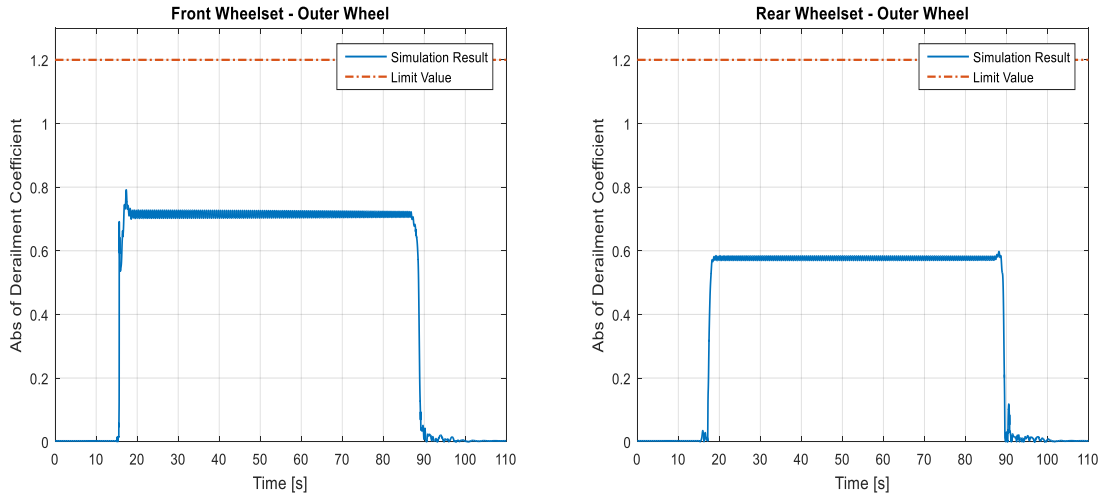

Figure 112 - Twisted track assessment EN14363 [128] - method 2

4.3.2 Second stage assessment

The second stage assessment, regarding dynamic performances, is performed according to EN14363 [128]. First, the dynamic performance on curved track is verified, secondly the stability. In Table 19 the track cases used for the assessment of the dynamic performance on curved track

are shown. An additional case of a 600 m curve is introduced with respect to the four (4) test zones specified in the standard.

Table 19 - Track cases for dynamic performance assessment on curved track

Test zone	Unit	1	2	x	3	4
Radii	m	10279	1500	600	400	250
Cant	mm	0	13.3	150	150	150
Cant deficiency	mm	20	100	100	100	100
Speed	km/h	132.0	120.0	112.8	92.1	72.8

In Table 20 the achieved results are reported as percentage of the threshold level. Thus,

$$(.) = \frac{assessment\ variable}{threshold\ level} * \mathbf{100}\%. \quad \textbf{(62)}$$

The missing values in the table are not required for the assessment. In all the studied cases, the vehicle is proven to be safe.

Table 20 - Dynamic performance assessment on curved track results

		Percentiles	Wheelset	Test Zone									
				1		2		x		3		4	
				Left HC	Right HC	Left HC	Right HC	Left HC	Right HC	Left HC	Right HC	Left HC	Right HC
Sum of Guiding Forces		h=0.15 %	Front	24%	34%	-	57%	-	50%	-	51%	-	58%
			Rear	25%	38%	-	66%	-	67%	-	50%	-	48%
		h=99.85 %	Front	38%	27%	53%	-	57%	-	51%	-	58%	-
			Rear	38%	23%	71%	-	64%	-	52%	-	38%	-
Derailment Ratio		h=0.15 %	Front	-	-	-	15%	-	23%	-	47%	-	53%
			Rear	-	-	-	16%	-	16%	-	17%	-	41%
		h=99.85 %	Front	-	-	16%	-	27%	-	47%	-	56%	-
			Rear	-	-	17%	-	16%	-	17%	-	42%	-
Acceleration in Vehicle Body	Lateral	h=0.15 %		18%	19%	-	13%	-	15%	-	12%	-	11%
		h=99.85 %		17%	18%	16%	-	16%	-	11%	-	13%	-
	Vertical	h=0.15 %		-	-	10%	10%	10%	10%	10%	10%	9%	9%
		h=99.85 %		-	-	13%	13%	13%	13%	12%	13%	10%	11%

According to EN14363 [128], a vehicle with admissible speed between 100 and 300 km/h must ensure stability up to 110 % of its admissible speed. For the two-axle vehicle the maximum admissible speed 120 km/h, so it's necessary to prove that the vehicle is running safely on a straight track at a speed of 132 km/h. Three equivalent conicity cases are compared to ensure stability on a wide range of possibilities. The wheel-rail combinations chosen to produce the desired equivalent conicities are shown in Table 21.

Table 21 – Wheel – Rail combinations

Case n.	Wheel profile	Rail profile	Track gauge	Rail inclination	Conicity
(a)	S1002	UIC60	1435	1:40	0.18
(b)	S1002	UIC60	1435	1:20	0.01
(c)	S1002	UIC60	1430	1:30	0.4

The equivalent conicity as functions of wheelset displacement for the three cases are reported in Figure 113.

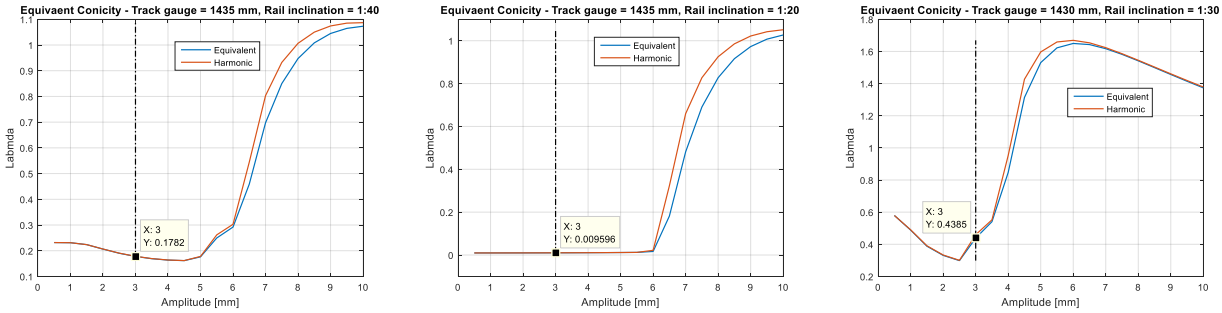

Figure 113 - Conicity profiles: case a (left), case b (center) and case c (right)

For each conicity case the assessment is performed with three different track irregularity profiles. The first one is the synthetic ERRI_High [131] while the other two are measured data provided by Huddersfield University in the following, called track_110 and track_160. For each case the assessment is performed on a speed range from 60 to 260 km/h with a speed step of 2.5 km/h. Both track shift force and wheelset lateral acceleration assessments quantities are considered for the critical speed evaluation. In Figure 114, Figure 115 and Figure 116 the results obtained for conicity case a), b) and c) respectively are shown. The left figures show results evalauated as track shift force and in the right figures as acceleration. In Table 20, the results are shown as percentage of the threshold level.

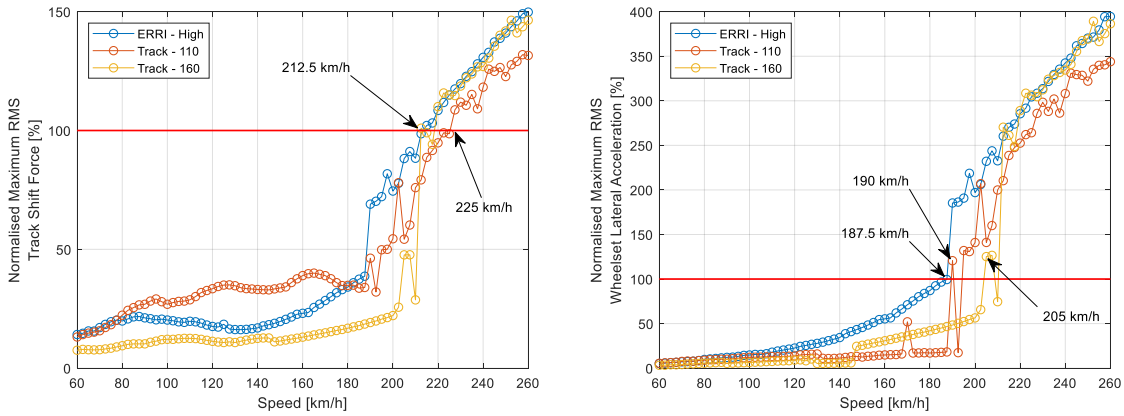

Figure 114 - Stability assessment, case a): track shift force (left), wheelset acceleration (right)

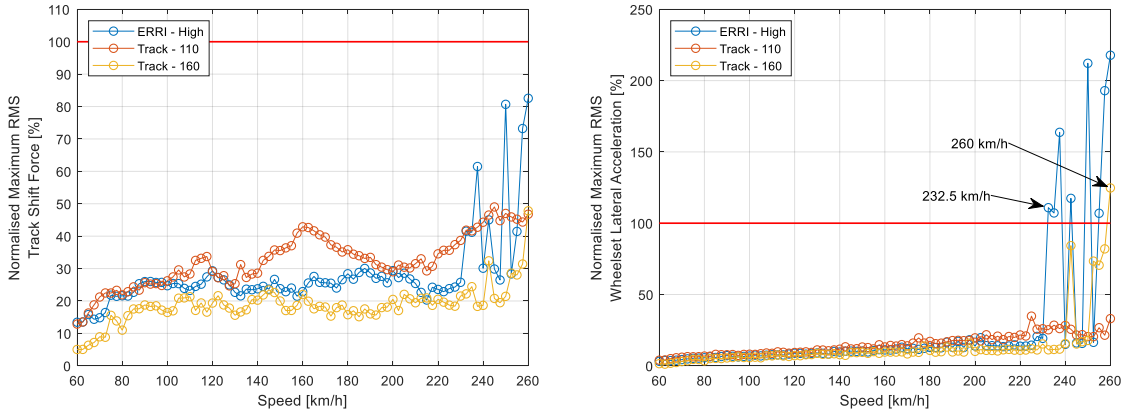

Figure 115 - Stability assessment, case b): track shift force (left), wheelset acceleration (right)

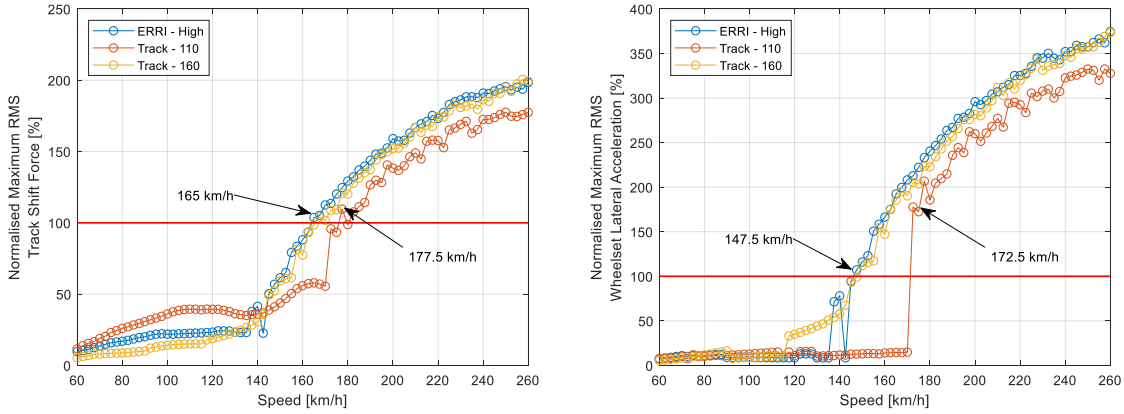

Figure 116 - Stability assessment, case c): track shift force (left), wheelset acceleration (right)

The results are summarized in Table 22, which shows the lowest critical speed of the front and rear wheelsets. The vehicle is stable within the requirements of the standard. Moreover, in the worst condition, the vehicle is stable up to 122% of its admissible speed.

Table 22 - Stability assessment results as critical speed

Case	Track irregularities	Critical speed [km/h]	
		Track shift force	Wheelset lateral acceleration
Case (a) Conicity: 0.18 Track gauge: 1435 Rail cant: 1:40	ERRI_High	212.5	187.5
	Track_110	225	190
	Track_160	212.5	205
Case (b) Conicity: 0.01 Track gauge: 1435 Rail cant: 1:20	ERRI_High	>260	232.5
	Track_110	>260	>260
	Track_160	>260	260
Case (c) Conicity: 0.4 Track gauge: 1430 Rail cant: 1:30	ERRI_High	165	147.5
	Track_110	177.5	172.5
	Track_160	165	147.5

4.4 WHEELSET STEERING OF SOLID-AXLE WHEELSET

Wheelset steering of a solid axle wheelset can principally be setup in two different ways, either with the actuator in parallel with the existing longitudinal wheelset guidance or with the actuator in series with the existing longitudinal wheelset guidance. With the actuator in parallel, the passive wheelset guidance will ensure stability and this guidance must therefore be rather stiff. It also means that the actuator must overcome this stiffness when trying to yaw the wheelset into an approximately radial position. To do this, the actuator must have a high force capability. With the actuator in series with the existing longitudinal wheelset guidance, the actuator can be designed for a much lower force than with the actuator in parallel. A third option would be to install a frequency dependent (but still passive) wheelset guidance. This option is explored in Section 4.4.3.

4.4.1 Actuator in parallel with spring

To improve the performances of the two-axle vehicle with solid wheelset in terms of wear, the use a feedback approach for the actuator in parallel with the spring solution was initially considered. Hence, the yaw angle of the wheelset relative to the carbody would be part of a closed loop control. In a first attempt it is searched which position the wheelsets must take to reduce the wear during curve negotiation. Then, the best signal to be used for feeback control is sought for. In this stage the wheelset lateral position and angle of attack with respect to the centre line are considered to be known without uncertainty. Nevertheless, the control logic applied is kept simple to resemble a real-life application. The chosen control logics are Proportional (P) or Proportional Integral Derivative (PID) controllers. Four different reference signals are compared. Radial steering (Section 2.5.2.3 – 1.a) and Creepage steering (Section 2.5.2.3 – 1.b.1) are applied together with two new approaches called Front Radial steering (FRS) and Combined steering. Front Radial steering only forces the front wheelset to be in radial position without applying any action to the rear one. Combined steering forces the front wheelset to be in radial position and the rear one to have lateral position always at the centre line of the track. Figure 117, Figure 118, Figure 119 and Figure 120 show the control schemes for Radial steering, FRS, Combined steering and Creepage steering respectively. Here, y stands for the lateral wheelset position, ψ for the attack angle while subscript 1 stands for front wheelset and 2 for rear wheelset.

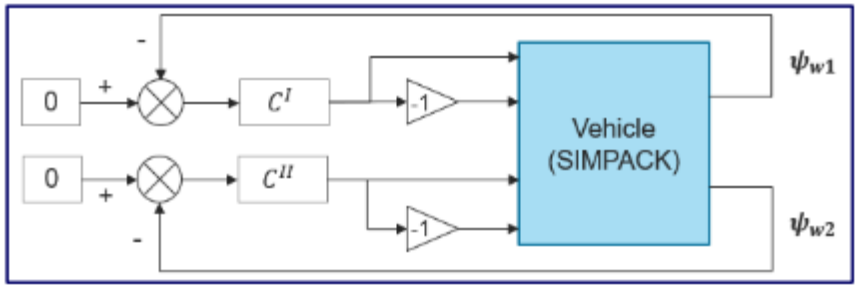

Figure 117 - Radial steering control scheme

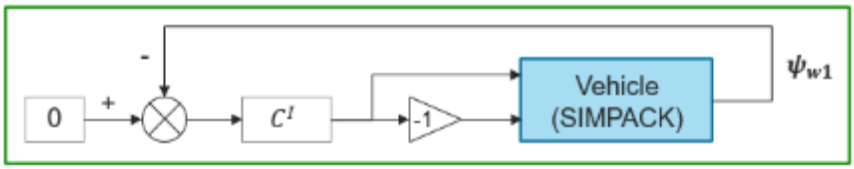

Figure 118 - FRS control scheme

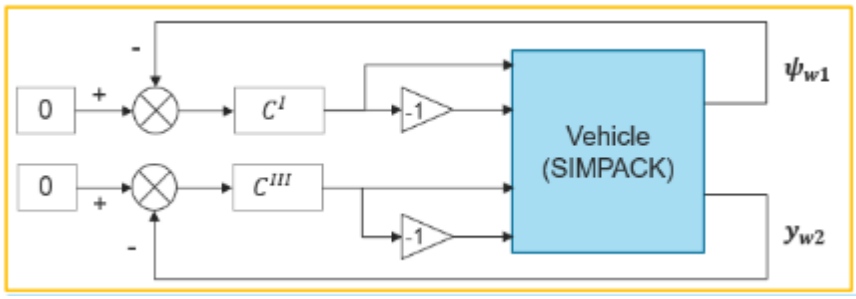

Figure 119 - Combined steering control scheme

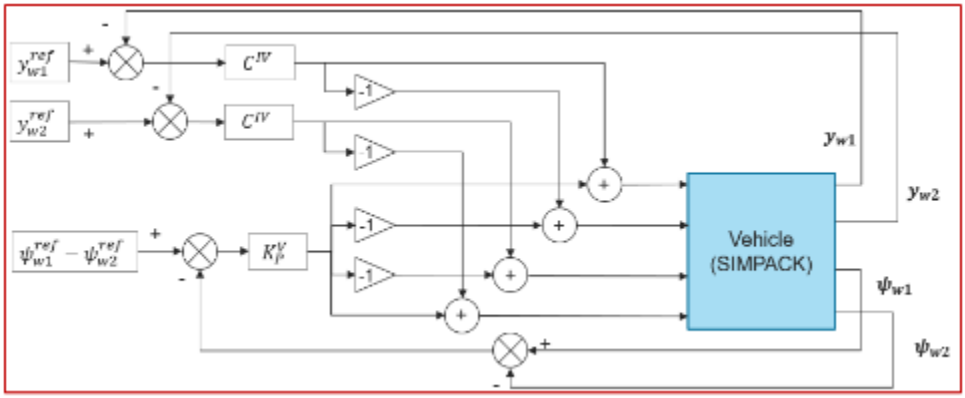

Figure 120 - Creepage steering control scheme

The reference signals are applied to the conicity cases of Table 21. Each reference signal on each conicity is applied on five different curves with twelve different Non-compensated Lateral Acceleration (NLA) for each curve. This generates a table of five by twelve velocities. The first speed for each curve is set to 10 km/h to verify the behaviour of the controlled system at a very low speed with the vehicle running at cant excess. The considered curves and speeds are shown in Table 23.

Table 23 - Running conditions for steering performance evaluation

		V											
		km/h											
			NLA [m/s^2]										
Radius	Cant		-0.26	-0.17	-0.11	-0.08	-0.05	0	0.05	0.09	0.18	0.34	0.65
100	0.06	10	13	17	19	20	21	23	24	25	27	31	37
250	0.15	10	48	51	53	54	55	56	58	59	61	65	73
400	0.1	10	45	50	53	55	56	58	60	62	66	72	82
600	0.08	10	45	52	56	59	61	64	67	69	74	82	96
1066	0.06	10	43	55	62	66	69	74	78	82	89	101	120

The results achieved with the different approaches are shown in Figure 121 and Figure 122 for the front and rear wheelset respectively in terms of total wear number in the circular curve. In each

figure the wear distribution for the passive two-axle vehicle is displayed as reference. In each graph the x-axis is NLA in which, for simplicity of representation, -0.4 m/s^2 corresponds to 10 km/h. The y-axis shows the curve radius. The wear number is shown in a logarithmic scale where red color corresponds to high values of wear while blue corresponds to low ones.

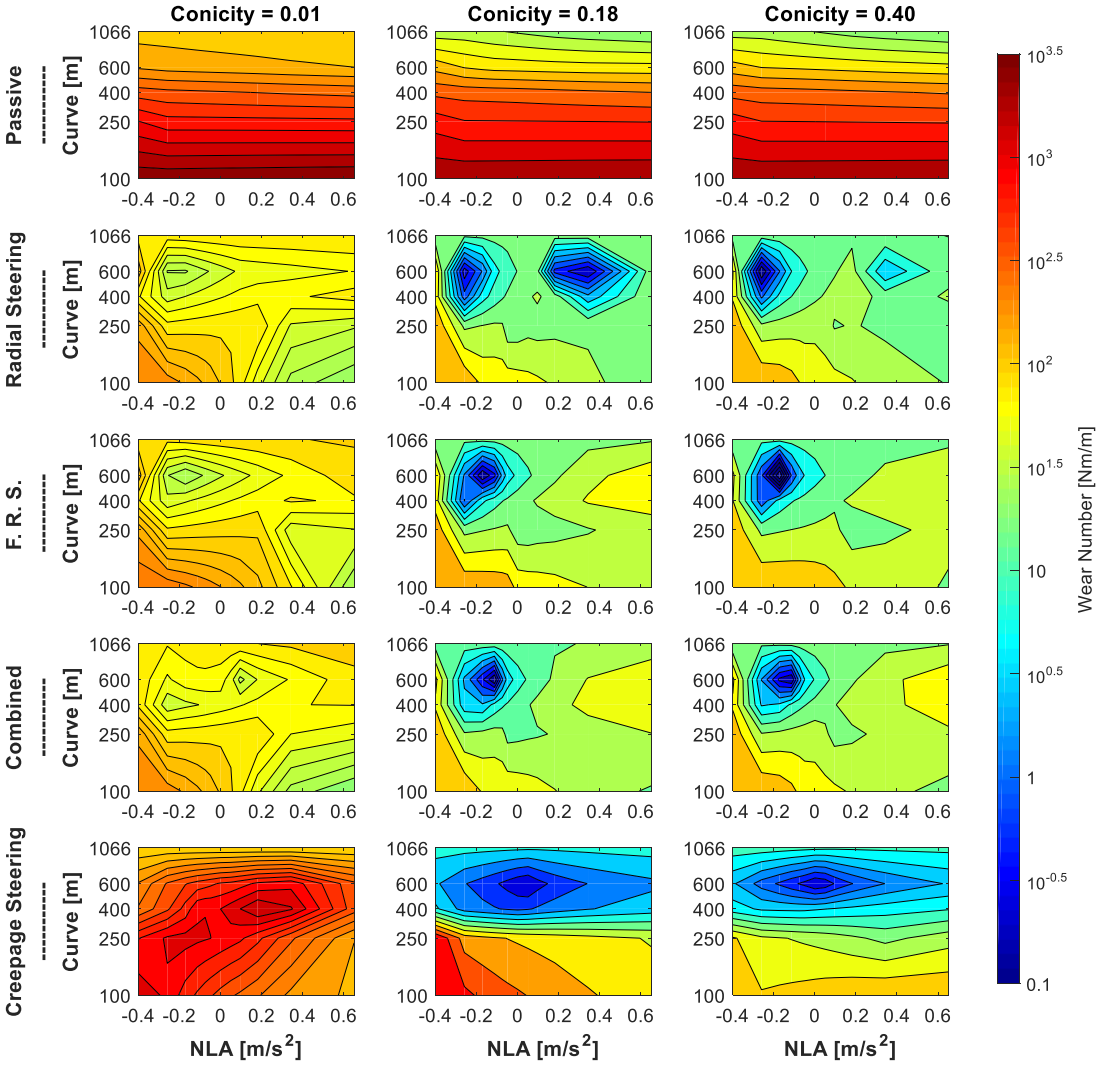

Figure 121 - Front wheelset wear distribution - Feedback approach

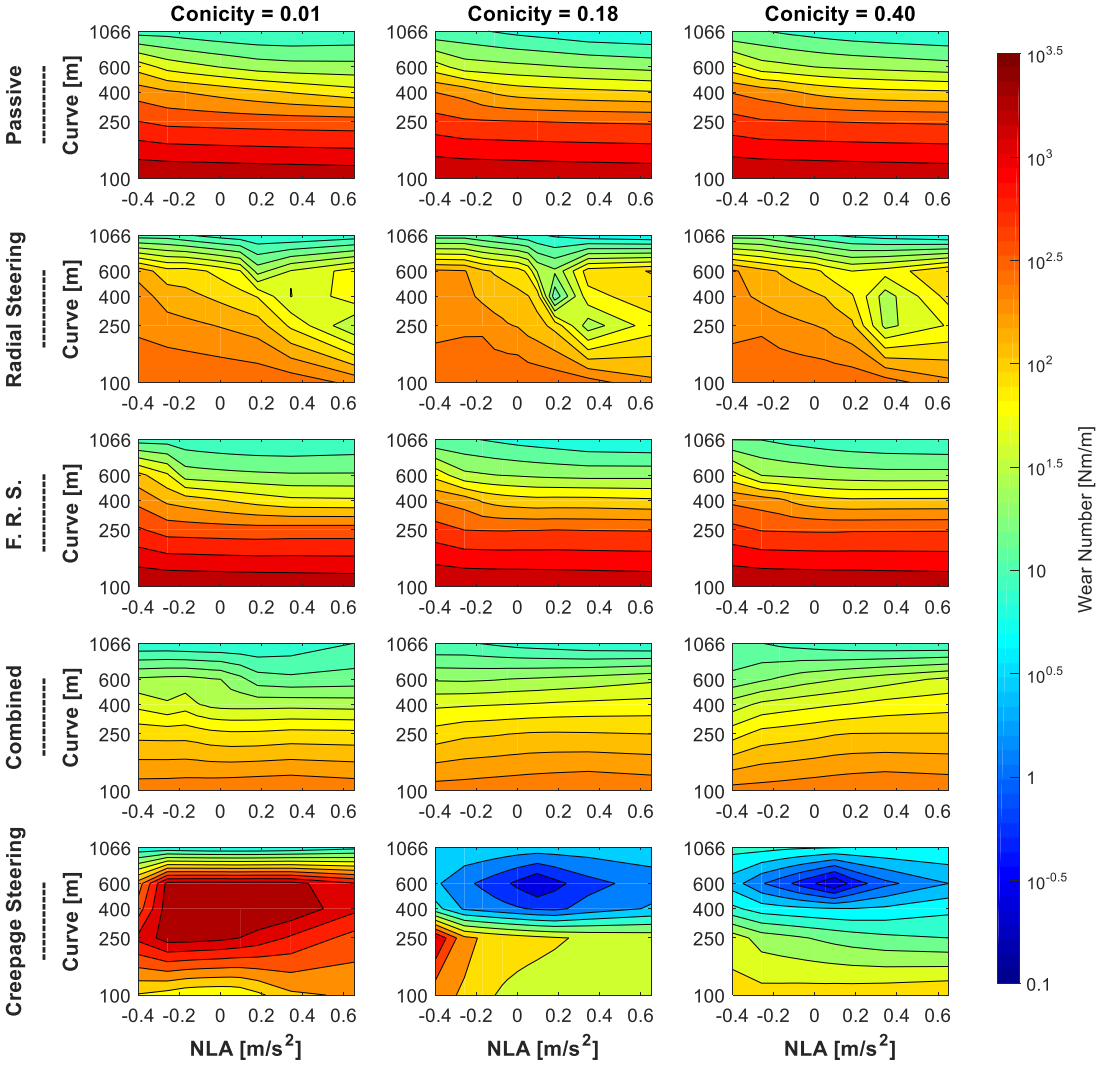

Figure 122 - Rear wheelset wear distribution - Feedback approach

Additionally, for a better comparison, Figure 123 and Figure 124 show the reduction achieved by each approach in in terms of wear with respect to the passive two-axle vehicle. The reduction is calculated as:

$$\boldsymbol{Reduction} = \frac{\boldsymbol{Wear_{Passive} - Wear_{Active}}}{\boldsymbol{Wear_{Passive}}}. \quad \textbf{(63)}$$

The reduction factor so achieved is again plotted against NLA and curve radius. Blue color means high wear reduction and so a positive influence of the proposed control, while red means a negligible or negative wear reduction (not displayed) of the proposed control.

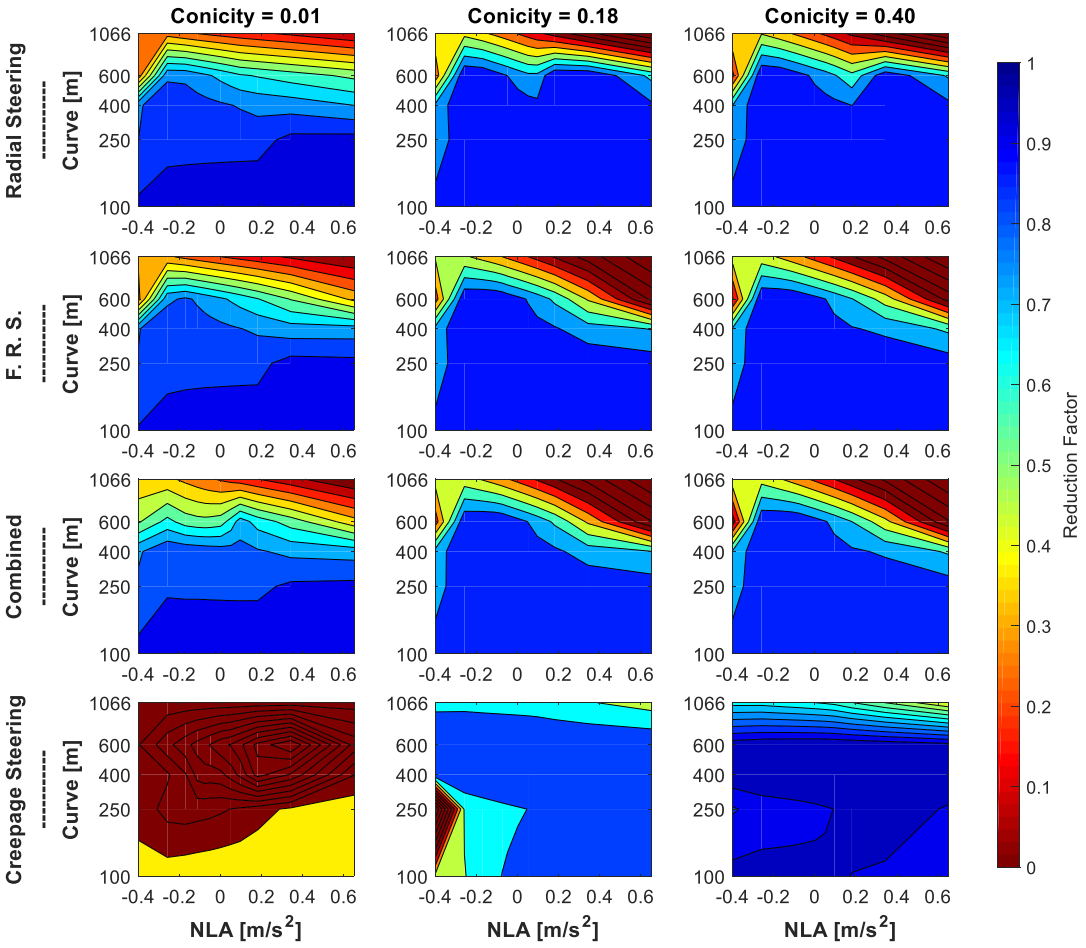

Figure 123 - Front wheelset wear reduction distribution - Feedback approach

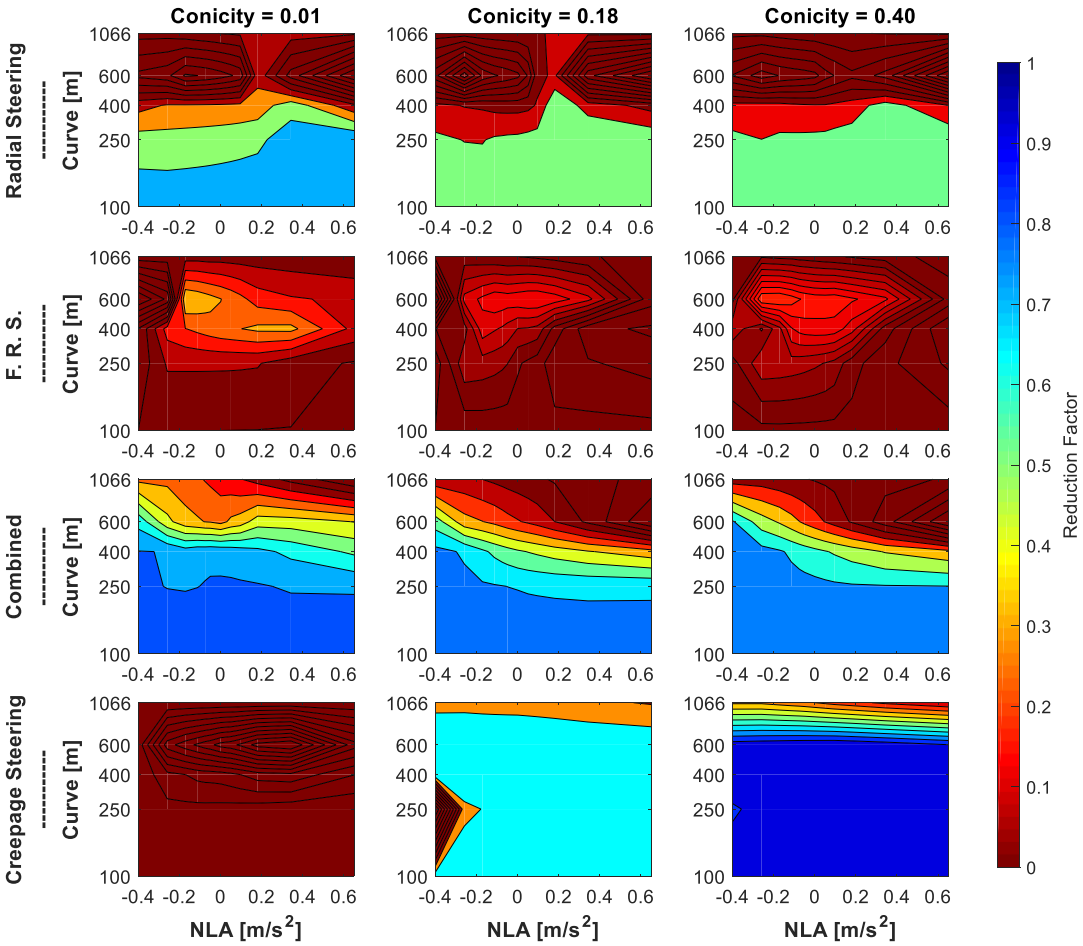

Figure 124 - Rear wheelset wear reduction distribution - Feedback approach

Considering the front wheelset, Figure 121 and Figure 123, it can be said that:

- Radial steering, FRS and Combined steering performed similarly and they improved the performance especially for small curve radius and low NLA for all the considered conicities.
- Creepage steering is the best solution in all curves and NLA for equivalent conicities of 0.18 and 0.4, but it fails for the lowest conicity of 0.01.

Considering the rear wheelset, Figure 122 and Figure 124, it can be said that:

- Radial steering performs well for small curve radius, but it fails for larger ones.
- FRS fails in improving the situation compared with the passive vehicle
- Combined Steering gradually decreases its effect with the increase of both curve radius and NLA.
- Creepage steering repeats the pattern obtained for the front wheelset.

None of the tested solutions can be considered optimal. Thus, a new feed-forward approach is searched. The feed-forward approach introduces the benefit of removing the necessity of measurement of wheelset lateral position or angle of attack. Nevertheless, the knowledge of the NLA at which the vehicle is running will be required.
First a benefit function is created. The function compares the feedback approaches and takes into account the absolute wear number, the achieved reduction, and the requested actuator force to achieve that condition. The so-defined function will favour the control approach that generates the lowest wear number with the highest reduction requiring the lowest possible actuator force.
The benefit function minimum between the four tested control approaches is then found for each point of Table 23. The actuator forces corresponding to the benefit function minimum are stored. An almost bi-linear relation between the stored forces and NLA and curvature is found for the front and rear wheelset. The force distribution generated from the benefit function minimum is shown in Figure 125.

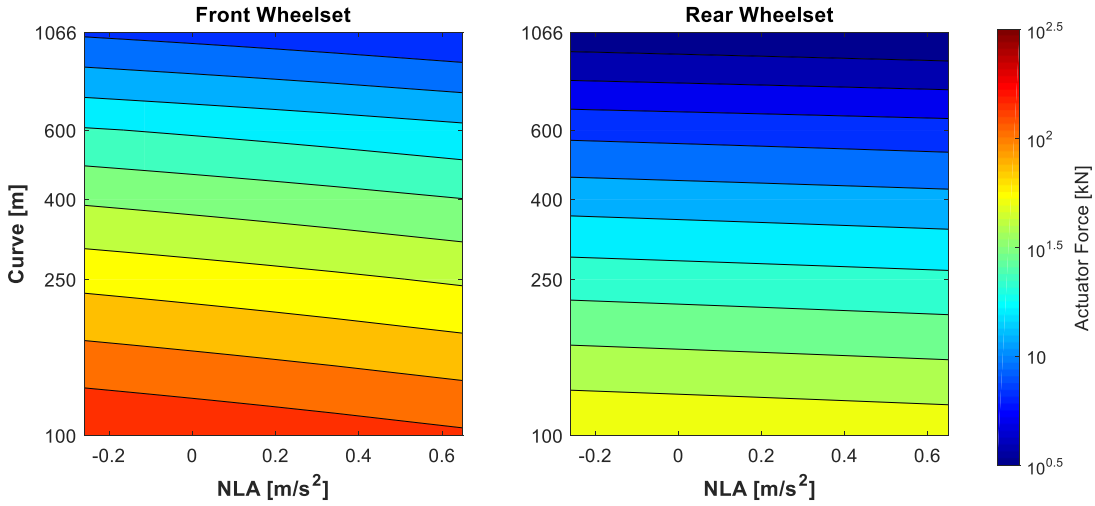

Figure 125 - Feedforward force distribution

The feed-forward approach so defined is applied to the set running cases. The maximum required force is approximately 180 kN, which is needed in 100 m curves while running at cant excess. To resemble a more realistic installation the required force is limited to 50kN. In Figure 126 and Figure 127 the achieved results with the feed-forward approach (limited and not limited) are shown in terms of absolute wear number for the front and rear wheelset respectively. The passive vehicle wear distribution is given as reference. Additionally, the benefit function minimum wear distribution is displayed.

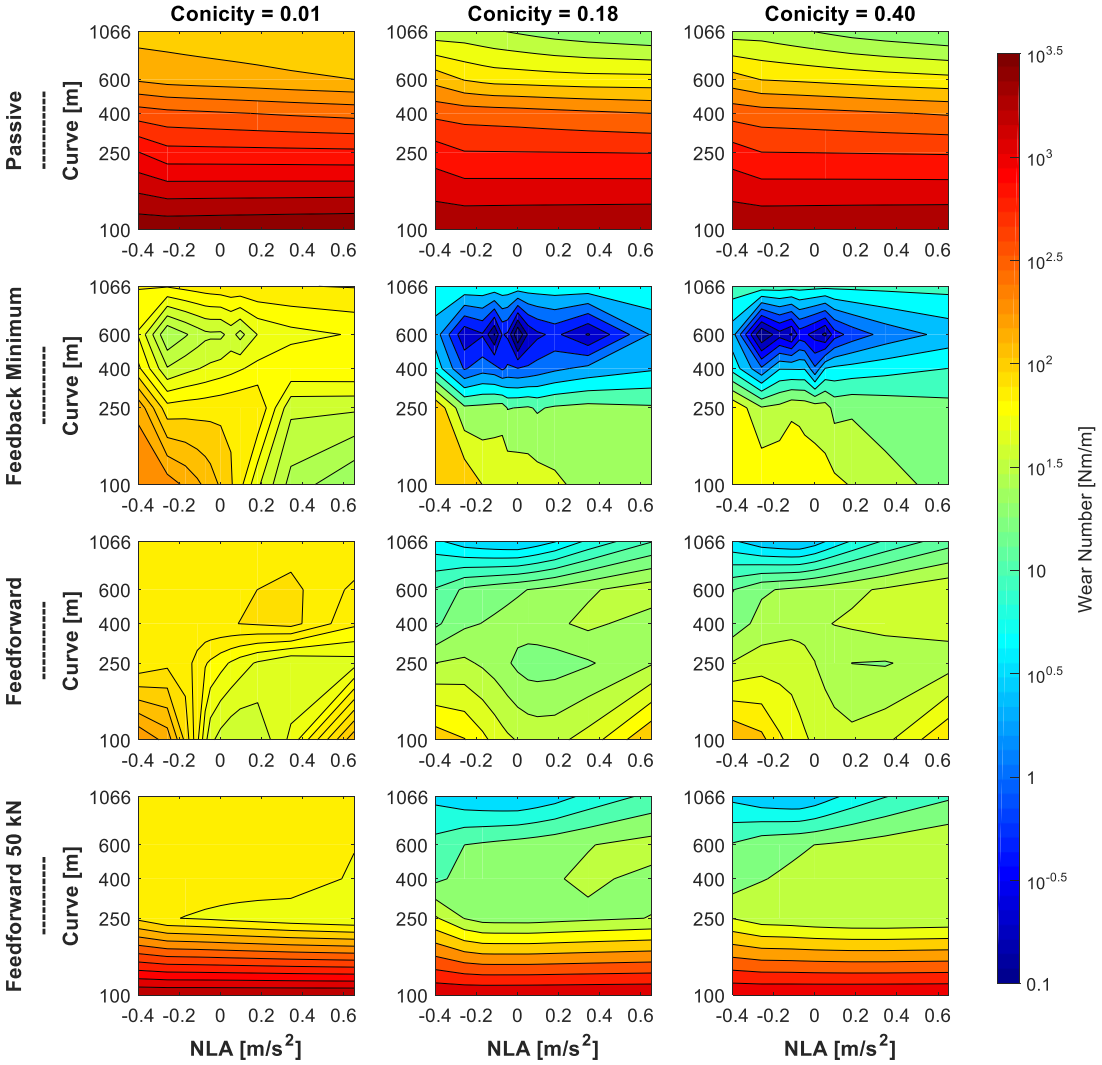

Figure 126 - Front wheelset wear distribution - Feedforward approach

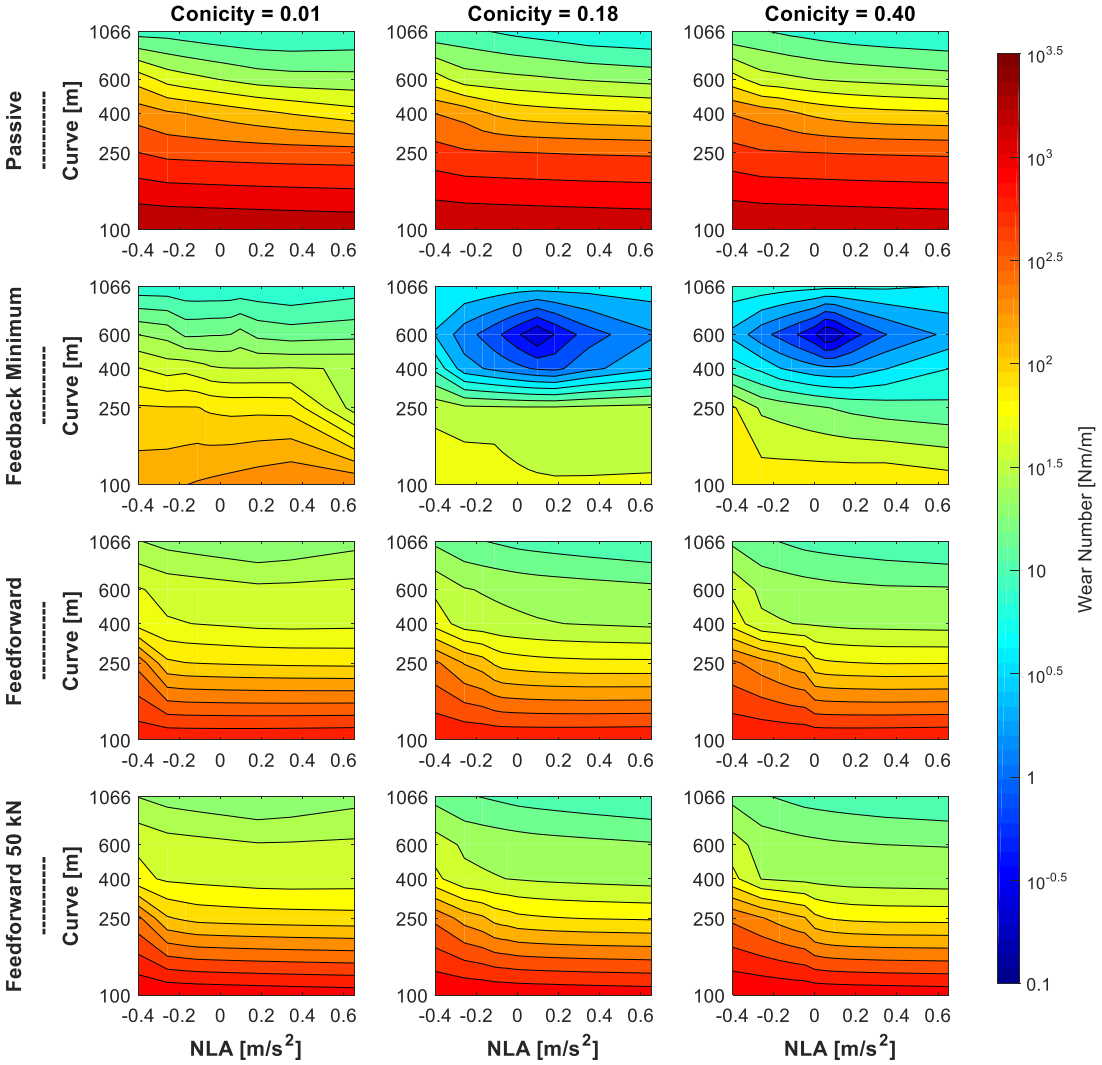

Figure 127 - Rear wheelset wear distribution - Feedforward approach

As for the feedback approach, the results are shown in terms of reduction achieved by the solution with respect to the passive vehicle. In Figure 128 and Figure 129 the results are shown for the front and rear wheelset respectively.

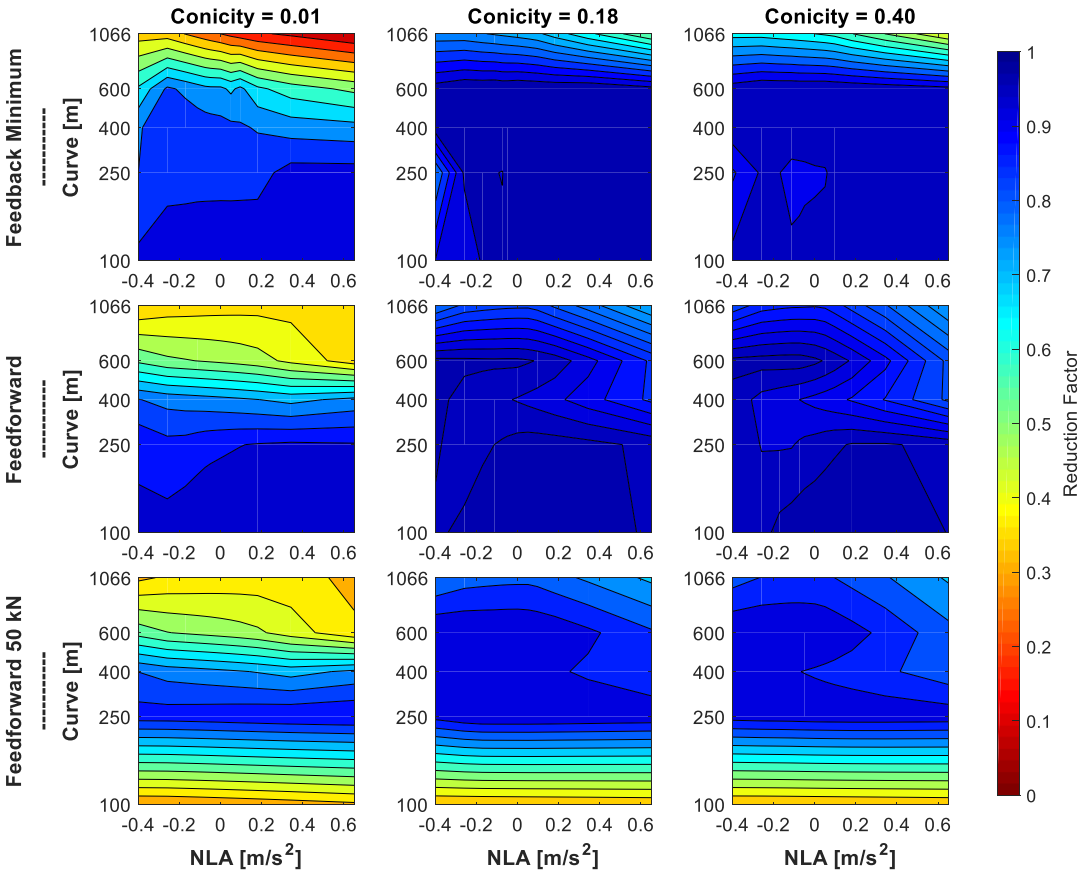

Figure 128 - Front wheelset wear reduction distribution - Feedforward approach

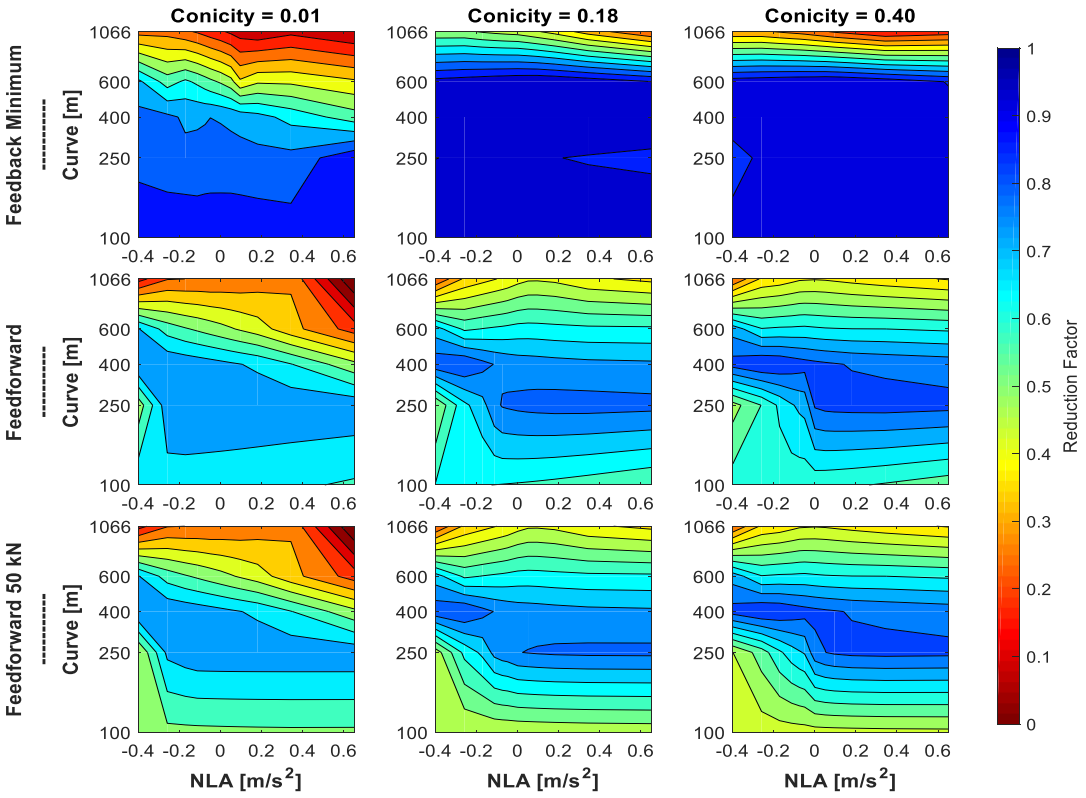

Figure 129 - Rear wheelset wear reduction distribution - Feedforward approach

Considering the results for the front wheelset, Figure 126 and Figure 128, it can be said that:

- The feedforward approach performs almost independently from the conicity and the achieved wear distribution is close to the feedback minimum especially for low conicity and low curvatures.
- The 50 kN limitation reduces the control action in narrow curves still producing improvements with respect to the passive vehicle reaching the lowest reduction of 30 % at 10 km/h for a 100 m curve.

Considering the results for the rear wheelset, Figure 127 and Figure 129, it can be said that:

- The 50 kN limitation doesn't influence the result.
- The feedforward approach is far from the feedback minimum especially for high conicities and narrow curves, but it still reduces the wear in most studied conditions and it is robust for conicity variations.

In conclusion, the feedforward approach is a simple and robust solution that can improve the two-axle vehicle with solid axels and actuator in parallel with spring in terms of wear condition.

4.4.2 Actuator in series with spring

In this section, a yaw relaxation control strategy is applied to the two-axle vehicle for the solid-axle configuration. Here the 'actuator in series with spring' means the linear actuator is connected in series with the primary guidance components (rubber bushing in this case), which provide the main yaw stiffness in the longitudinal direction. The purpose of this configuration is to utilize the different frequency response features of the actuator and serial stiffness to improve the curving performance without affecting the vehicle's stability [84].

It is known that the solid-axle wheelset has the natural steering capacity due to its physical configuration. With a low yaw stiffness, the solid axle wheelset has a good curving performance. However, the hunting motion can be a big issue with too low yaw stiffness. Figure 130 shows the wheelset lateral displacement of the passive solid-axle vehicle with a very low yaw stiffness during a curve negotiation. In this scenario, the curve radius is 400 m and cant is 100 mm. The vehicle speed is 82 km/h, meaning a cant deficiency condition with an uncompensated acceleration of 0.65 m/s^2. It can be seen from the simulation result that the hunting motion is very obvious, albeit the wheelset is trying to negotiate curve.

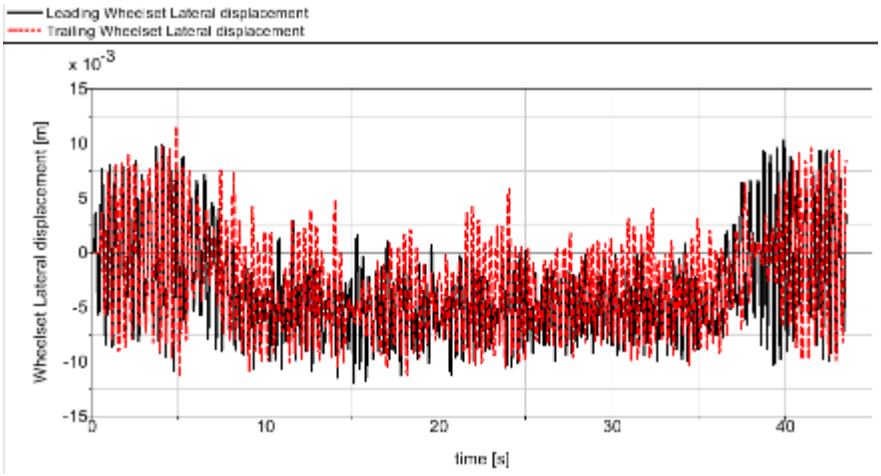

Figure 130 - Wheelset lateral displacements for passive solid-axle vehicle with low yaw stiffness (with track irregularities)

To deal with this problem, one option is to apply a control strategy to achieve the stability, but such a control system should not affect the quasi-static curving performance. In fact, the steady-state curving behaviour can be properly controlled by a low-frequency linear actuator. The yaw relaxation approach utilizes the natural steering effect of the wheelset to negotiate the curve by releasing the internal steady-state loads of the actuators. This actuator only needs to provide very low frequency steering forces, whereas the instability of the wheelset can be resisted at higher frequencies by its serial spring having a relatively large stiffness. In this actuation system, the electromechanical actuator is selected for this application due to its low cost and relatively high reliability. The sensor

required for this control scheme is only a load cell or a displacement transducer inside the electromechanical actuator. Figure 131 exhibits the general layout of the yaw relaxation control system. The actuator length is the observed variable, whilst the output of the controller is the desired force to be realised.

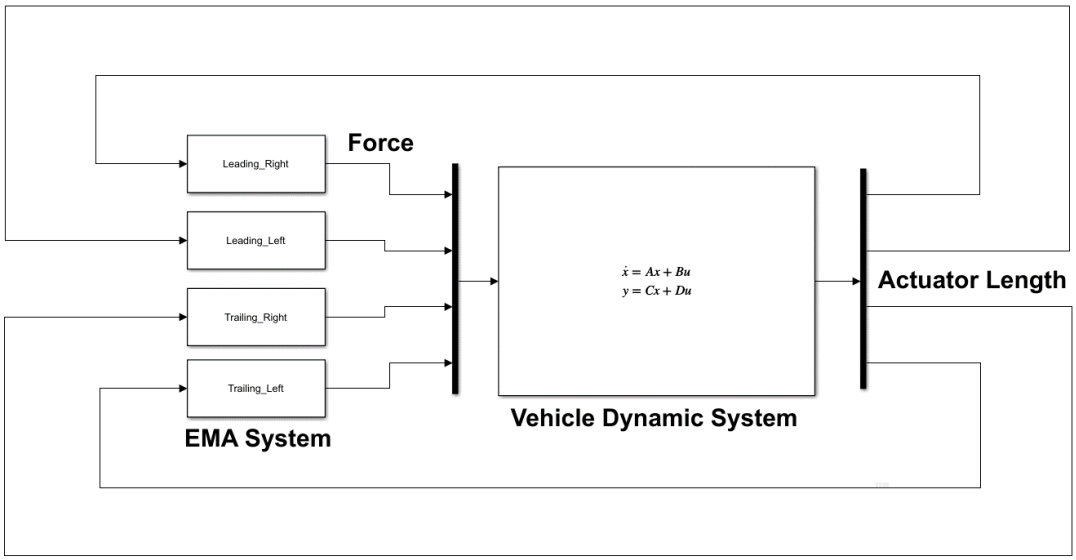

Figure 131 - General layout of yaw relaxation system

Figure 132 demonstrates the electromechanical actuator model used in this application. Inside this actuator model, the PID controller is used to control the position of the screw nut to release the low-frequency internal load by adjusting the quasi-static motor torque to zero (and hence the force applied via the series spring to the longitudinal suspension). Since the actuation process only takes place at very low frequencies, the controller is designed to have low frequency response features with a high-frequency cut-off effect.

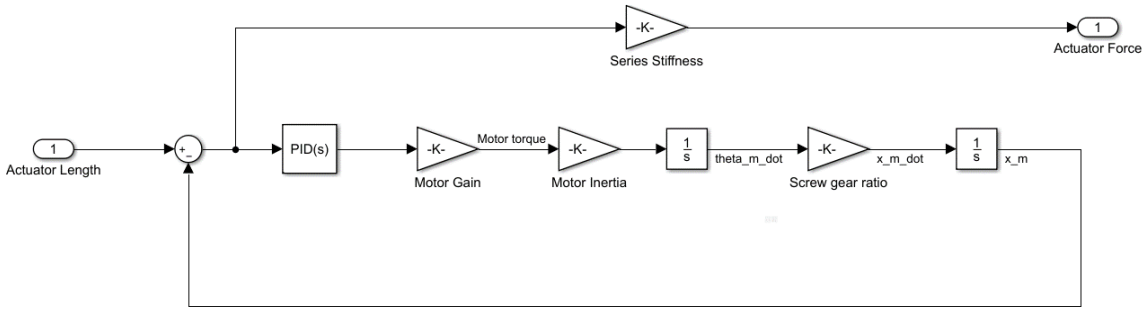

Figure 132 - Electromechanical actuation model

Figure 133 to Figure 137 exhibit the vehicle dynamic performances with the yaw relaxation control for the same track case used in the passive vehicle (400 m curve, corresponding to Figure 130). In Figure 133, it can be seen from the wheelset displacements that the hunting motion disappears with this yaw relaxation approach. In Figure 134, all the lateral wheel/rail forces of two wheelsets have low values without flange contacts. In Figure 135, both wheelsets exhibit the similar attack angles towards the curve centre, forming the lateral creep forces to counteract the cant deficiency. The leading and trailing wheelsets exhibit very similar behaviours and represent the ideal curving features. From Figure 136, it can be realized that the maximum actuation force for the curve negotiation takes place in the transition, whereas the actuation force is very small during the circular curve. As mentioned previously, the curving behaviour is controlled by the actuator in the adjustment of its own length. The actuation system needs to adjust the actuator length continuously in the transition, but almost does not need to adjust its length on the circular curve. From Figure 137, it is obvious that the wheel wear numbers are very small with this control approach. Similar to the actuation force, the maximum wear index occurs on the transition rather than the circular curve.

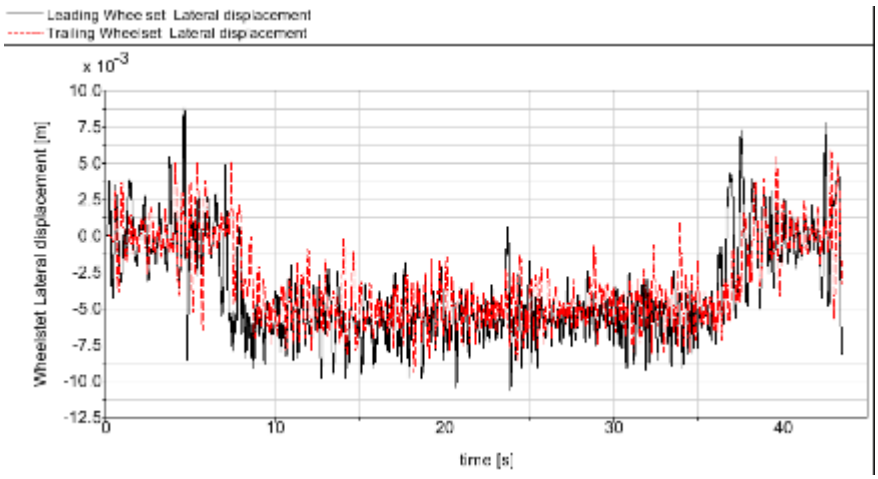

Figure 133 - Wheelset lateral displacements for yaw relaxation control (with track irregularities)

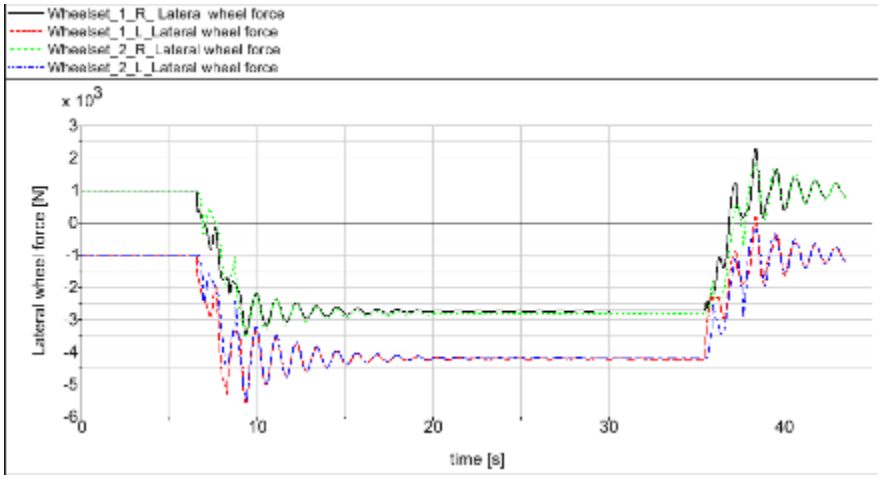

Figure 134 - Wheel/rail lateral forces for yaw relaxation control (without track irregularities)

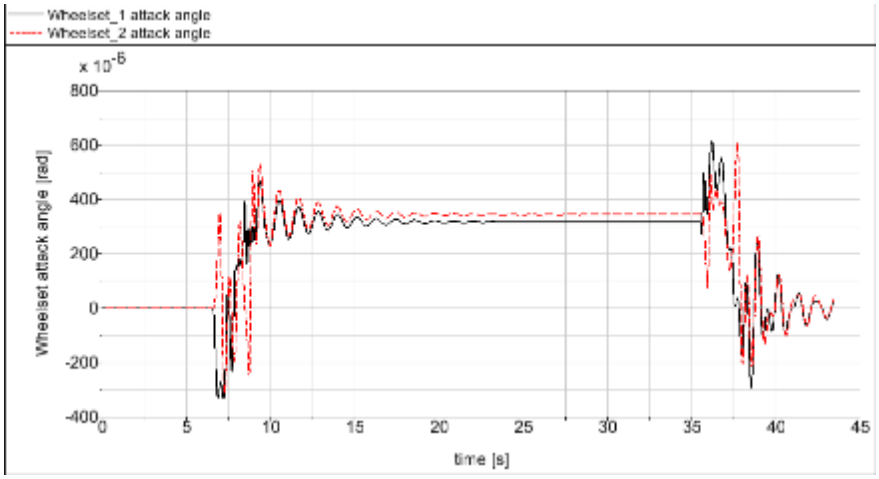

Figure 135 - Wheelset attack angles for yaw relaxation control (without track irregularities)

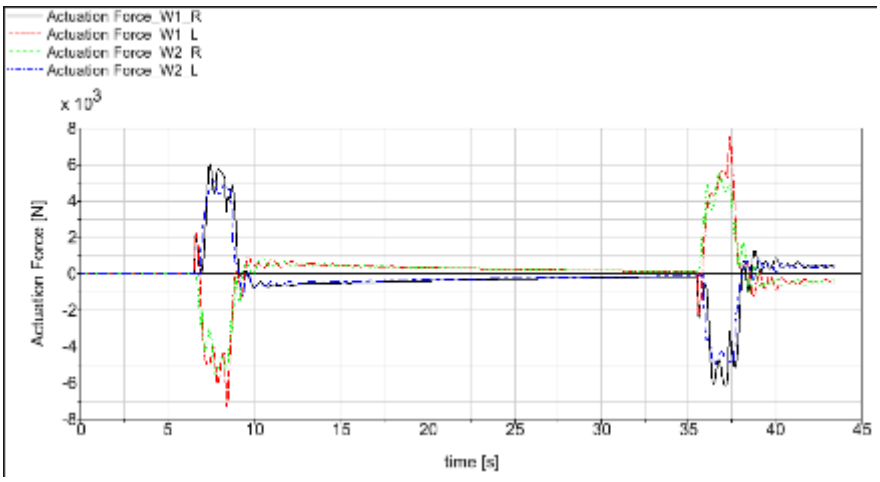

Figure 136 - Actuator Forces for yaw relaxation control (without track irregularities)

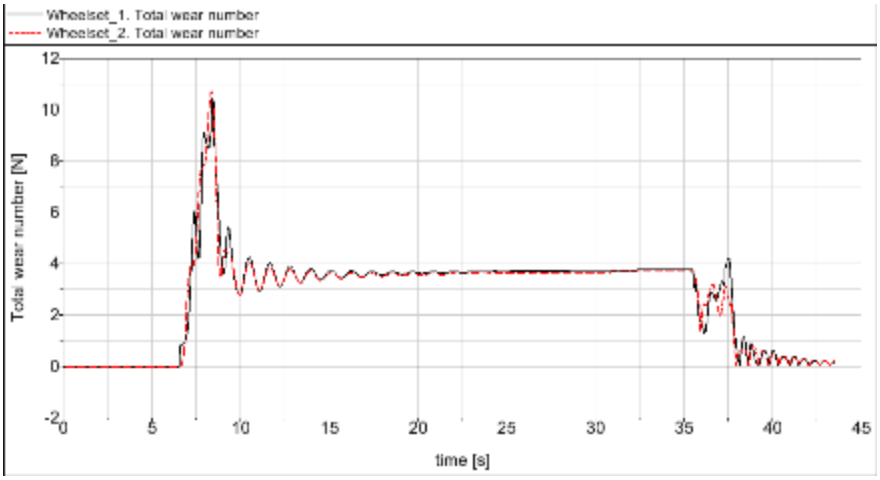

Figure 137 - Wheelset wear indexes for yaw relaxation control (without track irregularities)

From Figure 136, the actuation system mainly acts in the transition curve with a relatively low actuation force, which has a very low power requirement. This technique can provide very effective results in reducing the wheel/rail wear for the curve negotiation at a very low cost. For the stability issue, the hunting motion is actually resisted in the passive way. The low-frequency actuator almost rigid above 1 Hz. The hunting motion of the wheelset, which normally has higher frequency than 1 Hz, can be prevented by relatively large stiffness of the serial spring. Even though the actuator force appears to be larger under the high-frequency excitations from simulation results, mainly by hunting motion, in fact the actuator almost does not react to these high-frequency disturbances meaning very little energy consumption for high-frequency responses.

As agreed by the simulation group of Run2Rail project, the track cases, including the curved tracks with the radii of 250 m, 400 m, 600 m and 1500 m, are utilized to test the dynamic performances of the target concept vehicles. Here the track cases are employed to investigate the curving performances of the two-axle vehicle with the yaw relaxation control system, as shown in Table 24 and Table 25. It can also be noticed that the larger actuator forces are required to negotiate the smaller radius curves. From Table 24 and Table 25, for the same curve, larger actuator forces are needed at the higher speed due to shorter response time for the actuation system. Additionally, the stability of the vehicle can be guaranteed with a properly tuned actuator response.

Table 24 - Curving indexes for yaw relaxation control at 0.65 m/s² uncompensated acceleration

Track case: Radius [m] / Cant [mm]	Speed [km/h]	Wheelset lateral displacement [mm]	Maximum Wheel/rail lateral force [kN]	Derailment coefficient [-]	Wheelset attack angle [mrad]	Wear number - Curve [N]	Wear number - Transition [N]	Max. Actuator Force [kN]	Actuator Power [W]
250 / 150	72.7	7.3	4.45	0.07	0.32	5.54	11.6	7.0	14.32
400 / 100	82.2	6.2	4.21	0.067	0.35	3.78	10.7	7.54	19.6
600 / 80	95.5	4.9	4.66	0.074	0.39	3.32	9.5	8.27	15.89
1500 / 60	142.4	2.1	4.88	0.078	0.43	3.0	4.07	4.0	5.95

Table 25 - Curving indexes for yaw relaxation control at balanced speeds

Track case: Radius [m] / Cant [mm]	Speed [km/h]	Wheelset lateral displacement [mm]	Wheel/rail lateral force - Curve [kN]	Derailment coefficient [-]	Wheelset attack angle [mrad]	Wear number - Curve [N]	Wear number - Transition [N]	Max. Actuator Force [kN]	Actuator Power [W]
250 / 150	56.4	7.3	1.05	0.019	0.09	3.11	8.35	5.54	7.19
400 / 100	58.2	6.2	0.78	0.015	0.078	1.52	5.36	5.75	7.53
600 / 80	63.8	4.8	0.83	0.015	0.064	0.9	4.33	5.49	8.2
1500 / 60	87.3	2.0	0.99	0.018	0.036	0.33	1.61	2.61	2.63

4.4.3 Frequency dependent axle guidance

To improve the two-axle vehicle with solid axles, it is possible to replace the rubber bushing of Figure 107 with a Hydraulic bush (also called HALL = Hydraulisches AchsLenkerLager in German). This will avoid the necessity of an active control. The hydraulic bush is visualized in Figure 138 left and it can be modelled as in Figure 138 right.

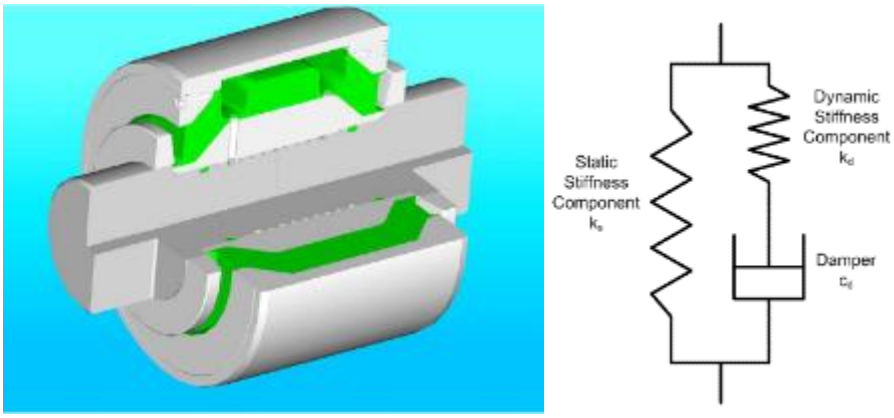

Figure 138 - Hydraulic bush (HALL): view (left) and model (right) [130]

This hydraulic bush has a frequency dependent stiffness. With reference to Figure 139 right, at low frequencies the bush shows a stiffness equal to the static stiffness K_s while at higher frequencies the stiffness becomes the sum of the static K_s and dynamic K_d. The setting of the static stiffness to a low value will allow the wheelset by self-radial steering to take an approximately radial position. To ensure the stability, the sum of the dynamic and static stiffness is set equal to that of the standard rubber bushing. The ratio between the two stiffnesses is set to 4 and the cut off frequency to 0.1 Hz (according to [130]). The frequency domain behaviour of the designed bush is shown in Figure 139. The transfer function between force and displacement is given as follow:

$$\frac{F}{\Delta x} = T_f(s) = K_s + \frac{K_d C_d s}{C_d s + k_d} = K_s + \frac{K_s K_d s}{K_s s + (K_s + K_d) 2\pi f} \quad (64)$$

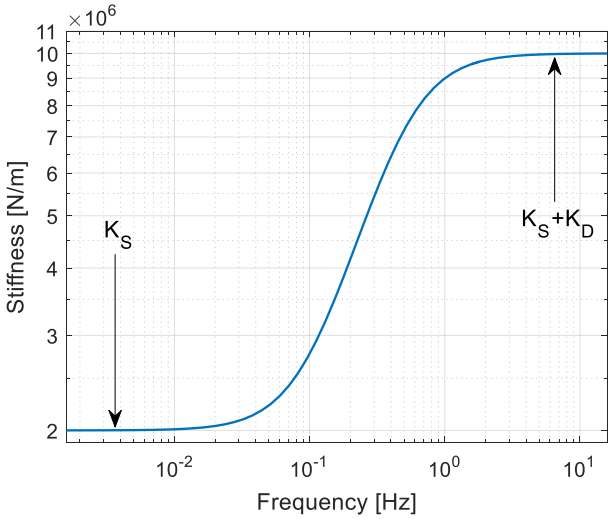

Figure 139 - Hydraulic bush frequency behaviour

The replacement of the rubber bushing with the hydraulic one can influence the critical speed of the vehicle. Thus, the stability analysis is repeated. According to Table 22, ERRI_High track irregularities [131] give the lowest critical speed. The analysis is therefore repeated for the three conicity cases defined in Table 21 with the ERRI_High track irregularities. In Figure 140 and Figure 141 the results are compared for the three conicities for the track shift force and acceleration methods respectively. On the left is shown the behaviour of the front wheelset while on the right the rear one.

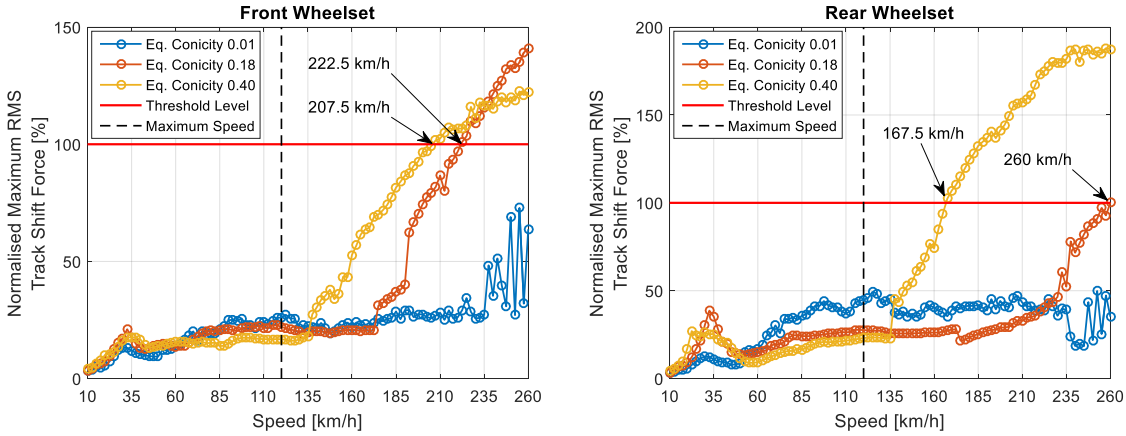

Figure 140 - HALL stability assessment - Track shift force front (left) and rear (right) wheelset

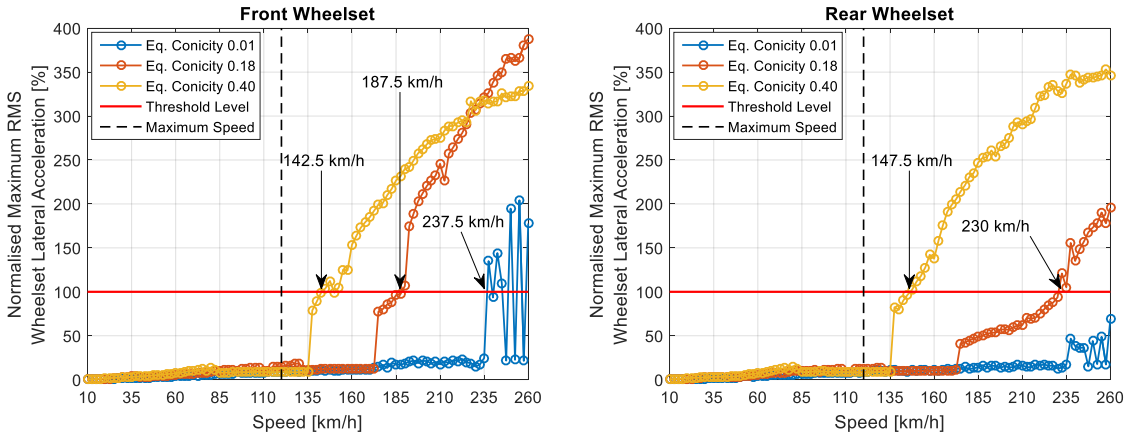

Figure 141 - HALL stability assessment - Acceleration front (left) and rear (right) wheelset

In Table 26 the critical speed for the different applied methods, wheelset and conicity are summarized. The vehicle is found stable at speed exceeding the requirements in the EN standard. The results are very similar to the ones reported with the standard bushing in Table 22. The lowest critical speed is now 142.5 km/h compared to 147.5 km/h for the standard bushing.

Table 26 - HALL stability assessment results, ERRI high track irregularities

Case	Wheelset	Critical speed [km/h]	
		Track shift force	Wheelset lateral acceleration
Case(a) Conicity: 0.18 Track gauge: 1435 Rail cant: 1:40	Front	222.5	187.5
	Rear	260	230
Case(b) Conicity: 0.01 Track gauge: 1435 Rail cant: 1:20	Front	>260	237.5
	Rear	>260	>260
Case(c) Conicity: 0.4 Track gauge: 1430 Rail cant: 1:30	Front	207.5	147.5
	Rear	167.5	142.5

The effectiveness of the HALL bush on curving performance is evaluated running the vehicle on the curve conditions defined in Table 23 for all the three defined conicity cases. The results achieved are compared in terms of wear distribution in the circular curve with the feedforward control defined in Section 4.4.1 and the passive vehicle. The feedforward control considered is the one with 50 kN limitation of the maximum actuator force. In Figure 142 and Figure 143 results are shown for the front and rear wheelset respectively.

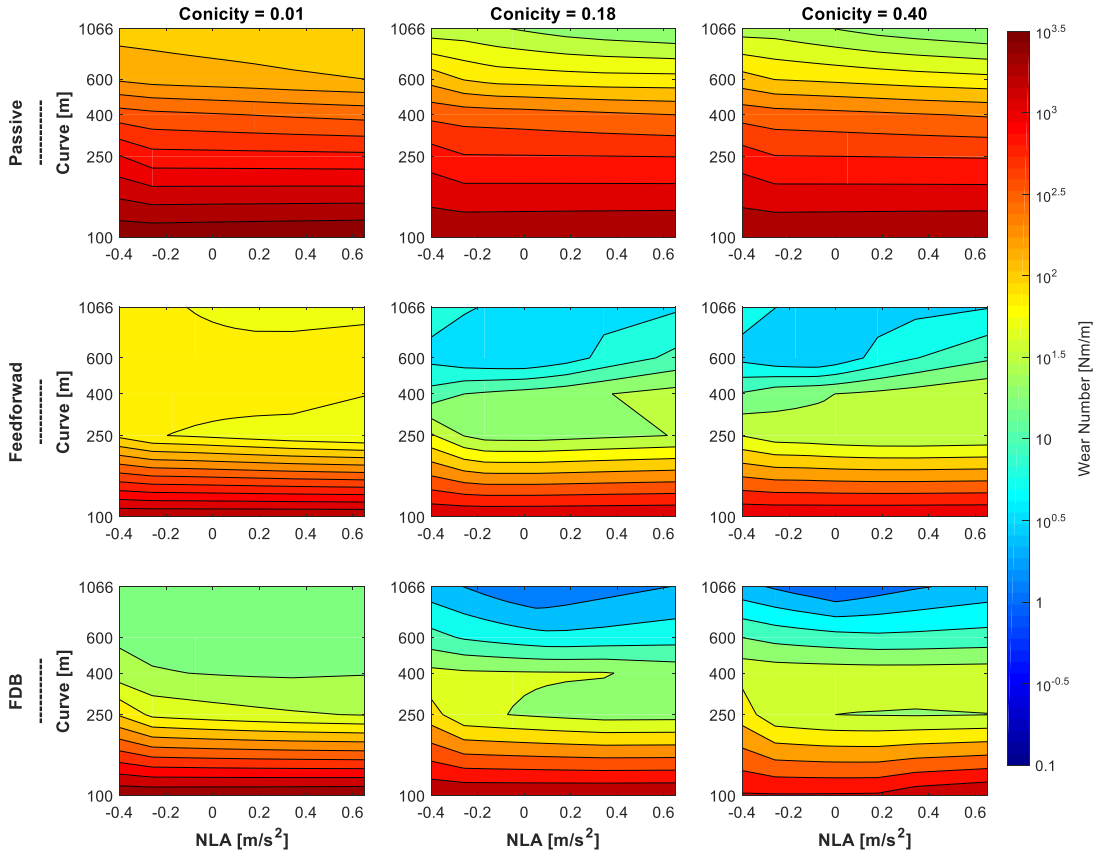

Figure 142 - Front wheelset wear distribution – HALL bush

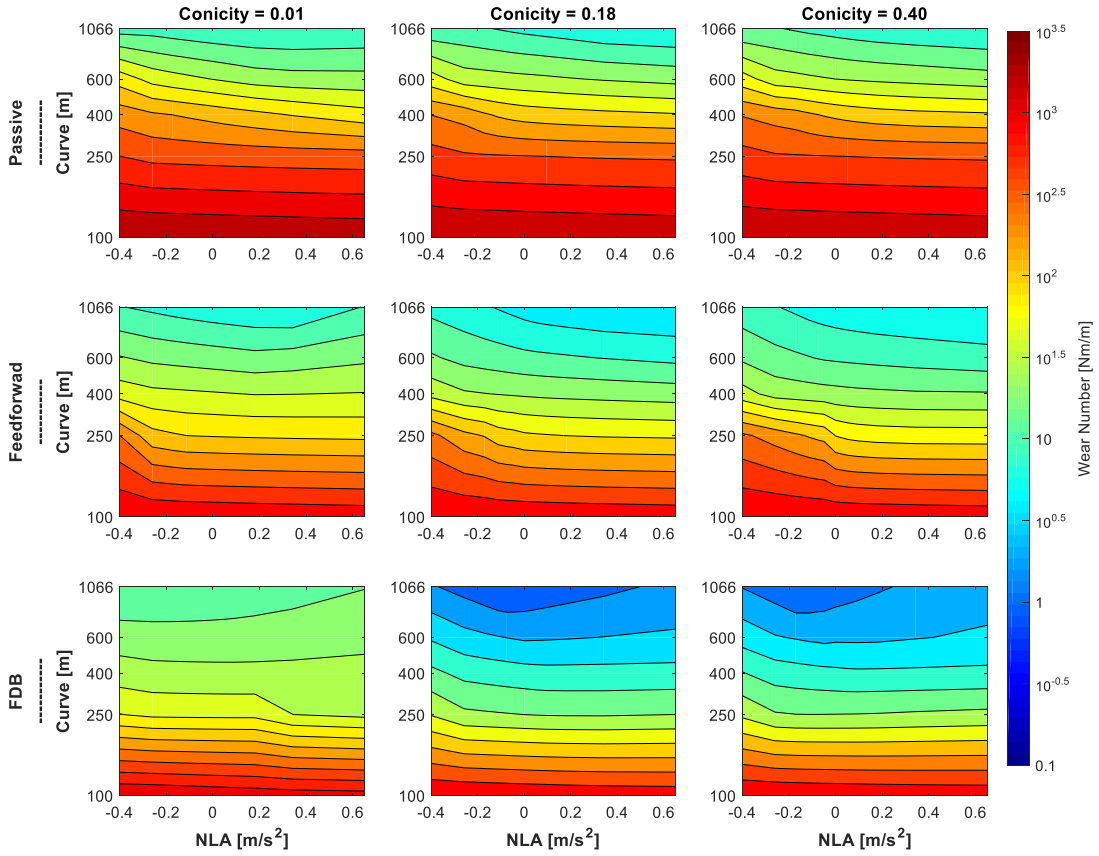

Figure 143 - Rear wheelset wear distribution – HALL bush

As made in Section 4.3.1 the wear reduction with respect to the passive two-axle vehicle with solid axle is shown in Figure 144 and Figure 145 for the front and rear wheelset respectively.

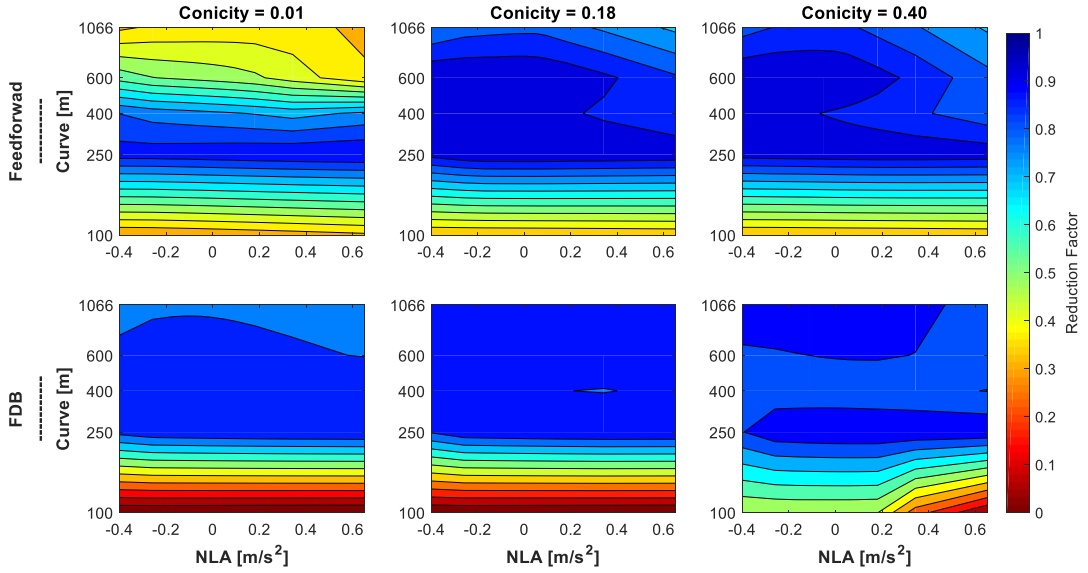

Figure 144 - Front wheelset wear reduction distribution - HALL bush

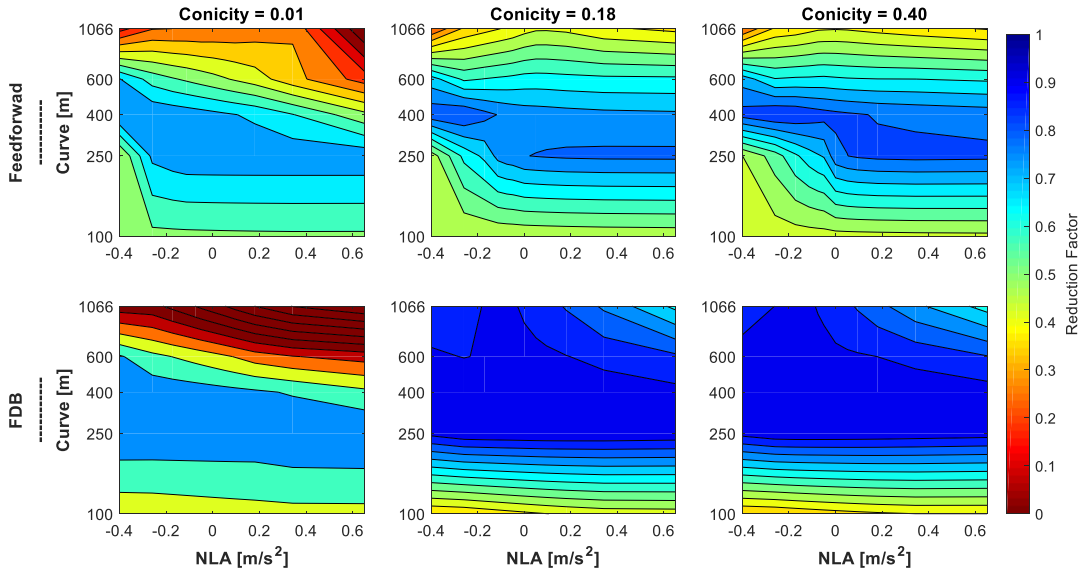

Figure 145 - Rear wheelset wear reduction distribution - HALL bush

Considering the results for the front wheelset, Figure 142 and Figure 144, it can be said that:

- HALL bush improves performances for large curves and conicities while it less effective for tight curves similarly to feedforward control.

- The HALL bush is robust against conicity variation, but it fails in achieving good results for very tight curves where the feedforward action limited to 50 kN still produces a reduction of 30 % with respect to the passive vehicle.

Considering the results for the rear wheelset, Figure 143 and Figure 145, it can be said that:

- For high conicities HALL bush greatly improves the wear condition reaching a minimum improvement of 40 % reduction with respect to the passive vehicle.
- For the lowest conicity and the tightest curve the HALL bush produces less benefits than the feedforward action.

In conclusion, the HALL bush (frequency dependent guidance) can be considered as an attractive alternative to active steering control.

4.5 ACTIVE STEERING OF INDEPENDENTLY ROTATING WHEELS

4.5.1 Passive independently rotating wheels

Compared with the solid axle wheelset of the railway vehicle, the passive independently rotating wheel (IRW) is not well suited for curve negotiation due to its limited capacity in providing the necessary steering torque for the wheelset. This feature may result in severe wheel/rail wear and large wheel/rail contact forces during the curve negotiation with the occurrence of a flange contact. In addition, due to the lack of the longitudinal creep force, it is difficult for the passive independently rotating wheelset to keep the alignment with the track centre under the disturbance of the track irregularity. These factors hinder many further applications of the IRW system, especially at a higher speed, even though this system has distinct advantages in lower maintenance cost, the reduced vehicle floor level and relatively easy stability control.

Figure 146 to Figure 148 show the dynamic behaviours of a passive IRW vehicle during a curve negotiation. With the same track case, the curve radius is 400 m and cant is 100 mm. The vehicle speed is 82 km/h. It can be seen from Figure 146 to Figure 148 that the flange contacts result in severe wheel/rail interactions with very large track forces and serious wheel wears.

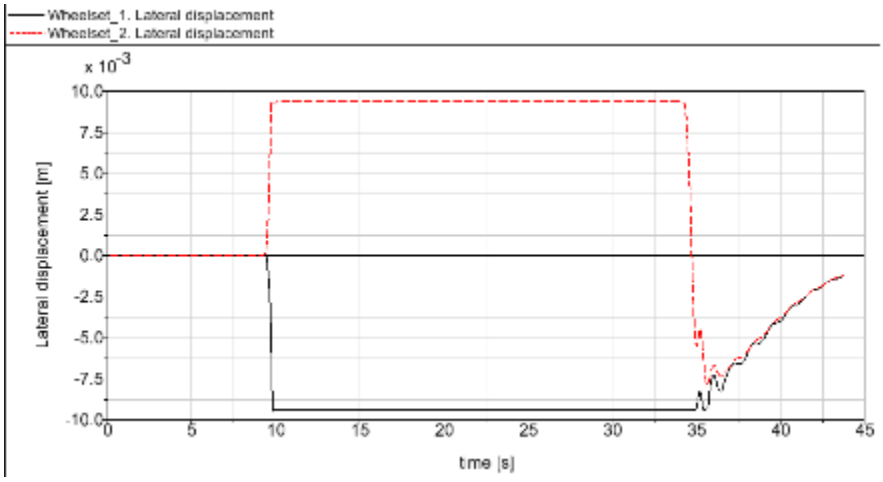

Figure 146 - Wheelset lateral displacements for passive IRW vehicle (without track irregularities)

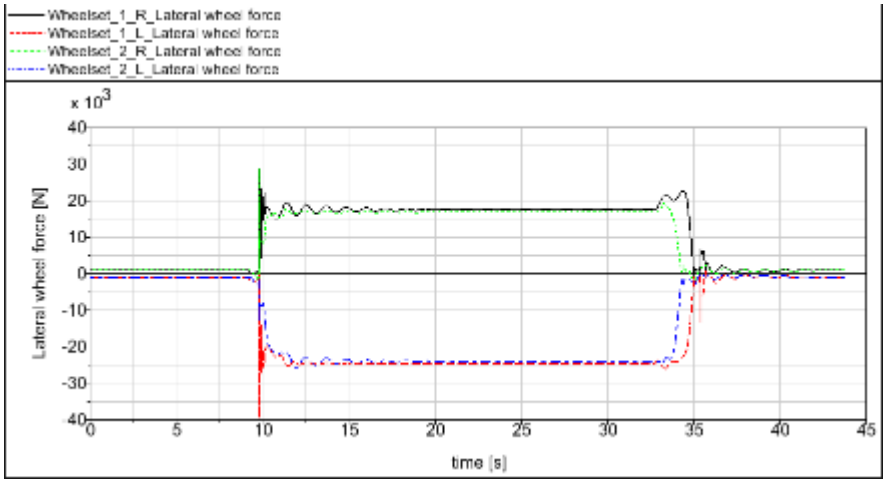

Figure 147 - Wheel lateral forces for passive IRW vehicle (without track irregularities)

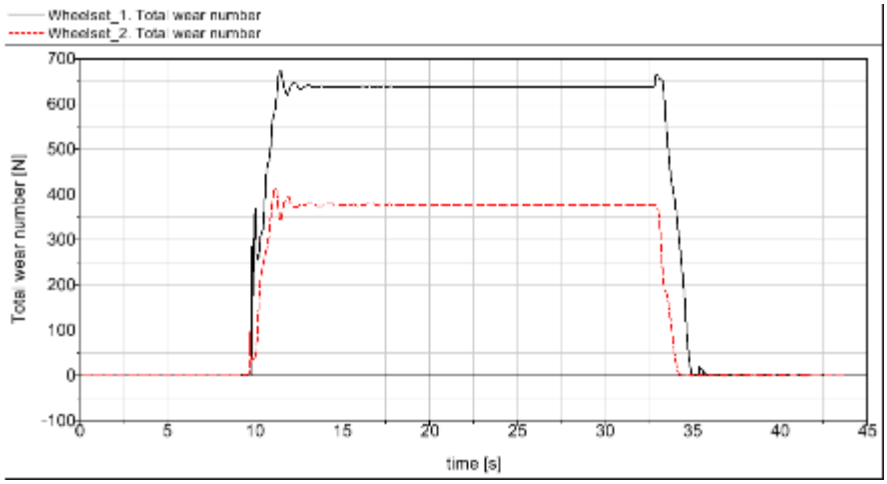

Figure 148 - Wheelset total wears for passive IRW vehicle (without track irregularities)

However, due to the basic mechanism of IRW, in which the independent wheels can rotate freely from each other, it could theoretically be feasible for an active IRW system to realize an optimized curve negotiation with less vehicle/track interaction. The relevant control approach can be achieved by the use of linear actuators or independently driven motors. These realization approaches are introduced in the following sub-sections.

4.5.2 Motorized wheels

Aiming at the improvement of the dynamic performance of the motorized IRW system, this section presents a simple control solution to realize the target with low-cost and robust techniques. The modern independently-driven motors can provide fast responses within a wide frequency-band under the control signals of traction and braking, which can also facilitate the design of the control system dedicated to the vehicle dynamic behaviour.

The principle of this concept is to apply opposite rotational torques with the same value (differential torques) to the wheel pair on the same axle. The differential torques lead to the differences of the rotational speeds of velocities (differential velocities) and generate the longitudinal creep torque. The differential speed can be obtained by tachometers mounted for both wheels, often in fact included for motor control anyway. With a suitable PID controller, it is feasible to control the relationship of the differential velocity and torque via a closed-loop system. This loop has a fast response and is regarded as the inner loop of the control system.

However, the differential control loop is an unstable system. The differential control can lead to the instability of the wheelset due to the wheel tread conicity, resulting in lateral and yaw oscillations of the wheelset [117, 119]. In order to solve the instability for this two-axle vehicle, a gyro control

loop is added to stabilize the differential loop by measuring the yaw angular velocity of the frame. The yaw-rate control loop functions as a 'Ground-hook damping' in the yaw motion of the wheelset. Since the sensors are all current technology with low costs and robust performances, this control scheme is named as 'Practical Dual-loop' control. Figure 149 demonstrates the general layout of this dual-loop control scheme.

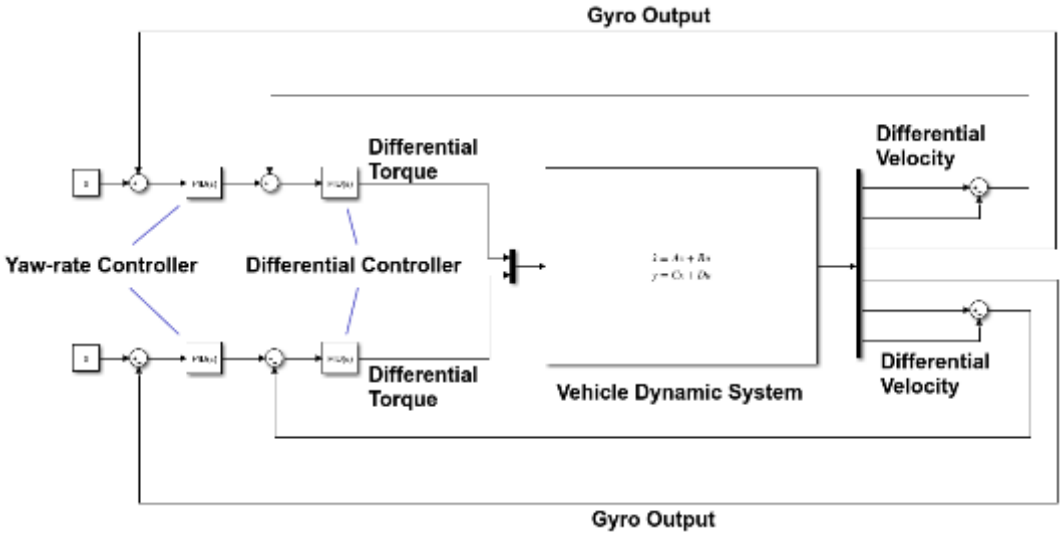

Figure 149 - Dual-loop control scheme for motorized IRW

Furthermore, another control loop with the wheel/rail lateral displacement measurement as the output can be added to control the yaw-rate loop. With this approach, the wheelset is able to stay at the track centreline for the steady state, particularly for the curve negotiation. However, more sophisticated techniques would be needed to achieve this measurement, such as the laser scanner, advanced pattern recognition, etc., and could involve high costs and perhaps unsatisfactory reliabilities at present. Figure 150 exhibits the general layout of the tri-loop control scheme.

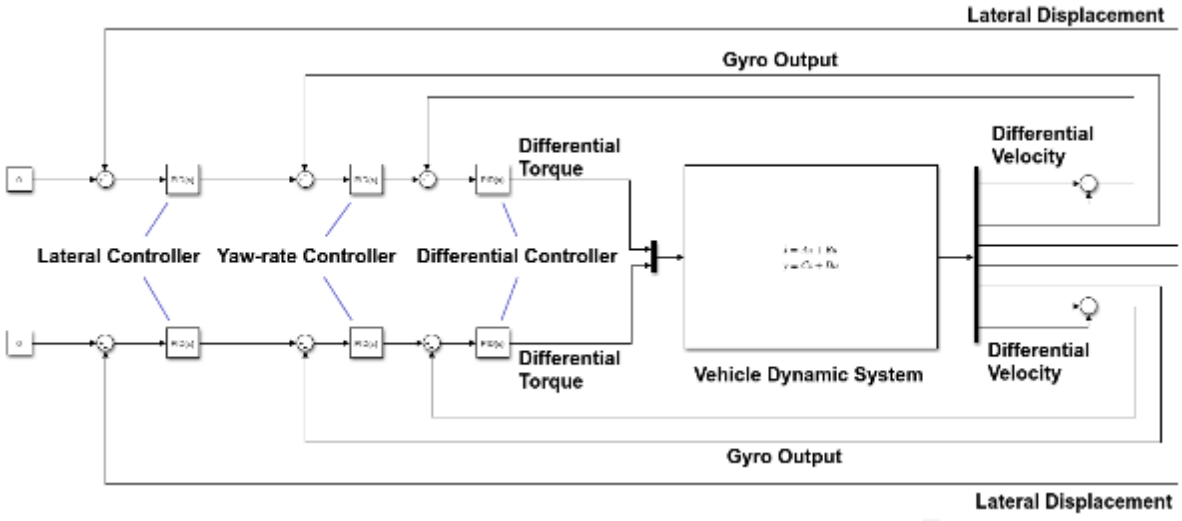

Figure 150 - Tri-loop control scheme for motorized IRW

Considering the curving case mentioned, 400 m radius curve with a 100 mm at speed of 82 km/h, Figure 151 and Figure 152 exhibit the wheelset lateral displacements of the IRW system with the dual-loop and tri-loop control strategies respectively. Both dual-loop and tri-loop control approaches exhibit steering improvements in the curve negotiations without resulting in flange contacts or instabilities. The dual-loop and tri-loop controls exhibit the similar features under the disturbance of track irregularities. For the curve negotiation, the IRW wheelset with the practical dual-loop control utilizes the wheel tread conicity, i.e. the wheel radius difference, to negotiate the curve with almost the same rotational velocities for both wheels. In contrast, with the tri-loop control method, the IRW wheelset stays at the track centreline during the curve; it means the two wheels use the different rotational speeds to negotiate the curve with almost the same wheel radius.

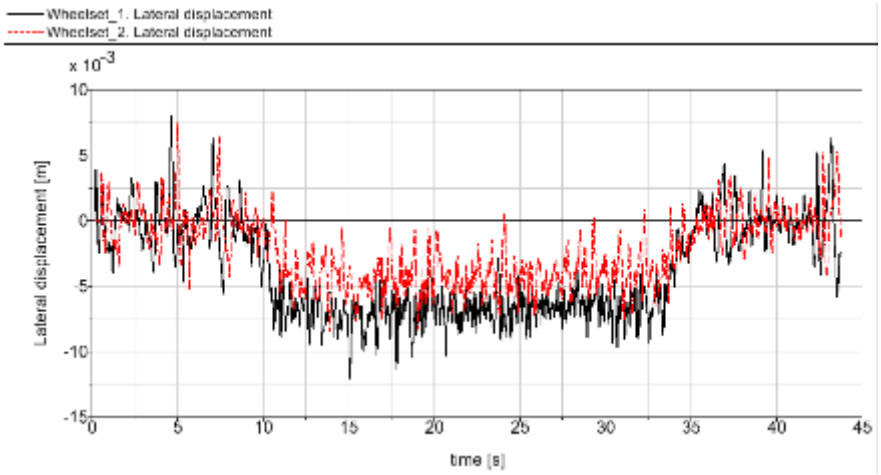

Figure 151 - Wheelset lateral displacement for dual-loop-control motorized IRW (with track irregularities)

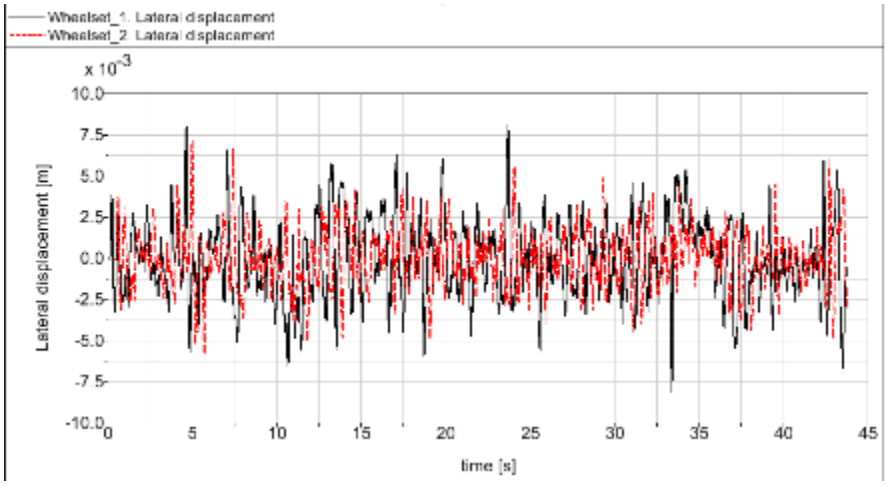

Figure 152 - Wheelset lateral displacement for tri-loop-control motorized IRW (with track irregularities)

Figure 153 to Figure 156 exhibit several dynamic indexes for the dual-loop control scheme. Since the dynamic performances by the dual-loop and tri-loop controls are very similar, here only the dynamic behaviours of the dual-loop control are illustrated. From Figure 153, it can be noticed that the wheel/rail lateral forces are considerably smaller than that of the passive system and almost evenly distributed. In Figure 154, the attack angles of two wheelsets are relatively small and almost the same. The small attack angles generate the lateral creep forces to counterbalance the uncompensated centrifugal forces. These phenomena represent an ideal curving feature of the vehicle. In Figure 155, the total wear index for each axle is very small and the flange contact does not happen during curve negotiation. These control configurations are obviously superior to the passive IRW (see Figure 146 to Figure 148), as the wheel/rail interactions are alleviated to a large extent. In Figure 156, the differential motor torques for the two wheel pairs are in the opposite directions in the curve, which is to realize the radial positions. The motor torques required for the steering functions are relatively small compared with the traction torque to achieve 1 m/s^2 [approximate 2.5 kNm].

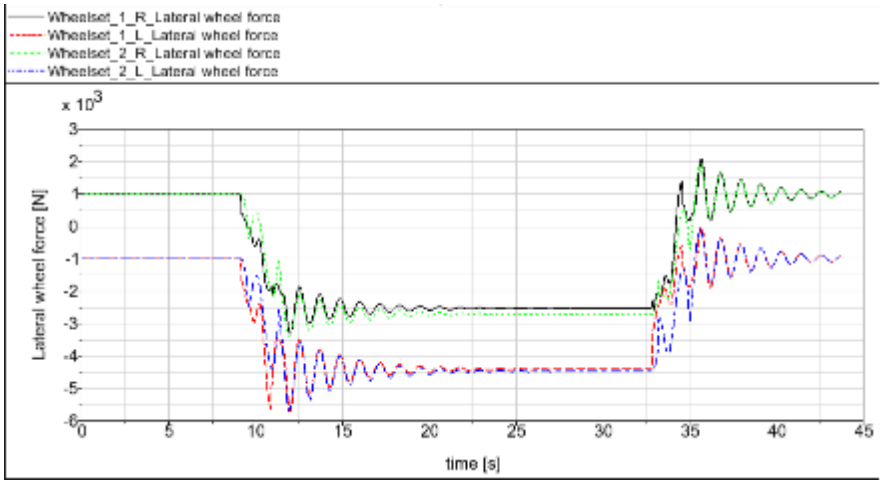

Figure 153 - Wheel/rail lateral forces for dual-loop-control motorized IRW (without track irregularities)

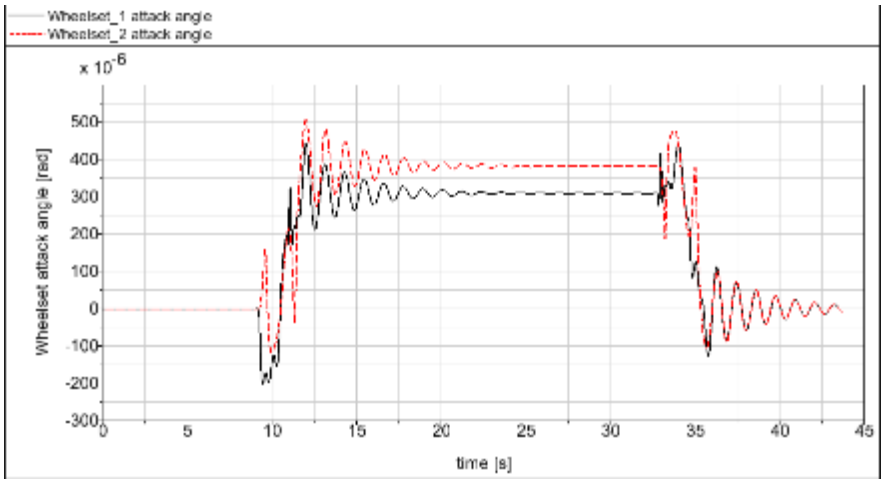

Figure 154 - Wheelset attack angles for dual-loop-control motorized IRW (without track irregularities)

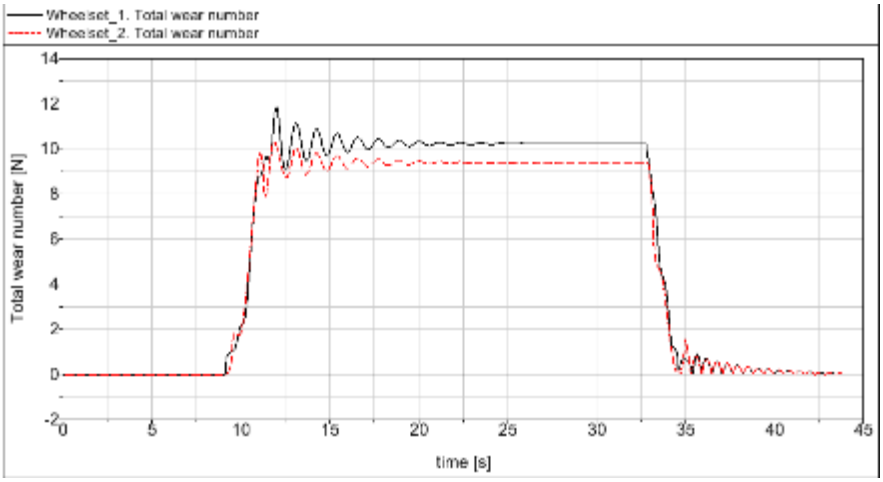

Figure 155 - Wheelset total wears for dual-loop-control motorized IRW (without track irregularities)

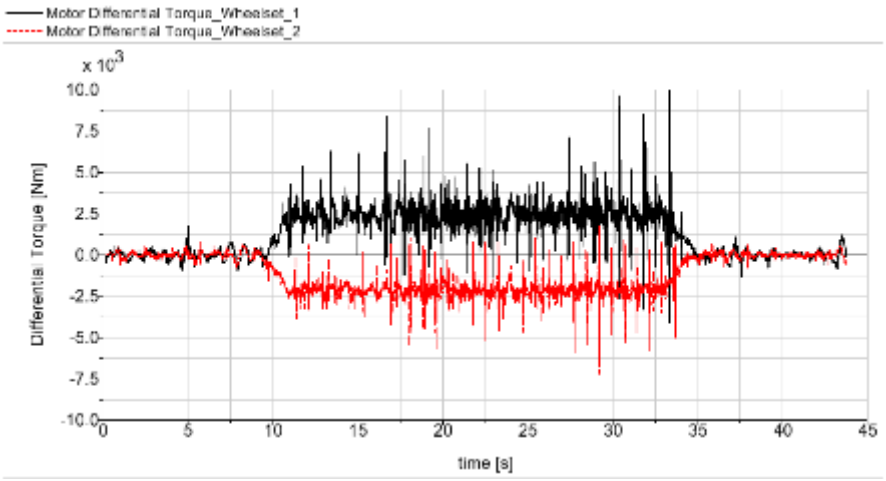

Figure 156 - Differential motor torques for dual-loop-control motorized IRW (with track irregularities)

Considering the track cases proposed in this project, including the curved tracks with the radii of 250 m, 400 m, 600 m and 1500 m, several simulations are carried out to investigate the curving performances of the target control system (see Table 27 to Table 30). It can be seen that no flange contacts take place for these track cases from the total wear numbers. Even though the dual-loop control utilizes rolling radius difference in the curving process, the IRW vehicle can still negotiate the 250 m curve without flange contact. The dual-loop control and tri-loop control provide comparable results in the curve negotiations. It can also be noticed that the motor torque required to negotiate the curve is inversely proportional to the curve radius. In contrast, the motor torque is almost independent of the vehicle speed. The motor torque required for the curve is also found to be proportional to the yaw stiffness. The very low yaw stiffness is favourable for the curve

negotiation with a lower motor torque, however, the stability is affected and the vehicle needs much higher motor torques in the guidance of the track irregularities.

Because the creep law of the wheel/rail interface is dependent upon the vehicle speed, it is likely that different sets of PID controller gains should be applied for different operational speeds. However, it is found many PID controllers can function well within a wide range of speeds. Within the vehicle speed range, the yaw-rate loop control provides enough stability for the vehicle in avoidance of the unstable yaw mode of the frame. This is another very practical issue related to the worn profile. The worn wheel profile normally leads to higher conicities and could cause an instability problem, however, it is found that many PID gains are not very sensitive to the profile conicity issue. Particularly, a larger yaw-rate control gain is more likely to be less sensitive to the worn wheel profile.

Table 27 - Curving indexes for dual-loop-control motorized IRW at cant deficiencies with 0.65 m/s² uncompensated acceleration

Track case: Radius [m] / Cant [mm]	Speed [km/h]	Wheelset lateral displacement [mm]	Maximum Wheel/rail lateral force [kN]	Derailment coefficient [-]	Wheelset attack angle [mrad]	Total wear number [N]	Motor Torque [kNm]
250 / 150	72.7	8.0	5.1	0.08	0.35	20.9	3.8
400 / 100	82.2	6.8	4.5	0.07	0.38	10.2	2.45
600 / 80	95.5	5.8	4.7	0.08	0.41	6.4	1.69
1500 / 60	142.4	3.0	5.0	0.08	0.45	3.7	0.76

Table 28 - Curving indexes for dual-loop-control motorized IRW at balanced speeds

Track case: Radius [m] / Cant [mm]	Speed [km/h]	Wheelset lateral displacement [mm]	Maximum Wheel/rail lateral force [kN]	Derailment coefficient [-]	Wheelset attack angle [mrad]	Total wear number [N]	Motor Torque [kNm]
250 / 150	56.4	7.8	1.66	0.032	0.16	19.1	3.7
400 / 100	58.2	6.6	1.01	0.019	0.09	7.56	2.36
600 / 80	63.8	5.4	0.92	0.017	0.07	3.7	1.6
1500 / 60	87.3	2.4	0.98	0.018	0.04	0.88	0.64

Table 29 - Curving indexes for tri-loop-control motorized IRW at cant deficiencies with 0.65 m/s2 uncompensated acceleration

Track case: Radius [m] / Cant [mm]	Speed [km/h]	Wheelset lateral displacement [mm]	Maximum Wheel/rail lateral force [kN]	Derailment coefficient [-]	Wheelset attack angle [mrad]	Total wear number [N]	Motor Torque [kNm]
250 / 150	72.7	1.4	5.2	0.08	0.53	27.2	3.84
400 / 100	82.2	1.7	5.1	0.08	0.50	12.3	2.44
600 / 80	95.5	1.8	5.1	0.08	0.49	7.24	1.67
1500 / 60	142.4	1.1	5.1	0.08	0.48	3.82	0.74

Table 30 - Curving indexes for tri-loop-control motorized IRW at balanced speeds

Track case: Radius [m] / Cant [mm]	Speed [km/h]	Wheelset lateral displacement [mm]	Maximum Wheel/rail lateral force [kN]	Derailment coefficient [-]	Wheelset attack angle [mrad]	Total wear number [N]	Motor Torque [kNm]
250 / 150	56.4	0.8	1.01	0.02	0.09	21.4	3.7
400 / 100	58.2	0.85	1.03	0.019	0.05	7.93	2.32
600 / 80	63.8	0.8	1.0	0.019	0.04	3.45	1.55
1500 / 60	87.3	0.5	0.99	0.018	0.01	0.55	0.62

4.5.3 Non-motorized wheels

Unlike the solid axle wheelset or motorized IRW, for the non-motorized IRW, it is impossible to steer the non-motorized IRWs via the longitudinal creep forces. In contrast, the non-motorized IRW requires an external steering force / torque applied on the axle-bridge to guide the wheelset. Associated with the experiences and results from Section 4.4.1, the controlling of the wheelset yaw motion is found to be a very efficient way to steer and stabilize the IRW system. In this section, the active actuation system is also developed on the basis of the yaw control approach.

In fact, the controlled yaw torque acting on the IRW can play the similar role as the longitudinal creep forces in the steering. Furthermore, the pure rolling of the wheels can be realized with this approach. In the previous section, the differential method is utilized for the steering of the wheelset, while the ground-hook damping in the yaw motion is very effective in the stability control. In this sense, it is not difficult to consider applying the similar control principle to the non-motorized IRW system. It is reasonable and feasible to modify the dual-loop control approach to apply on the non-motorized IRW system. By several numerical experiments, it is found that the yaw-rate control loop should function as the inner control loop with a fast response, while the differential loop should be

the outer loop to control the yaw motion. In this configuration, it is relatively easy to realize a high bandwidth control in the yaw motion, since the actuation torque (or force) is applied to the yaw direction. The general dual-loop control scheme for non-motorized IRW is shown in Figure 157.

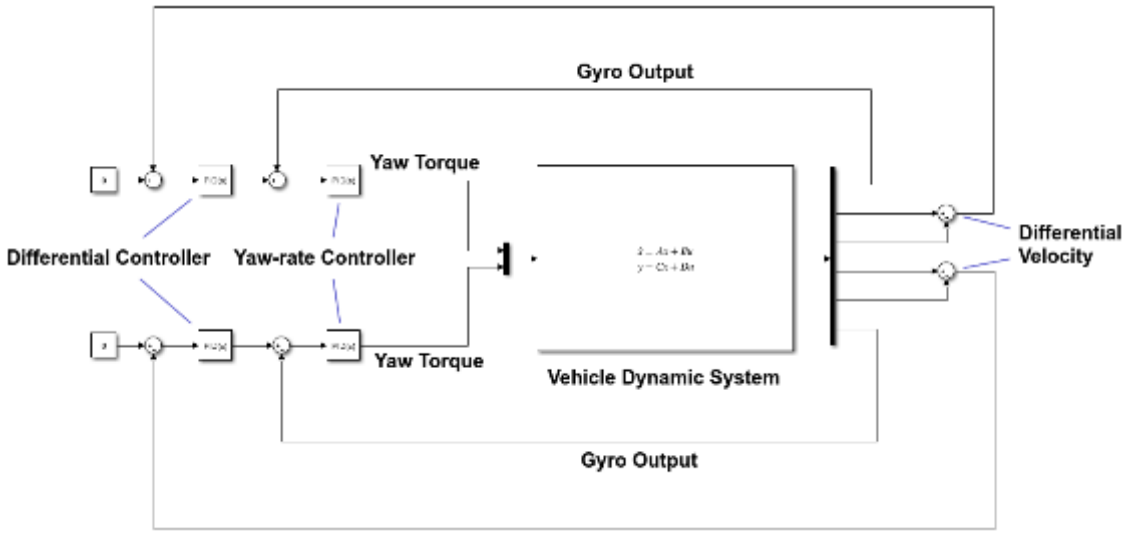

Figure 157 - Dual-loop control scheme for non-motorized IRW

In this control strategy, the yaw-rate control is applied to stabilize the unstable motion of the wheelset with the active 'ground-hook' damping. The differential loop is utilized to keep the wheelset in the right position of the track with almost the same rotational velocity of the two wheels, mainly at low frequencies. During the curve negotiation, the controlled yaw torque steers the wheelset with a small attack angle generating a lateral creep force to counterbalance the uncompensated centrifugal force. Meanwhile, the lateral creep force guides the wheelset to the proper lateral position of the track with a suitable radius difference for the pure rolling. In the whole process, only lateral creep guides the wheelset through the curve; in particular no longitudinal creep is involved in the curve negotiation.

In this vehicle, a very low yaw stiffness is adopted with only the horizontal shear stiffness of the coil spring. In fact, it is found that a very low yaw stiffness is favourable for the stability of the IRW vehicle, on the condition that a ground-hook damping is applied. The actuation power can be relatively low, since the two wheels can rotate freely with respect to each other without slip.

It can be realized that the longitudinal creep is not mandatory for the steering of the wheelset. In the IRW system, a controlled yaw torque is able to realize the same steering function as the longitudinal creep. As the longitudinal creep is not used in the guidance, it is not only longitudinal curving wear, but the hunting motion can be avoided. At the same time, a low yaw stiffness is also very suitable for the requirements for the actuation power of the IRW wheelset. In this perspective,

the curve negotiation performance and stability may no longer be contradictory, given that an optimized yaw-controlled IRW system is provided.

Figure 158 to Figure 162 show several dynamic behaviours of the IRW vehicle with the dual-loop control scheme. In Figure 158, it can be seen the wheelsets almost follow the track irregularity, since the longitudinal creep is no longer involved in the guidance. From Figure 159, it can be noticed that the wheel/rail lateral forces are considerably smaller than that of the passive system and are similar to the dual-loop-controlled motorized IRW. In Figure 160, the attack angles of two wheelsets, almost the same and relatively small, generate lateral creep forces to counterbalance the uncompensated centrifugal forces due to the cant deficiency. These behaviours demonstrate a perfect curving feature of the vehicle. In Figure 161, the total wear index for each axle is even smaller than that of the motorized IRW, since longitudinal creeps are eliminated in the curve negotiations. This control strategy is able to guarantee the satisfactory curving performance and the stability simultaneously, since the stability and curving performance of the vehicle can be controlled homogenously. In Figure 162, the active yaw torques for the two wheelsets are applied in the opposite directions in the curve negotiation, which is the same case as the controlled motorized-IRW. The active yaw torques required for the steering are very small, because a low yaw stiffness is adopted.

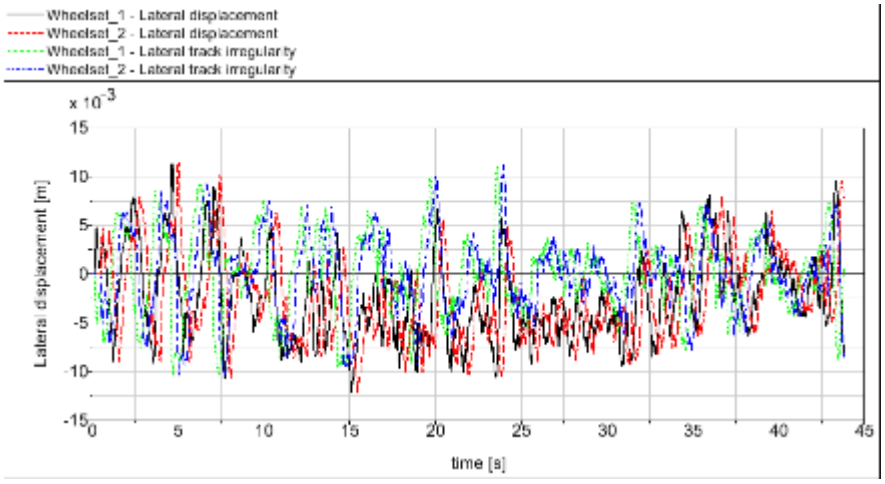

Figure 158 - Wheelset lateral displacements for dual-loop-control non-motorized IRW and lateral track irregularities

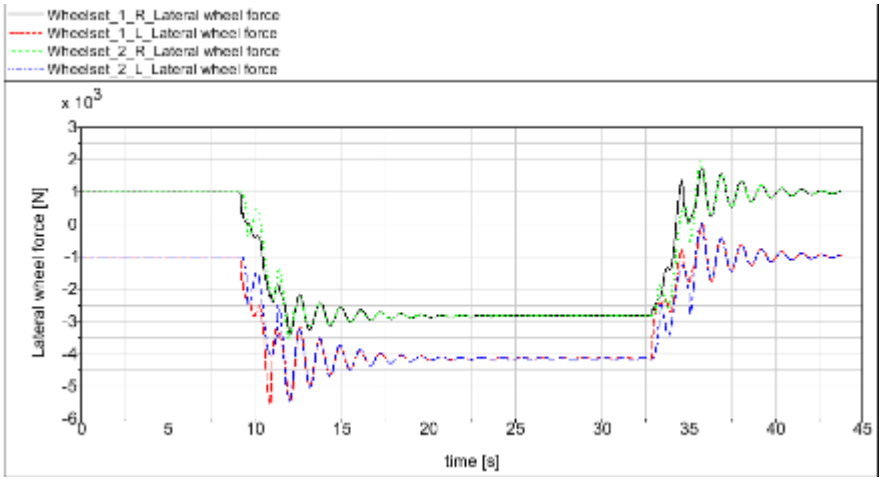

Figure 159 - Wheel/rail lateral forces for dual-loop-control non-motorized IRW (without track irregularities)

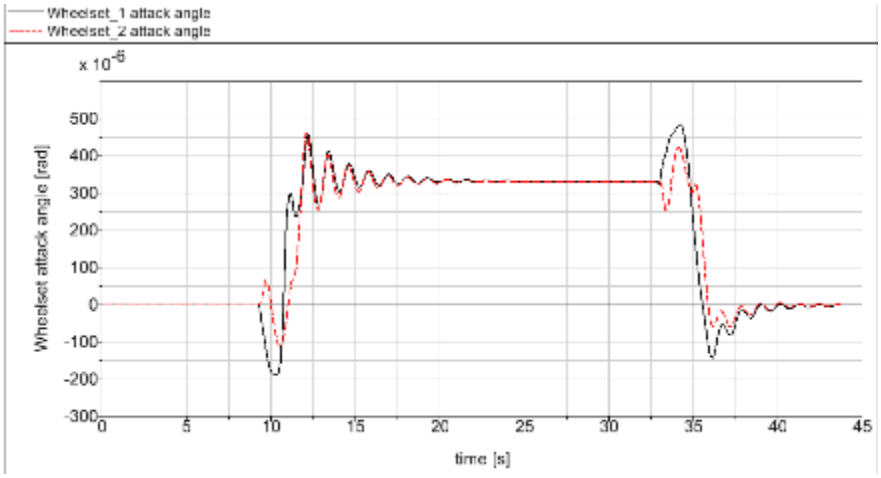

Figure 160 - Wheelset attack angles for dual-loop-control non-motorized IRW (without track irregularities)

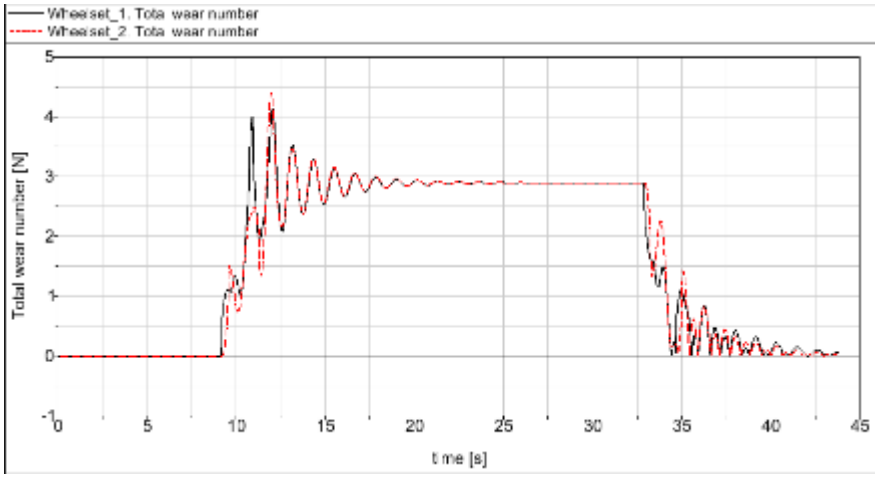

Figure 161 - Wheelset total wears for dual-loop-control non-motorized IRW (without track irregularities)

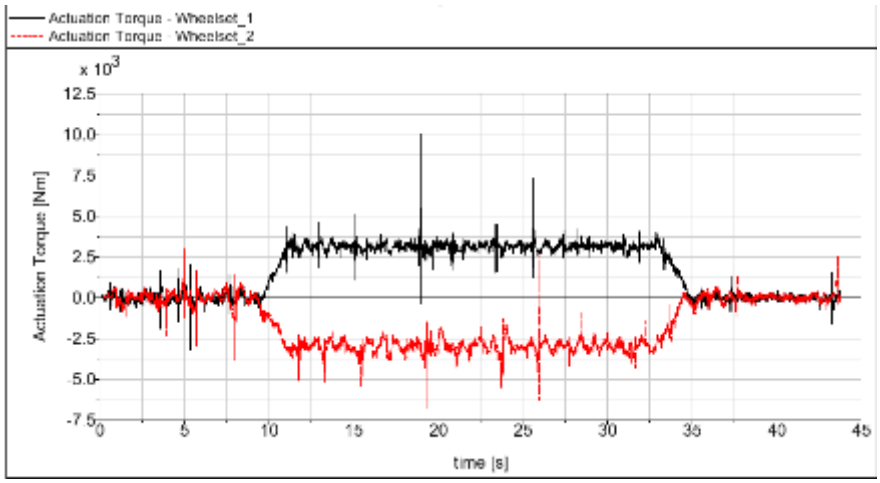

Figure 162 - Active yaw torques for dual-loop-control non-motorized IRW (with irregularities)

From the Table 31 and Table 32, it is obvious that the wheel/rail interaction indexes are very low with this active steering approach. The wear index can be reduced to a very low level, especially for the balanced speeds, since lateral creep forces are only necessary to counteract the centrifugal forces during the curve negotiations. Because there is no constraint between the two wheels of the wheelset, the required yaw torque is very small compared with the value for steering a solid axle wheelset. It can also be noticed that the yaw torque required to negotiate the curve is inversely proportional to the curve radius. In contrast, the yaw torque is almost independent of the vehicle speed. Additionally, since the Run2Rail WP2 is dedicated to the investigation of the application of light-weight materials to the railway vehicle, such as carbon fibre composite material, several experimental simulations are carried out with a light-weight running gear configuration. It is found that the reduction of the unsprung mass, especially the yaw inertia of the IRW wheelset, can

enhance the controllability of the running gear with this approach and contribute to the improvement of the overall dynamic performances.

Table 31 - Curving indexes for dual-loop-control non-motorized IRW at cant deficiencies with 0.65 m/s² uncompensated acceleration

Track case: Radius [m] / Cant [mm]	Speed [km/h]	Wheelset lateral displacement [mm]	Maximum Wheel/rail lateral force [kN]	Derailment coefficient [-]	Wheelset attack angle [mrad]	Total wear number [N]	Yaw Actuation Torque [kNm]
250 / 150	72.7	7.1	4.21	0.067	0.31	3.33	4.9
400 / 100	82.2	5.9	4.14	0.066	0.33	2.89	3.2
600 / 80	95.5	4.4	4.53	0.072	0.38	2.83	2.2
1500 / 60	142.4	1.8	4.84	0.078	0.43	2.94	0.98

Table 32 - Curving indexes for dual-loop-control non-motorized IRW at balanced speeds

Track case: Radius [m] / Cant [mm]	Speed [km/h]	Wheelset lateral displacement [mm]	Maximum Wheel/rail lateral force [kN]	Derailment coefficient [-]	Wheelset attack angle [mrad]	Total wear number [N]	Yaw Actuation Torque [kNm]
250 / 150	56.4	7.1	0.94	0.017	0.087	0.82	4.8
400 / 100	58.2	5.9	0.67	0.013	0.069	0.57	3.0
600 / 80	63.8	4.3	0.77	0.014	0.062	0.46	2.0
1500 / 60	87.3	1.8	0.98	0.018	0.032	0.24	0.81

4.6 ACTIVE SUSPENSIONS FOR IMPROVED RIDE COMFORT

The vibrational ride comfort can be heavily affected by the absence of a second level of suspensions. To improve it, fully active control is considered for the two-axle vehicle. Active vertical and lateral control are considered. An advantage will be shown to be the combination of vertical and lateral control. Comfort indexes (according to EN12299 [24]) will be compared for different control approaches. A limit value both in vertical and lateral direction for the achieved comfort index is set to 0.25 m/s². As will be shown, the vehicle with passive suspension is far from meeting this limit, but with fully active control it is possible to reach satisfactory results. Simulations are carried out on a 1000 m tangent track with ERRI_High track irregularities [131] at 100 km/h.
To implement active control the dampers are replaced by actuators (Figure 107). In Figure 163 the actuators and sensors locations are shown. The sensors are assumed to be accelerometers.

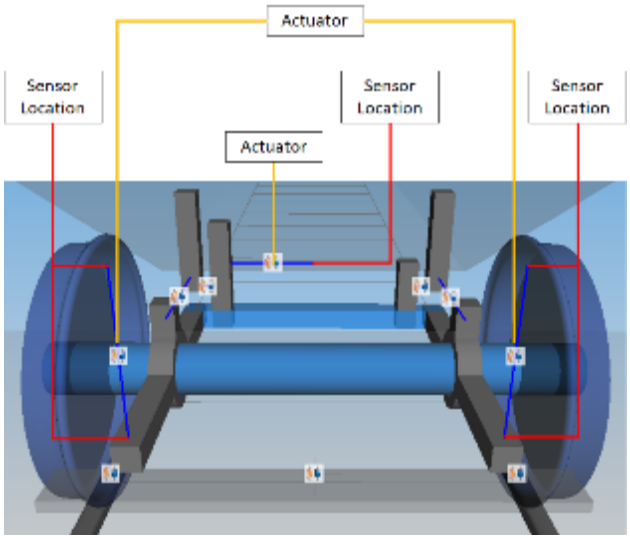

Figure 163 - Ride comfort actuators and sensors locations

4.6.1 Control of vertical motions

Vertical dampers are initially substituted by ideal actuators. A simple modal control is applied to verify the possibility of ride comfort improvement. The applied control takes the carbody accelerations (Figure 163) and decouples them into bounce, roll and pitch modes. A simple skyhook approach is then applied to the decoupled modes and the requested forces are computed. The control logic is shown in Figure 164.

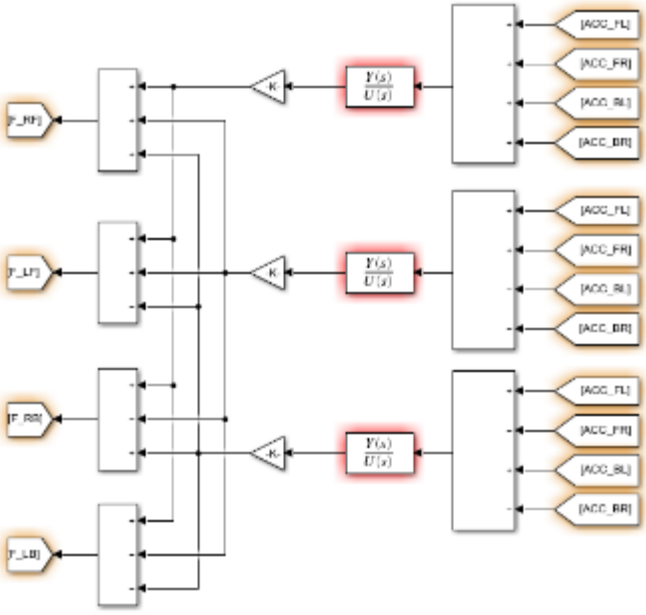

Figure 164 - Modal vertical control

The achieved result is shown in terms of acceleration power spectral density in Figure 165. A huge reduction of the energy frequency content is achieved in the region between 0 and 30 Hz.

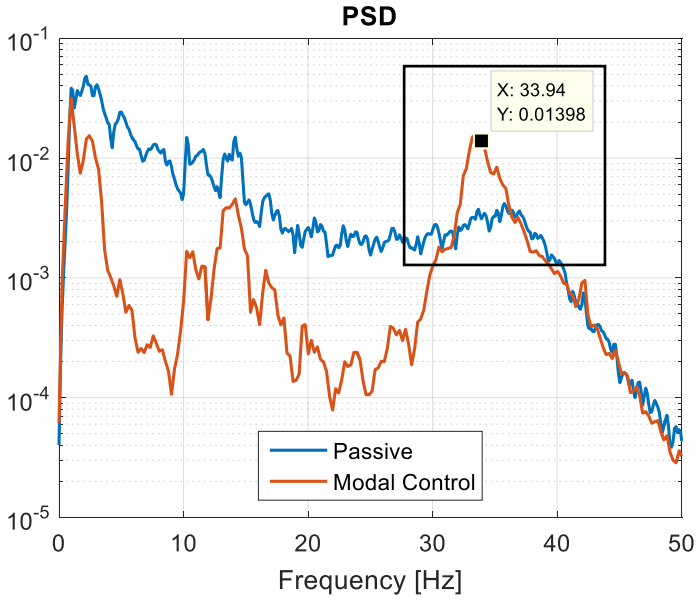

Figure 165 - Vertical modal control acceleration PSD, ideal actuator

Nevertheless, an increase of the frequency content in the region between 30 and 40 Hz is experienced. The reason must be sought in the mode shapes of the vehicle. The modes shapes are described in Table 33 and Table 34 for the 4th mode (bounce) and the 14th (interfering mode). The representation of the two modes is given in Figure 166 left (bounce) and Figure 166 (interfering mode) right. As can be seen, the two modes have opposite phase between car-body motion and frames motion. This implies that the same action on the car-body will generate an opposite effect on the frame response eventually resulting in a worsening of the response in the frequency region of the 14th mode. This effect will remain significant if and only if the actuator will be capable to provide effective control action in the frequency range between 30 and 40 Hz.

Table 33 - 4th Mode – Correlation between carbody and frame movements

	Front Left	*Front Right*	*Rear Left*	*Rear Right*
Car-body	1	1	1	1
Frame	-0.6	-0.6	-0.6	-0.6

Table 34 - 14th Mode - Correlation between carbody and frame movements

	Front Left	*Front Right*	*Rear Left*	*Rear Right*
Car-body	0.1	0.1	0.1	0.1
Frame	1	1	1	1

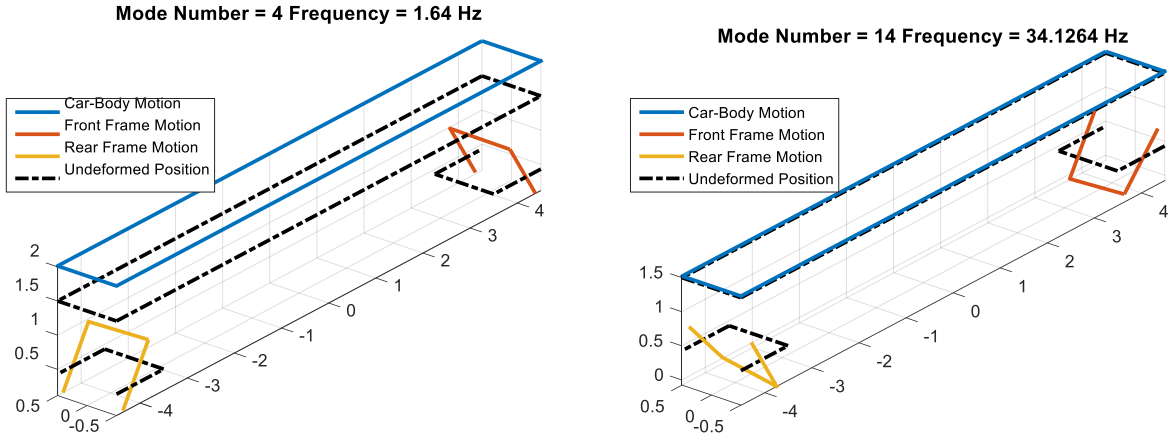

Figure 166 - Modes shapes representation: 4th mode (left) and 14th mode (right)

A double acting electrohydraulic actuator (EHA) (Figure 167) is introduced in the system replacing the ideal actuator. This actuator is selected to have a maximum stroke of ± 100 mm allowing for a maximum admissible displacement of ± 90 mm. The actuator parameters are set to fit a supplier's empirical model.

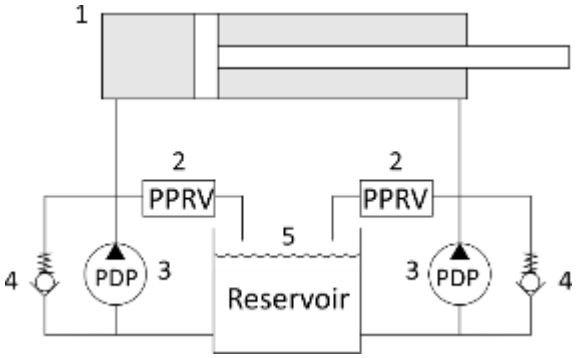

Figure 167 - Double acting hydraulic actuator

The modal control of Figure 164 is applied and the results are compared in Figure 168. The presence of the actuator reduces the effectiveness of the control in the frequency region between 0 and 30 Hz but has the positive effect of removing the problem experienced between 30 and 40 Hz. This is essentially due to the reduced ability of the actuator to act above a certain frequency.

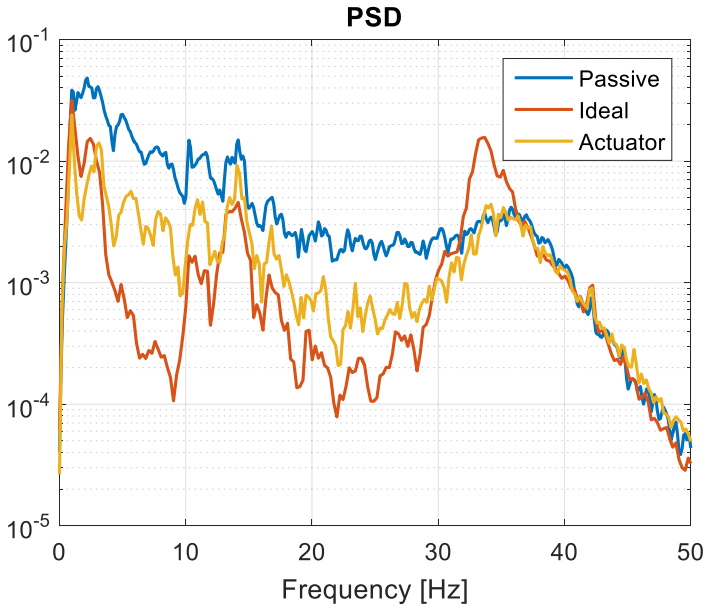

Figure 168 - Modelled vs Ideal actuator vertical modal control acceleration PSD

To further improve the performance, two approaches are studied and combined. The first one concerns the type of integration used while the second one applied a more advance control logic. In Figure 169 are shown the integration functions used compared with the ideal integration. The High-Pass Integration (HPI) is generally used to remove the quasi-static part from the acceleration. The Extended Range Integration (ERI) is introduced here to extend the actuator frequency range. Here a derivative action is introduced between 10 and 22 Hz.

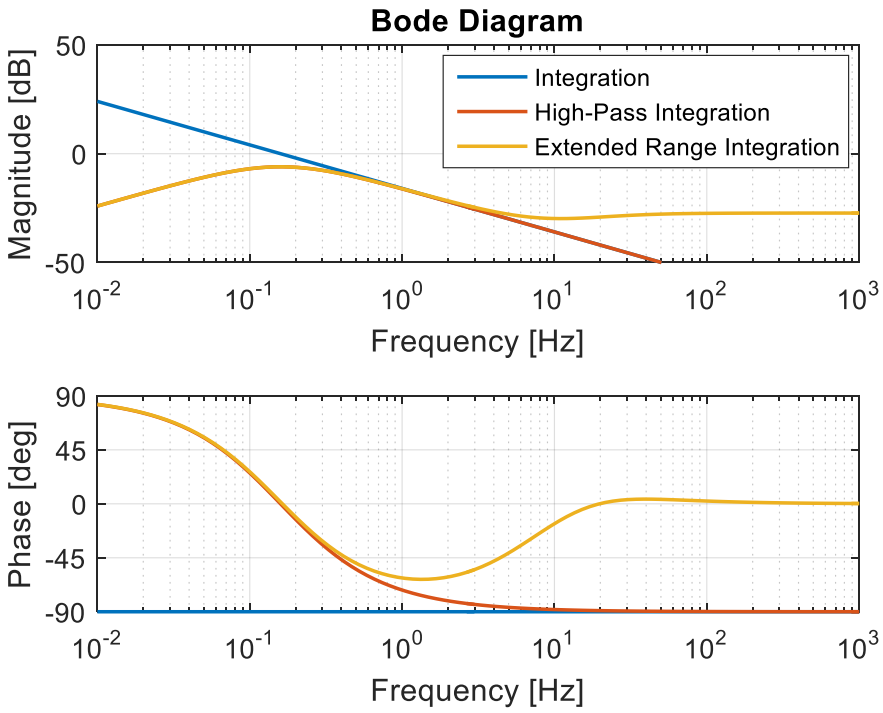

Figure 169 - Integration functions

The integration functions are combined with the modal control defined before (Figure 164) and an approach introduced here called blended control. In blended control a portion of the frame acceleration is subtracted from the car-body acceleration. The frame sensor's location is shown in Figure 163. The four combinations between control logics and integration functions are compared in Figure 170.

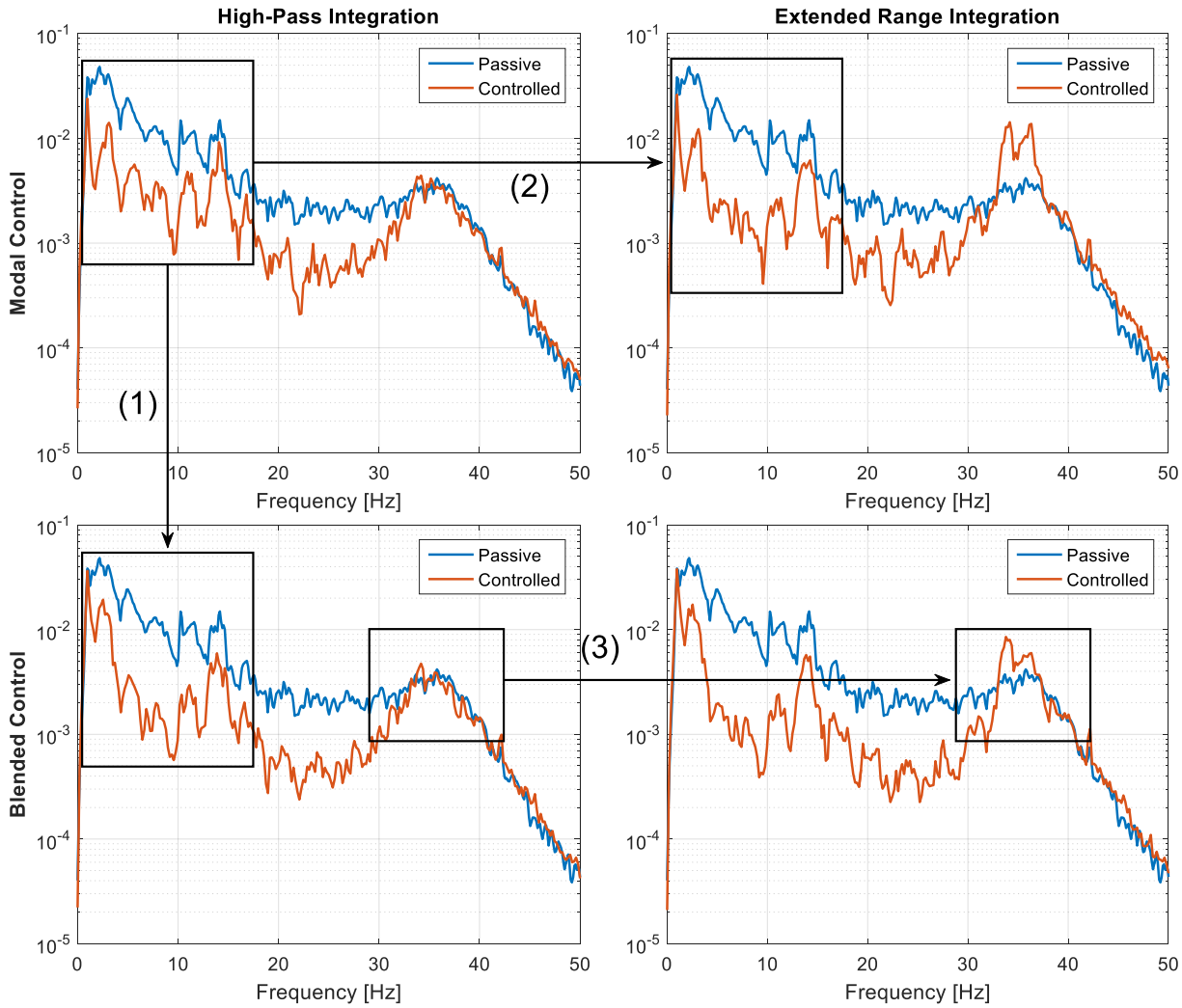

Figure 170 - Vertical comfort control comparison

Following the arrows' order in Figure 170, it can be said that:

1. Blended control improves the performances by reducing the frequency content in the first frequency region especially increasing the frequency.
2. ERI improves the performances by reducing the frequency content in the first frequency region.
3. ERI worsens the situation in the frequency region between 30 and 40 Hz due to extension of the actuator range. Blended control performs better in this region with respect to Modal control even if ERI is applied.

The results are better compared through the usage of EN12299 ([24]) in terms of comfort indexes. The achieved comfort is reported in Table 35.

Table 35 - Average vertical comfort [m/s^2], weighted according to EN12299

	Front Left	*Front Right*	*Rear Left*	*Rear Right*
Passive	0.428	0.428	0.425	0.424
Modal HPI	0.241	0.240	0.225	0.223
Modal ERI	0.225	0.223	0.208	0.206
Blended HPI	0.215	0.216	0.205	0.205
Blended ERI	0.204	0.204	0.194	0.191

Blended control generally performs better with respect to modal control as well as ERI with respect to HPI. Despite the need for four additional sensors with respect to a more standard modal control, the benefits on the comfort achieved with blended control suggest that it could be a reliable solution.

4.6.2 Control of lateral motions

Lateral dampers are substituted by actuators and the car-body accelerations are measured at the actuator locations. The location of actuators and sensors is provided in Figure 163. Initially a simple local (decentralized) control is applied using a skyhook approach together with an ideal actuator. In a second stage, a model of a electro-mechanical actuator is replacing the ideal actuator. The results, in terms of carbody acceleration PSD above the leading running gear, are shown for passive, active suspension with ideal actuator and active suspension with modelled actuator in Figure 171. As it is possible to see, the presence of the non-ideal actuator does not influence the system significantly. Moreover, a large reduction of the frequency content can be easily achieved in lateral direction from 0 to 35 Hz.

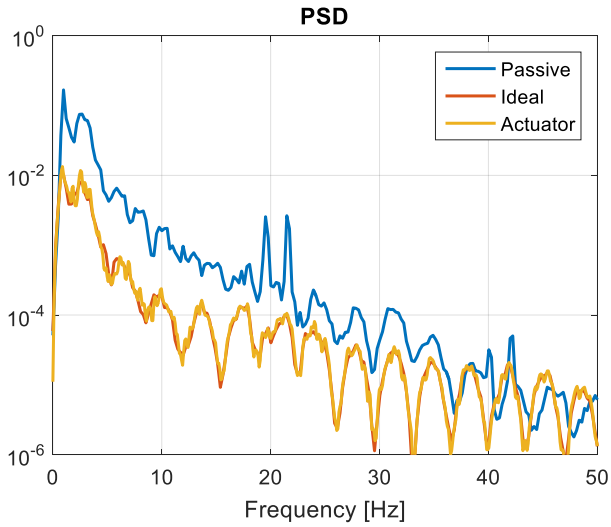

Figure 171 - Real vs Ideal actuator lateral decentralized control acceleration PSD

To improve the control performances a modal control is applied in which the car-body accelerations are decoupled in pure lateral and yaw motions. A modal skyhook is then applied to the decoupled motions. A simple High-Pass integration is used. The schematic control logic is shown in Figure 172.

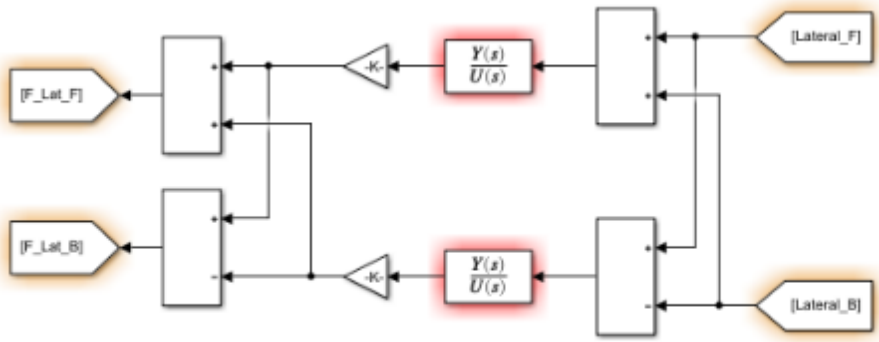

Figure 172 - Modal control for lateral control

The benefits of applying a modal control in lateral direction is shown in Figure 173. The effectiveness of the decoupling between pure lateral and yaw motions is evident in the low frequency region in which the amplitude of the response is about half of the decentralized one. Above 5 Hz the two controllers perform closely the same. According to EN12299 ([24]) the most sensitive region is below 5 Hz for comfort in lateral direction. Thus, a good benefit could be expected from the modal control. It is possible to notice that the rear part of the vehicle is more sensitive in the very low frequency region with respect to the front one.

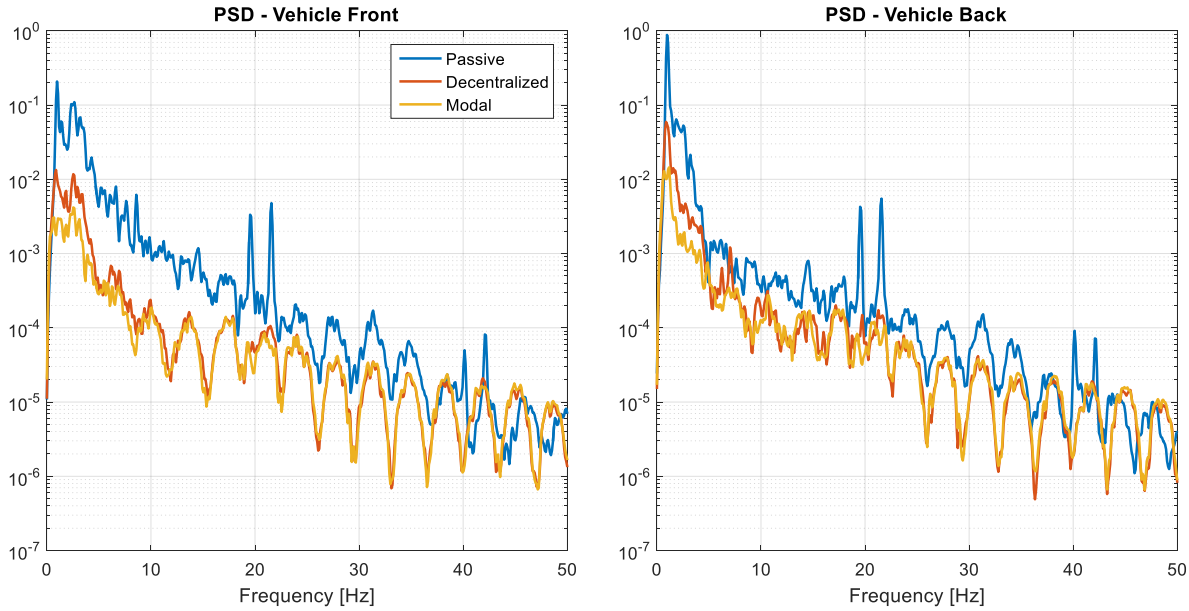

Figure 173 - Lateral comfort control comparison

To better compare the results the frequency weighting according EN12299 ([24]) is applied. In Table 36 the comfort indexes achieved with the different control logics are compared to the original passive vehicle comfort. Modal control further improves the performance compared to the decentralized control without introducing a significantly higher complexity and is a good choise. The improvement by introducing active suspension becomes large in lateral direction and the target on vibrational ride comfort of 0.25 m/s^2 can easily be met with an EMA. The large improvement relates to the evaluation weighting curve in lateral direction, which focuses on the low frequency accelerations where active suspension is very effective. This is particularly true when the performance of the passive vehicle is poor as it is in this case.

Table 36 - Average lateral comfort [m/s^2], weighted according EN12299

Control	Front	Rear
Passive	0.381	0.553
Decentralized	0.130	0.203
Modal	0.077	0.113

4.6.3 Combination of Vertical and Lateral vibration control

Generally, in two level of suspension vehicles the lateral and vertical motions are decoupled. In the case of the innovative two-axle vehicle the interaction between car-body and frames additional benefit is found in the simultaneous application of vertical and lateral control.

In Figure 175 the first six modes are shown. As it is possible to see, the first and second mode are almost purely lateral modes, while the fourth and the fifth mainly vertical. Instead, the third and the sixth share some components in vertical and lateral directions. It can be expected that these last modes will have benefits in the simultaneous application of vertical and latral control. In Figure 174 a measure of this effect is given through the modal controllability. In Figure 174 left, centre and right the effect of applying only vertical, only lateral respectively vertical simultaneously lateral control is compared in terms of modes controllability. Here, the higher the mode's energy the higher the controllability and thus the highest the achievable benefit on that specific mode.
It is possible to notice that vertical control has a great effect on the fourth and the fifth modes, lateral control mainly has an effect on the first one still having some effect on second and third mode. The combination of the two takes advantage of both the benefits increasing the controllability of the third and sixth modes with respect to the separated ones.

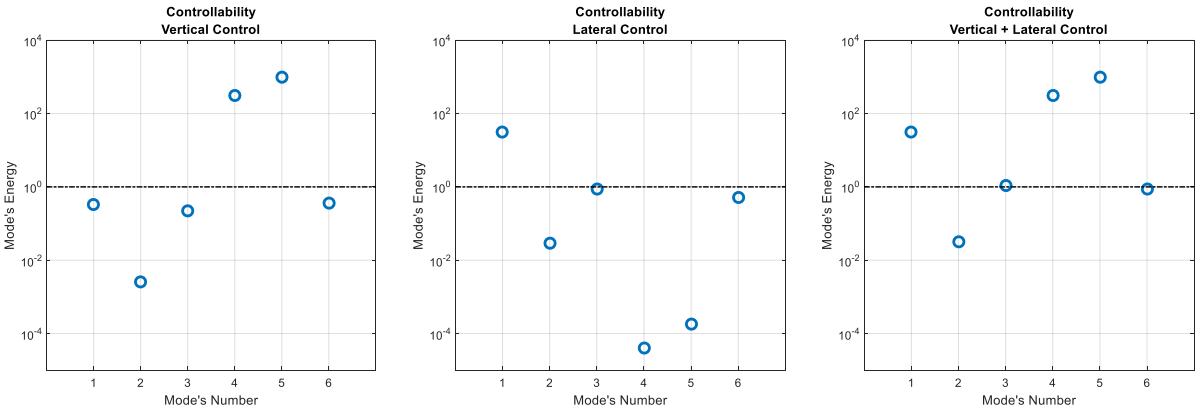

Figure 174 - Modes comtrollability for different control approach: Vertical control (left), Lateral control (center) and Vertical plus Lateral control (right)

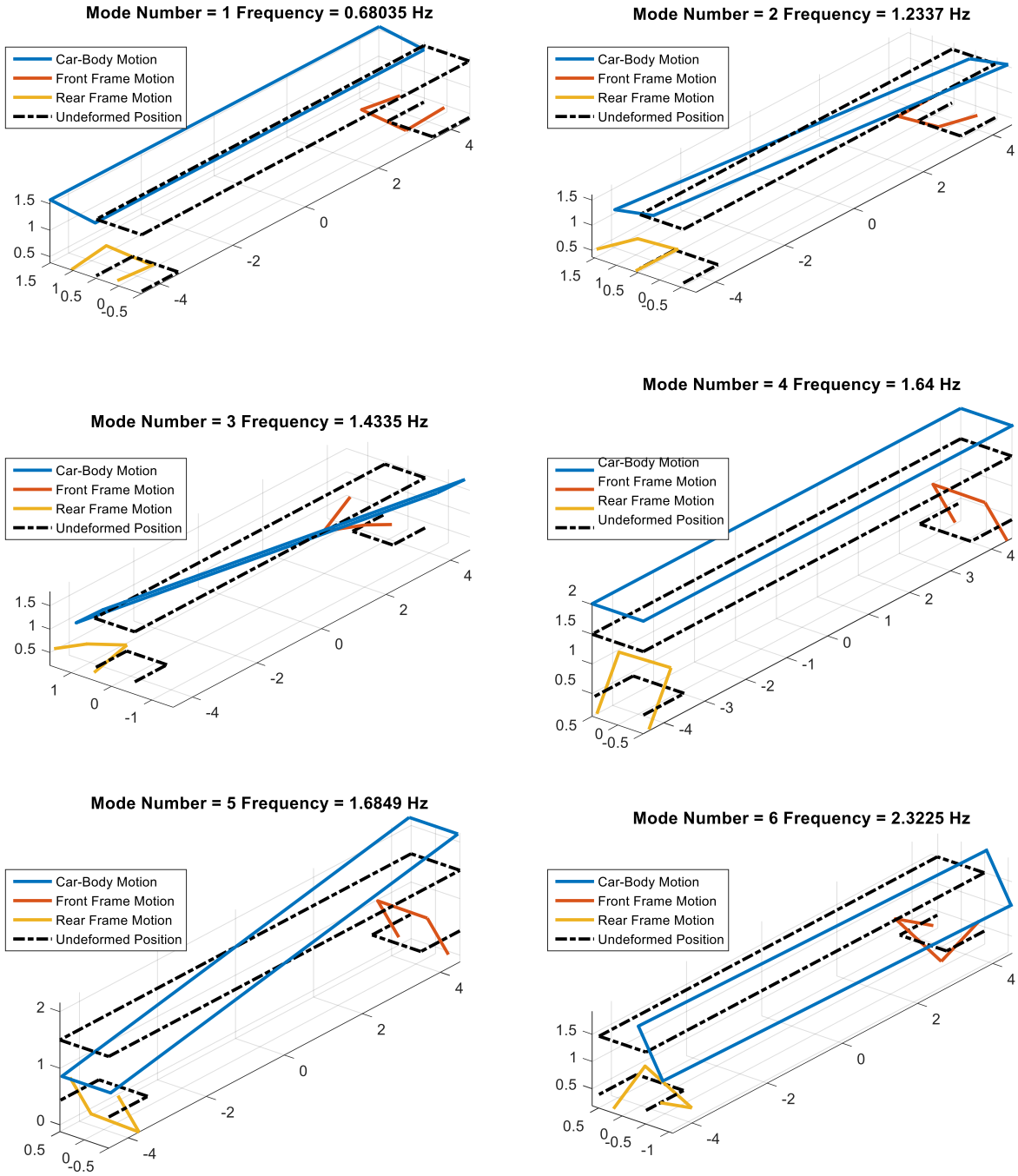

Figure 175 - Two-axle vehicle first six modes

In this section the best options achieved in Section 4.6.1 and 4.6.2 are applied simultaneously Blended control using ERI in vertical direction together with Modal control using HPI in lateral direction. Results achieved in terms of acceleration PSD are shown for the vertical direction in Figure 176 left and for lateral direction in Figure 176 right. The combination of the control strategies is more effective in the vertical direction rather than in lateral direction.

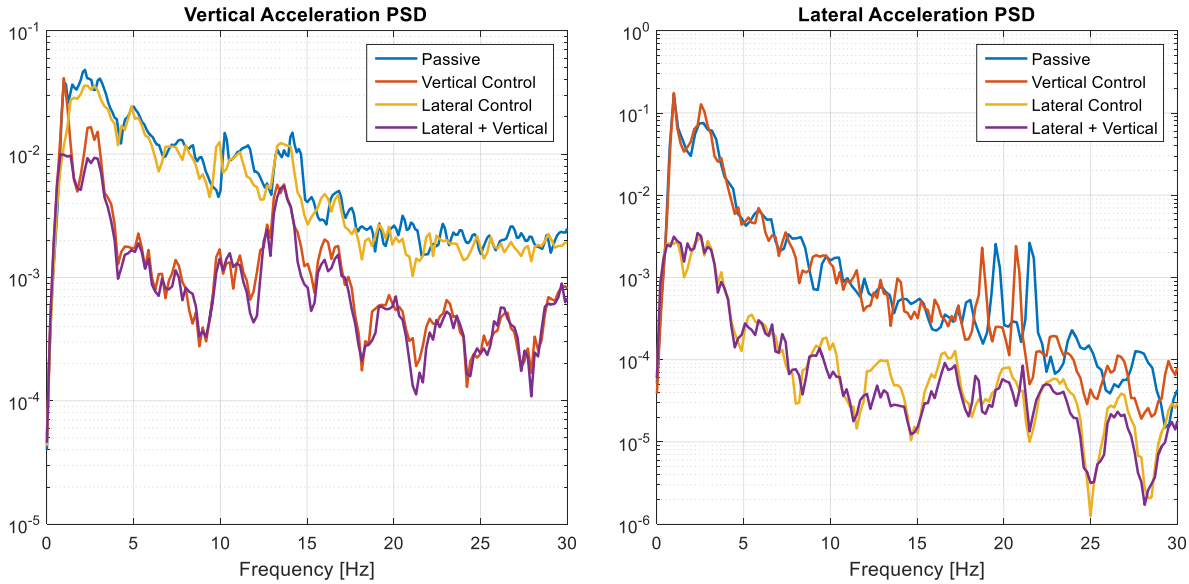

Figure 176 - Vertical and Lateral comfort comtrol comparison: vertical acceleration PSD (left), lateral acceleration PSD (right)

The results are again compared in terms of comfort indexes. In Table 37 the results for the vertical comfort are shown while in Table 38 the ones related to the lateral comfort are given. As mentioned, the effectiveness of the simultaneous application of lateral and vertical control on the two-axle vehicle is more relevant in the vertical direction. Additionally, if only one of the two controls is applied the other direction will not have significant benefit.

Table 37 - Average vertical comfort for combined vertical and lateral control [m/s^2], EN12299

	Front Left	*Front Right*	*Rear Left*	*Rear Right*
Passive	0.428	0.428	0.425	0.424
Vertical	0.204	0.204	0.194	0.191
Lateral	0.397	0.396	0.393	0.393
Vertical + Lateral	0.178	0.178	0.171	0.170

Table 38 - Average lateral comfort for combined vertical and lateral control [m/s^2], EN12299

Control	Front	Rear
Passive	0.381	0.553
Vertical	0.398	0.548
Lateral	0.077	0.113
Vertical + Lateral	0.076	0.109

4.7 CONCLUSIONS ON ACTIVE SUSPENSION FOR SINGLE AXLE RUNNING GEARS

A single axle running gear has potential for significant weight savings compared to conventional bogie designs. The savings come from reduced size of the components and reduced number of components. A conventional bogie vehicle with passive suspension can be designed to provide an acceptable vibration ride comfort and wheel wear. A single axle running gear with just one suspension stage (a conventional bogie has two) has fewer possibilities to provide an acceptable vibration ride comfort and level of wheel wear.

Wheelset steering of solid axle
The simulations comparing a vehicle with conventional bogies and a single axle running gear with a solid wheelset showed that the wear on wheel and rail will be worse for the single axle running gear. This is caused by the longer wheelbase for the two-axle vehicle compared to the bogie. The wheelset yaw stiffness is here selected to fulfil the stability requirements according to EN 14363, hence there is no possibility to reduce the wheelset yaw stiffness further. Three solutions have been investigated to improve the situation:

1. Install an active wheelset steering system with the actuator placed in parallel with the longitudinal wheelset guidance. In this case, the longitudinal wheelset guidance will ensure safety. The drawback is that the active system must overcome the stiffness of the passive longitudinal wheelset guidance, which leads to an actuator with high force capability.
2. Install an active wheelset steering system with the actuator placed in series with the longitudinal wheelset guidance. In this case, the actuator must be designed with a high internal stiffness to ensure safety. The advantage is that the actuator can have a much lower force capability than for 1) above.
3. A frequency dependent bush can replace the passive wheelset guidance. This will be a passive solution with less cost for installation and maintenance

All investigated solutions will improve the wear issue to become an advantage compared to a vehicle with conventional bogies. The active wheelset steering system with the actuator placed in series with the longitudinal wheelset guidance brings the best performance of the three investigated solutions, but it may also be the solution with the most challenging safety case. The frequency dependent bush gives good performance in most cases, the exception is the 100 m curve radius

negotiation, where the bushing allows the wheelset to steer opposite to the intended direction for difficult combinations of wheel and rail profiles. Still, considering the ratio between performance and simplicity, the frequency dependent bush becomes an attractive alternative for a single axle running gear with a solid wheelset.

Wheelset steering of independently rotating wheels
The single axle running gear can also be equipped with independently rotating wheels. Compared with the solid axle wheelset of the railway vehicle, the passive independently rotating wheel is not well suited for curve negotiation due to its limited capacity in providing the necessary steering torque for the wheelset. Two solutions have been investigated.

1. For motorized wheels it is possible to control the motors to yaw the wheel pair in a more advantageous position. The wheels can either be controlled to rotate with about the same speed on different wheel radii or to different speeds at about the same wheel radii.
2. For un-motorized wheels, it is not possible to steer the wheel pair via the longitudinal creep. The yaw torque must here be applied by actuators. As high yaw stiffness is unnecessary to ensure stability, the actuator can be quite modest in force capability.

Both studied solutions show superior performance compared to a vehicle with conventional bogies with very low expected wear on wheel and rail.

Active suspensions to improve vibrational ride comfort
The simulations comparing a vehicle with conventional bogies and a single axle running gear showed that vibrational ride comfort would be worse for the single axle running gear and worse than could be considered as acceptable. This is caused by single stage suspension, which is unable to attenuate the vibrations initiated by the track irregularities. An active suspension will improve the situation to become an advantage compared to a vehicle with conventional bogies. Active suspension is needed in both vertical and lateral directions. Combining vertical and lateral control will give better performance than controlling each direction separately. This is due to the coupling between some carbody and running gear frame motion modes. As control is needed in both directions anyhow, it is recommended to combine the control.

5. CONCLUSIONS

Wheelset steering

Active wheelset steering will significantly improve the curving performance by controlling the angle of attack between wheel to rail. Solutions with and without a passive spring in parallel with the actuators have been studied for both conventional bogie designs as well as for single axle running gears. Simulations show that the wear could be reduced by 70 – 90% compared to what a vehicle with conventional bogie produce. The performance without the parallel spring is superior to solutions with the parallel spring in narrow curves as the spring restricts the wheelset to take an ideal position. Another advantage is that the actuator force could be kept much lower. Independently rotating wheels were studied for the single-axle running gear, giving even better curving performance than for the rigid wheelset. Motorized independently rotating wheels is an particularly interesting solution as no actuator must be added to the tractions motors, which is needed anyhow.

Different control strategies can be used for active wheelset steering. The control can be built on force or position. The force control can only be used for actuators in parallel to the passive spring. A reference is needed for both force and position controlled actuation. Track curvature is the natural reference source as the curvature has direct correlation to the needed wheelset yaw. The track curvature can be derived in to two ways, either by measuring properties on-track or store the information in a database and use geo-localisation technology to pick the correct data from the database. The first way involves some kind of evaluation of the measured data and therefore risk to create a somewhat late reference, impairing the curving performance on curve transitions where the reference change.

Active wheelset steering has a relation to running safety and is therefore interesting to study what impact a failure may have. A method to evaluate the severity of different failure modes and fault-tolerant capability of various actuation schemes for wheelset steering is proposed. The quantified severity factor and Risk Priority Number can provide a good base for assessing and comparing different active steering schemes in regard to their tolerance to faults. Solutions with a passive spring in parallel is found more fault tolerant than solutions without a passive spring. Implementing a redundant actuation scheme is an effective method to improve the fault tolerance.

Semi-active and active suspensions to improve vibrational ride comfort

A conventional bogie design can often offer a proper vibrational ride comfort using passive springs and dampers. Semi-active suspension has a good ratio between benefit and complexity and become an attractive choice to improve the vibrational ride comfort. The control for the semi-active suspension can be either two-stage or continuous, the latter produce better attenuating effects than two-state and is therefore recommended. Maximum Power Point Tracking and Modified Maximum

Power Point Tracking are two suggested control strategies showing promising results for semi-active suspension.

For a single axle running gears with only one suspension step, the vibrational comfort tends to be inferior to the conventional bogie and even worse than can be accepted. In this case the choice falls on a fully active suspension as a semi-active suspension will not bring sufficient benefits. Active suspension is needed in both vertical and lateral directions. The actuator for vibrational ride comfort may have as low force capability as ± 5 kN, making the size of the actuator similar to a passive damper. Control including mode separation is recommended in lateral direction to attenuate carbody yaw movements effectively without risking interaction with roll modes. Combining vertical and lateral control gives better performance than controlling each direction separately.

REFERENCES

[1] R. M. Goodall and W. Kortüm, “Active Controls in Ground Transportation—Review of the State-of-the-Art and Future Potential,” *Veh. Syst. Dyn.*, vol. 12, no. 4–5, pp. 225–257, 1983.

[2] R. M. Goodall, “Active railway suspensions: Implementation status and technological trends,” *Veh. Syst. Dyn.*, vol. 28, pp. 87–117, 1997.

[3] T. X. Mei and R. M. Goodall, “Recent Development in Active Steering of Railway Vehicles,” *Veh. Syst. Dyn.*, vol. 39, no. 6, pp. 415–436, 2003.

[4] S. Bruni, R. Goodall, T. X. Mei, and H. Tsunashima, “Control and monitoring for railway vehicle dynamics,” *User Model. User-adapt. Interact.*, vol. 45, no. 7–8, pp. 743–779, 2007.

[5] R. M. Goodall, T. X. Mei, and S. Iwnicki, “Active Suspensions,” in *Handbook of Railway Vehicle Dynamics*, 2006, pp. 327–357.

[6] R. Persson, R. M. Goodall, and K. Sasaki, “Carbody tilting - Technologies and benefits,” *Veh. Syst. Dyn.*, vol. 47, no. 8, pp. 949–981, 2009.

[7] W. Van Dorn and P. Beemer, “Suspension for vehicles,” vol. US Patent, 1938.

[8] Anon., “Tilting Train,” *http://en.wikipedia.org/wiki/Tilting*. .

[9] Anon., “Talgo,” *https://en.wikipedia.org/wiki/Talgo*. .

[10] Talgo, “Talgo XXI,” *http://www.talgo.es/pdf/T21ingles.pdf*. .

[11] H. Zamzuri, A. C. Zolotas, and R. M. Goodall, “Intelligent control approaches for tilting railway vehicles,” *Veh. Syst. Dyn.*, vol. 44, no. SUPPL. 1, pp. 834–842, 2006.

[12] R. Zhou, A. Zolotas, and R. Goodall, “Integrated tilt with active lateral secondary suspension control for high speed railway vehicles,” *Mechatronics*, vol. 21, no. 6, pp. 1108–1122, 2011.

[13] R. Zhou, A. Zolotas, and R. Goodall, “Robust system state estimation for active suspension control in high-speed tilting trains,” *Veh. Syst. Dyn.*, vol. 52, no. SUPPL. 1, pp. 355–369, 2014.

[14] A. Facchinetti, E. Di Gialleonardo, F. Resta, S. Bruni, and V. Brundisch, “Active Control of Secondary Airspring Suspension,” *Proc. 22nd Int. Symp. Dyn. Veh. Roads Tracks (IAVSD 2011)*, pp. 1–7, 2011.

[15] S. Alfi, S. Bruni, and A. Facchinetti, “Active Control of Airspring Secondary Suspension to Improve Ride Comfort in Presence of Random Track Irregularity,” in *Proceedings of international symposium on speed-up safety and service technology for railway and maglev systems (STECH’09)*, 2009.

[16] E. F. Colombo, E. Di Gialleonardo, A. Facchinetti, and S. Bruni, “Active carbody roll control in railway vehicles using hydraulic actuation,” *Control Eng. Pract.*, vol. 31, pp. 24–34, 2014.

[17] G. Jacazio, D. Risso, M. Sorli, and L. Tomassini, “Adaptive control for improved efficiency of hydraulic systems for high-speed tilting trains,” *Proc. Inst. Mech. Eng. Part F J. Rail Rapid Transit*, vol. 226, no. 3, pp. 272–283, 2012.

[18] G. Hauser, “Alstom’s Tiltronix anticipative tilt control,” *Le Rail*, vol. 129, 2006.

[19] R. Persson, B. Kufver, and M. Berg, “On-track test of tilt control strategies for less motion sickness on tilting trains,” *Veh. Syst. Dyn.*, vol. 50, no. 7, pp. 1103–1120, 2012.

[20] S. Alfi, S. Bruni, G. Diana, A. Facchinetti, and L. Mazzola, “Active control of airspring secondary

suspension to improve ride quality and safety against crosswinds," *Proc. Inst. Mech. Eng. Part F J. Rail Rapid Transit*, vol. 225, no. 1, pp. 84–98, 2011.

[21] A. Orvnäs, S. Stichel, and R. Persson, "Aspects of Using Active Vertical Secondary Suspension To Improve Ride Comfort," in *Proceedings of the 22nd International Symposium on Dynamics of Vehicle on Roads and Tracks (IAVSD 2011)*, 2011, pp. 1–6.

[22] T. Mei X and R. Goodall M, "Use of multiobjective genetic algorithms to optimize inter-vehicle active suspensions," *Proc. Inst. Mech. Eng. Part F-journal Rail Rapid Transit*, vol. 216, no. 1, pp. 53–63, 2002.

[23] J. Zhou, L. Ren, G. Shen and T. Zhong. "Inter-vehicle active suspension control strategies to improve lateral riding quality in high-speed railway trains" vol. 06, 2004.

[24] CEN ; EN12299, *Railway Applications - Ride Comfort for Passengers - Measurement and Evaluation*. 2009.

[25] ORE, C116/RP8/D, "Wechselwirkung zwischen Fahrzeugen und Gleis," 1977.

[26] A. Orvnäs and A. L. Survey, *Methods for Reducing Vertical Carbody Vibrations of a Rail Vehicle: A Literature Survey*. 2010.

[27] D. Karnopp, "Active and semi-active vibration isolation," *Trans. ASME-L-Journal Vib. Acoust.*, pp. 177–185, 1995.

[28] A. Orvnäs, *Active Secondary Suspension in Trains A Literature Survey of Concepts and Previous Work*. 2008.

[29] A. Qazizadeh, R. Persson, and S. Stichel, "Preparation and Execution of On-track Tests with Active Vertical Secondary Suspension," *Int. J. Railw. Technol.*, 2015.

[30] A. Qazizadeh, R. Persson, and S. Stichel, "On-track tests of active vertical suspension on a passenger train," *Veh. Syst. Dyn.*, vol. 53, no. 6, pp. 798–811, 2015.

[31] Y. Sugahara, A. Kazato, T. Takigami, and R. Koganei, "Suppression of Vertical Vibration in Railway Vehicles by Controlling the Damping Force of Primary and Secondary Suspensions," *Q. Rep. RTRI*, vol. 49, no. 1, pp. 7–15, 2008.

[32] Y. Sugahara, T. Takigami, and R. Koganei, "Suppression of Vertical Bending Vibration in Railway Car Bodies By Primary Suspension Damping Control (Results of Running Tests Using Shinkansen Vehicles)," in *Proceedings of the 21st International Symposium on Dynamics of Vehicle on Roads and Tracks (IAVSD 2009)*, 2009, pp. 1–12.

[33] L. V. V. Gopala Rao and S. Narayanan, "Sky-hook control of nonlinear quarter car model traversing rough road matching performance of LQR control," *J. Sound Vib.*, vol. 323, no. 3–5, pp. 515–529, 2009.

[34] A. Pacchioni, R. M. Goodall, and S. Bruni, "Active suspension for a two-axle railway vehicle," *Veh. Syst. Dyn.*, vol. 48, no. SUPPL. 1, pp. 105–120, 2010.

[35] P. E. Orukpe, X. Zheng, I. M. Jaimoukha, A. C. Zolotas, and R. M. Goodall, "Model predictive control based on mixed H2/H∞control approach for active vibration control of railway vehicles," *Veh. Syst. Dyn.*, vol. 46, no. SUPPL.1, pp. 151–160, 2008.

[36] H. Li and R. M. Goodall, “Linear and non-linear Sky-hook damping control laws for active railway suspensions,” *Control Eng. Pract.*, vol. 7, pp. 843–850, 1999.

[37] A. Turnip, K. S. Hong, and S. Park, *Control of a semi-active MR-damper suspension system: A new polynomial model*, vol. 17, no. 1 PART 1. IFAC, 2008.

[38] H. Hammood and T. X. Mei, “Gain-sheduling control for railway vehicel semi-actibe suspension.pdf,” in *Proceedings of the 25th International Symposium on Dynamics of Vehicle on Roads and Tracks (IAVSD 2017)*, 2017, pp. 893–899.

[39] H. Md Yusof, R. Goodall, and R. Dixon, “Controller Strategies for Active Secondary Suspension Actuators,” in *Proceedings of the 22nd International Symposium on Dynamics of Vehicle on Roads and Tracks (IAVSD 2011)*, 2011.

[40] T. Hirata and R. Takahashi, “H_inf Control of Railroad Vehicle Active Suspension,” in *Proceedings of the 32nd Conference on Decision and Control*, 1993, pp. 2937–2942.

[41] T. Hirata, S. Koizumi, and R. Takahashi, “H_inf Control of Railroad Vehicle Active Suspension,” *Automatica*, vol. 31, no. 1, pp. 13–24, 1995.

[42] T. Kamada, K. Hiraizumi, and M. Nagai, “ACTIVE VIBRATION SUPPRESSION OF LIGHTWEIGHT RAILWAY VEHICLE BODY BY COMBINED USE OF PIEZOELECTRIC ACTUATORS AND LINEAR ACTUATORS,” in *Proceedings of the 21st International Symposium on Dynamics of Vehicle on Roads and Tracks (IAVSD 2009)*, 2009, pp. 1–6.

[43] T. Kamada, T. Mikazuki, and M. Nagai, “Active Vibration Suppression of Railway Vehicle by Air Actuators,” in *Proceedings of the 22nd International Symposium on Dynamics of Vehicle on Roads and Tracks (IAVSD 2011)*, 2011, pp. 1–6.

[44] T. Kamada and T. Makino, “Active Vertical Elastic Vibration Suppression of Railway Vehicle by Air Spring Suspension,” in *Proceedings of the 23rd International Symposium on Dynamics of Vehicle on Roads and Tracks (IAVSD 2013)*, 2013, pp. 1–7.

[45] A. S. Leblebici and S. Türkay, “An H∞and Sky-hook Controller Design for a High Speed Railway Vehicle,” *IFAC-PapersOnLine*, vol. 51, no. 9, pp. 156–161, 2018.

[46] D. Gong, J. Zhou, W. Sun, and R. Goodall, “Effects of Active Primary Suspension on Vertical Ride Quality Control of Flexible Car Body and Its,” *Proc. 22nd Int. Symp. Dyn. Veh. Roads Tracks (IAVSD 2011)*, vol. 1, no. 1, pp. 1–6, 2011.

[47] A. S. Leblebici and S. Türkay, “Track Modelling and Control of a Railway Vehicle,” *IFAC-PapersOnLine*, vol. 49, no. 21, pp. 274–281, 2016.

[48] M. Nagarkar, Y. Bhalerao, G. V. Patil, and R. Z. Patil, “Multi-Objective Optimization of Nonlinear Quarter Car Suspension System - PID and LQR Control,” *Procedia Manuf.*, vol. 20, pp. 420–427, 2018.

[49] L. A. Zadeh, “Fuzzy Sets,” *Inf. Control*, vol. 8, pp. 338–353, 1965.

[50] R. Guclu and M. Metin, “Fuzzy logic control of vibrations of a light rail transport vehicle in use in Istanbul traffic,” *JVC/Journal Vib. Control*, vol. 15, no. 9, pp. 1423–1440, 2009.

[51] M. Metin and R. Guclu, “Active vibration control with comparative algorithms of half rail vehicle

model under various track irregularities," *JVC/Journal Vib. Control*, vol. 17, no. 10, pp. 1525–1539, 2011.

[52] S. Sezer and A. E. Atalay, "Application of fuzzy logic based control algorithms on a railway vehicle considering random track irregularities," *JVC/Journal Vib. Control*, vol. 18, no. 8, pp. 1177–1198, 2012.

[53] A. Orvnäs, S. Stichel, and R. Persson, "Active lateral secondary suspension with H∞ control to improve ride comfort: Simulations on a full-scale model," *Veh. Syst. Dyn.*, vol. 49, no. 9, pp. 1409–1422, 2011.

[54] Y. Sugahara, T. Kojima, Y. Akami, and Y. Igarashi, "Development of a vertical semi-active suspension system using variable hydraulic dampers," in *Proceedings of the 15th International Conference on Railway Engineering Design and Operation (CR 2016)*, 2016.

[55] D. H. Allen, "Active bumpstop Hold-Off Device," in *Proc IMechE Conference Railtech 94*, 1994, p. paper C478/5/013.

[56] A. Orvnäs, S. Stichel, and R. Persson, "Ride Comfort Improvements in a High-Speed Train with Active Secondary Suspension," *J. Mech. Syst. Transp. Logist.*, vol. 3, no. 1, pp. 206–215, 2010.

[57] S. M. Savaresi, E. Silani, and S. Bittanti, "Acceleration-Driven-Damper (ADD): An Optimal Control Algorithm For Comfort-Oriented Semiactive Suspensions," *J. Dyn. Syst. Meas. Control*, vol. 127, no. 2, p. 218, 2005.

[58] S. M. Savaresi and C. Spelta, "Mixed Sky-Hook and ADD: Approaching the Filtering Limits of a Semi-Active Suspension," *J. Dyn. Syst. Meas. Control*, vol. 129, no. 4, p. 382, 2007.

[59] K. Hudha, M. H. Harun, M. H. Harun, and H. Jamaluddin, "Lateral suspension control of railway vehicle using semi-active magnetorheological damper," *IEEE Intell. Veh. Symp. Proc.*, no. Iv, pp. 728–733, 2011.

[60] D. H. Wang and W. H. Liao, "Semi-active suspension systems for railway vehicles using magnetorheological dampers. Part I: System integration and modelling," *Veh. Syst. Dyn.*, vol. 47, no. 11, pp. 1305–1325, 2009.

[61] D. H. Wang and W. H. Liao, "Semi-active suspension systems for railway vehicles using magnetorheological dampers. Part II: simulation and analysis," *Veh. Syst. Dyn.*, vol. 47, no. 12, pp. 1439–1471, 2009.

[62] L. H. Zong, X. L. Gong, S. H. Xuan, and C. Y. Guo, "Semi-active H∞ control of high-speed railway vehicle suspension with magnetorheological dampers," *Veh. Syst. Dyn.*, vol. 51, no. 5, pp. 600–626, 2013.

[63] M. G. Pollard and N. J. A. Simons, "Passenger Comfort—the Role of Active Suspensions," *Proc. Inst. Mech. Eng. Part D Transp. Eng.*, vol. 198, no. 3, pp. 161–175, 2007.

[64] A. Stribersky, S. Steidl, H. Müller, and B. Rath, "On Dynamic Analyses of Rail Vehicles With Electronically Controlled Suspensions," *Veh. Syst. Dyn.*, vol. 25, no. sup1, pp. 614–628, 2007.

[65] A. Stribersky, H. Müller, and B. Rath, "The development of an integrated suspension control technology for passenger trains," *Proc. Inst. Mech. Eng. Part F J. Rail Rapid Transit*, vol. 212, no. 1,

pp. 33–42, 1998.

[66] A. Stribersky, A. Kienberger, G. Wagner, and H. Müller, “Design and Evaluation of a Semi-Active Damping System for Rail Vehicles,” *Veh. Syst. Dyn.*, vol. 29, no. 1, pp. 669–681, 2007.

[67] Trafikverket, “Gröna Tåget, available online at: http://www.gronataget.se.” .

[68] J. Park, Y. Shin, H. Hur, and W. You, “A practical approach to active lateral suspension for railway vehicles,” *Meas. Control (United Kingdom)*, pp. 1–15, 2019.

[69] K. Tanifuji, S. Koizumi, and R. H. Shimamune, “Mechatronics in Japanese rail vehicles: Active and semi-active suspensions,” *Control Eng. Pract.*, vol. 10, no. 9, pp. 999–1004, 2002.

[70] Y. Maruyama, K. Ishihara, T. Matsui, and S. Koizumi, “The Sumitomo Search,” vol. 59, pp. 108–112, 1997.

[71] K. Sasaki, S. Kamoshita, and M. Enomoto, “A design and bench test of multi-modal active suspension of railway vehicle,” pp. 2011–2016, 2002.

[72] K. Asano, “JR East High-Speed Rolling Stock Development,” *JR East Tech. Rev.*, vol. 36, pp. 1–6, 2015.

[73] O. Goto, “Development of Active Suspension System with Electromechanical Actuators for Railway Vehicles,” no. 105, 2013.

[74] H. R. O’Neill and G. D. Wale, “Semi-active suspension improves rail vehicle ride,” *Comput. Control Eng. J.*, vol. 5, no. 4, pp. 183–188, 2005.

[75] P.-A. Roth and M. Lizell, “A Lateral Semi-Active Damping System For Trains,” *Veh. Syst. Dyn.*, vol. 25, no. sup1, pp. 585–598, 2007.

[76] Y. J. Shin, W. H. You, H. M. Hur, and J. H. Park, “Semi-active control to reduce carbody vibration of railway vehicle by using scaled roller rig,” *J. Mech. Sci. Technol.*, vol. 26, no. 11, pp. 3423–3431, 2012.

[77] Y. J. Shin, W. H. You, H. M. Hur, and J. H. Park, “H∞ control of railway vehicle suspension with MR damper using scaled roller rig,” *Smart Mater. Struct.*, vol. 23, no. 9, 2014.

[78] Y. J. Shin, W. H. You, H. M. Hur, J. H. Park, and G. S. Lee, “Improvement of Ride Quality of Railway Vehicle by Semiactive Secondary Suspension System on Roller Rig Using Magnetorheological Damper,” *Adv. Mech. Eng.*, vol. 2014, 2014.

[79] M. K. Kwak, J. H. Lee, D. H. Yang, and W. H. You, “Hardware-in-the-loop simulation experiment for semi-active vibration control of lateral vibrations of railway vehicle by magneto-rheological fluid damper,” *Veh. Syst. Dyn.*, vol. 52, no. 7, pp. 891–908, 2014.

[80] H. C. Kim, Y. J. Shin, W. You, K. C. Jung, J. S. Oh, and S. B. Choi, “A ride quality evaluation of a semi-active railway vehicle suspension system with MR damper: Railway field tests,” *Proc. Inst. Mech. Eng. Part F J. Rail Rapid Transit*, vol. 231, no. 3, pp. 306–316, 2017.

[81] O. Polach, “Curving and stability optimization of locomotive bogies using interconnected wheelsets,” *Veh. Syst. Dyn.*, vol. 41, no. suppl., pp. 282–291, 2004.

[82] R. M. Goodall, S. Bruni, and A. Facchinetti, “Active control in railway vehicles,” *Int. J. Railw. Technol.*, vol. 1, no. 1, pp. 57–85, 2012.

[83] T. X. Mei and R. M. Goodall, “Wheelset control strategies for a two-axle railway vehicle,” *Veh. Syst. Dyn.*, vol. 33, no. suppl, pp. 653–664, 1999.
[84] G. Shen and R. Goodall, “Active Yaw Relaxation For Improved Bogie Performance,” *Veh. Syst. Dyn.*, vol. 28, pp. 273–289, 1997.
[85] G. Diana, S. Bruni, F. Cheli, and F. Resta, “Active Control of the Running Behaviour of a Railway Vehicle: Stability and Curving Performances,” *Veh. Syst. Dyn.*, vol. 37, no. sup1, pp. 157–170, 2002.
[86] F. Braghin, S. Bruni, and F. Resta, “Active yaw damper for the improvement of railway vehicle stability and curving performances: Simulations and experimental results,” *Veh. Syst. Dyn.*, vol. 44, no. 11, pp. 857–869, 2006.
[87] S. A. Simson and C. Cole, “Idealized steering for hauling locomotives,” *Proc. Inst. Mech. Eng. Part F J. Rail Rapid Transit*, vol. 221, no. 2, pp. 227–236, 2007.
[88] S. A. Simson and C. Cole, “Simulation of traction curving for active yaw - Force steered bogies in locomotives,” *Proc. Inst. Mech. Eng. Part F J. Rail Rapid Transit*, vol. 223, no. 1, pp. 75–84, 2009.
[89] S. A. Simson and C. Cole, “Simulation of active steering control for curving under traction in hauling locomotives,” *Veh. Syst. Dyn.*, vol. 49, no. 3, pp. 481–500, 2011.
[90] M. Chi, H. Zhang, and Q. Huang, “Research on the Curved Negotiation Performance of the New Type Low Floor Bogie with Independent Wheels,” *Roll. Stock*, vol. 43, pp. 1–5, 2005.
[91] J. Pérez, J. M. Busturia, and R. M. Goodall, “Control strategies for active steering of bogie-based railway vehicles,” *Control Eng. Pract.*, vol. 10, no. 9, pp. 1005–1012, 2002.
[92] S. Shen, T. X. Mei, R. M. Goodall, J. Pearson, and G. Himmelstein, “A study of active steering strategies for railway bogie,” *Veh. Syst. Dyn.*, vol. 41, no. suppl, pp. 282–291, 2004.
[93] J. T. Pearson *et al.*, “Design and experimental implementation of an active stability system for a high-speed bogie,” *Veh. Syst. Dyn.*, vol. 41, no. suppl, pp. 43–52, 2004.
[94] T. X. Mei and R. M. Goodall, “Stability control of railway bogies using absolute stiffness: Sky-hook spring approach,” *Veh. Syst. Dyn.*, vol. 44, no. SUPPL. 1, pp. 83–92, 2006.
[95] R. Goodall and T. X. Mei, “Mechatronic strategies for controlling railway wheelsets with independently rotating wheels,” *2001 IEEE/ASME Int. Conf. Adv. Intell. Mechatronics. Proc. (Cat. No.01TH8556)*, vol. 1, no. July, pp. 225–230, 2001.
[96] J. Perez, L. Mauer, and J. M. Busturia, “Design of Active Steering Systems for Bogie-Based Railway Vehicles with Independently Rotating Wheels,” *Veh. Syst. Dyn.*, vol. 37, no. sup1, pp. 209–220, 2002.
[97] B. Kurzeck and L. Valente, “A novel mechatronic running gear : concept , simulation and scaled roller rig testing,” *9th World Congr. Railw. Res.*, pp. 1–10, 2011.
[98] J. Carballeira, L. Baeza, A. Rovira, and E. Garcia, “Technical characteristics and dynamic modelling of Talgo trains,” *Veh. Syst. Dyn.*, vol. 46, no. SUPPL.1, pp. 301–316, 2008.
[99] A. Meyer, “Wheel sets or independently rotating wheels – from theory to practice,” *Siemens AG*, pp. 1–12, 2016.
[100] Y. Cho and J. Kwak, “Development of a new analytical model for a railway vehicle equipped with

independently rotating wheels," *Int. J. Automot. Technol.*, vol. 13, no. 7, pp. 1047–1056, 2012.

[101] H. Sugiyama, R. Matsumura, Y. Suda, and H. Ezaki, "Analysis of independently rotating wheel system using multibody dynamics approach," *Proc. ASME 2009 Int. Des. Eng. Tech. Conf. Comput. Inf. Eng. Conferemce*, pp. 1–8, 2009.

[102] T. X. Mei and R. M. Goodall, "Wheelset control strategies for a two-axle railway vehicle," *Veh. Syst. Dyn.*, vol. 33, no. Supplement, pp. 653–664, 1999.

[103] M. Gretzschel, L. Bose, and DRL, "A mechatronic approach for active influence on railway vehicle running behaviour," *Veh. Syst. Dyn.*, vol. 33, no. Supplement, pp. 418–430, 1999.

[104] P. Aknin, J. B. Ayasse, and A. Devallez, "Active steering of railway wheelsets," *Proc. 12th IAVSD Conf.*, 1992.

[105] L. Baeza, J. Carballeira, A. Roda, and J. E. Tarancón, "Method for obtaining the modal properties of articulated trains equipped with independently rotating wheels," *Veh. Syst. Dyn.*, vol. 44, no. 11, pp. 841–854, 2006.

[106] X. Wu, M. Chi, J. Zeng, W. Zhang, and M. Zhu, "Analysis of steering performance of differential coupling wheelset," *J. Mod. Transp.*, vol. 22, no. 2, pp. 65–75, 2014.

[107] Y. Suda, W. Wang, M. Nishina, S. Lin, and Y. Michitsuji, "Self-steering ability of the proposed new concept of independently rotating wheels using inverse tread conicity," *Veh. Syst. Dyn.*, vol. 50, no. SUPPL. 1, pp. 291–302, 2012.

[108] T. X. Mei and R. M. Goodall, "Robust control for independently rotating wheelsets on a railway vehicle using practical sensors," *IEEE Trans. Control Syst. Technol.*, vol. 9, no. 4, pp. 599–607, 2001.

[109] T. X. Mei and R. M. Goodall, "Practical Strategies for Controlling Railway Wheelsets Independently Rotating Wheels," *J. Dyn. Syst. Meas. Control*, vol. 125, no. 3, p. 354, 2003.

[110] T. X. Mei and J. W. Lu, "On the interaction and integration of wheelset control and traction system," *Veh. Syst. Dyn.*, vol. 41, no. Supplement, pp. 123–132, 2004.

[111] J. Pérez, J. M. Busturia, T. X. Mei, and J. Vinolas, "Combined active steering and traction for mechatronic bogie vehicles with independently rotating wheels," *Annu. Rev. Control*, vol. 28, no. 2, pp. 207–217, 2004.

[112] M. Gretzschel and L. Bose, "A new concept for integrated guidance and drive of railway running gears," *Control Eng. Pract.*, vol. 10, no. 9, pp. 1013–1021, 2002.

[113] B. Liang and S. D. Iwnicki, "An experimental study of independently rotating wheels for railway vehicles," *Proc. 2007 IEEE Int. Conf. Mechatronics Autom. ICMA 2007*, pp. 2282–2286, 2007.

[114] B. Liang and S. D. Iwnicki, "Independently rotating wheels with induction motors for high-speed trains," *J. Control Sci. Eng.*, vol. 2011, 2011.

[115] H. Ahn, H. Lee, S. Go, Y. Cho, and J. Lee, "Control of the lateral displacement restoring force of IRWs for sharp curved driving," *J. Electr. Eng. Technol.*, vol. 11, no. 4, pp. 1044–1050, 2016.

[116] Z. G. Lu, Z. Yang, Q. Huang, and X. C. Wang, "Robust active guidance control using the μ-synthesis method for a tramcar with independently rotating wheelsets," *Proc. Inst. Mech. Eng. Part F J. Rail Rapid Transit*, vol. 0, no. 0, pp. 1–16, 2018.

[117] T. X. Mei, H. Li, R. M. Goodall, and A. H. Wickens, “Dynamics And Control Assessment Of Rail Vehicles Using Permanent Magnet Wheel Motors,” *Veh. Syst. Dyn.*, vol. 37, no. sup1, pp. 326–337, 2002.

[118] Y. Ji, L. Ren, and J. Zhou, “Boundary conditions of active steering control of independent rotating wheelset based on hub motor and wheel rotating speed difference feedback,” *Veh. Syst. Dyn.*, vol. 3114, pp. 1–16, 2018.

[119] B. Kurzeck, A. Heckmann, C. Wesseler, and M. Rapp, “Mechatronic track guidance on disturbed track: The trade-off between actuator performance and wheel wear,” *Veh. Syst. Dyn.*, vol. 52, no. SUPPL. 1, pp. 109–124, 2014.

[120] G. Grether, “Dynamics of a running gear with IRWs on curved tracks for a robust control development,” *Pamm*, vol. 17, no. 1, pp. 797–798, 2017.

[121] A. Heckmann, L. Daniel, G. Grether, and A. Keck, “From Scaled Experiments of Mechatronic Guidance to Multibody Simulations of DLR ’ s Next Generation Train Set,” *Dyn. Veh. Roads Tracks Proc. 25th Int. Symp. Dyn. Veh. Roads Tracks (IAVSD 2017), 14-18 August 2017, Rockhampton, Queensland, Aust.*, 2017.

[122] A. H. Wickens, “Dynamic stability of articulated and steered railway vehicles guided by lateral displacement feedback,” *Veh. Syst. Dyn.*, vol. 23, no. Supplement, pp. 541–553, 1994.

[123] A. H. Wickens, “Comparative stability of bogie vehicles with passive and active guidance as influenced by friction and traction,” *Veh. Syst. Dyn.*, vol. 47, no. 9, pp. 1137–1146, 2009.

[124] A. Powell, “Mechatronic control of an actively guided rail vehicle,” *Veh. Syst. Dyn.*, vol. 33, no. Supplement, pp. 442–452, 1999.

[125] Y. Michitsuji and Y. Suda, “Running performance of power-steering railway bogie with independently rotating wheels,” *Veh. Syst. Dyn.*, vol. 44, no. SUPPL. 1, pp. 71–82, 2006.

[126] M. Gretzschel and A. Jaschinski, “Design of an active wheelset on a scaled roller rig,” *Veh. Syst. Dyn.*, vol. 41, no. 5, pp. 365–381, 2004.

[127] W. Geuenich, Ch. Günther and R. Leo, “The Dynamics of Fiber Composite Bogies with Creep-controlled Wheelsets,” *Veh. Sys. Dyn.*, vol. 12, no. 1-3, pp. 134-140, 1983

[128] CEN, EN14363, Railway applications — Testing and Simulation for the acceptance of running characteristics of railway vehicles — Running Behaviour and stationary tests, 2016

[129] CEN, EN60812, Failure modes and effects analysis (FMEA and FMECA), 2018

[130] Evans, J. “Application of the “Hall” Hydraulic Radial Arm Bush to a 200 km/h inter-city coach”, IAVSD 2011

[131] ERRI (ORE) B176 Report 1, Appendix 6. Bogie with steered or steering wheelset - Design and proof calculations relating to running behaviour

[132] A. Qazizadeh, S. Stichel, and R. Persson, “Proposal for systematic studies of active suspension failures in rail vehicles,” *Proc. Inst. Mech. Eng. Part F J. Rail Rapid Transit*, vol. 232, no. 1, pp. 199–213, 2018